SYNTHESIS AND CHARACTERISATION OF THERMO-RESPONSIVE MICROCARRIERS BASED ON POLY(*N*-ISOPROPYLACRYLAMIDE)

Jinnan Zhang

Hertford College



Institute of Biomedical Engineering
Department of Engineering Science
University of Oxford

A thesis submitted for the degree
Doctor of Philosophy
Hilary Term 2013

To my mother and father

Abstract

Cell cultivation on the surface of microcarriers in suspension bioreactors is widely used for large scale expansion of anchorage-dependent cells. Proteolytic enzyme treatment is most commonly used to detach cells from colonized microcarriers for cell harvest or scale-up. One advantage of thermo-responsive microcarrier is that it may facilitate non-enzymatic harvest of cultured cells. In this thesis, the synthesis and characterisation of thermo-responsive microcarriers grafted with poly(*N*-isopropylacrylamide) (PNIPAAm) is discussed, potentially allowing cell-harvesting by temperature alternation, and without enzyme treatment.

To prepare the PNIPAAm-grafted microcarriers, three grafting techniques were employed, namely grafting-to, grafting-from and seeded polymerization. In each technique, the methods for regulating PNIPAAm grafting parameters, including grafting density, grafted amount, molecular weight, and molecular architecture were investigated, as the grafting parameters may affect the efficiency of cell attachment, proliferation and detachment. In the grafting-to technique, chain transfer polymerization was employed to synthesise and control the molecular weight of end-functionalized PNIPAAm polymers. The grafting density of PNIPAAm was regulated by changing the feed concentration of the polymers. However, the grafting density (or amount) was limited by steric hindrance and reached a plateau at around 27 μmol/g (300 mg/g). Apart from linear PNIPAAm molecular architecture, the methods for preparation of looped and double-layer looped PNIPAAm chain were also investigated. In the grafting-from technique, an azo-initiator, 4,4′-azobis(4-cyanovaleric acid) (ACVA), and an atom transfer radical polymerization (ATRP) initiator, 2-bromopropionyl bromide, were immobilized respectively onto the surface of microspheres before PNIPAAm chains were grown from these initiators. Both initiator grafting density and PNIPAAm molecular weight can be regulated. The achievable PNIPAAm grafted amount (~697 mg/g) is much higher than that prepared by the grafting to technique. Different preparations of PNIPAAm molecular architecture were investigated, namely linear PNIPAAm chain, cross-linked PNIPAAm hydrogel and branched PNIPAAm chain. Using seeded polymerization, cross-linked PNIPAAm hydrogel (up to 143mg/g) was grafted to the carboxyl functionalized polystyrene microspheres. The grafted amount of PNIPAAm hydrogel can also be regulated.

The PNIPAAm-grafted microspheres with different grafting parameters were cultured with cells to investigate cytotoxicity, cell attachment and cell detachment behaviour. All the PNIPAAm-grafted microcarriers with appropriate treatments are not found to inhibit cell proliferation. However, cell attachment and thermally-induced detachment behaviour were not observed on these microcarriers. Potential reasons for these observations were systematically discussed. Finally, two conceptual bioreactor designs, using thermo-responsive microcarriers, are described which would be suitable for future detailed evaluation.

Acknowledgements

As a D.Phil student working in two labs with five supervisors, I have received support and advice from many people in many places during the time spent on my thesis. I am grateful to you all and would like to give some personal thanks.

Firstly, thank you to all my supervisors in Department of Engineering Science for giving me such a wonderful opportunity to work on the exciting project with an interdisciplinary nature in this amazing university. To Dr. Hua Ye, whose unwavering support and guidance have contributed immeasurably. To Prof. Zhanfeng Cui, whose brilliant ideas of the bioreactor design and his introduction to the big picture of this project provided insight into the world of tissue engineering. To Prof. Robert Field, whose help always came in time when I needed him.

I also would like to thank Prof. Mark Moloney, my supervisor in Chemistry Research Laboratory (CRL), for his genuine belief in my abilities and his continuous and professional support throughout my research. His supervision technically transformed me from a pure-bred engineer to a competent chemist.

Thank you to Prof. Stephen Rimmer, my supervisor based in Sheffield University, and his group, for sharing with me their comprehensive knowledge of polymer synthesis and purification. The experience I learned there has proven to be the foundation of my entire research.

Many thanks must go to Dr. Robert Jacobs from CRL for his helps on FTIR and XPS characterization and providing patient guidance on result analysis. I also would like to thank Dr. Richard Laga from Department of Oncology for his continuous help on HPLC measurements even though I screwed up the HPLC machine once.

I owe many thanks to past and present members of Cui's group in IBME and the MGM group in CRL for making it such a pleasurable few years. In particular, to Dr. Julian George for all your help relating to every aspect of my research work, you are the superman of this lab. To Miss Maria Higson, thanks for the grammatical guidance and the Friday Cakes. To Dr. Emily Parker, thanks for always reminding me to wear lab goggles and keep myself safe, in addition to all your other incredible help. To Dr. Apichat Aphaiwong, thank you for generously sharing your fume hood and work desk with me for three years.

Mum and Dad, I wish you could be here to see this, I know how proud it would make you. For the first twenty eight years of my life you gave everything you had, supported, guided and always encouraged me. I will forever be indebted to you. This is the fruit of your labours as much as it is mine, and I dedicate this, together with every other achievement in my future, to you both.

Content

Abstract.....I

Acknowledgements II

Content..... III

Nomenclature XII

1 Introduction..... 1

1.1 Background 1

1.2 Aims of this thesis..... 3

1.3 Thesis outline 5

2 Literature review 7

2.1 Stimuli-responsive polymer and PNIPAAm..... 7

2.2 Thermal-responsive behaviour of surface-grafted PNIPAAm..... 12

2.3 Thermo-responsive surfaces for cell culture 17

2.3.1 Introduction to cell sheet engineering 17

2.3.2 Cellular interactions with PNIPAAm-grafted surfaces 21

2.3.2.1 Cell attachment to and detachment from PNIPAAm-grafted surface 21

2.3.2.2 Effects of characters of PNIPAAm-grafted surface 23

2.4 Microcarrier cell culture..... 26

2.5 Preparation methods of thermo-responsive microcarriers 28

2.5.1 “Grafting-to” approach..... 28

2.5.2 “Grafting-from” approach 32

2.5.2.1 Conventional free radical grafting polymerization 32

2.5.2.2 Controlled/living free radical polymerization 34

2.5.2.3 Redox initiated grafting polymerization 39

2.5.2.4 Vinyl group copolymerization 39

2.5.3 Bulk cross-linked PNIPAAm hydrogel beads 40

2.5.3.1 Precipitation polymerization using a mold 40

2.5.3.2 Suspension polymerization 42

2.5.4 Seeded polymerization 44

2.5.5 Non-covalent adsorption 47

2.6 Thermo-responsive microcarriers on cell culture 48

3 ‘Grafting-to’ technique for microsphere modification 54

3.1 Introduction 54

3.2 Materials and methods 55

3.2.1 Materials 55

3.2.2 Preparation of PNIPAAm polymers and copolymers 56

3.2.2.1 Synthesis of PNIPAAm 56

3.2.2.2 Synthesis of PNIPAAm-COOH 56

3.2.2.3 Synthesis of PNIPAAm-OH 57

3.2.2.4 Synthesis of PNIPAAm-NH_2 57

3.2.2.5 Synthesis of poly(NIPAAm-*co*-AAc) 58

3.2.3 Grafting PNIPAAm polymer or copolymer to microsphere surfaces 59

3.2.3.1 Preparation of PS-O-OC-PNIPAAm microspheres 59

3.2.3.2 Preparation of PS-CO-O-PNIPAAm microspheres 60

3.2.3.3 Preparation of PS-CO-NH-PNIPAAm microspheres 60

3.2.3.4 Preparation of PS-(looped PNIPAAm) microspheres 61

3.2.3.5 Preparation of PS-(double-layer looped PNIPAAm) microspheres 61

3.2.4 Characterizations and measurements 62

3.2.4.1 FTIR spectroscopy measurements 62

3.2.4.2 HPLC measurements 62

3.2.4.3 Combustion analysis 62

3.2.4.4 SEM observations 63

3.2.4.5 Determination of LCST 63

3.2.4.6 NMR measurements 64

3.3 Results and discussion 64

3.3.1 Synthesis of end-functionalized PNIPAAm 64

3.3.2 Phase transition of PNIPAAm-COOH 72

3.3.3 Conjugation of end-functionalized PNIPAAm to microspheres 74

3.3.4 Synthesis of PNIPAAm copolymers 79

3.3.5 Phase transition of PNIPAAm copolymers 83

3.3.6 Synthesis of looped PNIPAAm and double-layer looped PNIPAAm grafted microsphere 85

3.4 Summary 88

4 'Grafting-from' technique for microsphere modification 91

4.1 Introduction 91

4.2 Materials and methods 92

4.2.1 Materials 92

4.2.2 Conventional radical grafting polymerization 93

4.2.2.1 Azo-initiator immobilization 93

4.2.2.2 Surfaced-initiated radical grafting polymerization 94

4.2.2.3 Preparation of microspheres grafted with PNIPAAm hydrogel 94

4.2.2.4 Preparation of microspheres grafted with comb-type PNIPAAm hydrogel 95

4.2.2.4.1 Preparation of PNIPAAm macromonomer 95

4.2.2.4.2 Preparation of comb-type hydrogel grafted microspheres 95

4.2.2.5 Preparation of microspheres grafted with branched PNIPAAm 96

4.2.2.5.1 Synthesis of poly(2-hydroxylethyl acrylate) grafted polystyrene (PS-PHEA) microspheres 96

4.2.2.5.2 Synthesis of poly(styrene-co-HEA) grafted polystyrene (PS-PSHEA) microspheres 96

4.2.2.5.3 Synthesis of PNIPAAm branches via 'grafting-to' technique 96

4.2.2.5.4 Immobilization of ACVA moieties to PS-PHEA or PS-PSHEA microspheres 97

4.2.2.5.5 Synthesis of PNIPAAm branches via 'grafting-from' technique 97

4.2.3 Atom transfer radical polymerization (ATRP) 97
4.2.3.1 ATRP initiator immobilization 98
4.2.3.2 ATRP of NIPAAm 98
4.2.4 Characterizations and measurements 99
4.2.4.1 FTIR spectroscopy measurements 99
4.2.4.2 Combustion analysis 99
4.2.4.2.1 Conventional radical grafting polymerization 99
4.2.4.2.2 ATRP 101
4.2.4.3 SEM observations 102
4.2.4.4 NMR measurements 102
4.3 Results and discussion 103
4.3.1 Conventional free radical grafting polymerization 103
4.3.1.1 Azo-initiator immobilization 103
4.3.1.2 Surface-initiated radical polymerization 106
4.3.1.2.1 Thermal decomposition of grafted ACVA 106
4.3.1.2.2 Surface-initiated polymerization 109
4.3.1.2.3 Reaction termination and molecular architecture of grafted PNIPAAm 113
4.3.1.3 Preparation of microspheres grafted with PNIPAAm hydrogel 114
4.3.1.4 Preparation of microspheres grafted with branched PNIPAAm 118
4.3.1.4.1 Synthesis of the backbone 119

4.3.1.4.2 Branch incorporation via ‘grafting-to’ technique 119

4.3.1.4.3 Branch incorporation via ‘grafting-from’ technique 121

4.3.2 Surface-initiated ATRP 124

4.3.2.1 Immobilization of ATRP initiator 125

4.3.2.2 Aqueous ATRP 126

4.4 Summary 132

5 Seeded precipitation polymerization for microsphere modification 134

5.1 Introduction 134

5.2 Materials and methods 135

5.2.1 Materials 135

5.2.2 Preparation of PNIPAAm hydrogel-modified microsphere 135

5.2.3 Characterizations and measurements 136

5.2.3.1 FTIR spectroscopy measurements 136

5.2.3.2 Combustion analysis 136

5.3 Results and discussion 137

5.4 Summary 140

6 Characterisation of thermo-responsive properties of modified microspheres for cell culture 141

6.1 Introduction 141

6.2 Materials and methods 142

6.2.1 Materials 142

6.2.2 Methods 142

6.2.2.1 Isolation of rADSCs 142

6.2.2.2 Preparation of GFP cells 143

6.2.2.3 Monolayer cell cultivation 143

6.2.2.4 Preparation of microcarriers for culture 144

6.2.2.5 Cytotoxicity assays 144

6.2.2.5.1 Standard curve 145

6.2.2.5.2 Cell inoculation with microcarriers 146

6.2.2.5.3 AB assay for cell proliferation 146

6.2.2.5.4 Removal of copper ions 147

6.2.2.6 Cell attachment experiments 147

6.2.2.7 Cell detachment experiments 148

6.3 Results and discussion 148

6.3.1 Cytotoxicity assay of cross-linked dextran based microcarriers 148

6.3.2 Cytotoxicity assay of cross-linked polystyrene based microcarriers 152

6.3.3 Cell attachment experiments 155

6.3.3.1PS-O-OC-PNIPAAm microspheres 155

6.3.3.2 PS-(looped PNIPAAm) and PS-(double-layer looped PNIPAAm) microspheres 157

6.3.3.3 PS-ACVA-PNIPAAm microspheres 158

6.3.3.4 PS-ACVA-homopolymer hydrogel and PS-ACVA-comb type hydrogel microspheres 159

6.3.3.5 PS-PSHEA-ACVA-PNIPAAm microspheres 161

6.3.3.6 PS-COOH-hydrogel microspheres 161

6.3.3.7 PNIPAAm-modified Sephadex® G-50 microcarriers 163

6.3.3.8 PNIPAAm-modified Cytodex®-1 microcarriers 164

6.3.4 Cell detachment experiments 166

6.4 Summary 168

7 Conclusion and future work 171

7.1 Preparation of PNIPAAm-grafted microspheres 171

7.2 PNIPAAm-grafted microspheres for cell culture 175

7.3 Future work 179

7.3.1 Microsphere modification using RAFT polymerization 179

7.3.2 Bioreactor design 182

7.3.2.1 Design A: tapered fluidized-bed bioreactor 183

7.3.2.1.1 Conceptual design and justifications 183

7.3.2.1.2 Cell culture procedure 185

7.3.2.2 Design B: columnar fluidized-bed bioreactor 188

7.3.2.2.1 Conceptual design and justifications 188

7.3.2.2.2 Cell culture procedure 189

Appendix A: Combustion analysis characterization 192

Appendix B: FTIR characterization..... 198

Appendix C: ^{1}H-NMR characterization 201

Appendix D: SEM characterization..... 203

References..... 205

Nomenclature

AAc	acrylic acid
AAm	acrylamide
AB	alamarBlue®
ACVA	4,4′-azobis(4-cyanovaleric acid)
AEMA	*N*-aminoethyl methacrylate
AIBN	2,2′-azobis(2-methylpropionitrile)
AMPTMA	(3-acrylamidopropyl)-trimethylammonium chloride
APS	ammonium persulfate
ATP	adenosine triphosphate
ATR	attenuated total reflectance
ATRP	atom transfer radical polymerization
BPOEA	2-(2-bromopropionyloxy) ethyl acrylate
CCYMEA	5-(4-carboxy-2-cyanobutan-2-ylimino)-4-methylpent-4-enoic acid
CEA	4-cyanopent-4-enoic acid
CHO-K1	Chinese hamster ovary cells
CIPAAm	2-carboxyisopropylacrylamide
CLD	cross-linked dextran
CME	chloromethyl methyl ether
COA	4-cyanopentanoic acid
CRP	controlled/living radical polymerization
DCC	*N*,*N*′-dicyclohexylcarbodiimide
DCM	dichloromethane
DDOA	4,5-dicyano-4,5-dimethyloctanedioic acid
DEAE	*N*,*N*-diethylaminoethyl
DI	deionised

DIC	*N*,*N*′-diisopropylcarbodiimide
DMAP	4-(dimethylamino)pyridine
DMSO	dimethyl sulfoxide
DPBS	Dulbecco's Phosphate-Buffered Saline
DVB	divinylbenzene
ECM	deposited extracellular matrix
ECP	ethyl-2-chloropropionate
ECP	ethyl-2-chloropropionate
EDC	*N*-(3-dimethylaminopropyl)-*N*′-ethylcarbodiimide hydrochloride
EDTA	ethylenediaminetetraacetic acid
FBS	fetal bovine serum
FCs	fetal chondrocytes
FTIR	Fourier transform infrared
GFP	green fluorescent protein
GRGDY	Glysine-Arginine-Glycine-Aspartic acid–Tyrosine
hBMMSCs	human bone marrow-derived mesenchymal stem cells
HBPS	hyperbranched poly(siloxysilane)
HCST	higher critical solution temperature
HEA	hydroxyethyl acrylate
HG-DMEM	Dulbecco’s modified Eagle’s medium – high glucose
HMTETA	1,1,4,7,10,10-hexamethyltriethylenetetramine
HPLC	high-performance liquid chromatography
LCST	lower critical solution temperature
MBAAm	*N*,*N*′-methylenebis(acrylamide)
Me_6TREN	tris[2-(dimethylamino)ethyl]amine
MEA	2-mercaptoethylamine
MetOH	2-mercaptoethanol
M_n	number average molecular weight

MPA	3-mercaptopropionic acid
M_w	weight average molecular weight
MW	molecular weight
N/A	not applicable
N/D	not determined
NHS	*N*-hydroxysuccinimide
NIPAAm	*N*-isopropylacrylamide
NMR	nuclear magnetic resonance
P(NIPAAm-*co*-BMA)	poly(*N*-isopropylacrylamide-*co*-*n*-butyl methacrylate)
PD	polydispersity
PDMS	poly(dimethylsiloxane)
PEG	poly(ethylene glycol)
PHEA	poly(2-hydroxyethyl acrylate)
PHEMA	poly(2-hydroxyethylmethacrylate)
PLGA–PEG–PLGA	poly(DL-lactide-*co*-glycolide-*b*-ethylene glycol-*b*-DL-lactide-*co*-glycolide)
PNIPAAm	poly(*N*-isopropylacrylamide)
PNIPAAm-COOH	carboxyl-terminated PNIPAAm
PNIPAAm-NH_2	amine-terminated PNIPAAm
PNIPAAm-OH	hydroxyl-terminated PNIPAAm
poly(NIPAAm-*co*-AAc)	poly(*N*-isopropylacrylamide-*co*-acrylic acid)
poly(NIPAAm-*co*-AAm)	poly(*N*-isopropylacrylamide-*co*-acrylamide)
PS	polystyrene
PS-COOH	polystyrene A COOH microspheres
PSHEA	poly(styrene-*co*-2-hydroxyethyl acrylate)
PS-NH_2	(aminomethyl)polystyrene microspheres
PS-OH	(hydroxymethyl)polystyrene microspheres
rADSCs	rat adipose-derived stem cells
RAFT	reversible addition-fragment chain transfer

RGD	Arginine-Glycine-Aspartic acid
RGDS	Arginine-Glycine-Aspartic acid–Serine
RT	room temperature
SEM	scanning electron microscope
SD	standard deviation
SVF	stromal–vascular fraction
TCPS	tissue culture polystyrene
TEMED	*N,N,N′,N′*-tetramethylethylenediamine
UCST	upper critical solution temperature
UV-VIS	ultraviolet-visible

1 Introduction

1.1 Background

Reliable methods for the culture of large number of cells with defined phenotype are a critical requirement for clinical and industrial applications, such as tissue engineering, cell transplantation and biological production (Malda and Frondoza 2006; Collett et al. 2007; Yang et al. 2010; Tamura et al. 2012a). For example, a therapeutic treatment for adult human liver will require large quantities of competent cells (of the order of 10^9-10^{10}) (Park et al. 2010). However, conventional two-dimensional culture methodology suffers from the inherent limitation of a flat surface, leading to its unsuitability for scale-up to large quantities in industrial manufacturing (Oh et al. 2009). Therefore, a large-scale cell culture method is required to meet such a clinical and industrial need. The microcarrier cell culture technique was introduced by van Wezel in 1967 (Van Wezel 1967), and it allows anchorage-dependent cells to attach, spread and proliferate on the surface of synthetic particles, which are usually suspended in culture medium by gentle stirring (Kim et al. 2003). This technique provides an attractive alternative to conventional two-dimensional cell culture due to its high surface area-to-volume ratio (Kim et al. 2003). In addition, microcarrier-based bioreactors offer easier monitoring and control of culture parameters in a homogeneous culture system (Eibes et al. 2010). Thus, the microcarrier cell culture technique has been extensively used in industry for amplification of various types of anchorage-dependent cells on a large scale to mass produce many biologicals, such as growth factors, vaccines and antibodies (Phillips et al. 2008).

For cell harvest or scale-up, proteolytic enzyme treatments (e.g. trypsinization) are most commonly employed for detaching cells from microcarriers. However, such proteolytic enzyme treatments have many drawbacks. First, proteolytic enzymes degrade cell membrane proteins and deposited extracellular matrix (ECM), resulting in the reduction of cell viability (Tamura et al. 2012a). The disruption of deposited ECMs is also responsible for the decreased grafting efficiency when cells are used for transplantation (Yang et al. 2010). Second, proteolytic enzymes are usually animal-derived proteins and bring obvious risks of the transmission of disease when cells are used for therapeutic applications (Collett et al. 2007). Third, it is reported that proteolytic enzymes might have potential to alter cell phenotype (Collett et al. 2007). Fourth, proteolytic enzyme treatment is complicated and labour-intensive, because it requires further treatments such as enzyme deactivation and cell washing (Yang et al. 2010).

In order to circumvent these difficulties, a thermo-responsive polymer, poly(N-isopropylacrylamide) (PNIPAAm), has received particular attention for cell detachment. PNIPAAm exhibits a sharp phase transition at its lower critical solution temperature (LCST) of about 32 ℃ in aqueous solution. At temperatures below 32 ℃, the polymer shows a hydrophilic state with a highly hydrated and extended ‘random coil’ conformation. At temperatures above 32 ℃, however, the polymer shows a hydrophobic nature with an extensively dehydrated and collapsed ‘globular’ conformation (Yamada et al. 1990; Kim et al. 2003; Mittal et al. 2007a). This thermo-responsive hydrophobic/hydrophilic change of PNIPAAm can be used for the regulation of cell attachment and detachment on PNIPAAm-grafted microcarriers by simply changing the temperature. Thus, on PNIPAAm modified microcarriers, cells can adhere and proliferate on the hydrophobic surface at temperatures higher than 32 ℃ and may

be detached spontaneously from the hydrophilic surfaces without enzymatic digestion by reducing the temperature below 32 ℃ (Figure **1.1**).

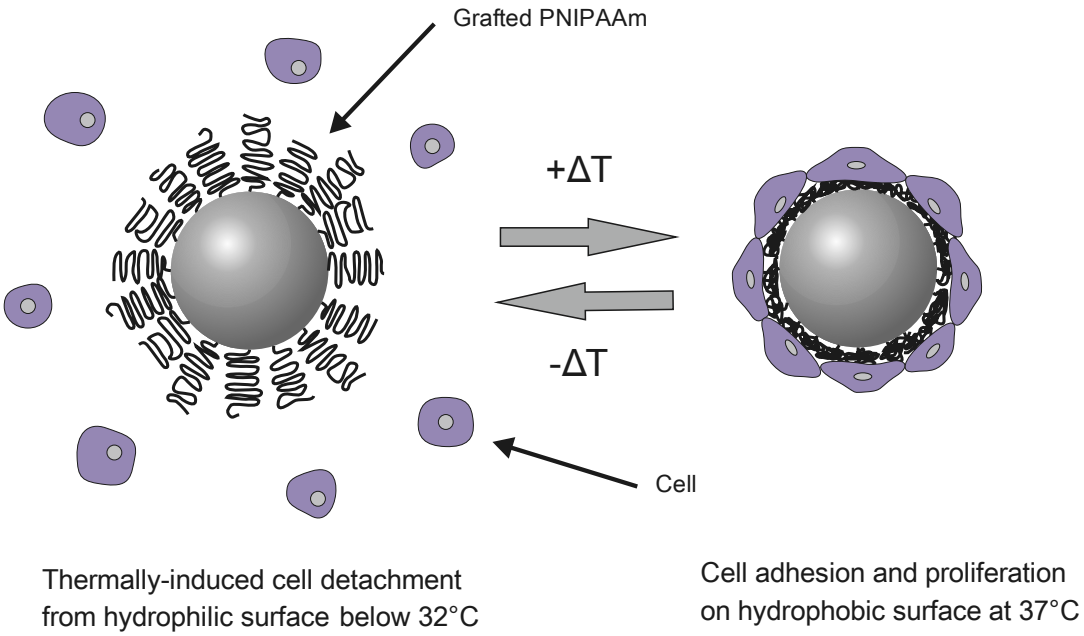


Figure 1.1 Schematic illustration of cell attachment to and thermally-induced detachment from thermo-responsive microcarrier based on PNIPAAm.

1.2 Aims of this thesis

The overall aim of this thesis is to develop a thermo-responsive microcarrier grafted with PNIPAAm allowing cell-harvesting by temperature reduction without enzyme treatment. It consists of four steps: (i) to develop reliable methods for the construction of PNIPAAm modified microspheres and characterise the modified microspheres; (ii) to manipulate the PNIPAAm grafting parameters, such as grafting density grafted amount, molecular weight and molecular architecture; (iii) to investigate their suitability as use for microcarriers; and (iv) to design a bioreactor which would be used for cell harvesting using thermo-responsive microcarriers.

A PNIPAAm-grafted surface has already been applied to two-dimensional cell culture. Several different methods have been used to fabricate the thermo-responsive surfaces, such as electron-beam polymerization (Yamada et al. 1990), plasma polymerization (Canavan et al. 2005), ultraviolet (UV) light irradiation (Von Recum et al. 1999), and surface-initiated polymerization (Ista et al. 2001). However, most of these methods are not suitable for grafting PNIPAAm onto the surface of spherical particles. An applicable method for thermo-responsive microcarrier preparation requires two important features: 1) that it can be used to modify or fabricate beads bigger than 50 μm in diameter; 2) that the grafted PNIPAAm has to be distributed on the outermost surface of the microspheres. It is necessary to investigate and optimise reliable PNIPAAm grafting techniques for conjugation to various microspheres. It is reported that PNIPAAm grafting density, molecular weight and molecular architecture will affect the efficiency of cell adhesion, proliferation and thermally-induced cell detachment (da Silva et al. 2007). Therefore, methods for controlling the grafting parameters to optimise the cellular interaction with PNIPAAm-grafted surface have to be investigated. The investigation of the suitability of the modified microspheres for use as microcarriers includes two parts: 1) cell cytotoxicity of the modified microspheres and 2) the properties of the modified microspheres on cell attachment and thermally-induced detachment behaviour. Furthermore, critical to this work is the development of a bioreactor specifically designed for thermo-responsive microcarriers which would fully make use of the advantages of thermally-induced cell detachment and simplify the cell harvest procedure and most further operations. In this thesis, two conceptual designs are described which would be suitable for future detailed evaluation.

1.3 Thesis outline

Chapter 2 presents a literature review that describes the categories of stimuli-responsive polymers, focusing on the thermal-responsive polymers and PNIPAAm, and demonstrating the effect of grafting parameters on thermal-responsive behaviour of surface-grafted PNIPAAm. Cell sheet engineering is also introduced as an important application of thermo-responsive surfaces in tissue engineering. Microcarrier cell culture and the preparation of thermo-responsive microcarriers are also discussed, leading to a detailed comparison among the thermo-responsive microcarriers, focusing on their physicochemical properties and cell culture efficiency.

Chapter 3 demonstrates the synthesis and characterization of end-functionalized PNIPAAm and PNIPAAm copolymer before conjugating them to microspheres' surface via grafting-to technique. The regulation of PNIPAAm molecular weight and grafting density is presented. Apart from linear PNIPAAm molecular architecture, the methods for preparation of looped and double-layer lopped PNIPAAm chain are also described.

Chapter 4 describes the microsphere modification via grafting-from technique. In the grafting-from approach, PNIPAAm chains grow directly from the polymerization initiators first immobilized on microspheres' surface. This chapter presents the methods of controlling initiator grafting density and molecular weight of PNIPAAm chains grown from two types of initiators. Preparation of three types of PNIPAAm molecular architecture is discussed, namely (1) linear PNIPAAm chain, (2) cross-linked PNIPAAm hydrogel and (3) branched PNIPAAm chain.

In Chapter 5, the encapsulation of PNIPAAm hydrogel onto the carboxyl-functionalized polystyrene microspheres via seeded precipitation polymerization is discussed. This chapter also demonstrates the methods to regulate the grafted amount of hydrogel.

Chapter 6 describes the study designed to investigate the cytotoxicity of PNIPAAm-grafted microcarriers and the effects of physicochemical properties of PNIPAAm-grafted microcarriers on cell attachment and thermally-induced detachment behaviour.

Chapter 7 presents a summary of the thesis contributions and conclusions derived from this work. Avenues for future work, in particular the design of bioreactors for thermo-responsive microcarriers, are discussed.

2 Literature review

After describing the nature of stimuli-responsive polymers, in particular PNIPAAm and its thermo-responsive behaviour, this chapter reviews the effects of PNIPAAm grafting parameters on the thermal-responsive behaviour of surface-grafted PNIPAAm. Alongside the introduction to cell sheet engineering and its recent developments, the mechanisms of cell attachment to and detachment from PNIPAAm-grafted surfaces are also discussed. In addition, this chapter describes how the grafting parameters affect the cellular interactions with PNIPAAm-grafted surfaces. Conventional microcarrier cell culture and its applications on tissue engineering are introduced briefly before systematically discussing the potential methods for the preparation of thermo-responsive microcarriers. Finally, a detailed comparison is given of thermo-responsive microcarriers, discussing their physicochemical properties and cell culture efficiency.

2.1 Stimuli-responsive polymer and PNIPAAm

Stimuli-responsive polymers (also known as smart polymers, intelligent polymers or environmental-sensitive polymers) represent a new class of polymers that are able to undergo fast and reversible conformational rearrangement responding to the external chemical or physical stimuli (Gil and Hudson 2004; Maharjan et al. 2008). Chemical stimuli, such as pH, ionic strength and chemical agents, will ‘change the interactions between polymer chains or between polymer chains and solvents at the molecular level’. The physical stimuli, such as temperature, light or radiation forces, ultrasound, electric or magnetic fields, and mechanical stress, will ‘affect the level of various energy

sources and alter molecular interactions at critical onset points' (Jeong and Gutowska 2002). A stimuli-responsive polymer system can be tailored to recognize one specific stimulus as well as to respond simultaneously or independently to two or more stimuli (Mano 2008; Brun-Graeppi et al. 2010). The physical forms of stimuli-responsive polymer can be categorized into three classes: 1) linear free chains in solution, 2) cross-linked hydrogels and 3) chain adsorbed or surface-grafted form (Kumar et al. 2007; Maharjan et al. 2008). Depending on the polymer system, the responses upon stimulation may be changes in one or more of the following: shape, surface characteristics, solubility, formation of an intricate molecular self-assembly or a sol-to-gel transition and others. (Jeong and Gutowska 2002; Kikuchi and Okano 2002). These stimuli-responsive changes have enabled several novel applications in drug delivery, protein folding, bioseparations, microfluidics, actuators, sensors, membranes, chromatography, and tissue engineering (Jeong and Gutowska 2002; Kumar et al. 2007).

Temperature is the most widely studied stimulus in stimuli-responsive polymer systems, because a change of temperature is relatively easy to control and this stimulus is easily applicable both *in vitro* and *in vivo* (Gil and Hudson 2004; Maharjan et al. 2008). Thermo-responsive (or temperature-responsive) polymers exhibit a phase transition at a certain critical temperature, which causes a reversible and abrupt change in the salvation state (Schmaljohann 2006). Polymers, which become less solvated with increasing temperature and eventually precipitate from solution, have a lower critical solution temperature (LCST) (Cole et al. 2009). On the contrary, polymers that become soluble with increasing temperature have an upper critical solution temperature (UCST) (Schmaljohann 2006). Typical LCST polymers include PNIPAAm, poly(*N*,*N*-diethylacrylamide), poly(methyl vinyl ether), poly(*N*-vinylcaprolactam), poly(ethylene glycol), poly(propylene glycol), poly(4-hydroxybutyl vinyl ether), poly[2-(2-

ethoxy)ethoxyethyl vinyl ether], and poly(2-isopropyl-2-oxazoline) (Figure **2.1**) (Schmaljohann 2006; Cole et al. 2009) and the values of their LCST range from 30 to 50 ℃. Typical UCST polymers (or systems) include poly(DL-lactide-*co*-glycolide-*b*-ethylene glycol-*b*-DL-lactide-*co*-glycolide) (PLGA–PEG–PLGA) triblock copolymer and the interpenetrating polymer networks based on poly(acrylic acid) and (Aoki et al. 1994; Cole et al. 2009). The range of UCST values for these polymers is 5 to 60 ℃.

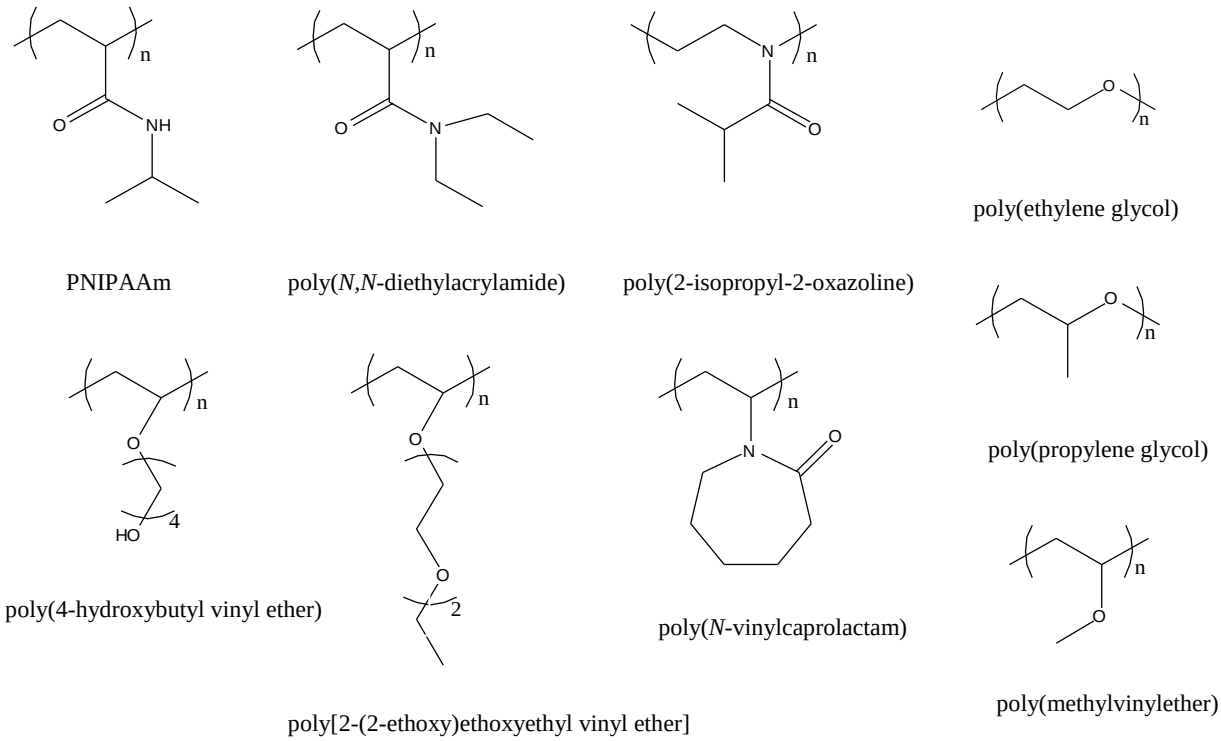


Figure 2.1 Molecular structure of selected LCST polymers

PNIPAAm is the most representative and extensively investigated thermo-responsive polymer with an aqueous solution LCST of 32 ℃ (Maharjan et al. 2008). The sharpness of its phase transition, its biocompatibility and the close proximity of its LCST to the physiological temperature has made it an attractive thermo-responsive material for potential bio-related applications (Cole et al. 2009; Brun-Graeppi et al. 2010). PNIPAAm has both hydrophilic (N-H, C=O) and hydrophobic (isopropyl) groups. The

driving force for the phase transition response is dependent on temperature-specific molecular interactions, consisting mainly of hydrogen bonding and the hydrophobic effect (Lin et al. 1999). Below the LCST, hydrogen bonding between the PNIPAAm amide groups and the water molecules leads to dissolution of the polymer chains (Jeong and Gutowska 2002) and shielding of the central hydrophobic isopropyl groups (Lin et al. 1999) (Figure **2.2**). The dissolved polymer chains exhibit an extended random coil conformation with a hydrophilic nature. Above the LCST, the hydrogen bonding with surrounding water molecules is disrupted and the intramolecular bonding between the C=O and N-H groups dominates over the external hydrogen bonding (Mittal et al. 2007b). Simultaneously, the hydrophobic isopropyl groups are exposed to the outer layer (Lin et al. 1999). Water molecules are expelled from the polymer and the polymer chains transform into a more collapsed globular form that has hydrophobic nature, leading to aggregation and precipitation of the polymer (Jeong and Gutowska 2002; Mittal et al. 2007b).

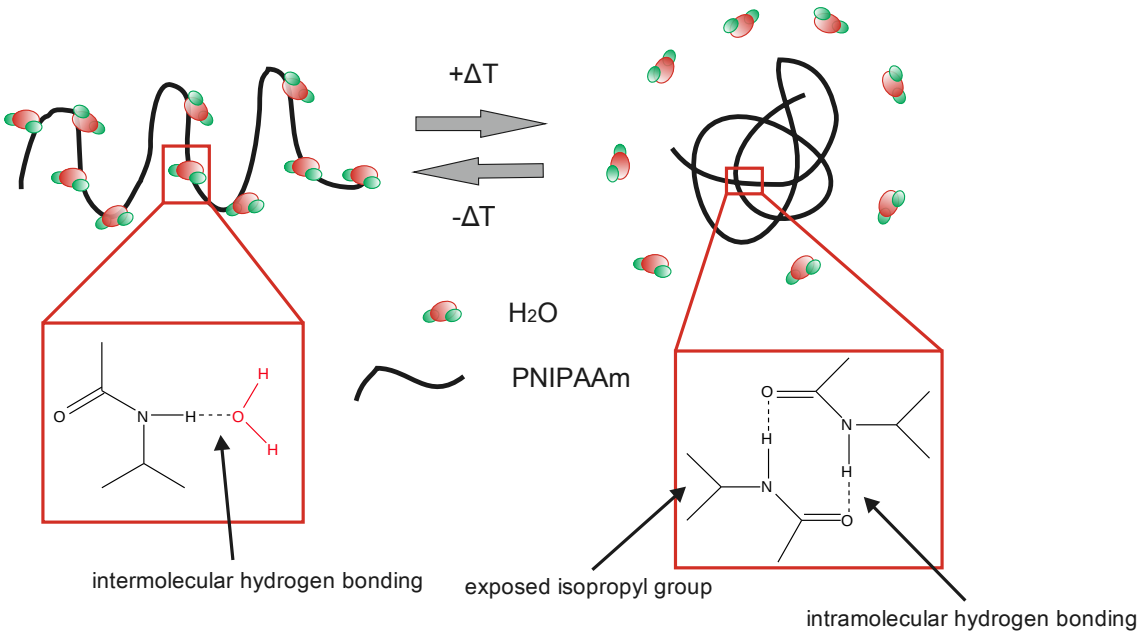


Figure 2.2 Reversible phase transition of PNIPAAm below and above the LCST

The LCST of a thermo-responsive polymer is determined by a balance between attractive polymer-water interactions and polymer-polymer interactions. Structure factors that enhance polymer-water interactions lead to the increase of the LCST, while those enhance polymer-polymer interactions result in the decrease of the LCST (Brun-Graeppi et al. 2010). Because the attractive polymer-water interactions rely on the hydrophilicity of the polymer molecules, the incorporation of more hydrophilic (polar or ionic) moieties into the molecular structure can increase the attractive polymer-water interactions, leading to the increase of the LCST. For example, the co-polymerization of NIPAAm monomers with acrylamide (AAm) and acrylic acid (AAc) causes the LCST of the resulting copolymer to shift to higher temperature and even disappear (Gil and Hudson 2004; Brun-Graeppi et al. 2010). In contrast, the attractive polymer-polymer interactions are dependent on the hydrophobicity of the polymer molecules. The incorporation of less polar or more hydrophobic moieties into the molecular structure can increase the attractive polymer-polymer interactions, leading to the decrease of the LCST. It is the case of co-polymerization of NIPAAm monomers with vinyl laurate and *N-tert*-butylacrylamide (N-tBAAm) (Hoffman et al. 2000; Brun-Graeppi et al. 2010). Therefore, the LCST could be adjusted to a desired value by incorporation of hydrophilic or hydrophobic moieties. For instance, it is essential to adjust the LCST to near body temperature for drug delivery application (Gil and Hudson 2004).

2.2 Thermal-responsive behaviour of surface-grafted PNIPAAm

The model of conformation transition (i.e. coil-globule transition) behaviour of a single free PNIPAAm molecule in dilute solution is well established (Binder et al. 2006). However, the phase transition behaviour of surface-grafted PNIPAAm is still poorly understood, because the issue of surface confinement (or tethering constraint) arises (Cole et al. 2009). Surface confinement limits the entropic space and the segmental mobility in the ordering of grafted PNIPAA chains as they dehydrate, leading to, for example, a more gradual phase transition (Cole et al. 2009). The polymer segments near to the substratum form a dense, incompressible and structurally restricted core. The core maintains dehydration over a large range of temperatures. In contrast, the outer segments form a dilute, compressible and freely mobile layer. This layer undergoes a thermally induced hydration/dehydration change (Balamurugan et al. 2003; Plunkett et al. 2006; Tamura et al. 2012b). The nearer the grafted PNIPAAm chain to the substratum, the stronger is the dehydration and the likely restriction of chain mobility (Matsuda et al. 2007).

To describe the phase behaviour of end-grafted PNIPAAm, Mendez et al (2004) developed a computational model using self-consistent field theory and predicted that the chain collapse would depend on both the grafting density and the molecular weight. According to the model of Mendez et al. (2004), the magnitude of conformational change (characterized by layer thickness change) is greatest at intermediate grafting density, and the grafting density required for maximum conformational change varies inversely with molecular weight of end-grafted PNIPAAm. This may indicate that the

effects of grafting density and molecular weight are interacting with each other on the thermo-responsive behaviour of end-grafted PNIPAAm. However, the magnitude of conformational change of end-grafted PNIPAAm chain is known to increase with increasing the molecular weight of PNIPAAm (Plunkett et al. 2006; Tamura et al. 2012a). Yim et al. (2003; 2004; 2006) used neutron reflectivity to study a broad range of molecular weight (13,000-230,000 g/mol) and grafting density (0.0001-0.0054 chains/$Å^2$) of surface-grafted PNIPAAm chains. It was proposed that the greatest conformational change was observed for PNIPAAm brushes with intermediate densities and high molecular weight (~ 152,000 g/mol). On the other hand, PNIPAAm brushes with low molecular weight (< 75,000 g/mol) demonstrated only a slight or no conformational change (Yim et al. 2004; Cole et al. 2009). In addition, Malham and Bureau (2009) studied the swelling ratio (i.e. the ratio of the swollen to the collapsed thickness) of PNIPAAm brushes of given high molecular weight (~ 475,000 g/mol) with densities ranging from 0.0002 to 0.004 chains/$Å^2$. The swelling ratio was found to decrease noticeably (from ~7 to ~3) with increasing the grafting density. Also, Plunkett et al. (2006) studied the end-grafted PNIPAAm chain collapse with a range of molecular weight (51,000-263,000 g/mol) and grafting density (~0.0005 to ~0.0044 chains/$Å^2$). It was proposed that the chain conformational change was only evident at high molecular weight and high grafting density and the change decreased with decreasing grafting density and molecular weight. Above the LCST, the surface hydrophobicity (wettability) also increased sharply on PNIPAAm films of high molecular and grafting density, while the change was less significant with PNIPAAm brushes of low molecular weight at lower densities (Plunkett et al. 2006). All these experimental findings were in good qualitative agreement with the model of Mendez et al. (2004).

As well as the grafting density and molecular weight of PNIPAAm, the molecular architecture of grafted PNIPAAm also significantly affects the ability to thermo-responsively change the hydrophilicity of a modified surface (Takei et al. 1994; Yoshida et al. 1995; Yakushiji et al. 1998; 1999). Takei et al. (1994) compared the magnitude and rate of change in surface wettability between thermally-grafted (Figure **2.3 a**) and multipoint-grafted PNIPAAm surfaces (Figure **2.3 b**). The thermally-grafted surface was prepared by conjugating aminated glass with carboxyl group end-functionalized PNIPAAm, whilst the multipoint-grafted surface was prepared using a copolymer of NIPAAm and acrylic acid (P(NIPAAm-*co*-AAc)) with reactive moieties along the polymer chain. It was found that the terminally-grafted surface demonstrated a more rapid and significant change in surface wettability than that observed for the multipoint-grafted surface. This is mainly because the multipoint graft architecture constrains the dehydration of polymers and prevents aggregation of the dehydrated polymers, whilst the polymer chains of the terminally-grafted architecture are only fixed at a single point, such that they are more mobile and elastic, and free to respond to temperature change. Yakushiji et al. (1998) prepared four types of PNIPAAm-grafted surfaces to investigate the effects of the grafted PNIPAAm architecture on the change in surface wettability. The four surfaces with different molecular architecture are: 1) terminally-grafted surface (free mobile chain density: 20 μmol/m^2), 2) multi-point grafted surface with short polymer loops, 3) multi-point grafted surface with longer polymer loops (Figure **2.3 c**) (looped chain density: 23 μmol/m^2), and looped PNIPAAm chain surface grafted with freely mobile PNIPAAm chains (Figure **2.3 d**) (referred as the combination surface; free mobile chain density: 62 μmol/m^2, and looped chain density: 23 μmol/m^2) . In this study, dioxane/toluene mixed solvent was used to regulate the looped polymer chain length on the multi-point grafted surface. The multi-

point grafted surface with longer polymer loops showed a larger and observed discontinuous change in surface wettability. This is because the longer loops retain a relatively larger mobility and thus larger dynamic motion caused by thermal-responsive polymer hydration/dehydration. The multi-point grafted surface also showed a phase transition temperature at ~27 ℃, which is lower than the LCST of free PNIPAAm in aqueous solution (32 ℃). This is attributed to the restricted conformational transitions for the multi-point grafted surface. Further, Yakushiji et al. (1998) grafted free mobile PNIPAAm chains on the looped PNIPAAm chains to prepare a combination surface. Similar with the terminally-grafted surface, the combination surface showed drastic and discontinuous change in surface wettability over the temperature range 32-35 ℃. This is due to the existence of terminally-grafted PNIPAAm on the basal looped chains. Terminally-grafted PNIPAAm chains retain a highly mobile nature and respond rapidly to temperature changes. However, the combination surface demonstrated a larger change in surface wettability than that of terminally-grafted surface. This is attributed to the increased density of freely mobile PNIPAAm chains and the existence of basal PNIPAAm-looped chains, both of which can induce stronger hydrophobic aggregation upon temperature change. Yoshida et al. (1995) compared the de-swelling rate between a conventional homopolymer PNIPAAm hydrogel (Figure **2.3 e**) and a comb-type PNIPAAm hydrogel. The comb-type PNIPAAm hydrogel (Figure **2.3 f**) was synthesised by copolymerizing free mobile acrylate-terminated PNIPAAm chains with NIPAAm monomers and a cross-linker, such that the free mobile PNIPAAm chains were grafted onto cross-linked networks. It was found that the conventional homopolymer PNIPAAm hydrogel shrank very slowly after the temperature was increased, requiring more than one month to reach equilibrium, whilst the comb-type PNIPAAm hydrogel reached full de-swelling in about 20 minutes. The rapid deswelling

of comb-type hydrogel was attributed to the immediate dehydration of these free mobile PNIPAAm chains grafted on the network. The dehydration of free chains occurred before the shrinkage of the cross-linked network due to the mobility of the free chains. These collapsed chains then formed hydrophobic nuclei which subsequently accelerated aggregation of the cross-linked network, leading to rapid expulsion of water from the comb-type hydrogel matrix. In contrast, as the conventional PNIPAAm homopolymer hydrogel shrank very slowly from the surface inwards, a dense and collapsed polymer layer impermeable to water was formed near the hydrogel surface before the bulk gel collapse was initiated (Yoshida et al. 1992a; 1992b). This layer limited the water permeation from the hydrogel interior outwards, leading to longer period of gel dehydration. However, such a layer was not formed in the comb-type structure. These results demonstrate that the surface wettability responses to temperature changes are strongly influenced by the molecular architecture of grafted PNIPAAm because of differences in the mobility and thus dynamic motion of grafted polymer chains.

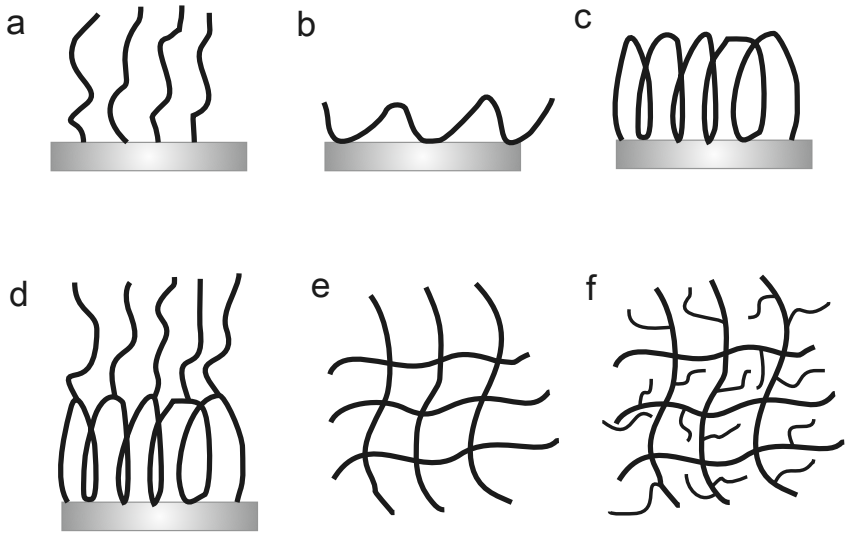


Figure 2.3 PNIPAAm molecular architectures: (a) PNIPAAm terminally-grafted surface, (b) multi-point grafted surface with short polymer loops, (c) multi-point grafted surface with long polymer loops, (d) looped PNIPAAm chain surface grafted with freely mobile PNIPAAm chains, (e) cross-linked PNIPAAm homopolymer hydrogel, and (f) comb-type PNIPAAm hydrogel. Adapted fromYoshida et al. (1995); Yakushiji et al. (1998).

It was also proposed that the substrate surface property might have effects on thermally induced collapse of PNIPAAm (Cole et al. 2009). The nature of the interfacial forces might be involved in the phase transition. However, the researches regarding this aspect are very limited. Cole et al. (2009) suggested that the substrate influence should be studied by using substrate with different surface properties, but the grafted-PNIPAAm chains on different substrates should be identical in terms of chain length, grafting density and polydispersity.

In conclusion, the (extent of) collapse of surface-grafted PNIPAAm is affected by a number of grafting parameters such as molecular weight, grafting density, molecular architecture and substrate surface property. However, the mechanisms behind such effects are poorly understood. There is a still a need for further insight and fundamental studies on PNIPAAm-grafted surfaces (Cole et al. 2009).

2.3 Thermo-responsive surfaces for cell culture

2.3.1 Introduction to cell sheet engineering

In conventional cell culture dishes, consisting of tissue culture polystyrene (TCPS), cells are grown to confluency (i.e., the whole culture dish is covered by cells) and subsequently harvested by disrupting cell-cell junctions and cell-surface junctions (i.e. ECM) through use of a calcium chelating agent such as ethylenediaminetetraacetic acid (EDTA) and proteolytic enzymes such as trypsin or dispase (da Silva et al. 2007; Yamato et al. 2007). However, non-specific proteases can damage crucial cell membrane proteins such as ion channels and growth factor receptors, leading to an

adverse impact on cell vitality (Yamato et al. 2007; Cole et al. 2009). Moreover, all the cells are harvested as single cells due to the disruption of cell-cell junctions and ECM.

In 1990, the Okano group demonstrated a pioneering approach using thermo-responsive polymers in cell culture, in the form of a PNIPAAm grafted culture dish, facilitating the detachment of both single cells and whole cell sheets (Yamada et al. 1990; Yang et al. 2005) (Figure **2.4**). The dish enables rapid detachment of single cells or entire cell sheets from the culture surface through a simple reduction in temperature without using proteolytic enzymes and chelating agents. At temperatures above 32 ℃, PNIPAAm grafted surfaces are hydrophobic. This is due to extensive dehydration of PNIPAAm molecules, allowing adsorption of serum proteins and subsequent cell attachment and proliferation similar to that of normal polystyrene dishes (Cole et al. 2009). By lowering the temperature below 32 ℃, the surface can be suddenly changed to become hydrophilic, due to swelling and hydration of PNIPAAm coatings, which leads to the spontaneous detachment of cells from the surface. Cells may detach separately or, in particular, as an entire cell sheet if the growth in the culture dish has become confluent. The manipulation technique of cell sheets is well known as 'cell sheet engineering', which has been notably established by the Okano group (Yang et al. 2005).

Cell sheet engineering is advantageous compared to conventional tissue engineering strategies. By avoiding enzymatic digestion, cell-to-cell and cell-to-ECM connections are completely preserved and the cells are detached as a contiguous cell sheet along with their ECM (Matsuda et al. 2007). Because ECM works as an adhesive agent, the harvested cell sheets can readily adhere to various surfaces including culture dishes, other cell sheets and host tissues (Matsuda et al. 2007; Yamato et al. 2007). This enables direct transplantation of single cell sheet or multiple-layered cell sheets (three-

dimensional constructs) to host tissues without scaffolds, fixation, or sutures (Yang et al. 2005).

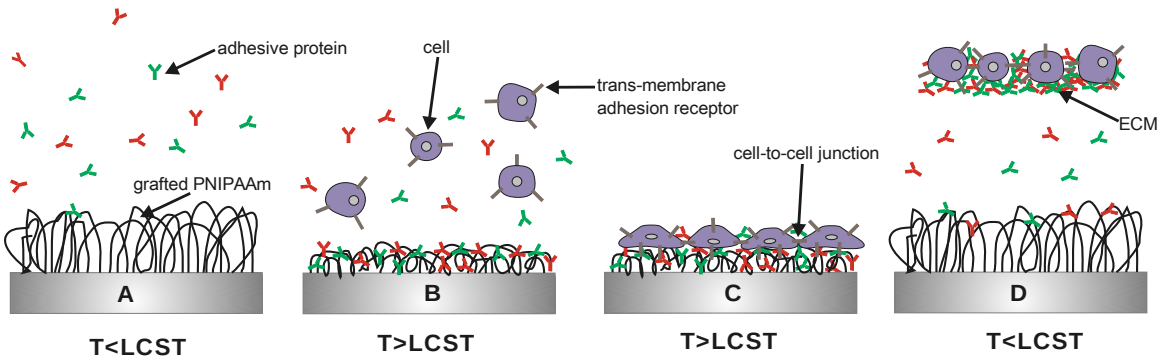


Figure 2.4 Temperature-responsive culture dishes. (A) Below the LCST, the surface is hydrated and resists adsorption of adhesive protein and thus cell attachment. (B) Above the LCST, the surface is dehydrated and allows adsorption of adhesive proteins and cell attachment. (C) After morphological change to spread, cells deposit ECM molecules and form cell-to-cell junctions, leading to contiguous cell sheets. (D) By simply reducing the temperature, cell sheets can be recovered along with their associated ECM proteins. With typical proteolytic treatment, both ECM and cell-to-cell junction proteins are degraded for cell recovery.

Cell sheet engineering is advancing further with demonstrations of co-cultured cell sheet using patterned dual thermo-responsive surfaces. The surfaces consist of two thermo-responsive domains with different LCSTs, allowing spatial controls of surface hydrophobicity and subsequent site-selective cell adhesion. Cell culture dishes were first modified with PNIPAAm, followed by patterning with a copolymer of NIPAAm and *n*-butyl methacrylate (P(NIPAAm-*co*-BMA)) using electron beam polymerization method and porous metal masks (Tsuda et al. 2005; Cole et al. 2009). The incorporation of hydrophobic BMA monomers to PNIPAAm was to decrease the LCST of the patterned area (Tsuda et al. 2004). At 27 ℃, seeded cells were seen to attached exclusively onto hydrophobic, dehydrated P(NIPAAm-*co*-BMA) domains, but not onto neighbouring hydrophilic, hydrated PNIPAAm domains (Tsuda et al. 2005). Subsequently, a different cell type could attach to the remaining dehydrated PNIPAAm coated area upon increasing the temperature to 37 ℃, achieving patterned co-cultures.

By reducing the system below the LCST of the two polymers, co-cultured patterned cell monolayers could be released as continuous cell sheets with heterotypic cell interactions and intact ECM (Tsuda et al. 2005) (Matsuda et al. 2007). Through overlaying the recovered co-cultured cell sheets, tissue-mimicking multi-layer materials can be prepared, potentially allowing the re-creation of higher-order structures such as the kidney and liver (Yang et al. 2005).

Other advances in cell sheet engineering have been underpinned by immobilization of cell-adhesion peptides such as RGDS (Arg-Gly-Asp-Ser) and cell growth factors such as insulin onto PNIPAAm, allowing accelerated cell adhesion and proliferation, or serum-free cell culture (Cole et al. 2009). For biomolecule immobilization, NIPAAm was copolymerizes with its carboxyl-derivatized analog, 2-carboxyisopropylacrylamide (CIPAAm), and simultaneously grafted to tissue culture dishes by electron beam-irradiated polymerization (Hatakeyama et al. 2006). RGDS and/or insulin were subsequently immobilized to CIPAAm carboxyl groups through amidation. At 37 ℃, the grafted thermo-responsive copolymer shrinks to expose immobilized RGD ligands to cell membrane integrin receptors. However, upon reducing the temperature to 20 ℃, the grafted copolymer suddenly swells and extends outwards to shield the RGD ligands from integrin access, leading to decreased binding affinity between integrin and RGD ligands (Yamato et al. 2007; Ebara et al. 2008). As a result, cells are pushed out from the surface.

2.3.2 Cellular interactions with PNIPAAm-grafted surfaces

2.3.2.1 Cell attachment to and detachment from PNIPAAm-grafted surface

Cell adhesion onto a material surface can be divided into three phases. The first phase comprises the adsorption of adhesive proteins (e.g. fibronectin, vitronectin, laminin) to the substrate (Grinnell 1978). In particular, fibronectin is a cell surface protein important in controlling cell shape and cell-to-cell interactions and promotes cell adhesion to tissue culture substrates (Grinnell and Feld 1979). It must be adsorbed on the substrate surface to achieve spreading of a variety of cell types on tissue culture substrates (Grinnell and Feld 1979). The second phase is termed 'passive adhesion'. In this phase, there is only a direct physical adsorption of the cells onto the substrate surface. This adsorption is controlled by physicochemical interactions including hydrophobic, coulombic, and van der Waals forces between the substrate surface, adsorbed proteins and cell membranes (Okano et al. 1995; Kikuchi and Okano 2005). Therefore, the cell adsorption in this stage is reversible and it is independent of the viability or metabolic state of the cells (Grinnell et al. 1977; Kikuchi and Okano 2005). The cellular morphology in this phase shows a shape slightly flattened but still spherical. Finally, the third phase is considered as 'active adhesion' due to the participation of cellular metabolic process (Kikuchi and Okano 2005). In this phase, cells adsorbed on the substrate spontaneously activate receptor-mediated processes, forming bonds between trans-membrane adhesion receptors (e.g. integrin) and absorbed adhesion proteins (LaFlamme et al. 1992). Then, free receptors diffuse into contact area between cell and substrate to form more interactions with adhesive proteins and increase the size of the contact area (Weisz and Schnaar 1991). The cells change their morphology to spread and expend metabolic energy (i.e. ATP) in order to stabilize the interface

between their membrane and the underlying substrate. (Okano et al. 1995; Kikuchi and Okano 2005). The spread cells then deposit and construct a basement membrane-like ECM between the basal surface of the cells and the substrate surface (Yamato et al. 1999). The spread cells cannot detach spontaneously from the substrates without reversing events associated with morphology changes from spread to round shapes and release of surface-engaged receptors (Kikuchi and Okano 2005). Thus, treatment with trypsin and EDTA has been a commonly used method for detaching actively adherent cells from culture dishes (Yamato et al. 1999). EDTA chelates divalent cations such as Ca^{2+} required by integrin receptors for ECM binding, while trypsin degrades the ECM proteins and its receptors (Yamato et al. 1999; Kikuchi and Okano 2005).

Spontaneous cell detachment from PNIPAAm-grafted surface is initiated by the hydration of grafted PNIPAAm leading to reduced cell-surface interactions. Further cell detachment from the PNIPAAm-grafted surface requires adherent cells change their membrane shape, consuming internal metabolic energy (Okano et al. 1995). It was found that cells treated with an ATP synthesis inhibitor, sodium azide, and with a tyrosine kinase inhibitor, genistein, did not change their morphologies and remain adherent on hydrated PNIPAAm-grafted surface below the LCST (Okano et al. 1995; Yamato et al. 1999). Furthermore, Yamato et al. (1999) reported that cell detachment was also inhibited by adding an actin filament stabilizer, phalloidin, and its depolymerizer, cytochalasin D. These findings indicate cell detachment from hydrated PNIPAAm-grafted surfaces is mediated by cellular metabolic processes and reorganization of the cytoskeleton (Yamato et al. 1999; da Silva et al. 2007). Moreover, cells of different phenotypes require varying optimum temperatures for detachment, depending on their differing temperature sensitivities for cellular metabolic processes (Okano et al. 1995; da Silva et al. 2007). For example, the optimum temperature for cell

detachment was 10 ℃ for hepatocytes while 20 ℃ for endothelial cells (Okano et al. 1995). After detachment, ECM proteins can be recovered together with the confluent cell sheet (Akiyama et al. 2004). However, since cells mainly interact with the ECM at focal points, the ECM proteins which do not have strong interactions with cells may be left in the substrate (Canavan et al. 2005).

2.3.2.2 Effects of characters of PNIPAAm-grafted surface

Okano's group investigated cellular interactions with PNIPAAm-grafted surfaces with different grafting thickness prepared by electron-beam polymerization (Kwon et al. 2000; Akiyama et al. 2004; Kikuchi and Okano 2005; Matsuda et al. 2007). It was reported that temperature-controlled cell attachment and detachment were only observed for grafting thickness in the range of 15-20 nm. On PNIPAAm-grafted surfaces with grafting thickness less than 15 nm, cell attach and proliferate appropriately at 37 ℃ but never detach from the surface when reducing the temperature to around 20 ℃. On the other hand, cells do not adhere to surfaces with a PNIPAAm layer thicker than 30 nm. In addition, surface wettabilities were also determined by captive bubble methods. It was reported that the changes in surface wettability were observed for all grafting thicknesses between 20 and 37 ℃, however the higher grafting thickness of PNIPAAm produced lower aqueous contact angles at both temperatures. This indicated that the hydrophilicity of the surface was increased with increasing grafting thickness. Akiyama et al. (2004) proposed that the immobilization of PNIPAAm chains dramatically restricted the molecular motion, and the restrictions on molecular mobility would be more significant in the vicinity of the rigid polystyrene surface. The restriction produces extensive hydrophobic aggregates and limited hydration of the polymer chain. Therefore, the outmost PNIPAAm chains have more

degree of freedom, lower chain density and thus higher hydration capability than inward chains. Based on these findings, Kikuchi and Okano (2005) proposed a three-layer model to demonstrate the influence of PNIPAAm grafting thickness on cell-adhesive characteristics (Figure **2.5**). The grafted PNIPAAm chains can be divided into (1) the aggregated layer, (2) the restricted layer, and (3) the relaxed layer. The aggregated layer is at the substrate interface. The chains in this layer are highly hydrophobic and aggregated due to strong hydrophobic interaction with the hydrophobic polystyrene substrate and have an entropic resistance to hydration. Therefore, this layer maintains dehydration over a large range of temperatures and do not let attached cells detach by lowing temperature. The strong hydrophobicity of the 'aggregated layer' also affects the adjacent layer, leading to the restricted chain mobility and limited hydration capabilities of PNIPAAm chains in the 'restricted layer'. The 'restricted layer' allows temperature-dependent cell attachment and detachment behaviour. The maximum thickness of the 'restricted layer' on the PNIPAAm-grafted surface can be considered in between 15 to 20 nm (Matsuda et al. 2007). The outmost part is the 'relaxed layer', which consists of relatively hydrated and less restricted PNIPAAm chains. PNIPAAm-grafted surfaces with grafting thicknesses more than 30 nm belong to this category. On such surfaces, cells cannot interact strongly with the PNIPAAm chains to adhere even at 37 ℃. da Silva et al. (2007) interpreted the model of Kikuchi and Okano in term of the concentration of isopropyl groups. At 37 ℃, the hydrophobic isopropyl groups point to the interface with the water, conferring hydrophobic properties on the surface (Cheng et al. 2005). At low grafting thicknesses, adhesive proteins will adsorb and cells can attach to the surface. As the grating thickness increases, the PNIPAAm chain density decreases, leading to low surface concentration of isopropyl groups. Thus the surface becomes unsuitable for cell attachment.

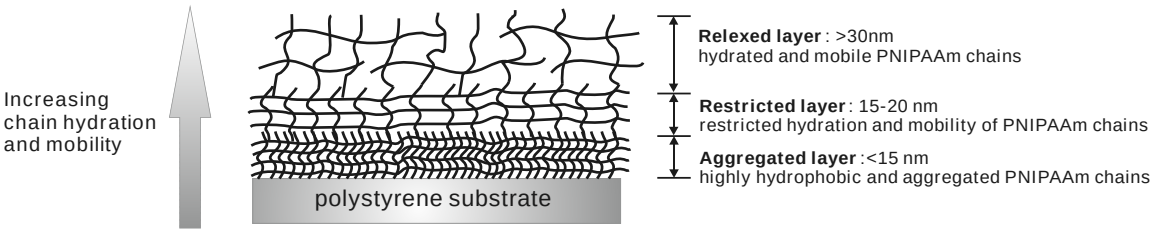


Figure 2.5 Influence of PNIPAAm-grafted polymer thickness on cell-adhesive characteristics. Adapted from Kikuchi and Okano (2005).

Cell attachment on PNIPAAm-grafted surfaces and subsequent thermally-induced cell detachment are mainly attributed to the surface hydrophobicity alternations. However, not everyone agrees this hypothesis. On the one hand, Griesser et al. (1994) reported that human endothelial cells and fibroblasts can adhere and proliferate on solid substrate surfaces with contact angle ranging from 33 to 96 °. The range encompasses the contact angle values reported for surface-grafted PNIPAAm under both expanded and collapsed conditions. On the other hand, the surfaces with similar values of contact angle demonstrated different abilities of cell-adhesiveness. Akiyama et al. (2004) prepared a thermo-responsive surface grafted with bulk cross-linked PNIPAAm hydrogel. This hydrogel surface showed a contact angle of 49.4 ° at 40 ℃ and it did not support cell attachment. In contrast, another PNIPAAm-grafted surface prepared by plasma polymerization showed similar contact angle (40 ° at 40 ℃) and supported reversible cell attachment and detachment (Cheng et al. 2005). Moreover, the contact angle results reported for PNIPAAm-grafted surfaces above LCST are typically below 90 °, meaning the surfaces are only partially dehydrated (Kwon et al. 2000; Akiyama et al. 2004; Cheng et al. 2005). Cole et al. (2009) proposed that the change in the cell-adhesiveness of PNIPAAm-grafted surface results from the changes in hydration and consequent mechanical properties of the polymer rather than the variance in hydrophobicity. Above the LCST, PNIPAAm coatings form a collapsed and aggregated conformation, and this

is considered to be akin to convention solid polystyrene surfaces. This surface supports cell attachment via the adsorption of adhesive proteins, such as fibronectin. Below the LCST, the PNIPAAm coatings (with appropriate thickness) are in a well-hydrated state. The solvation of the outmost PNIPAAm chains together with their great conformational freedom and hence entropy prevents the protein adsorption which, otherwise, would restrict the conformational mobility of the hydrated free PNIPAAm molecules (da Silva et al. 2007). The well-hydrated PNIPAAm coatings are also considered too soft to enable cell spreading.

2.4 Microcarrier cell culture

Microcarrier cell culture was introduced by van Wezel in 1967 (Van Wezel 1967). It allows anchorage-dependent cells to grow as monolayers on the surface of small beads (often referred to as microcarriers) in a homogenous suspension culture system (Kim et al. 2003; GE-Healthcare 2005). Microcarriers are manufactured from various materials including cellulose, chitosan, collagen, dextran, gelatin, glass, polyethylene, and polystyrene, with a diameter range of 50 to 400 μm (Martin et al. 2011; Tamura et al. 2012a). The specific density of the microcarriers (typically between 1.02 and 1.10) should be slightly higher than that of the surrounding culture medium, thus facilitating 1) easy maintenance of microcarrier in suspension by gentle agitation and 2) easy separation of cells and medium (Kim et al. 2003; Malda and Frondoza 2006).

Microcarrier cell culture has many advantages. First, microcarriers offer a very large culture surface area to volume ratio (e.g. 30 cm^2 in 1 mL using 5 mg Cytodex®-1 microcarriers), providing the maximum achievable cell density in a space-saving and

cost-effective manner compared with conventional two-dimensional cell culture (Tamura et al. 2012b). Also, the homogeneous culture system is easier to scale up as it facilitates oxygen and nutrient supply, and makes it easier to remove waste products(GE-Healthcare 2005). In addition, the microcarrier-based bioreactor allows an improved control of culture parameters, such as pH, gas tensions, levels of sheer, agitation and nutrient components (Malda and Frondoza 2006). Further, periodic sampling of a small amount of cells can be performed without causing disruption to the bulk of the cell-seeded microcarriers (Malda and Frondoza 2006). The microcarrier cell culture technique has been extensively used in industry for amplification of various types of anchorage-dependent cells on a large scale to mass produce many biologicals, such as growth factors, vaccines and antibodies (Phillips et al. 2008).

Microcarriers also have great potential in tissue engineering applications. First of all, the microcarrier system is a potential large-scale culture method for obtaining a sufficient number of therapeutic cells for tissue engineering, as large numbers of cells with defined phenotype are required for tissue repair and restoration of function (Tamura et al. 2012b). Moreover, the microcarrier culture system has been widely utilized as an *in vitro* research tool to study cell behaviour in response to various stimuli, such as biological, chemical, physical factors (Malda and Frondoza 2006; Martin et al. 2011). In particular, regulation of cell differentiation on microcarriers can be achieved by the addition of appropriate stimuli (Martin et al. 2011). Microcarriers can also serve as cell-delivery vehicles to repair and regenerate tissue (Demetriou et al. 1988; Kim et al. 2005b). Cell-seeded microcarriers can either be directly applied or incorporated into a larger scaffold and subsequently transplanted to damaged or degenerated tissue (Martin et al. 2011).

2.5 Preparation methods of thermo-responsive microcarriers

In the section, the five methods for the preparation of thermo-responsive microcarriers are summarized. An applicable method for thermo-responsive microcarrier preparation requires two important features: 1) it can be used to modify or fabricate beads bigger than 50 μm in diameter; 2) the grafted PNIPAAm has to be distributed on the outermost surface of the microspheres. Not all of the methods have already been applied for thermo-responsive microcarrier preparation, but many of them have been used for preparation of PNIPAAm-grafted particles for protein adsorption, drug delivery, and thermo-responsive chromatography. The methods for controlling PNIPAAm grafting density, molecular weight and molecular architecture are also outlined in this section.

2.5.1 "Grafting-to" approach

The "grafting-to" approach relies on the covalent tethering between preformed end-functionalized PNIPAAm and complementary reactive groups located on microsphere surfaces (Burtovyy et al. 2007; Xu et al. 2009). However, this definition could be considered too narrow, since useful grafting can also be achieved when appropriate functionality is located mid-chain. The "grafting-to" approach is widely used because it is experimentally simple and easy to control (Peleshanko and Tsukruk 2008; Xu et al. 2009). However, the grafting density obtained through this approach is limited due to steric hindrance caused by the already grafted polymer chains. Polymer chains have to diffuse through the existing polymer layer to reach the complementary reactive groups on the microsphere surface before they can be immobilised (Burtovyy et al. 2007).

A typical "grafting-to" procedure was demonstrated by Yang et al. (Yang et al. 2010) for the preparation of thermo-responsive microcarriers (Figure **2.6**). Carboxyl-terminated PNIPAAm (PNIPAAm-COOH) was prepared by chain transfer polymerization using 3-mercaptopropionic acid (MPA) as the chain transfer agent. The carboxyl group of PNIPAAm-COOH was then activated by *N*-(3-Dimethylaminopropyl)-*N′*-ethylcarbodiimide hydrochloride (EDC) and *N*-hydroxysuccinimide (NHS) to form succinimide esters, which in turn spontaneously reacted with the amine groups on the on Cytodex-3 microcarriers. The resulting PNIPAAm molecular architecture is reported to be a "free end linear chain" (Kikuchi and Okano 2002). It is worth mentioning that the molecular weight of PNIPAAm-COOH can be regulated by changing the feed amount of chain transfer agent (Takei et al. 1993).

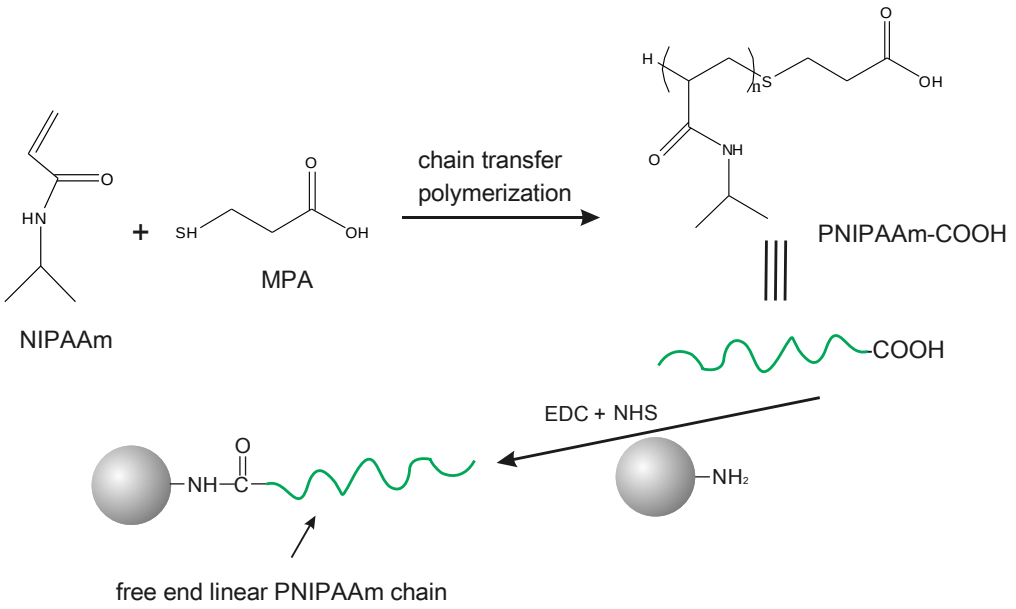


Figure 2.6 Synthesis of carboxyl-terminated PNIPAAm (PNIPAAm-COOH) and subsequent conjugation of PNIPAAm-COOH with Cytodex-3® microcarriers.

Functional groups can also be introduced to PNIPAAm mid-chain by co-polymerization. Takei et al. (1994) introduced carboxyl groups to PNIPAAm by co-polymerizing

NIPAAm and acrylic acid (AAc). This poly(*N*-isopropylacrylamide-*co*-acrylic acid) (poly(NIPAAm-*co*-AAc)) was grafted to aminated glass beads through amidation using EDC as a coupling agent (Figure **2.7**). However, the PNIPAAm molecular architecture in this case is a "looped chain" due to multi-point attachment between the poly(NIPAAm-*co*-AAc) and amine groups on the glass beads (Kikuchi and Okano 2002).

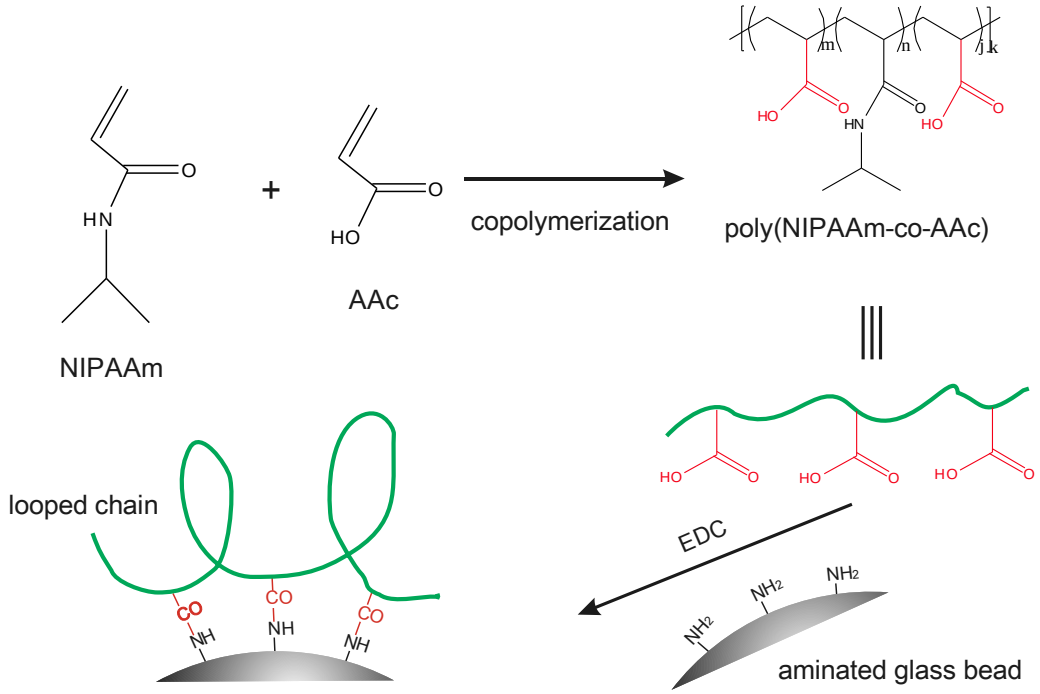


Figure 2.7 Synthesis of poly(NIPAAm-*co*-AAc) copolymer and subsequent conjugation of poly(NIPAAm-*co*-AAc) with aminated glass beads.

The grafting can also be conducted before the preparation of microspheres. Kim et al. (Kim et al. 2005a) grafted PNIPAAm-NH_2 to the carboxylate groups on sodium alginate through amidation mediated by *N*,*N*′-dicyclohexylcarbodiimide (DCC) and NHS to form an alginate-*g*-PNIPAAm copolymer. Then, by dropping the aqueous solution of the copolymer into $CaCl_2$ aqueous solution, alginate-*g*-PNIPAAm beads were prepared through ionic bond formation between Ca^{2+} and the remained carboxylate groups on

alginate-*g*-PNIPAAm (Figure **2.8**). With the increase of the content of PNIPAAm, the crossing linking density of alginate-*g*-PNIPAAm beads decreases, which regulates the swelling ratio of the beads.

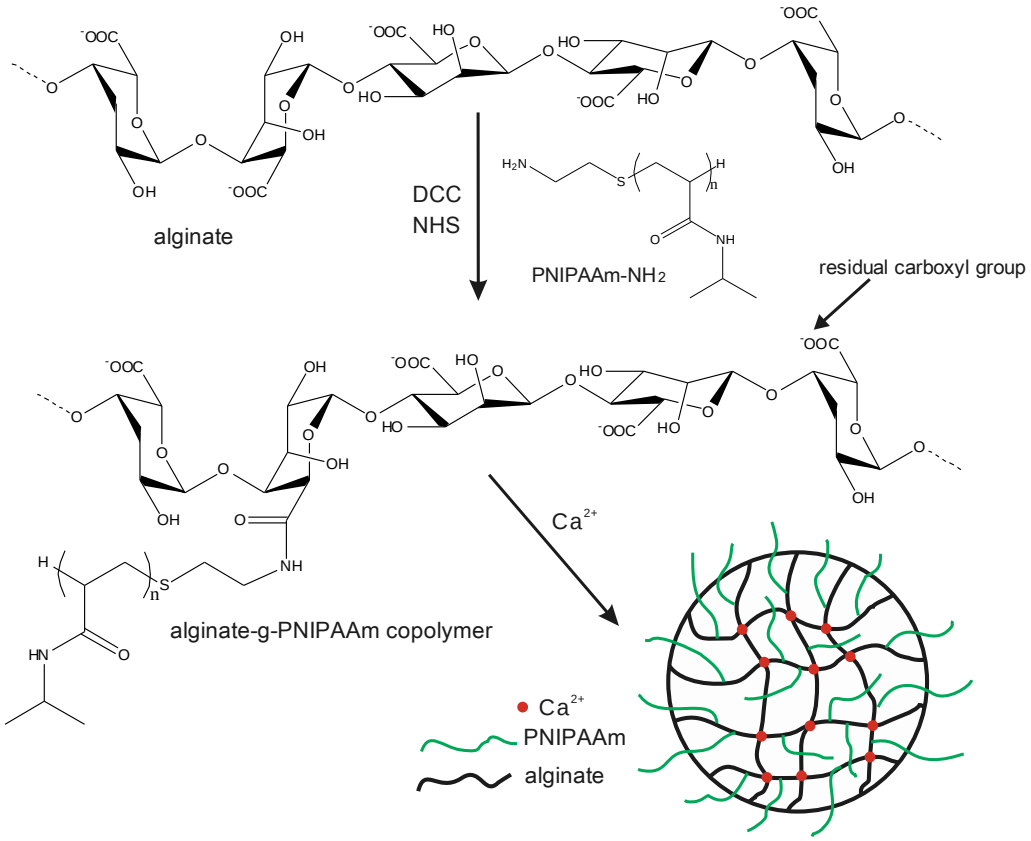


Figure 2.8 Synthesis of PNIPAAm grafted alginate and preparation of alginate beads

It is worth mentioning that Shi et al. (2006) prepared calcium alginate beads containing free PNIPAAm chains (semi-interpenetration beads). However, it is reported that free PNIPAAm chains assembled in the core of beads rather than on the surface above LCST, due to the strong collapsing force of the PNIPAAm chain network. This makes such semi-interpenetration beads not suitable for thermo-responsive microcarrier application.

2.5.2 “Grafting-from” approach

The “grafting-from” approach involves growing PNIPAAm chains directly from the reactive groups first immobilized covalently on microsphere surface. The reactive group is usually a polymerization initiator, and the process in this case is also referred as surface-initiated polymerization. However, other reactive groups can be used, which are able to generate or react with radicals under certain conditions. As the growing chain only reacts with monomers or oligomers, the process is less affected by steric hindrance and leads to higher grafting density.

2.5.2.1 Conventional free radical grafting polymerization

Conventional free radical grafting polymerization is usually initiated by thermal decomposition of azo or peroxy initiators first conjugated on particle surfaces (Prucker and Rühe 1998a; 1998b; Bachmann et al. 2007; Wang et al. 2008).

Yakushiji et al. (1999) immobilized an azo initiator, 4,4′-azobis(4-cyanovaleric acid) (ACVA), onto aminopropyl silica beads and the polymerization was subsequently initiated at 70 ℃ in the presence of NIPAAm and a cross-linker, *N*,*N*′-methylenebis(acrylamide) (MBAAm), to form a cross-linked PNIPAAm hydrogel layer (Figure **2.9**). This method incorporates a relatively large amount of PNIPAAm onto the surface in comparison with “grafting-to” approaches, but it offers little control over the resulting hydrogel thickness (Nagase et al. 2007). According to Prucker and Rühe (1998a), this method has many drawbacks. First, surface immobilization reduces the radical efficiency of azo initiators, and not all initiators can be easily thermally decomposed. Second, upon initiation, an azo initiator generates two macro-radicals: one attached to the surface and the second in solution. The latter grows to form a free

polymer chain in solution, which decreases the grafting efficiency. Third, bimolecular termination remains a major problem.

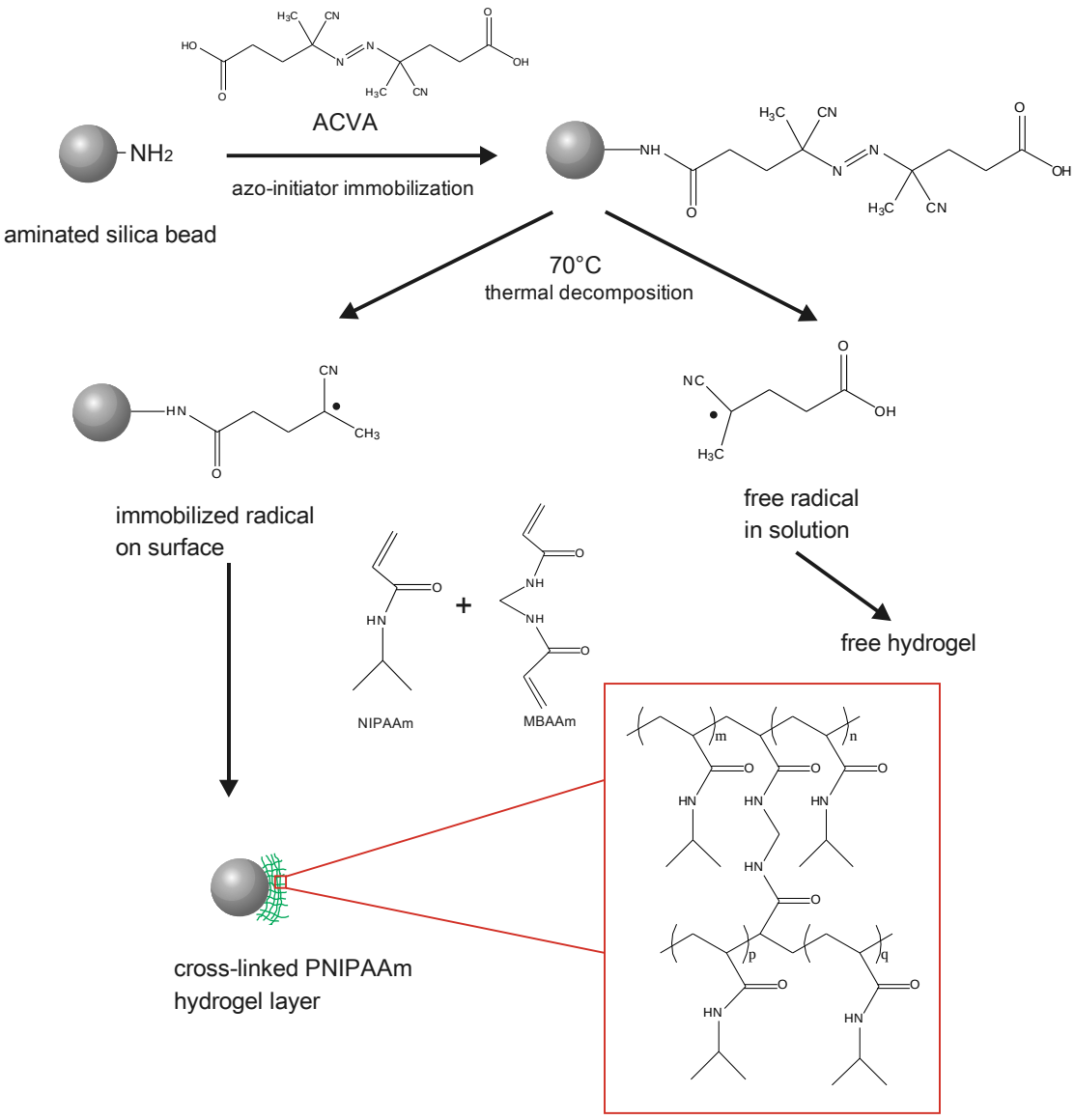


Figure 2.9 Reaction scheme for immobilization of azo-initiator to aminated silica beads and subsequent polymerization to prepare PNIPAAm hydrogel grafted surface.

2.5.2.2 Controlled/living free radical polymerization

To precisely control the grafting density and grafting thickness (i.e. chain length), many researchers prepared thermo-responsive microspheres by grafting PNIPAAm from microsphere surfaces using controlled/living radical polymerization (CRP) processes. Of the CRP methods, atom transfer radical polymerization (ATRP) is the most extensively studied and widely used, due to its simplicity and broad applicability (Matyjaszewski and Tsarevsky 2009).

ATRP involves the use of a transition metal halide and an appropriate nitrogen-based ligand to form a transition metal catalyst complex (Matyjaszewski 2001; Xu et al. 2009). It relies on a dynamic equilibrium between the growing chains (polymer terminated with a radical) and dormant chains (polymer terminated with halide), via a reversible redox process catalyzed by the transition metal complex (Siegwart et al. 2012) (Figure **2.10**). In ATRP, the transition metal complex at lower oxidation state abstracts a halogen atom from either an initiator or a dormant chain end, to form a radical, and promote the transition metal complex to a higher oxidation state. After activation of a dormant chain, more than one monomer unit can add to the chain (Matyjaszewski 2001). Then the growing chain is reversibly deactivated by transfer of halogen from the transition metal complex at higher oxidation state, leading to termination of the active chain. The equilibrium is designed to keep the concentration of propagating radicals at a sufficiently low level and the concentration of dormant chains at a higher level. This suppresses bimolecular termination and controls molecular weights (Matyjaszewski 2001; Xu et al. 2009; Siegwart et al. 2012). Most ATRP initiators are alkyl halides (Matyjaszewski and Tsarevsky 2009) and they provide the formed polymers with simple halogen as the end groups, which can be easily used for further functionalization

(Qiu et al. 2001). Copper halide complexed by a suitable ligand is the most commonly used metal catalyst complex in ATRP (Siegwart et al. 2012).

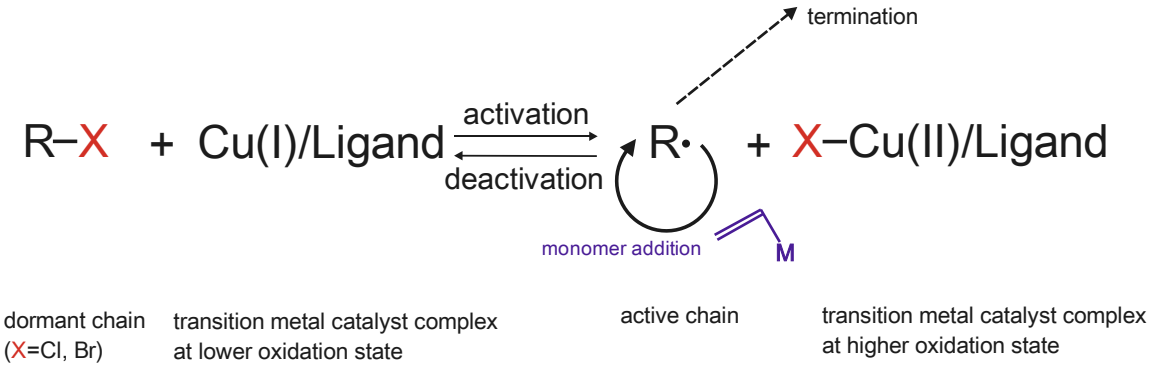


Figure 2.10 The mechanism of transition metal-catalyzed ATRP

Due to its controlled/living nature, ATRP allows the preparation of polymers with narrow molecular weight distribution, predetermined molecular weight, well-defined composition (e.g. gradient or block copolymer) and complex molecular architecture (e.g. branched or hyper branched polymers) (Xu et al. 2009). In surface-initiated ATRP, the polymer grafting density can be regulated by varying the concentration of ATRP initiator on surfaces, while the polymer chain length can be controlled by changing the ATRP reaction duration or the feed NIPAAm concentration.

Kim et al. (2003) attached an ATRP initiator, 2-bromopropionyl group, to the hydroxyl groups on the surface of cross-linked dextran beads (Sephadex® G-50) through esterification. NIPAAm was then polymerized from the initiator by employing aqueous ATRP with a catalytic system of CuBr and 2,2'-dipyridyl at room temperature. Using a similar procedure, Cetinkaya et al. (2011) fabricated a thermo-responsive microcarrier by grafting PNIPAAm from the highly cross-linked poly(2-hydroxyethylmethacrylate) (PHEMA) beads (Figure **2.11**).

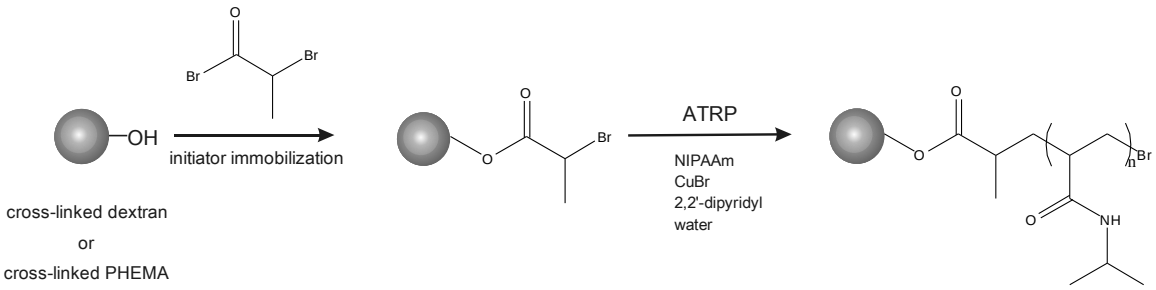


Figure 2.11 Immobilization of ATRP initiator to cross-linked dextran (or PHEMA) particle and subsequent growth of PNIPAAm chains by ATRP

Mittal et al. (2007a; 2007b) presented a process to graft PNIPAAm from polystyrene (PS) particles surface functionalized with a thin shell of ATRP initiator (Figure **2.12**). The acrylic-terminated ATRP initiator, 2-(2-bromopropionyloxy) ethyl acrylate (BPOEA), was synthesized by esterification between 2-hydroxylethyl acrylate and 2-bromopropionyl bromide, and subsequently immobilized to PS particles by seeded polymerization of BPOEA alone or along with styrene or a crosslinker (DVB). It was proposed that the initiator could be distributed homogenously on the particles under proper conditions, and the initiator density could be controlled by changing the styrene/BPOEA mole ratio before the initiator immobilization. PNIPAAm was grafted from the initiators through aqueous ATRP with a catalytic system of Cu powder, CuBr, $CuBr_2$ and 1,1,4,7,10,10-hexamethyltriethylenetetramine (HMTETA). It was reported the grafting thickness can be increased proportionally by increasing the feed NIPAAm concentration (Mittal et al. 2007b).

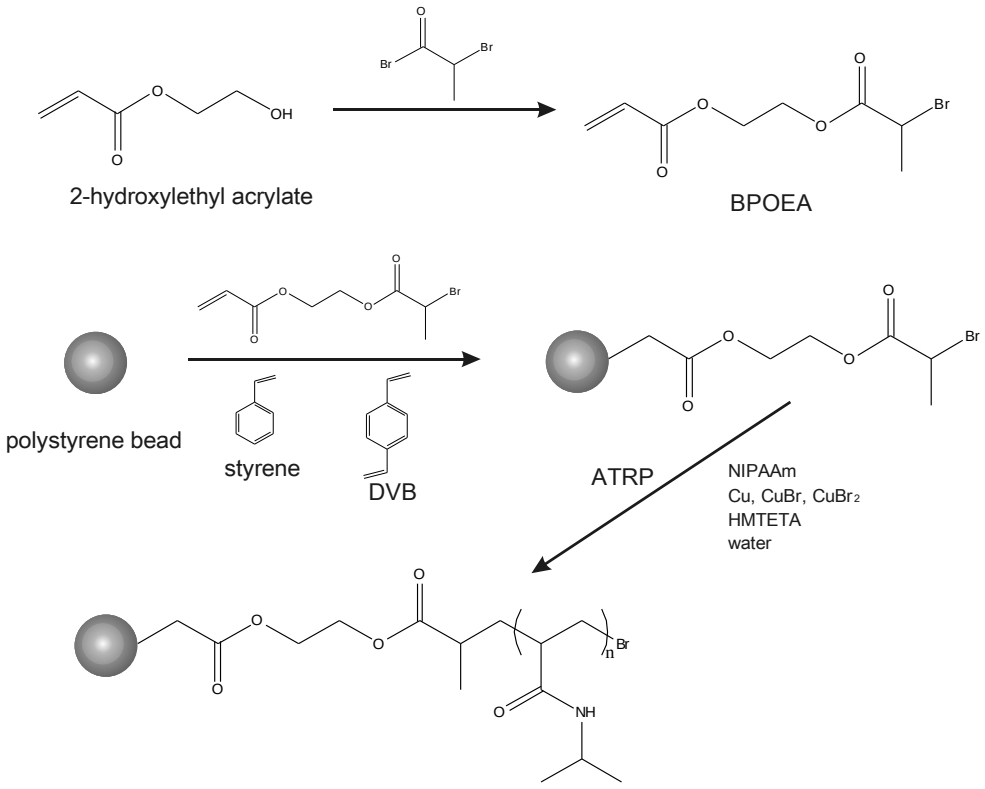


Figure 2.12 The reaction scheme for synthesis of BPOEA, immobilization of BPOEA to polystyrene beads and subsequent growth of PNIPAAm chains through ATRP

Mizutani et al. (2010) immobilized an ATRP initiator, chloromethyl methyl ether (CME) to polystyrene beads through Friedel-Crafts alkylation. The density of the ATRP initiator was modulated by varying the feed concentration of the CME, reaction duration and reaction temperature. Subsequently, NIPAAm was polymerized from the initiator by ATRP in 2-propanol with a catalytic system of CuCl, $CuCl_2$ and tris[2-(dimethylamino)ethyl]amine (Me_6TREN) at 25 ℃ (Figure **2.13**). Tamura et al. (2012a) used the same ATRP system to graft PNIPAAm from chloromethylated polystyrene beads to prepare thermo-responsive microcarriers, and regulated the PNIPAAm chain length by changing the feed concentration of the NIPAAm. Nagase et al. (2007) also regulated the chain length of grafted PNIPAAm on alkyl chloride initiator by varying the ATRP reaction duration.

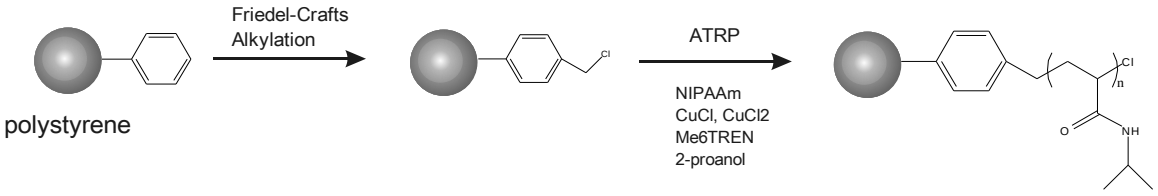


Figure 2.13 Scheme for immobilization of ATRP initiator to polystyrene beads by Friedel-Crafts alkylation and subsequent growth of PNIPAAm chains through ATRP

Apart from control of polymer grafting density and chain length, surface-initiated ATRP can be applied to prepare complex PNIPAAm molecular architecture. Seino et al. (2006) immobilized a macroinitiator, hyperbranched poly(siloxysilane) (HBPS), to silica beads. The HBPS macroinitiator has a hyperbranched structure with alkyl bromide in the end of each branch. Polymerisation of NIPAAm, mediated by ATRP, from each alkyl bromide initiator was then used to form a hyperbranched structure of PNIPAAm (Figure **2.14**).

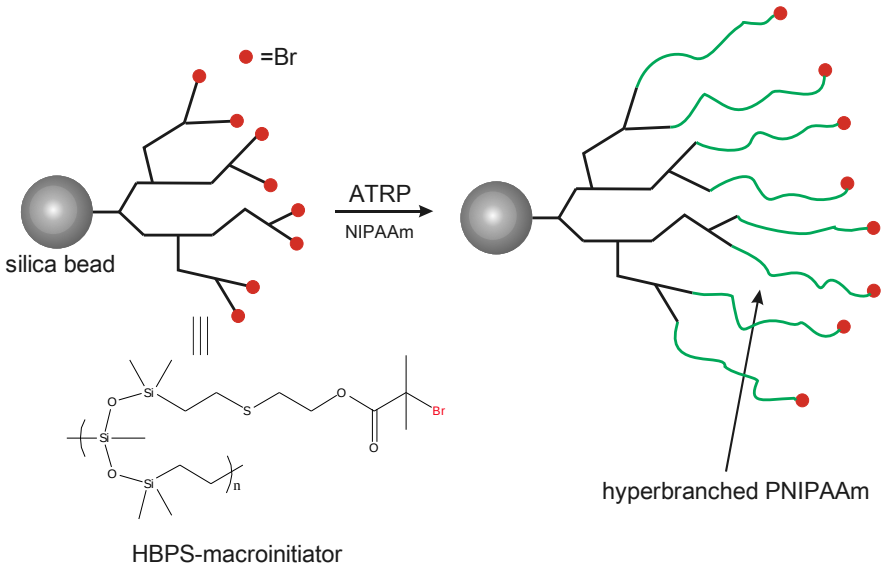


Figure 2.14 Schematic description of the preparation of hyperbranched PNIPAAm grafted microspheres

Another popular controlled/living free radical polymerization is reversible addition-fragment chain transfer (RAFT) polymerization. RAFT polymerization shares many

similar mechanistic features and advantages with ATRP and it was also applied to the preparation of PNIPAAm grafted microspheres (Pan et al. 2010).

2.5.2.3 Redox initiated grafting polymerization

Redox-initiated grafting polymerization was developed by Mino and Kaizerm (Mino and Kaizerman 1958) and it relies on a redox reaction between an oxidative metal ion (e.g. Ce^{4+} and Mn^{3+}) and a reductive group (e.g. hydroxyl and amino group) to generate free radicals capable of initiating vinyl polymerization in an acid aqueous solution (Ranby and Zuchowska 1987; Bamford and Al-Lamee 1994).

Wang et al. (2008) immobilized hydroxyl terminated poly(ethylene glycol) (PEG) on silica particles and subsequently initiated a free radical polymerization of NIPAAm through a redox reaction of Ce^{4+} with the hydroxyl groups on particle surfaces in a nitric acid solution (Figure **2.15**). However, it is reported that this redox system also failed to offer a precise control over PNIPAAm molecular weight and polydispersibility.

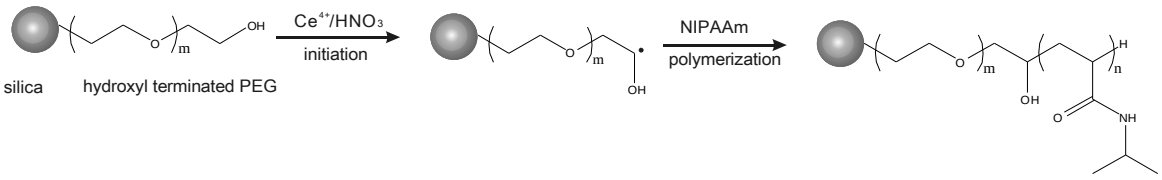


Figure 2.15 Schematic description of the mechanism of the redox-initiated grafting polymerization

2.5.2.4 Vinyl group copolymerization

This method relies on the copolymerization of NIPAAm and vinyl groups first immobilized on a microsphere surface. As the immobilized vinyl groups only react with NIPAAm monomers or oligomers, this method is considered in this review to be a "grafting-from" technique. However, vinyl group copolymerization might involve a

considerable number of side reactions so that NIPAAm monomers were polymerized to generate free linear polymers in solution.

Go et al. (Go et al. 1998) prepared PNIPAAm grafted silica particles by copolymerizing NIPAAm with 3-(methacryloxy)propyl moieties on silica surfaces in a water-organic (water-cyclohexanol) two-phase system (Figure **2.16**). It was proposed that the amount of immobilized PNIPAAm can be increased by increasing the feed ratio of NIPAAm to cyclohexanol.

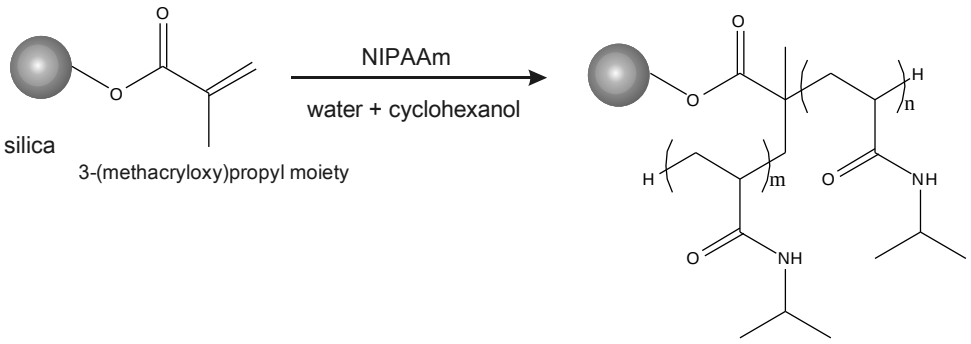


Figure 2.16 The synthesis scheme for the grafting polymerization from the surface of vinyl group functionalized microsphere.

2.5.3 Bulk cross-linked PNIPAAm hydrogel beads

2.5.3.1 Precipitation polymerization using a mold

Precipitation polymerization starts initially as a homogeneous system in a continuous phase (usually water), where NIPAAm monomers, an initiator and a cross-linker (usually MBAAm) are completely soluble. Upon initiation and propagation, the formed crosslinked PNIPAAm is insoluble in the medium and thus precipitates. It is proposed that this causes a continuous nucleation and coagulation process which leads to the formation of larger particles (Shimizu et al. 2009). Precipitation polymerization usually does not involve the use of surfactants (Gokmen and Du Prez 2012). It is worth

mentioning that many other literature reports indicate PNIPAAm precipitation is mainly caused because the reaction temperature is above the LCST in aqueous solution (Shamim et al. 2006; Shimizu et al. 2009). However, a more likely explanation is that the cross-linkage of PNIPAAm with MBAAm leads to insolubility of PNIPAAm and subsequent precipitation, because the precipitation polymerization of PNIPAAm can be easily conducted at room temperature.

Cross-linked PNIPAAm hydrogel particles were first prepared by precipitation polymerization of NIPAAm with MBAAm in an aqueous medium at 60 to 70 ℃ (Pelton and Chibante 1986). Shimizu et al. (2009) proposed that larger particles can be obtained with this method by increasing the concentration of initiator or electrolyte in the reaction mixture. However, the particle size is limited to the micron and submicron range (0.55~1.6 μm), which is unsuitable for cell culture application. To obtained larger hydrogel beads through precipitation, a mold is usually required.

Park and Hoffman (1992) prepared large and uniformly spherical cross-linked PNIPAAm hydrogel beads (2-3 mm in diameter) by using calcium alginate as polymerization molds for NIPAAm and MBAAm (Figure **2.17**). First, a solution of NIPAAm, MBAAm, sodium alginate and TEMED was dropped into calcium chloride solution containing APS. Calcium alginate gel mould beads were immediately formed and the solution of NIPAAm, MBAAm and TEMED was entrapped in the mould beads. APS in the medium then rapidly diffused into the mould beads and initiated the polymerization at room temperature. After the spherical cross-linked PNIPAAm hydrogel formed inside the mould beads, the calcium alginate mould was removed out by using calcium-chelating agents such as phosphate and EDTA. Kim et al. (2002) used this method to prepared thermo-responsive carriers by copolymerizing NIPAAm and *N*-

aminoethyl methacrylate (AEMA). The RGD moieties were also introduced onto the carrier by conjugating GRGDY to a primary amino group of AEMA unit in the hydrogel beads. The conjugation was conducted under the pre-collapsed state of hydrogel beads at 40 ℃ to prevent GRGDY from diffusing inside the beads, so that the RGD moieties only distributed on the external surface of the hydrogel beads.

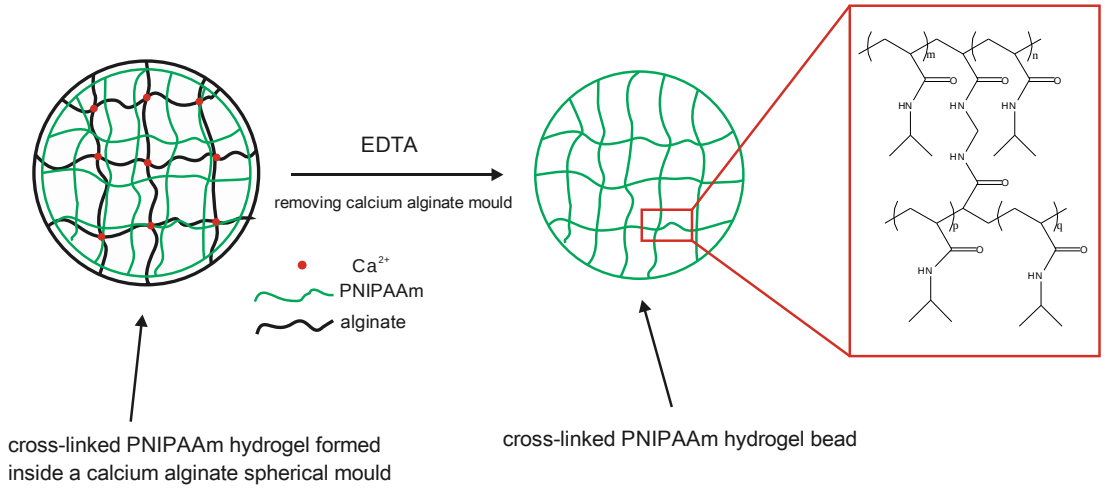


Figure 2.17 Preparation of cross-linked PNIPAAm hydrogel beads using calcium alginate as a spherical mold

2.5.3.2 Suspension polymerization

Suspension polymerization starts with dispersing aqueous droplets of NIPAAm and a cross-linker (e.g. MBAAm) in an oil-continuous phase by mechanical agitation with the aid of a surfactant (Figure **2.18**). A water-soluble initiator (e.g. APS) is added to drive both initiation and chain growth inside the aqueous droplets. The size of the final particles obtained from suspension polymerization is usually in the range of 20-2000 μm (Qiu et al. 2001), and it is mainly determined by the agitation speed and the shape of both the reactor and mechanical stirrer (Qiu et al. 2001; Gokmen and Du Prez 2012). The main drawback of suspension polymerization is the broad size distribution of final particles (Gokmen and Du Prez 2012).

Park and Hoffman (1990a; 1990b) synthesized cross-linked PNIPAAm beads (150 ~ 400 μm in diameter) through suspension polymerization at room temperature using paraffin oil as the continuous phase, Pluronic L-81 as the surfactant, and APS and TEMED as the initiators. Similarly, Teal et al. (Teal et al. 2000) used cyclohexane as the continuous phase and sorbitan monooleate as the surfactant to prepare cross-linked PNIPAAm beads of approximately 100 μm in average diameter.

It is worth mentioning that emulsion polymerization can be used to prepare PNIPAAm copolymer particles through NIPAAm macromonomer (i.e. vinyl-terminated PNIPAAm) (Takeuchi et al. 1993). However, emulsion polymerization usually leads to particles with submicron size (Qiu et al. 2001; Chern 2006), which is not satisfactory for microcarrier applications. The main difference between suspension polymerization and emulsion polymerization is that the former uses a monomer phase soluble initiator while the latter uses a continuous phase soluble initiator (Gokmen and Du Prez 2012), leading to a completely different mechanism.

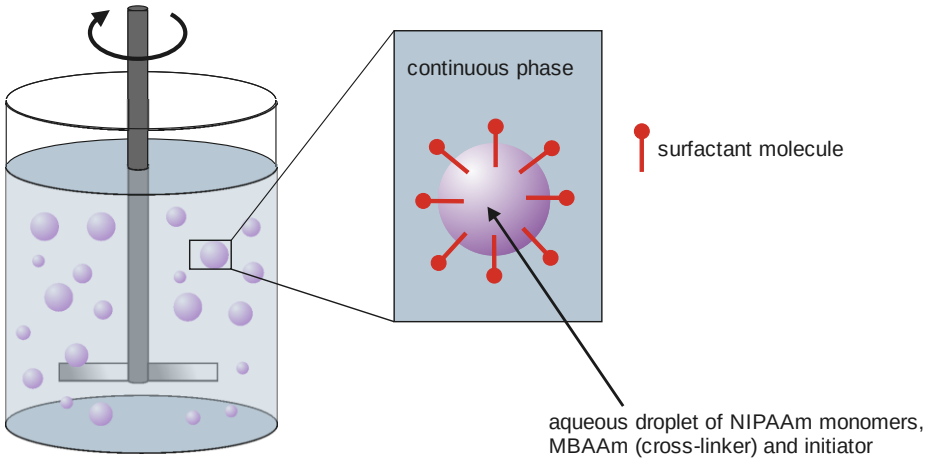


Figure 2.18 Schematic description of the suspension polymerization technique

2.5.4 Seeded polymerization

Seeded polymerization has been widely used to prepare thermo-responsive particles with a core-shell structure. It starts with a mixture containing NIPAAm monomers or NIPAAm macromonomers with a cross-linker in the presence of seed particles. Upon polymerization, the formed cross-linked polymer precipitates out and adsorbs on the surface of seed particles. Normally this method is used for preparation of PNIPAAm modified particles in sub-micron range. However, because the final particle size is mainly regulated by varying the size of seed particle, in this review this method is considered a potential way for PNIPAAm microcarrier fabrication.

Makino et al. (1994) prepared thermo-responsive core-shell particles by covering crosslinked PNIPAAm hydrogel layer on poly(styrene-*co*-NIPAAm) cores (Figure **2.19**). First, poly(styrene-*co*-NIPAAm) microspheres were prepared by soap-free emulsion copolymerization of NIPAAm with styrene. Then, a cross-linked PNIPAAm hydrogel layer was coated onto poly(styrene-*co*-NIPAAm) cores by seeded precipitation polymerization of NIPAAm with MBAAm as a crosslinker in the presence of the core particles in aqueous medium. Using a similar procedure, Andersson et al. (2006) synthesized core-shell thermo-responsive particles with a polystyrene core covered by crosslinked PNIPAAm hydrogel layer.

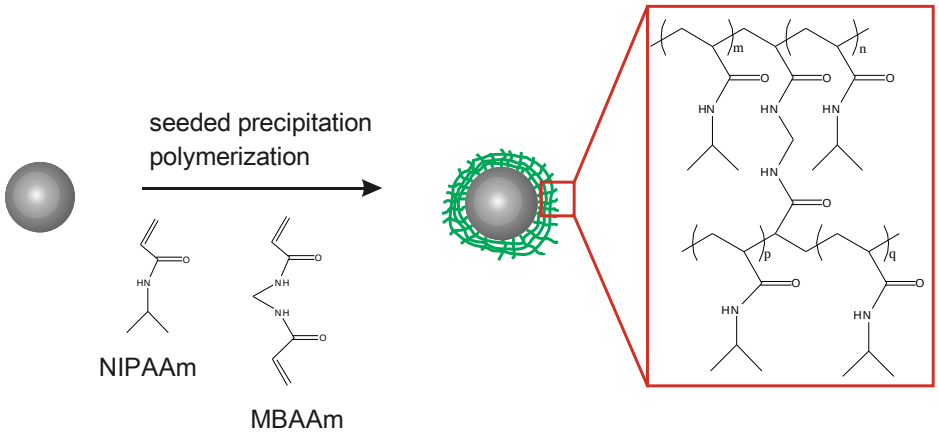


Figure 2.19 Schematic description of preparation of cross-linked PNIPAAm hydrogel grafted particles by seeded precipitation polymerization

Li et al. (2008) fabricated crosslinked PNIPAAm hydrogel layer on poly(methacrylic acid) microspheres through seeded distillation-precipitation polymerization. In this process, the crosslinked PNIPAAm hydrogel layer was formed simultaneously through a seeded precipitation polymerization manner during the distillation of the solvent (acetonitrile) from the reaction system. It was proposed that the synergic hydrogen-bonding interaction between the carboxylic acid groups on the seed particles and the amide groups of NIPAAm and MBAAm acted as a driving force for the construction of the hydrogel shell.

Shamim et al. (2006) and Lee et al. (2012) coated crosslinked PNIPAAm layer onto vinyl-functionalized magnetic and silica particles respectively by seeded precipitation polymerization of NIPAAm and MBAAm in the presence of vinyl-functionalized particles in an aqueous system at 70 ℃. The major role of the vinyl groups on seed particles was believed to be the promotion of the adsorption of the precipitated PNIPAAm (Lee et al. 2012), due to the hydrophobicity of both vinyl groups and PNIPAAm at a temperature above LCST.

The thickness of the cross-linked PNIPAAm hydrogel shell usually can be regulated by the dosage of NIPAAm in the shell preparation (Andersson et al. 2006; Li et al. 2008; Zhang and Wang 2008; Lee et al. 2012). Importantly, Lee et al. (2012) proposed a linear proportionate relationship between the shell thickness and feed NIPAAm concentration.

Rimmer et al. (1996) synthesized thermo-responsive core-shell particles consisting of a core of cross-linked polystyrene and a shell of poly(styrene-*g*-NIPAAm) (Figure **2.20**). The particles were prepared by seeded polymerization of styrene with a NIPAAm macromonomer in the presence of cross-linked polystyrene seeds. Because NIPAAm macromonomer contains a hydrophobic end-group, it is soluble in styrene and easily adsorbed onto the polystyrene core. The NIPAAm macromonomer was prepared by esterification between PNIPAAm-COOH and hydroxyethyl acrylate (HEA) and the reaction was mediated by DCC. Unlike the previous examples, the molecular architecture of PNIPAAm on the shell is a linear polymer chain rather than a cross-linked hydrogel.

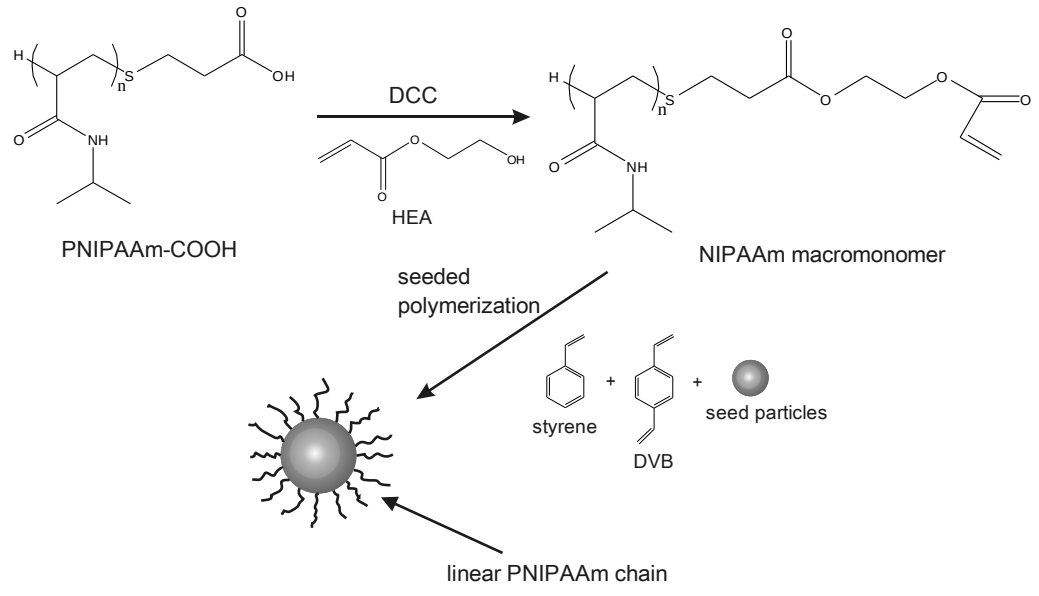


Figure 2.20 The reaction scheme for synthesis of NIPAAm macromonomer and preparation of PNIPAAm grafted polystyrene particle by seeded polymerization

2.5.5 Non-covalent adsorption

Non-covalent adsorption of PNIPAAm to particle surface usually relies on Coulombic interaction between charged segments on PNIPAAm and complementary groups on a particle surface.

Patrizi et al. (2009) introduced positively charged segments onto the end of PNIPAAm by block copolymerization of NIPAAm and (3-acrylamidopropyl)-trimethylammonium chloride (AMPTMA) using ATRP. First, the cationic poly-AMPTMA block was synthesized by ATRP using ethyl-2-chloropropionate (ECP) as an initiator. Subsequently, NIPAAm was polymerized from the chloride end group of poly-AMPTMA to form PNIPAAm block using ATRP again. Oddo et al. (2010) grafted the copolymer to calcium alginate microspheres through 'polycation-polyanion' interaction between the positively charged poly-AMPTMA block in the copolymer and the negatively charged alginate carboxylic groups (Figure **2.21**).

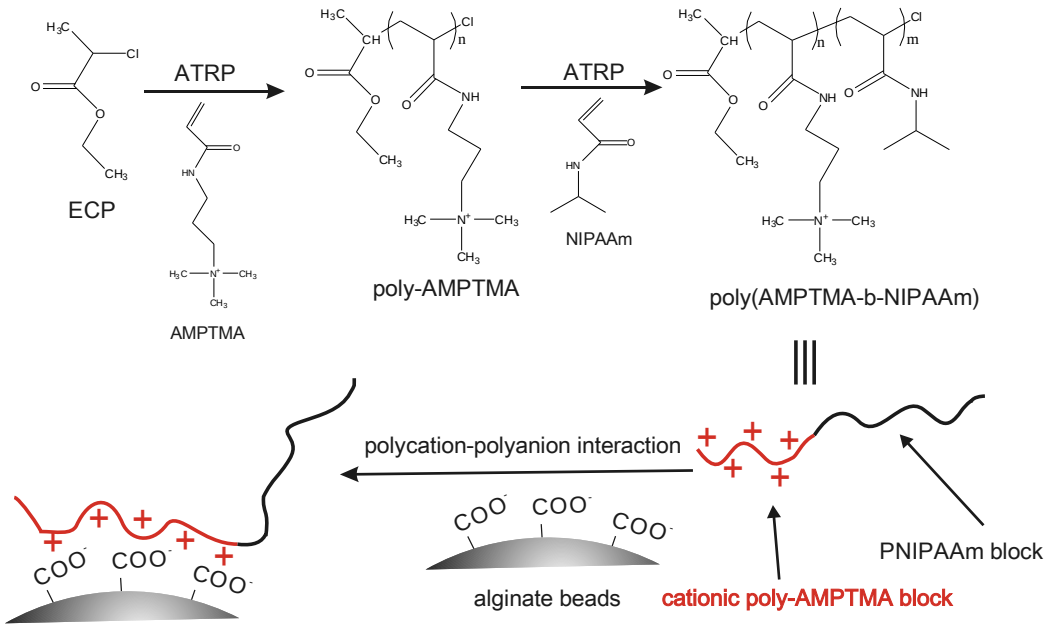


Figure 2.21 The reaction scheme for synthesis of poly(AMPTMA-b-NIPAAm) block copolymer and the adsorption of poly(AMPTMA-b-NIPAAm) to alginate beads by polycation-polyanion interaction

Hendrick et al. (2001) prepared thermo-responsive microcarriers by conjugating PNIPAAm to polystyrene beads by simultaneous oxidation of the polystyrene surface and adsorption of the PNIPAAm at room temperature in water containing sodium persulfate and TEMED (Figure **2.22**). The benzyl groups on the external surface of PS beads were oxidized to carboxylic groups, which after ionic interaction with amine groups on PNIPAAm gave a material equivalent to grafted polymer. It is appropriate to consider the molecular architecture of adsorbed PNIPAAm being a "looped chain".

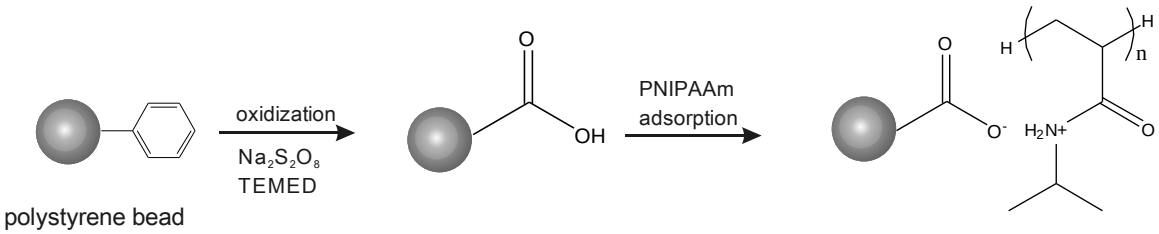


Figure 2.22 Simultaneous oxidation of the polystyrene surface and adsorption of the PNIPAAm

2.6 Thermo-responsive microcarriers for cell culture

The fabrication methods of the thermo-responsive microcarriers and corresponding cell attachment/detachment experiments are summarized and compared within Table **2.1** and Table **2.2** respectively.

Yang et al. (2010) fabricated thermo-responsive microcarriers by grafting PNIPAAm to the surface of Cytodex-3® microcarriers (170-380 μm in diameter). It was reported that human bone marrow-derived mesenchymal stem cells (hBMMSCs) were able to adhere, spread and proliferate on the PNIPAAm-grafted Cytodex-3® microcarriers by dynamic culture (spinner flask) with an attachment ratio of > 99% within 270 min. By dropping the temperature to 32 ℃ for 10 min, more than 82.5% of hBMMSCs were detached

from the confluent microcarriers spontaneously with the viability of approximately 92.2%. In addition, modified and unmodified microcarriers showed an almost identical cell attachment and proliferation profile.

Cetinkaya et al. (2011) carried out a cell attachment experiment with PNIPAAm grafted PHEMA microcarriers (327 ± 99 μm in diameter) using fetal chondrocytes (FCs) under a static culture condition (24-well plate). FCs were able to adhere on the microcarriers with an attachment ratio of 89% after 8h inoculation at 37 ℃. After proliferation, cells were detached by incubating the confluent microcarriers at 4 ℃ for 20 min with approximately 70% yield. It was reported that the PNIPAAm-grafted PHEMA microcarrier presented a lower cell attachment ratio and a slower cell growth rate than those of a commercial microcarrier, Cytodex®-1.

Tamura et al. (Tamura et al. 2012a; 2012b) studied the effects of the diameter of PNIPAAm-grafted microcarrier, the PNIPAAm grafting density and the PNIPAAm molecular weight on the efficiency of cell attachment, proliferation and thermally-induced detachment. Chinese hamster ovary cells (CHO-K1) were employed and cultured using both static (12-well plate) and dynamic (spinner flask) methods. It was proposed that the hydrophilicity of PNIPAAm-grafted surface is increased by increasing the molecular weight of PNIPAAm, which suppresses cell attachment and proliferation, while also increasing the efficiency of thermally-induced cell detachment. It is also believed that increasing PNIPAAm molecular weight increases the magnitude of the conformational change of PNIPAAm chain grafted on the surface, which leads to more rapid cell detachment upon the temperature reduction. Tamura et al. (2012b) found the PNIPAAm brush density has a negligible influence on the cell attachment efficiency at 37 ℃. However, when the temperature was reduced to 20 ℃, the PNIPAAm-grafted

microcarriers with an intermediate brush density exhibited the highest efficiency of thermally induced cell detachment. This might be due to the influence of the magnitude of the conformational change. Tamura et al. (2012a) also suggested PNIPAAm-grafted microcarriers with a relatively small diameter (~56 μm) exhibit higher efficiency for both cell adhesion and proliferation, due to the larger number of contacts between beads and cells. However, on smaller beads, cells can easily achieve confluence and the strong cell-cell junctions can decrease the thermally-induced cell detachment efficiency. To increase the cell harvest efficiency on small beads, Tamura et al. (2012c) designed a thermo-responsive microcarrier grafted with cationic copolymer consisting of NIPAAm, positively charged quaternary amine monomer, and hydrophobic monomer. The detachment efficiency was increased due to the highly hydrated nature of the positively charged quaternary amine moieties. In addition, the positively charged quaternary amine moieties were believed to suppress aggregation of the beads and consequently enhance the cell proliferation efficiency. Tamura et al. (2012a; 2012c) found, with increase of cell incubation duration, the cell detachment ratio decreased gradually and detached cells tended to aggregate due to the formation of cell-cell junctions.

Hendrick et al. (2001) prepared thermo-responsive microcarriers by adsorbing PNIPAAm onto polystyrene beads (120-250 μm in diameter). It was shown that Chinese hamster ovary cells (CHO-K1) were able to adhere and grow at 37 ℃ on the microcarriers under static culture conditions, while the cells did not adhere to the microcarriers under dynamic conditions (spinner flask). After 24 h and 48 h of cell culture, the cells were detached by incubating the confluent microspheres at 10 ℃ for 1 h with 100% detachment ratio for both cell culture durations.

Kim et al. (2002) prepared PNIPAAm hydrogel beads conjugated with RGD moieties (~2.2 mm at room temperature and ~0.9 mm at 37℃ in diameter). It was shown that chondrocytes were able to adhere at 37 ℃ on the beads under static culture conditions (24-well plate) and the cells were detached by lowering the temperature below 37 ℃ for 1.5 h. The cell detachment percentage was approximately 85% at 20 ℃. RGD moieties were able to significantly increase the efficiency of cell attachment in comparison with unconjugated hydrogel beads. The thermally-induced cell detachment was caused by not only the change of the surface hydrophobicity but also the decrease of RGD moiety density. The latter was brought about by bead swelling behaviour induced by temperature reduction.

Published literature	Fabrication method	Matrix	Surface (PNIPAAm architecture)	Microsphere diameter	Density	Specific surface area	PNIPAAm MW	PNIPAAm chain grafting density
Yang et al. (2010)	grafting-to technique	Cytodex-3 ® beads	linear PNIPAAm homopolymer	170-380 µm	1.04 g/mL[a]	2700 cm^2/g[a]	N/D	N/D
Kim et al. (2003)	grafting-from technique	cross-linked dextran beads (Sephadex G50)	linear PNIPAAm homopolymer	~273 µm (25 °C) ~314 µm (40 °C)	N/D	N/D	N/D	N/D
Catinkaya et al. (2011)	grafting-from technique	cross-linked PHEMA beads	linear PNIPAAm homopolymer	327 ±99 µm	1.05 g/mL	230 cm^2/g	N/D	N/D
Tamura et al. (2012 a)	grafting-from technique	chloromethylated polystyrene beads	linear PNIPAAm homopolymer	55.5 µm-189.1 µm	N/D	422-1030 cm^2/g	7,250-27,800	0.39-0.47 chains/nm^2
Tamura et al. (2012 b)	grafting-from technique	chloromethylated polystyrene beads	linear PNIPAAm copolymer	55.5 ±12.5 µm	N/D	1030 cm^2/g	N/D	N/D
Tamura et al. (2012 c)	grafting-from technique	chloromethylated polystyrene beads	linear PNIPAAm homopolymer	~100 µm	N/D	603-647 cm^2/g	3,400-23,000	0.29-0.77 chains/nm^2
Hendrick et al (2001)	adsorption	polystyrene beads	looped PNIPAAm homopolymer	120-250 µm	N/D	N/D	5.3×10^5	N/D
Kim et al. (2002)	Precipitation polymerization using a mold	cross-linked PNIPAAm hydrogel beads	RGD conjugated PNIPAAm hydrogel	~0.9 mm (37 °C) ~2 mm (RT)	N/D	N/D	N/A	N/A

a: manufacturer's data of Cytodex-3 ®

b: Kim et al. (2003)'s method was specifically designed for thermo-responsive microcarrier preparation, but no cell culture experiment was carried out.

N/D: not determined

N/A: not applicable

MW: molecular weight

RT: room temperature

Table 2.1 Preparation of thermo-responsive microcarriers

Literature reports	Cell type	Culture method	Microcarrier seeding density	Cell seeding density	Cell attachment temperature	Cell attachment duration	Density of attached cells	Cell attachment ratio [a]	Cell incubation duration [e]	Cell density before detachment	Cell detachment temperature	Cell detachment duration	Cell detachment ratio [b]	Cell viability	
														before cell detachment	after cell detachment
Yang et al. (2010)	hBMMSCs	dynamic (spinner flask)	5 mg/mL	2×10^5 cells/mL	37 °C	270 min	N/D	> 99%	5 days	~5×10^5 cells/mL	32 °C	10 min	>82.5%	N/D	~92.2%
Catinkaya et al. (2011)	fetal chondrocytes	Static (24-well plate)	10g/L	1×10^5 cells/mL	37 °C	8 h	N/D	89%	11 days	5×10^5 cells/mL	4 °C	20 min	~70%	N/D	N/D
Tamura et al. (2012 a)	CHO-K1	static (12-well plate)	2 cm^2 bead surface area/ well	1×10^5 cells/cm^2 of bead surface	37 °C	24 h	2×10^4 - 11×10^4 cells/cm^2 of bead surface[c]	20%-110%[d]	24 h	2×10^4 -11×10^4 cells/cm^2 of bead surface[c]	20 °C	120 min	60%-100%[c]	~100%	93%-100%[c]
		dynamic (spinner flask)	200 cm^2 bead surface /flask	5×10^3 cells/cm^2 of bead surface	37 °C	24 h (without stirring)	0-5×10^3 cells/cm^2 of bead surface[c]	0%-100%[d]	24h-168 h	0 -30×10^4 cells/cm^2 of bead surface[c]	20 °C	120 min	41.9%-100%[c]	N/D	N/D
Tamura et al. (2012 b)	CHO-K1	Static (12-well plate)	2 cm^2 bead surface area/ well (2 mg beads/well)	2.5×10^4 cells/cm^2 of bead surface	37 °C	24 h	2.5×10^4 - 3×10^4 cells/cm^2 of bead surface[c]	100%-120%[d]	24h-264h	2.5×10^4 - 40×10^4 cells/cm^2 of bead surface[c]	20 °C	120 min	40%-90%[c]	~100%	N/D
				1×10^5 cells/cm^2 of bead surface	37 °C	24 h	8.5×10^4 - 10×10^4 cells/cm^2 of bead surface[c]	85%-100%[d]	24 h	8.5×10^4 - 10×10^4 cells/cm^2 of bead surface[c]	20 °C	120 min	31.2%-90%[c]	N/D	>90%
Tamura et al. (2012 c)	CHO-K1	Static (12-well plate)	4 cm^2 bead surface area/ well	5×10^4 cells/cm^2 of bead surface	37 °C	24 h	2×10^4 - 4.5×10^4 cells/cm^2 of bead surface[c]	40%-90%[d]	24 h	2×10^4 -4.5×10^4 cells/cm^2 of bead surface[c]	20 °C	120 min	35%-100%[c]	N/D	N/D
Hendrick et al (2001)	CHO-K1	static	0.05g/mL	7.5×10^5 cells/ 5mL	37 °C	24 h	N/D	N/D	24 h-48 h	N/D	10 °C	1 h	100%	N/D	N/D
Kim et al. (2002)	chondrocytes	static (24-well plate)	12.6mg (dry weight)/well	1.4×10^6 cells/well (2.6×10^4 cells/bead)	37 °C	8h (without fetal bovine serum) + another 16 h	~30×10^3 cells/cm^2 of bead surface[c]	N/D	24h	N/D	20 °C-35°C	1.5 h	30%~85%[c]	N/D	N/D

a: cell attachment ratio=[number of attached cells]/ [total number of seeded cells] ×100%

b: cell detachment ratio=[number of detached cells]/ [total number of cells on microcarriers before detachment] ×100%

c: data taken from diagrams in the relevant literature reports

d: cell attachment ratios were calculated as: cell attachment ratio=[density of attached cells]/ [cell seeding density] ×100%; ratios more than 100% were perhaps caused by experimental errors or cell proliferation over prolonged incubation times.

e: cell incubation duration = total cell incubation time between cell seeding and cell detachment. When cell detachment is carried out immediately after cell attachment, cell incubation duration is equivalent to cell attachment duration.

N/D: not determined

Table 2.2 Cell culture on thermo-responsive microcarriers

3 ‘Grafting-to’ technique for microsphere modification

3.1 Introduction

In the grafting-to approach, PNIPAAm with appropriate functional groups was synthesised as reported previously, and subsequently grafted to microspheres by the covalent tethering between functional groups on PNIPAAm and complementary reactive groups located on microsphere surfaces. The grafting-to approach is a widely-used surface modification strategy due to its experimental simplicity and ease of control (Peleshanko and Tsukruk 2008; Xu et al. 2009). In this study, various functional groups were introduced to the ends of PNIPAAm homopolymer chains or the mid-chain of PNIPAAm copolymers. Thereafter, these polymers and copolymers were grafted onto the surfaces of cross-linked polystyrene microspheres with different complementary reactive groups. The molecular weight of end-functionalized PNIPAAm was controlled by regulating the feed concentration of chain transfer agent in chain transfer polymerization. The PNIPAAm grafting density (or amount) can be regulated by varying the feed amount of PNIPAAm homopolymer or copolymer in the conjugation reaction. Finally, three types of PNIPAAm molecular architecture were prepared, namely 1) linear PNIPAAm chain, 2) looped PNIPAAm chain and 3) double-layer looped PNIPAAm chain.

3.2 Materials and methods

3.2.1 Materials

1,4-Dioxane (99.8%), 2-mercaptoethanol (MetOH, ≥99.0%), 3-mercaptopropionic acid (MPA, ≥99%), 2-mercaptoethylamine (MEA, ≥98.0%), 4,4′-azobis(4-cyanovaleric acid) (ACVA, ≥98.0%), 2,2′-azobis(2-methylpropionitrile) (AIBN, 98%), diethyl ether (≥99.8%), acrylic acid (AAc, 99%), acrylamide (AAm, >99%), (aminomethyl)polystyrene microspheres (PS-NH_2, 70-90 mesh, -NH_2 group content: 1.0-1.5 mmol/g), (hydroxymethyl)polystyrene microspheres (PS-OH, 70-90 mesh, -OH group content: 2.0-3.0 mmol/g), methanol (HPLC grade, ≥99.9%), *N*,*N*′-diisopropylcarbodiimide (DIC, 99%), 4-(dimethylamino)pyridine (DMAP, 99%) and dichloromethane (DCM, ≥99.9%) were purchased from Sigma-Aldrich (UK) and used as received. Polystyrene A COOH microspheres (PS-COOH, 160-200 μm, -COOH group content: 0.8-1.2 mmol/g) were obtained from RAPP POLYMERE (Germany) and used as received.

N-Isopropylacrylamide (NIPAAm, 97%, Sigma-Aldrich) was purified by recrystallisation from hexane/toluene followed by filtration and drying. Typically, NIPAAm was dissolved in the minimum amount of 45-50 ℃ hexane/toluene (60/40, v/v) and the solution was filtrated into a beaker while it was still hot. The solution was then allowed to cool down and, after a while, it was further cooled by using an ice bath. The NIPAAm crystals were recovered by vacuum filtration. The NIPAAm was dried in a vacuum oven for 24 h. Deionised water (DI water) used in this study was obtained from an ultrapure water purification system (Elix®, Millipore).

3.2.2 Preparation of PNIPAAm polymers and copolymers

3.2.2.1 Synthesis of PNIPAAm

PNIPAAm homopolymer was synthesized by free radical polymerization using AIBN as an initiator according to the method reported by Schild (1992). NIPAAm (9 g, 0.08 mol) was dissolved in 60 mL dioxane and the solution was deoxygenated by nitrogen bubbling for 1 h at room temperature. AIBN (0.05 g, 0.3 mmol) was added to the solution and the polymerization was conducted at 70 ^{o}C for 24 h under nitrogen atmosphere. The resulting PNIPAAm was precipitated into an excess of diethyl ether from dioxane. To obtain PNIPAAm with a narrow molecular weight distribution, the precipitated PNIPAAm was dissolved in dioxane again and reprecipitated in diethyl ether. This procedure was repeated three times and then the PNIPAAm polymer was dried by vacuum suction for 1 h at room temperature.

3.2.2.2 Synthesis of PNIPAAm-COOH

Carboxyl-terminated PNIPAAm (PNIPAAm-COOH) was prepared by chain transfer polymerisation using MPA as a chain transfer agent (Takei et al. 1993). NIPAAm (9 g, 0.08 mol) was dissolved in dioxane (60 mL) and the solution was deoxygenated by nitrogen bubbling for 1 h at room temperature. MPA (various concentrations according to Table **3.1**) and ACVA (0.08 g, 0.29 mmol) were added to the solution and the polymerization was conducted at 70 ^{o}C for 24 h under nitrogen atmosphere. The resulting PNIPAAm-COOH was precipitated three times into an excess of diethyl ether from dioxane. Thereafter, the PNIPAAm-COOH was dried by vacuum suction for 1 h at room temperature.

Sample code	NIPAAm (g)	MPA (mL)	MPA concentration (mol/mL)	[MPA]/[NIPAAm] (mol/mol)	ACVA (g)	Dioxane (mL)
PNIPAAm-COOH (XS)	9.0	0.96	0.184	0.136	0.08	60
PNIPAAm-COOH (S)		0.48	0.092	0.068		
PNIPAAm-COOH (M)		0.24	0.046	0.034		
PNIPAAm-COOH (L)		0.12	0.023	0.017		
PNIPAAm-COOH (XL)		0.06	0.012	0.009		

Table 3.1 Synthesis of PNIPAAm-COOH of various molecular weights

3.2.2.3 Synthesis of PNIPAAm-OH

Hydroxyl-terminated PNIPAAm (PNIPAAm-OH) was prepared by chain transfer polymerisation using MetOH as a chain transfer agent. NIPAAm (9 g, 0.08mol) was dissolved in 60 mL dioxane and the solution was deoxygenated by nitrogen bubbling for 1 h at room temperature. MetOH (0.20 mL, 0.22 g, 2.85 mmol) and AIBN (0.05 g, 0.3 mmol) were then added to the solution and the polymerization was conducted at 70 ^{o}C for 24 h under nitrogen atmosphere. The resulting PNIPAAm-OH was precipitated three times into an excess of diethyl ether from dioxane. Thereafter, the PNIPAAm-OH was dried by vacuum suction for 1 h at room temperature. It shall be noted that MetOH is volatile and must be added after degassing.

3.2.2.4 Synthesis of PNIPAAm-NH_2

Amine-terminated PNIPAAm (PNIPAAm-NH_2) was prepared by chain transfer polymerisation using MEA as a chain transfer agent (Lee et al, 2010). NIPAAm (9 g, 0.08mol) and MEA (0.22 g, 2.85 mmol) were dissolved in 60 mL dioxane and the solution was deoxygenated by nitrogen bubbling for 1 h at room temperature. AIBN (0.05 g, 0.3 mmol) was then added to the solution and the polymerization was conducted for 24 h at 70 ^{o}C under nitrogen atmosphere. The resulting PNIPAAm-NH_2

was precipitated three times into an excess of diethyl ether from dioxane. Thereafter, the PNIPAAm-NH_2 was dried by vacuum suction for 1 h at room temperature.

3.2.2.5 Synthesis of poly(NIPAAm-*co*-AAc)

Poly(NIPAAm-*co*-AAc) was prepared by radical copolymerization of NIPAAm and AAc using ACVA as an initiator. A typical procedure (e.g. poly(NIPAAm-*co*-AAc-1%) in Table **3.2**) was as follows: NIPAAm (9 g, 0.08mol) and AAc (0.058 g, 0.8 mmol) were dissolved in 60 mL dioxane (mole ratio of AAc to NIPAAm, 1:100), and the solution was deoxygenated by nitrogen bubbling for 1 h at room temperature. ACVA (0.08 g, 0.29 mmol) was added to the solution and the polymerization was conducted at 70 ^{o}C for 24 h under nitrogen atmosphere. The resulting poly(NIPAAm-*co*-AAc) was precipitated three times into an excess of diethyl ether from dioxane. Thereafter, the poly(NIPAAm-*co*-AAc) was dried by vacuum suction for 1 h at room temperature. Similar experiments were performed by varying the mole ratio of AAc to NIPAAm added to the solution.

Sample code[a]	NIPAAm (g)	AAc (g)	[AAc]/[NIPAAm] (mol/mol)	ACVA (g)	Dioxane (mL)
poly(NIPAAm-*co*-AAc-1%)	9	0.058	1/100	0.08	60
poly(NIPAAm-*co*-AAc-2%)		0.116	2/100		
poly(NIPAAm-*co*-AAc-3%)		0.17	3/100		
poly(NIPAAm-*co*-AAc-5%)		0.29	5/100		
poly(NIPAAm-*co*-AAc-10%)		0.58	10/100		

a: Abbreviated as poly(NIPAAm-*co*-AAc-X%), where X% represents the molar ratio of AAc to NIPAAm.

Table 3.2 Synthesis of poly(NIPAAm-*co*-AAc) with various AAc contents

3.2.2.6 Synthesis of poly(NIPAAm-*co*-AAm)

Poly(NIPAAm-*co*-AAm) was prepared by radical copolymerization of NIPAAm and AAm using AIBN as an initiator. A typical procedure was as follows: NIPAAm (9 g,

0.08mol) and AAm (0.28 g, 4 mmol) (mole ratio of AAm to NIPAAm, 5:100) were dissolved in 60 mL dioxane and the solution was deoxygenated by nitrogen bubbling for 1 h at room temperature. AIBN (0.05 g, 0.3 mmol) was then added to the solution and the polymerization was conducted at 70 ℃ for 24 h under nitrogen atmosphere. The resulting poly(NIPAAm-*co*-AAm) was precipitated three times into an excess of diethyl ether from dioxane. Thereafter, the poly(NIPAAm-*co*-AAm) was dried by vacuum suction for 1 h at room temperature. Similar experiments were performed by varying the mole ratio of AAm to NIPAAm added to the solution, while keeping all other quantities constant (Table **3.3**).

Sample code[a]	NIPAAm (g)	AAm (g)	[AAm]/[NIPAAm] (mol/mol)	AIBN (g)	Dioxane (mL)
poly(NIPAAm-*co*-AAm-5%)	9	0.28	5/100	0.05	60
poly(NIPAAm-*co*-AAm-10%)		0.56	10/100		
poly(NIPAAm-*co*-AAm-15%)		0.84	15/100		
poly(NIPAAm-*co*-AAm-20%)		1.12	20/100		

a: Abbreviated as poly(NIPAAm-*co*-AAm-X%), where X% represents the molar ratio of AAm to NIPAAm.

Table 3.3 Synthesis of poly(NIPAAm-*co*-AAm) with various AAm contents

3.2.3 Grafting PNIPAAm polymer or copolymer to microsphere surfaces

3.2.3.1 Preparation of PS-O-OC-PNIPAAm microspheres

PS-O-OC-PNIPAAm microspheres were synthesized by conjugating PS-OH microspheres with PNIPAAm-COOH through esterification. A typical procedure was as follows: PS-OH microspheres (0.5 g), PNIPAAm-COOH (M) (3.0 g) and DMAP (0.224 g, 1.8 mmol) were added to 50 mL DCM. DIC (0.93 mL, 0.758g, 6 mmol) was added to the mixture. The reaction was kept under stirring at room temperature for 24 h. The

resulting PS-O-OC-PNIPAAm microspheres were washed thoroughly with methanol and DI water, and dried with vacuum suction for 1 h. Similar experiments were performed by varying the amount of PNIPAAm-COOH (M) (0.1 g, 0.3 g, 0.5 g, 1.5 g, 3.0 g, 4.5 g, 6 g and 9 g) added to the reaction mixture, while keeping all other quantities constant.

3.2.3.2 Preparation of PS-CO-O-PNIPAAm microspheres

PS-CO-O-PNIPAAm microspheres were synthesized by conjugating PS-COOH microspheres with PNIPAAm-OH through esterification. PS-COOH microspheres (0.5 g), PNIPAAm-OH (3.0 g) and DMAP (0.224 g, 1.8 mmol) were added to 50 mL DCM. DIC (0.93 mL, 0.758g, 6 mmol) was then added to the mixture. The reaction was kept under stirring at room temperature for 24 h. The resulting PS-CO-O-PNIPAAm microspheres were washed thoroughly with methanol and DI water, and dried with vacuum suction for 1 h.

3.2.3.3 Preparation of PS-CO-NH-PNIPAAm microspheres

PS-CO-NH-PNIPAAm microspheres were synthesized by conjugating PS-COOH microspheres with PNIPAAm-NH_2 through amidation. PS-COOH microspheres (0.5 g), PNIPAAm-NH_2 (3.0 g) and DMAP (0.224 g, 1.8 mmol) were added to 50 mL DCM. DIC (0.93 mL, 0.758g, 6 mmol) was then added to the mixture. The reaction was kept under stirring at room temperature for 24 h. The resulting PS-CO-NH-PNIPAAm microspheres were washed thoroughly with methanol and DI water, and dried with vacuum suction for 1 h.

3.2.3.4 Preparation of PS-(looped PNIPAAm) microspheres

PS-(looped PNIPAAm) microspheres were synthesized by conjugating PS-OH microspheres with poly(NIPAAm-*co*-AAc) copolymer through esterification. A typical procedure was as follows: PS-OH microspheres (0.5 g), poly(NIPAAm-*co*-AAc-1%) (3.0 g) and DMAP (0.224 g, 1.8 mmol) were added to 50 mL DCM. DIC (0.93 mL, 0.758g, 6 mmol) was then added to the mixture. The reaction was kept under stirring at 30 ℃ for 24 h. The resulting PS-(looped PNIPAAm) microspheres were washed thoroughly with methanol and dried with vacuum suction for 1 h. Similar experiments were performed by varying the amount of poly(NIPAAm-*co*-AAc-1%) (0.1 g, 0.2 g, 0.5 g, 1.5 g, 3.0 g, 4.5 g, and 6 g) added to the reaction mixture, while keeping all other quantities constant.

3.2.3.5 Preparation of PS-(double-layer looped PNIPAAm) microspheres

PS-(double-layer looped PNIPAAm) microspheres were synthesized by grafting poly(NIPAAm-*co*-AAm) copolymer to the residual carboxyl groups on PS-(looped PNIPAAm) microspheres through amidation. PS-(looped PNIPAAm) microspheres (0.5 g), poly(NIPAAm-*co*-AAm-10%) (3.0 g) and DMAP (0.224 g, 1.8 mmol) were added to 50 mL DCM. DIC (0.93 mL, 0.758g, 6 mmol) was then added to the mixture. The reaction was kept under stirring at 30 ℃ for 24 h. The resulting PS-(double-layer looped PNIPAAm) microspheres were washed thoroughly with methanol and dried with vacuum suction for 1 h.

3.2.4 Characterizations and measurements

3.2.4.1 FTIR spectroscopy measurements

Fourier transform infrared (FTIR) spectra were recorded using an FTIR spectrometer (FTS 6000, BIO-RAD) equipped with attenuated total reflectance (ATR) setup (DuraSampl*IR* II^{TM}, SensIR Technologies). 200 scans were averaged to yield the spectra at a resolution of 4.0 cm^{-1}. Before collecting sample spectra, the background spectrum was collected by measuring the response of the spectrometer without sample.

3.2.4.2 HPLC measurements

The weight average molecular weight (M_w), number average molecular weight (M_n) and polydispersity (PD) index of the polymers were determined by a high-performance liquid chromatography (HPLC) (Shimadzu, Japan) equipped with a TSK-GEL Super AW4000 column (Tosoh Bioscience, Japan). Methanol containing LiBr (10 mmol/L) was used as a mobile phase and eluted at a flow rate of 0.5 mL/min at a column temperature of 40 ℃. The polymer solution (0.5 mg/mL) was filtered through a 0.2 μm syringe filter (Acrodisc®, Pall Corp., USA) prior to the measurement.

3.2.4.3 Combustion analysis

The mass percentages of C, H and N of the unmodified and modified microspheres were tested by combustion analysis. The combustion analysis was conducted by MEDAC LTD (Surrey, UK). In this technique, a known weight of polymer is burnt in excess oxygen, and the ratio of C, H, and N determined from the weight of CO_2, H_2O and NO_x which is produced.

The grafted amount (m_p) of PNIPAAm or poly(NIPAAm-*co*-AAc) copolymer on PS-OH bead surface was calculated from an increment in nitrogen content derived from the amide bond of PNIPAAm or poly(NIPAAm-*co*-AAc) copolymer. It was calculated as follows:

$$m_p(\text{mg/g}) = \frac{N_p\% - N_0\%}{N_{p,theory}\% - N_0\%} \times 10^3$$

where $N_p\%$ and $N_0\%$ represent the nitrogen contents in modified and unmodified beads respectively, and $N_{p,theory}\%$ represents the theoretical nitrogen content of PNIPAAm or poly(NIPAAm-*co*-AAc) copolymer.

The grafting density of PNIPAAm on the PS-OH bead surface was calculated as follows:

$$Grafting\ density\ (\mu\text{mol/g}) = \frac{m_p}{M_n} \times 10^3$$

where M_n represents the number average molecular weight of PNIPAAm-COOH, which was determined by HPLC.

3.2.4.4 SEM observations

The surface morphology of the unmodified and modified microspheres was observed by a scanning electron microscope (SEM) (JOEL, JSM 840F) at an accelerating voltage of 3 kV. Before the SEM investigation, samples were coated with 10 nm platinum by sputtering for 20 min.

3.2.4.5 Determination of LCST

LCST of the prepared polymers was determined by measurement of the optical absorbance of aqueous polymer solution (0.5% wt/v, pH=7.4) at 500 nm using a

ultraviolet-visible (UV-VIS) spectrometer (Varian, Cary, 50 Bio) equipped with a single cell Peltier temperature controller (Varian, Cary). The aqueous polymer solution was prepared using Dulbecco's Phosphate-Buffered Saline (DPBS, PAA Laboratories GmbH, Austria). The pH of the solution was then adjusted to 7.4 by adding NaOH solution (1 mol/L). The temperature interval was 0.5 ℃ and 0.3 ℃ in the vicinity of the LCST. At each temperature, the sample was stabilized for 2 min before measurements. The LCST values were defined as the temperature producing a 50% increase of the total increase in optical absorbance (Luo et al. 2012).

3.2.4.6 NMR measurements

^{1}H nuclear magnetic resonance (NMR) spectra of polymers were recorded on Bruker DQX400 (400 MHz) spectrometers at 27 ℃ using methanol-d_4 (Sigma-Aldrich) as a solvent. Chemical shifts (δH) were reported in parts per million (ppm) and were referenced to the residual protonated solvent peak.

3.3 Results and discussion

3.3.1 Synthesis of end-functionalized PNIPAAm

The end-functionalization of PNIPAAm relies on free radical polymerization of NIPAAm in the presence of an appropriate chain transfer agent, chosen depending on

the desired end group. This reaction is referred as chain transfer polymerization or free radical telomerization (Takei et al. 1993; Sakamoto et al. 2004). In this study, carboxyl (-COOH), hydroxyl (-OH) and amino ($-NH_2$) end groups were incorporated to PNIPAAm polymer by using MPA, MetOH and MEA as chain transfer agents respectively (Figure **3.1**). These chain transfer agents are thiol compounds (RSH) containing the desired functional end groups. Thiols are very efficient chain transfer agents due to the weakness of its S-H bond and the high reactivity of the thiyl radicals (Henríquez et al. 2003). Taking the synthesis of PNIPAAm-COOH for example, the assumed mechanism of chain transfer polymerization is shown in Figure **3.2**. The polymerization is initiated by thermal decomposition of an azo-initiator generating free radicals. These radicals are then transferred to thiols (RSH) to produce thiyl radicals (RS•) by losing the hydrogen atoms from the S-H groups (Wardman and von Sonntag 1995). The thiyl radical subsequently adds to the unsaturated substrate (i.e. NIPAAm monomers) to form a carbon-centered radical (i.e. a growing PNIPAAm chain). Because the S-H bond strength is lower than that of many C-H bonds, the carbon-centered radical then reacts with a thiol molecule to give the final product (i.e. end-functionalized PNIPAAm) and a new thiyl radical, thus propagating the radical chain. This step is referred as chain transfer, involving the cleavage of an S-H bond and the subsequent hydrogen donation from the thiol molecule to the carbon-centered radical. Chain propagation occurs when on average the carbon-centered radical reacts more rapidly with the unsaturated substrate than with the chain-transferring thiol (Griesbaum 1970). The competition between chain elongation and chain transfer restricts the lifetime of the carbon-centered radical, leading to a limited chain length between a few hundred and several thousand. This competition can be adjusted by controlling the concentration of the thiol chain transfer agent. The final products (telomers) are usually small oligomers.

Finally, chain termination occurs when the combination of free radicals dominates over the chain transfer (Griesbaum 1970). After telomerization, each end-functionalized PNIPAAm molecule contains only one end group on average (Takei et al. 1993).

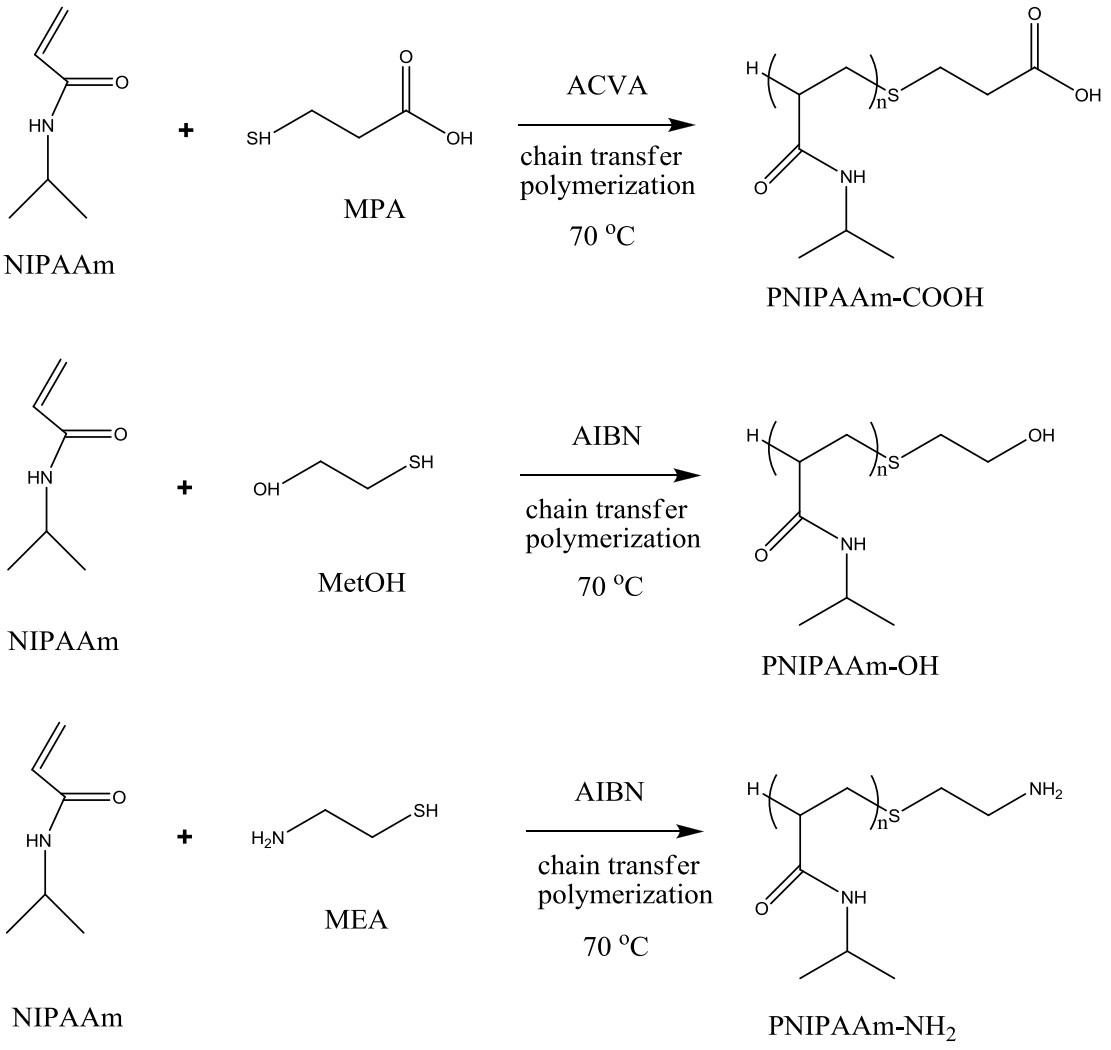


Figure 3.1 Synthesis of end-functionalized PNIPAAm

It is worth mentioning that the use of azo-initiators forms undesirable by-products, especially PNIPAAm chains directly growing from radicals on thermally-decomposed azo-initiators. These PNIPAAm chains contain the decomposed azo-initiators as end groups rather than the desired functional end groups from chain transfer agents. To minimize the amount of such by-product, in the case of PNIPAAm-COOH synthesis,

ACVA was used as an initiator. Because ACVA contains carboxyl groups, the by-products are still carboxyl end-functionalized. However, in the case of the synthesis of PNIPAAm-OH and PNIPAAm-NH_2, AIBN was used as an initiator to avoid the introduction of unwanted carboxyl groups.

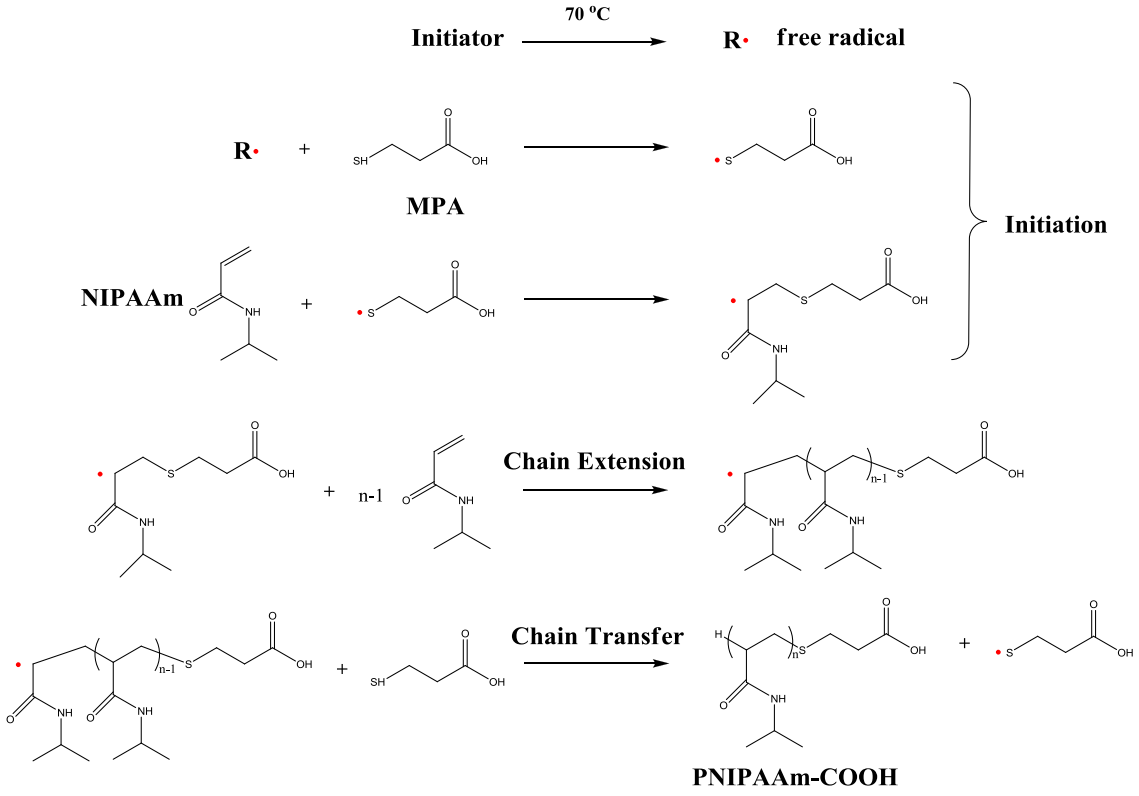


Figure 3.2 The mechanism of chain transfer polymerization

To confirm the nature of the polymerization of PNIPAAm-COOH, FTIR spectroscopy and ^{1}H-NMR spectroscopy were carried out. Figure **3.3** shows the FTIR spectra of NIPAAm, PNIPAAm and PNIPAAm-COOH. In the NIPAAm spectrum, peaks at 1618 cm^{-1} and 1409 cm^{-1} are assigned to C=C and CH_2=, which are characteristic of a vinyl monomer. In both the PNIPAAm and PNIPAAm-COOH spectra, the peaks disappeared, indicating that polymerization has taken place. In particular, in PNIPAAm-COOH spectrum, the C=O stretching bond attributed to the carboxyl end group of PNIPAAm-COOH was observed at 1705 cm^{-1}. This peak was absent in the PNIPAAm spectrum.

Figure **3.4**-**3.6** show the ^{1}H-NMR spectra of NIPAAm, PNIPAAm, and PNIPAAm-COOH. In the NIPAAm spectrum, signals around 1 ppm are assigned to $–CH_3$, the one around 4.0 ppm to –CH, and those around 5.6-6.2 ppm to CH_2=CH-. The signal at 3.3 ppm is ascribed to MeOD. On the other hand, in both PNIPAAm and PNIPAAm-COOH spectra, the signals around 1.6-2.1 ppm are due to $–CH_2$-CH- and no signal for the vinyl group was observed. In particular, in the PNIPAAm-COOH spectrum, the signals around 2.6-2.8 ppm are due to chain transfer agent (MPA) (Ju et al. 2001), which comprised the PNIPAAm-COOH end group. The signals were absent in PNIPAAm spectrum. These results together indicate PNIPAAm-COOH was successfully synthesized. The FTIR and ^{1}H-NMR spectra of PNIPAAm-NH_2 and PNIPAAm-OH are shown in Appendix **B** and **C** (Figure **B.1**, **C.1** and **C.2**). In a similar way, the polymerization of PNIPAAm-NH_2 and PNIPAAm-OH could be confirmed by the absence of the peak characteristic of vinyl monomers in both FTIR and ^{1}H-NMR spectra. Although the presence of amino and hydroxyl groups on PNIPAAm-NH_2 and PNIPAAm-OH could be confirmed by broad signals at about 3400 cm^{-1} in corresponding FTIR spectra, this did not indicate the identity of the end groups. Also, in the ^{1}H-NMR spectra of PNIPAAm-NH_2 and PNIPAAm-OH show peaks around 2.6-2.8 ppm attributed to the chain transfer agents (MEA and MetOH), which comprised the –NH_2 and –OH end groups of PNIPAAm-NH_2 and PNIPAAm end group respectively. No direct signals of amino and hydroxyl end groups were observed due to the possible hydrogen bonding and exchange effects. However, the presence of amino or hydroxyl groups were indirectly confirmed by successful DIC/DMAP coupling (see section **3.3.3**).

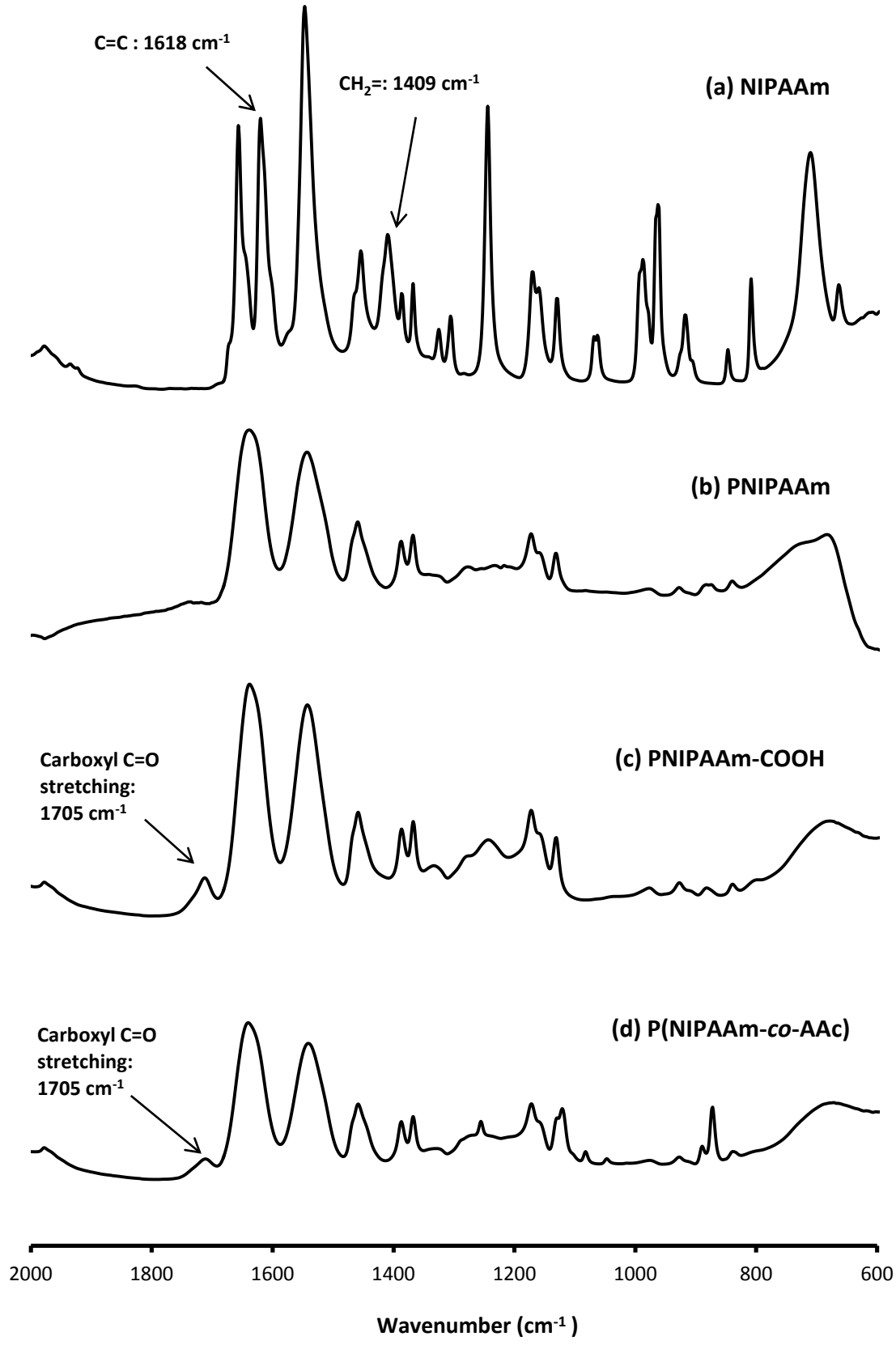


Figure 3.3 FTIR spectra of (a) NIPAAm monomer, (b) PNIPAAm homopolymer, (c) PNIPAAm-COOH and (d) P(NIPAAm-*co*-AAc) copolymer.

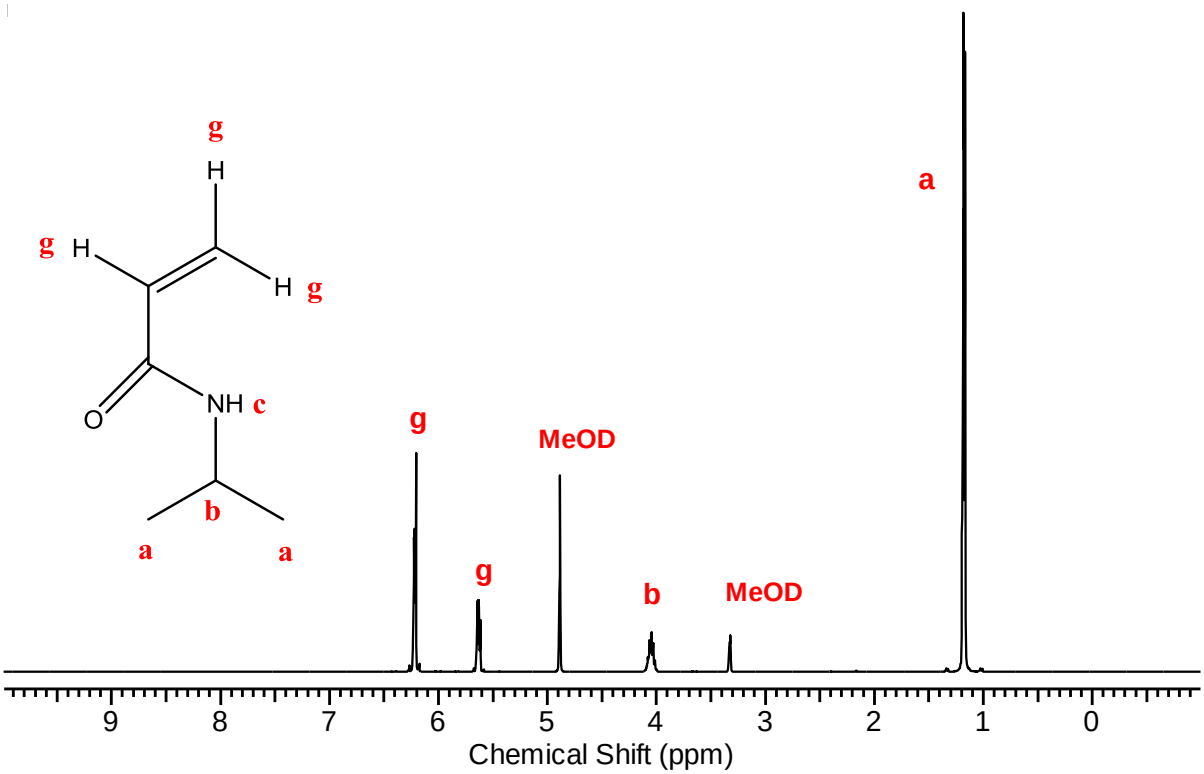


Figure 3.4 ^{1}H-NMR spectrum of NIPAAm monomer

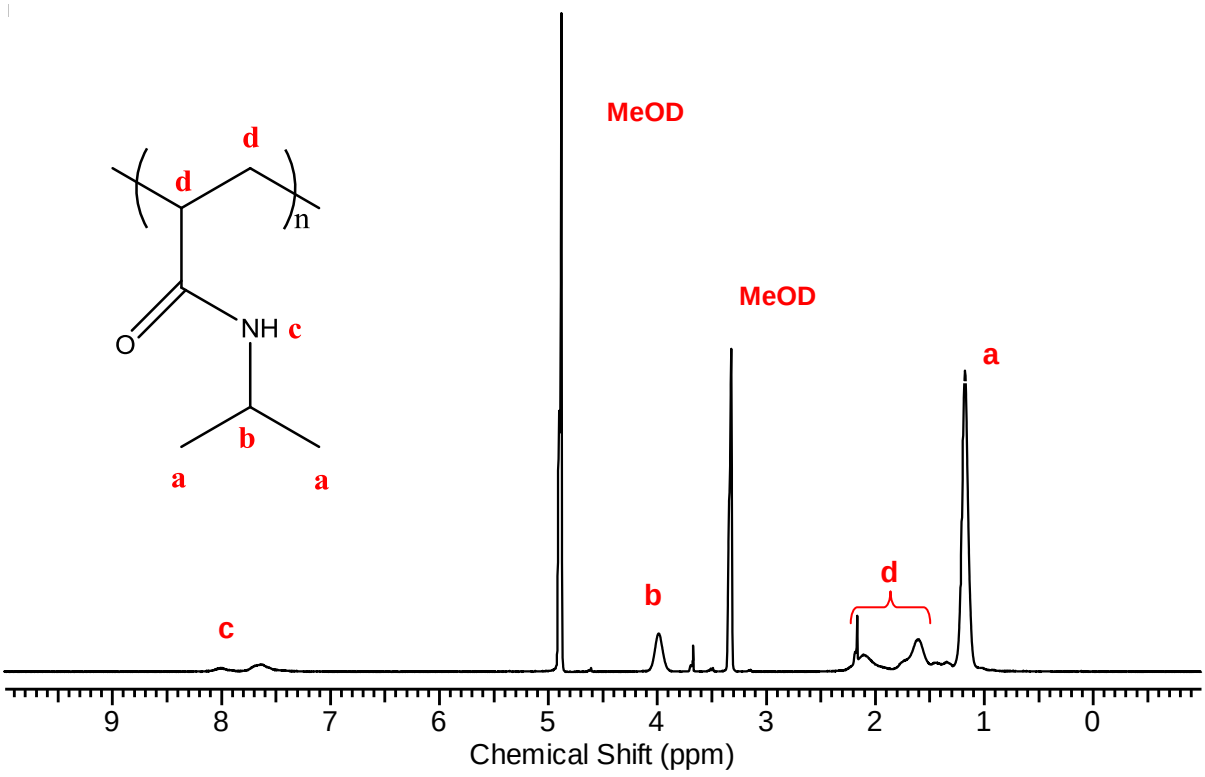


Figure 3.5 ^{1}H-NMR spectrum of PNIPAAm homopolymer

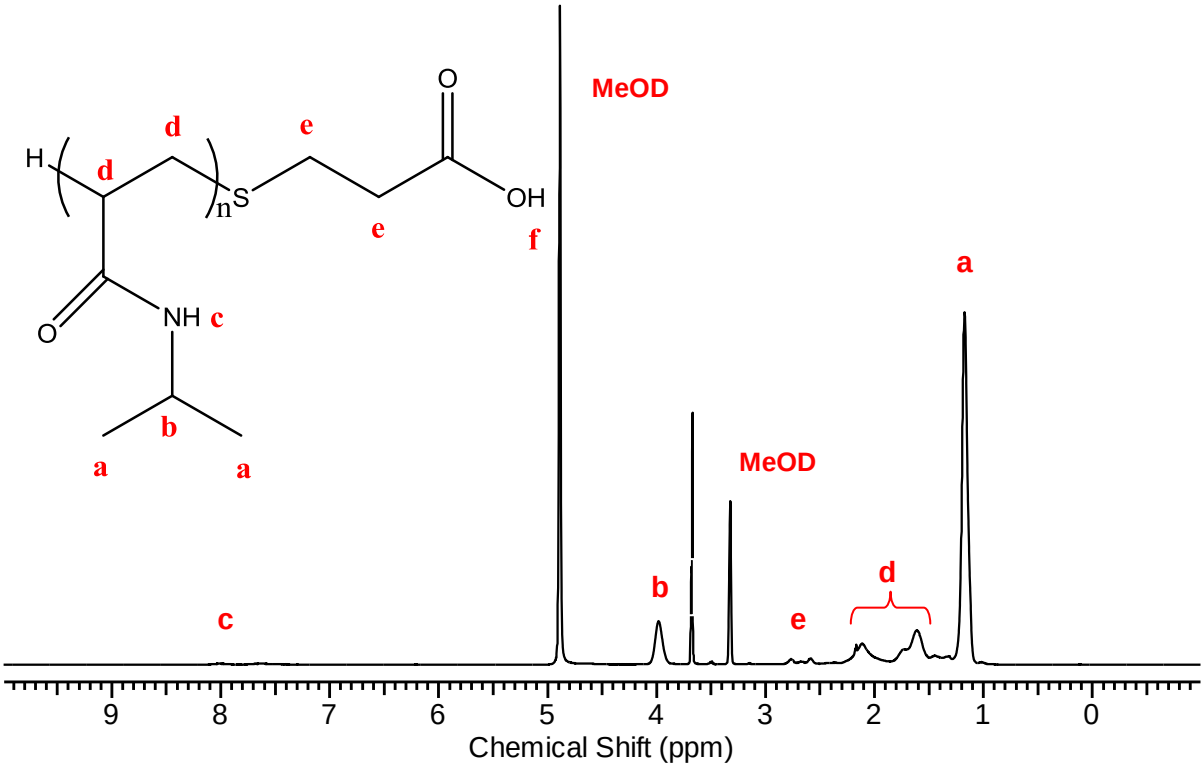


Figure 3.6 ^{1}H-NMR spectrum of PNIPAAm-COOH

Chain transfer polymerization produces polymer of lower molecular weight. The magnitude of this effect depends on the concentration of the chain transfer agents or the ratio of chain transfer agent to monomer (Shefer et al. 1993; Takei et al. 1993), as shown in Table **3.4**. In this study, the chain transfer polymerization of NIPAAm was conducted in the presence of different concentrations of MPA, while keeping all other quantities constant. The formed polymers were analyzed by HPLC. As expected, increases in the concentration of MPA resulted in lower molecular weight of PNIPAAm-COOH. This is because high concentration of MPA increases the rate of chain transfer, leading to shorter lifetime of the growing chain and consequent shorter chain length of the resulting PNIPAAm-COOH. In the absence of MPA, the ACVA initiated the polymerization of NIPAAm directly. The resulting PNIPAAm homopolymer had the highest molecular weight. The introduction of MPA resulted in a

significant reduction in overall polymer molecular weight. In addition, the molecular weight distribution was measured to find the polydispersity (PD), defined as the ratio of M_w to M_n. The PD value is always greater than or equal to 1. It directly reflects the non-homogeneity of a polymer molecular weight distribution, such that as homogeneity increases, the PD value decreases to approach unity (1). PNIPAAm had a PD value of about 3, but, in contrast, the PD values of PNIPAAm-COOH prepared by chain transfer polymerization were around 2. This indicates the addition of chain transfer agent can also reduce the polymer polydispersity. However, the polydispersity of PNIPAAm-COOH was still believed to be very broad due to the nature of free radical polymerization.

Sample code	MPA concentration (mol/mL)	[MPA]/[NIPAAm] (mol/mol)	M_n (g/mol)	M_w (g/mol)	Polydispersity (M_w/M_n)
PNIPAAm-COOH (XS)	0.184	0.136	1857	4196	2.26
PNIPAAm-COOH (S)	0.092	0.068	3763	8387	2.23
PNIPAAm-COOH (M)	0.046	0.034	10938	19435	1.78
PNIPAAm-COOH (L)	0.023	0.017	11735	23402	1.99
PNIPAAm-COOH (XL)	0.012	0.009	12428	24284	1.95
PNIPAAm	0	0	51622	152288	2.95

Table 3.4 The effects of MPA concentration on the molecular weight and polydispersity of PNIPAAm-COOH

3.3.2 Phase transition of PNIPAAm-COOH

The series of PNIPAAm-COOH samples in aqueous solution (0.5 wt%, PH=7.4) was examined for optical absorbance change at various temperatures (Figure **3.7**). All polymers demonstrated readily detectable phase transition behaviour with a LCST around 29.5 to 33.5 ℃. The phase transition phenomenon was attributed to the coil-

globule conformation transition of polymer chains, followed by the aggregation of individual globular polymer molecules mainly due to the intermolecular interaction between the hydrophobic isopropyl groups distributed across the polymer globular particle surfaces in aqueous medium (Fujishige et al. 1989; Gewehr et al. 1992). However, PNIPAAm-COOH with lower molecular weight demonstrated a higher phase transition temperature, decreased temperature-sensitivity (defined as the sharpness of phase transition), and reduced maximum absorbance value (possibly indicating reduced magnitude of aggregation). This is because the enriched presence of hydrophilic carboxyl end group moieties perturbs the hydrophobic intermolecular interaction and consequently disrupts aggregation of small PNIPAAm-COOH molecules. Therefore, it is believed that this phenomenon might disappear after the conjugation of PNIPAAm-COOH to microsphere surface by consuming the carboxyl end groups.

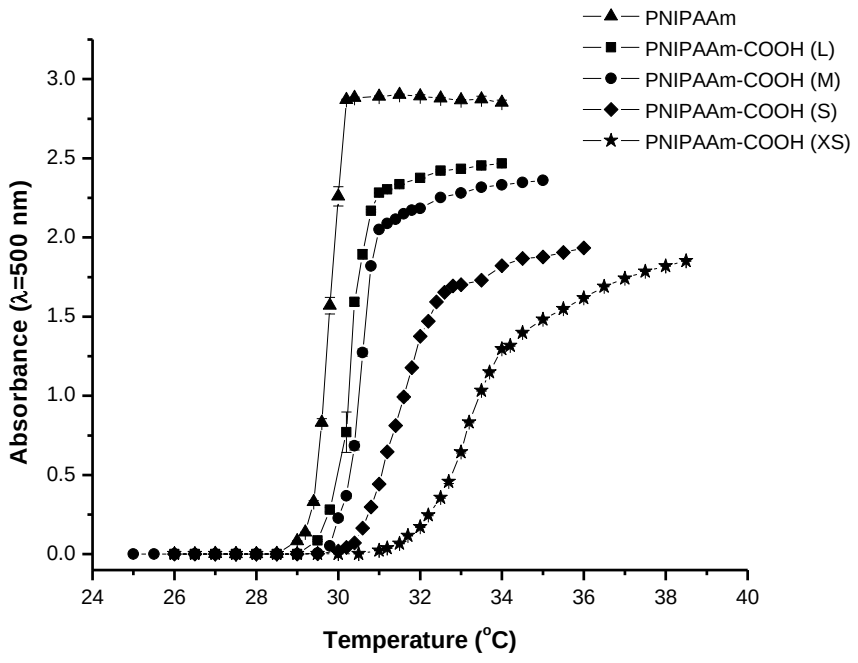


Figure 3.7 Phase transition profiles of PNIPAAm-COOH of various molecular weights in pH 7.4 PBS at 500nm. Polymer details refer to Table **3.4.**

3.3.3 Conjugation of end-functionalized PNIPAAm to microspheres

The conjugation of PNIPAAm to the microsphere surface relies on the covalent tethering between the end groups of the end-functionalized PNIPAAm and the surface complementary reactive groups. In this study, the end-functionalized PNIPAAm polymers were conjugated to various surface-functionalized particles via esterification or amidation, using DIC as a coupling agent and DMAP as a catalyst under mild liquid-phase conditions (Figure **3.8**). PNIPAAm-COOH was grafted to hydroxyl groups on PS-OH microspheres and conversely, PNIPAAm-OH was grafted to carboxyl groups on PS-COOH microspheres via esterification. Similarly, PNIPAAm-COOH was grafted to the amino groups on PS-NH_2 microspheres, and conversely PNIPAAm-NH_2 was grafted to carboxyl groups on PS-COOH microspheres via amidation.

The preparation of PS-O-OC-PNIPAAm microspheres is chosen here to demonstrate the common reaction mechanism, shown in Figure **3.9**. The carboxyl group of PNIPAAm-COOH is first activated by DIC to form an *O*-acylisourea intermediate. Then, DMAP, acting as a nucleophilic catalyst and acyl transfer reagent, reacts with the *O*-acylisourea to produce another reactive intermediate, which in turn undergoes rapid reaction with the hydroxyl group on the PS-OH microsphere. This generates an ester bond between the polymer and the microsphere.

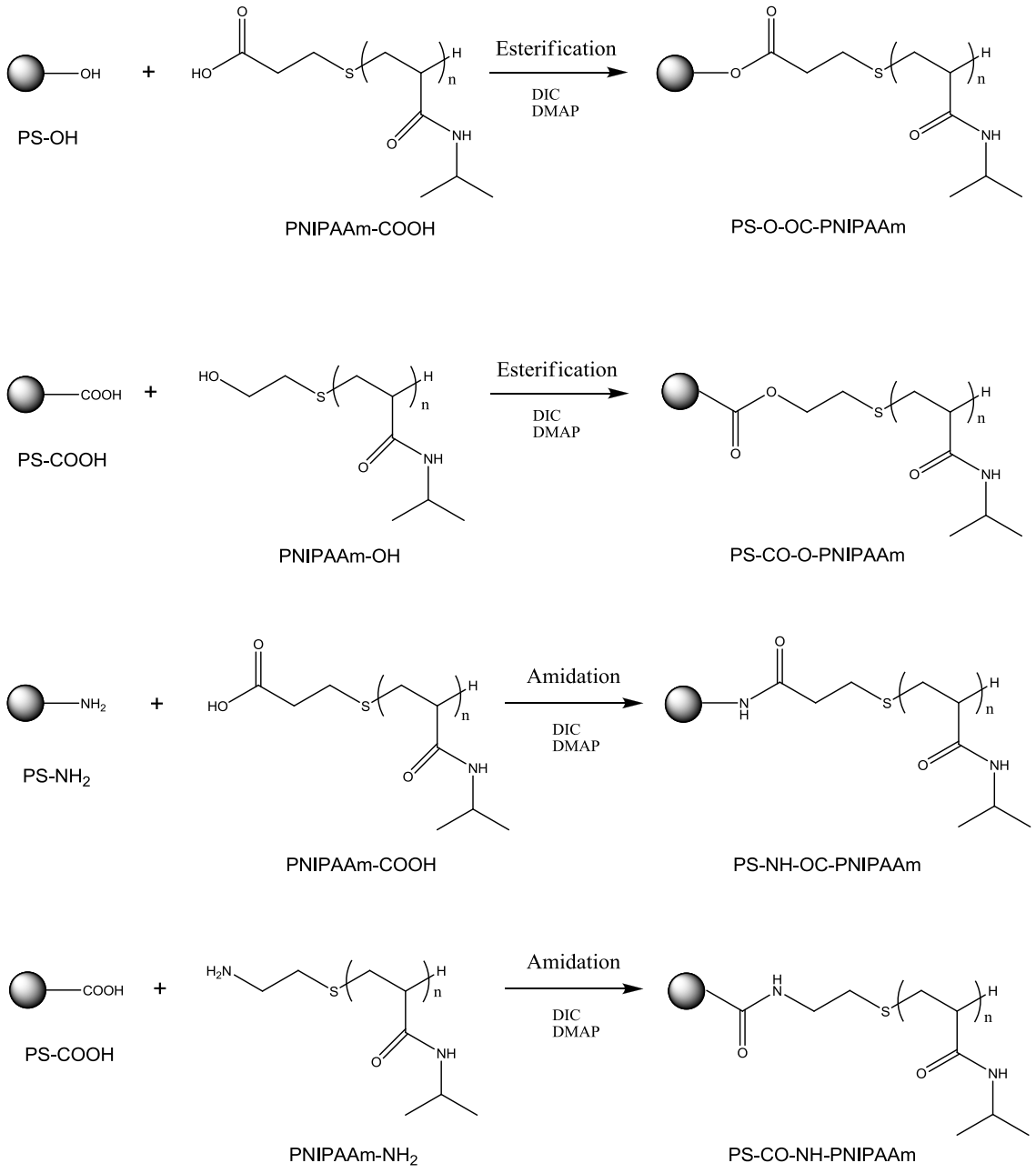


Figure 3.8 Conjugation of end-functionalized PNIPAAm to various microspheres

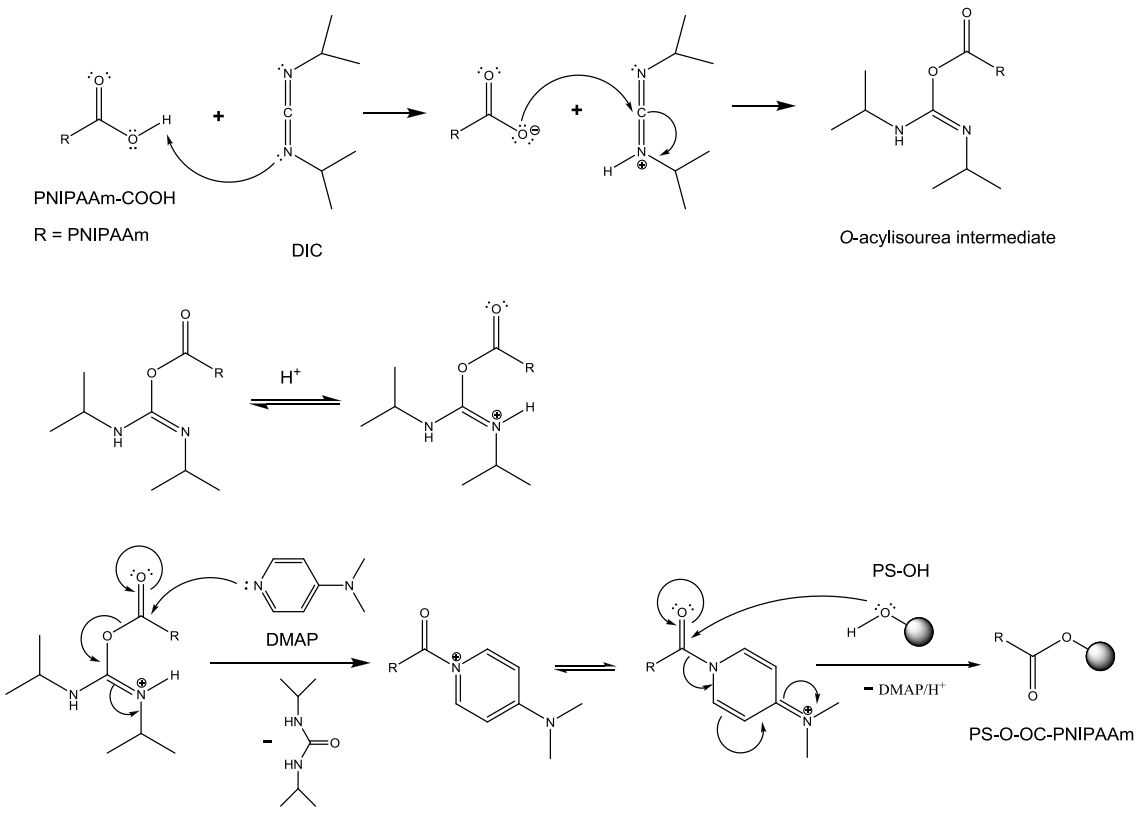


Figure 3.9 The mechanism of the conjugation of PNIPAAm-COOH polymer to the hydroxyl group of PS-OH bead using DIC as a coupling agent and DMAP as a catalyst.

The conjugation of PNIPAAm-COOH to the surface of PS-OH microspheres was confirmed by FTIR spectroscopy. The FTIR spectrum (Figure **3.10**) of PS-O-OC-PNIPAAm beads shows the peaks characteristic of PNIPAAm at 1640 cm^{-1} (amide I bond, arising from C=O stretching and little C-N stretching) and 1550 cm^{-1} (amide II bond, arising from N-H bending and C-N stretching), which were absent in the FTIR spectrum of unmodified PS-OH beads. In addition, the covalent ester bond connecting PNIPAAm-COOH and PS-OH bead was also confirmed by the peak at 1735 cm^{-1} (ester C=O stretching). Similarly, the preparation of PS-CO-O-PNIPAAm, PS-NH-OC-PNIPAAm and PS-CO-NH-PNIPAAm were confirmed by the peaks characteristic of PNIPAAm grafted to the particle surfaces (Appendix **B**: Figure **B.2** and **B.3**). It is worth mentioning that, in the spectra of PS-NH-OC-PNIPAAm and PS-CO-NH-PNIPAAm,

the signals of covalent amide bond connecting PNIPAAm and particles were overlapped with these of amide groups of modified PNIPAAm.

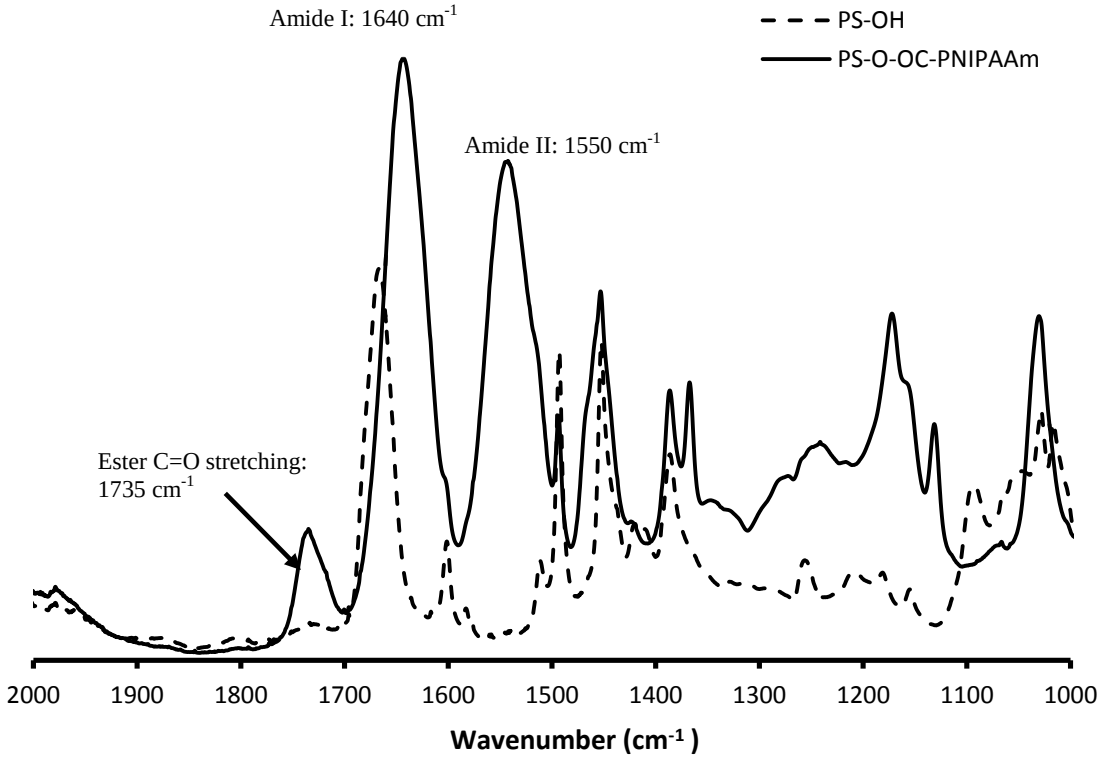


Figure 3.10 FTIR spectra of PS-OH and PS-O-OC-PNIPAAm microspheres.

The grafting density of PNIPAAm-COOH (M) on the PS-OH microsphere was regulated by varying the feed amount of PNIPAAm-COOH (M) (M_n=10938, PD=1.78). Between 0 – 4.5 g, increasing the amount of PNIPAAm-COOH polymer leads to increasing grafting density onto the PS-OH bead, but using more than 3.0 g does not produce any further increase (Table **3.5**). This is thought to be mainly due to the steric hindrance caused by the already grafted polymer chains. When the grafting density of PNIPAAm reached at about 27 μmol/g, unreacted PNIPAAm-COOH chains were not able to diffuse through the existing polymer layer to reach -OH groups on the microsphere surface.

Bead code[a]	Feed amount of PNIPAAm-COOH (g/50 mL)	Nitrogen content (wt%)	Grafted amount of PNIPAAm (mg/g)	Grafted density of PNIPAAm (μmol/g)
PS-OH	0	1.16 ±0.04	0	0
PS-O-OC-PNIPAAm-0.1	0.1	1.61 ±0.02	40.1 ±4.3	3.7 ±0.4
PS-O-OC-PNIPAAm-0.3	0.3	2.96 ±0.03	160.6 ±5.3	14.7 ±0.5
PS-O-OC-PNIPAAm-0.5	0.5	3.26 ±0.14	187.4 ±10.0	17.1 ±0.9
PS-O-OC-PNIPAAm-1.5	1.5	3.90 ±0.18	243.9 ±15.1	22.3 ±1.4
PS-O-OC-PNIPAAm-3.0	3.0	4.30 ±0.32	280.2 ±27.6	25.6 ±2.5
PS-O-OC-PNIPAAm-4.5	4.5	4.53 ±0.25	300.8 ±19.6	27.5 ±1.8
PS-O-OC-PNIPAAm-6.0	6.0	4.48 ±0.08	296.0 ±7.8	27.1 ±0.7
PS-O-OC-PNIPAAm-9.0	9.0	4.51 ±0.23	298.9 ±23.2	27.3 ±2.1

a: Abbreviated as PS-O-OC-PNIPAAm-X, where X represents the feed concentration of PNIPAAm-COOH (M)

b: The data were expressed as the mean ± SD; n=3

Table 3.5 Characterization of PS-O-OC-PNIPAAm beads with various amounts and densities of grafted PNIPAAm

The surface morphology of unmodified and modified microspheres was characterized by SEM. Figure **3.11** represents the SEM micrographs of unmodified PS-OH beads and modified PS-O-OC-PNIPAAm beads. Similar small patches of raised material were found on both the unmodified beads (as purchased) as well as on the modified beads (Figure **3.11** a&c – multiple beads). The modification process was not seen to affect the smooth surface of the beads. Similar results were obtained for other unmodified and modified beads (Appendix **D**: Figure **D.1** and **D.2**).

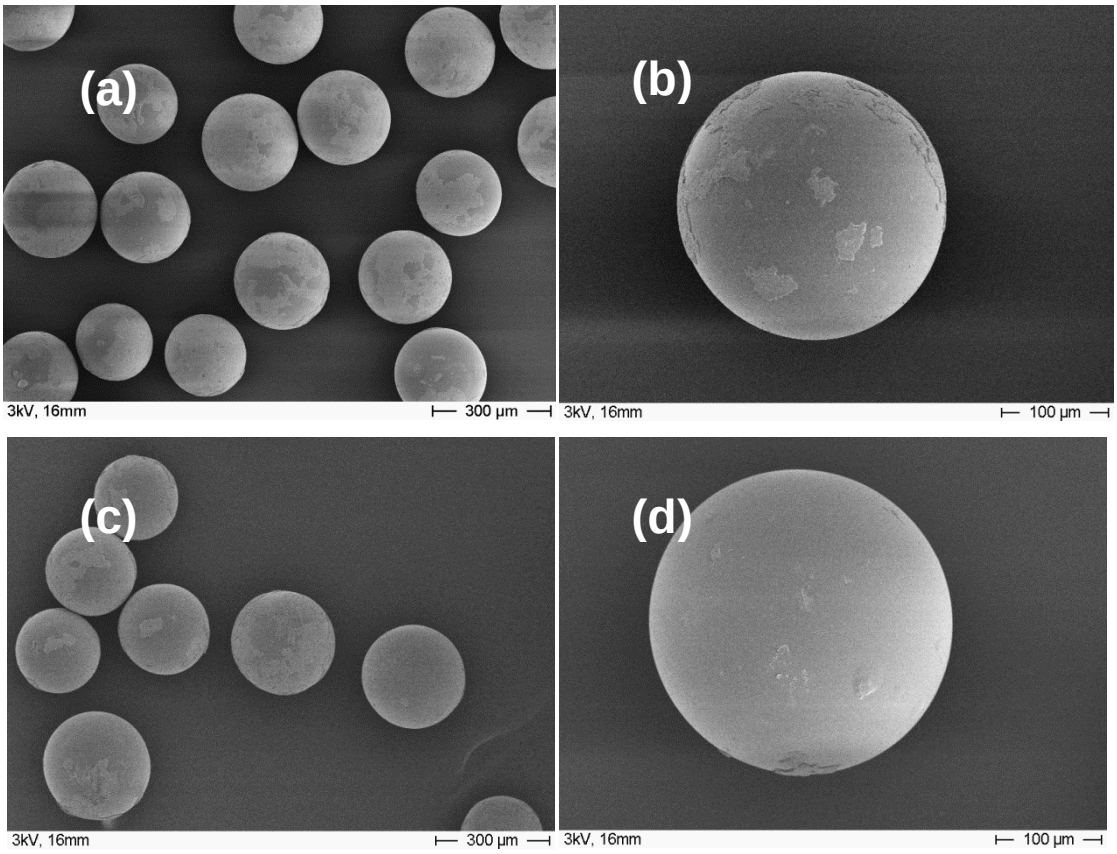


Figure 3.11 SEM characterization of (a) & (b) unmodified PS-OH microspheres, (c) & (d) PS-O-OC-PNIPAAm microspheres

3.3.4 Synthesis of PNIPAAm copolymers

Apart from end-functionalization of PNIPAAm via chain transfer polymerization, functional groups can also be introduced to PNIPAAm mid-chain by co-polymerization. In this study, carboxyl and amino groups were incorporated to PNIPAAm via radical copolymerization of NIPAAm with AAc and AAm respectively (Figure **3.12**). Copolymers with various carboxyl group or amino group contents were prepared by changing the feed mole ratio of AAc or AAm to NIPAAm. The M_n, M_w and polydispersity of the resulting copolymers were determined by HPLC (Table **3.6** and **3.7**). In comparison with PNIPAAm-COOH, PNIPAAm copolymers have much larger molecular weight and polydispersity.

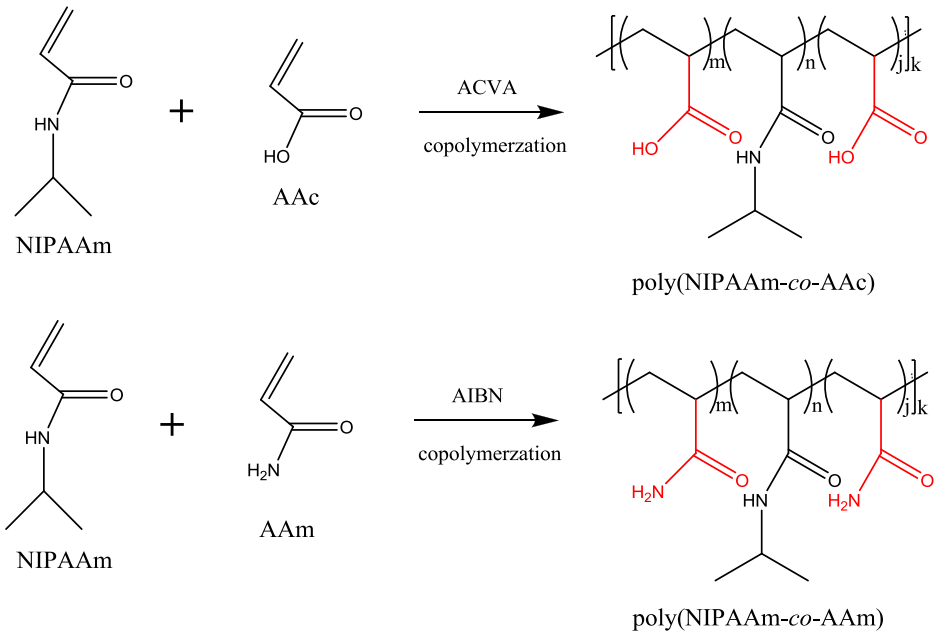


Figure 3.12 Introduction of carboxyl or amino groups to PNIPAAm through copolymerization

Sample code[a]	[AAc]/[NIPAAm] (mol/mol)	M_n	M_w	Polydispersity (M_w/M_n)
poly(NIPAAm-*co*-AAc-1%)	1/100	61013	214197	3.51
poly(NIPAAm-*co*-AAc-2%)	2/100	59378	177333	2.99
poly(NIPAAm-*co*-AAc-3%)	3/100	46185	156528	3.39
poly(NIPAAm-*co*-AAc-5%)	5/100	49627	166581	3.36
poly(NIPAAm-*co*-AAc-10%)	10/100	73105	253560	3.47

a: Abbreviated as poly(NIPAAm-co-AAc-X%), where X% represents the mole ratio of AAc to NIPAAm.

Table 3.6 The molecular weight and polydispersity of poly(NIPAAm-*co*-AAc) with various AAc contents.

Sample code[a]	[AAm]/[NIPAAm] (mol/mol)	M_n	M_w	Polydispersity (M_w/M_n)
poly(NIPAAm-*co*-AAm-5%)	5/100	61033	196938	3.23
poly(NIPAAm-*co*-AAm-10%)	10/100	59502	177210	2.98
poly(NIPAAm-*co*-AAm-15%)	15/100	66021	230271	3.49
poly(NIPAAm-*co*-AAm-20%)	20/100	49447	140860	2.85

a: Abbreviated as poly(NIPAAm-co-AAm-X%), where X% represents the mole ratio of AAm to NIPAAm.

Table 3.7 The molecular weight and polydispersity of poly(NIPAAm-*co*-AAm) with various AAm contents.

To confirm the incorporation of AAc or AAm units to the copolymers, FTIR spectroscopy and ^{1}H-NMR spectroscopy were carried out. Figure **3.3 (d)** shows the FTIR spectrum of poly(NIPAAm-*co*-AAc-10%) copolymer. The absence of peaks characteristic of the vinyl group in the spectrum indicates the polymerization has taken place. The C=O stretching signal assigned to the -COOH group of AAc moieties is observed at 1705 cm^{-1}, which is absent in the spectrum of PNIPAAm homopolymer (Figure **3.3 b**). This confirmed the presence of AAc moieties were successfully introduced to the poly(NIPAAm-*co*-AAc) copolymer. Figure **3.13** and **3.14** show the ^{1}H-NMR spectra of AAc monomer and poly(NIPAAm-*co*-AAc-10%). In the spectra of AAc, the signals around 5.8-6.5 ppm are assigned to CH_2=CH-. On the other hand, in the poly(NIPAAm-*co*-AAc-10%) spectrum, the absence of signals attributed to vinyl monomers indicates successful polymerization. The signals around 1 ppm are assigned to –CH_3, the one around 4.0 ppm to –CH, and those around 1.6-2.1 ppm to –CH_2-CH-. The signal at 3.3 ppm is ascribed to the solvent. However, in both spectra, no signal attributed to –COOH group of AAc was observed (usually at 12.0 ppm) due to the possible hydrogen bonding and dilution effect. The polymerization of poly(NIPAAm-*co*-AAm) was confirmed in a similar way (Appendix **C**: Figure **C.3** and **C.4**). However, the presence of –NH_2 group of AAm units in the copolymer was indirectly confirmed by successful DIC/DMAP coupling (see section **3.3.6**), because both FTIR and ^{1}H-NMR spectra of poly(NIPAAm-*co*-AAm) failed to show peak characteristic of –NH_2 group of AAm unites.

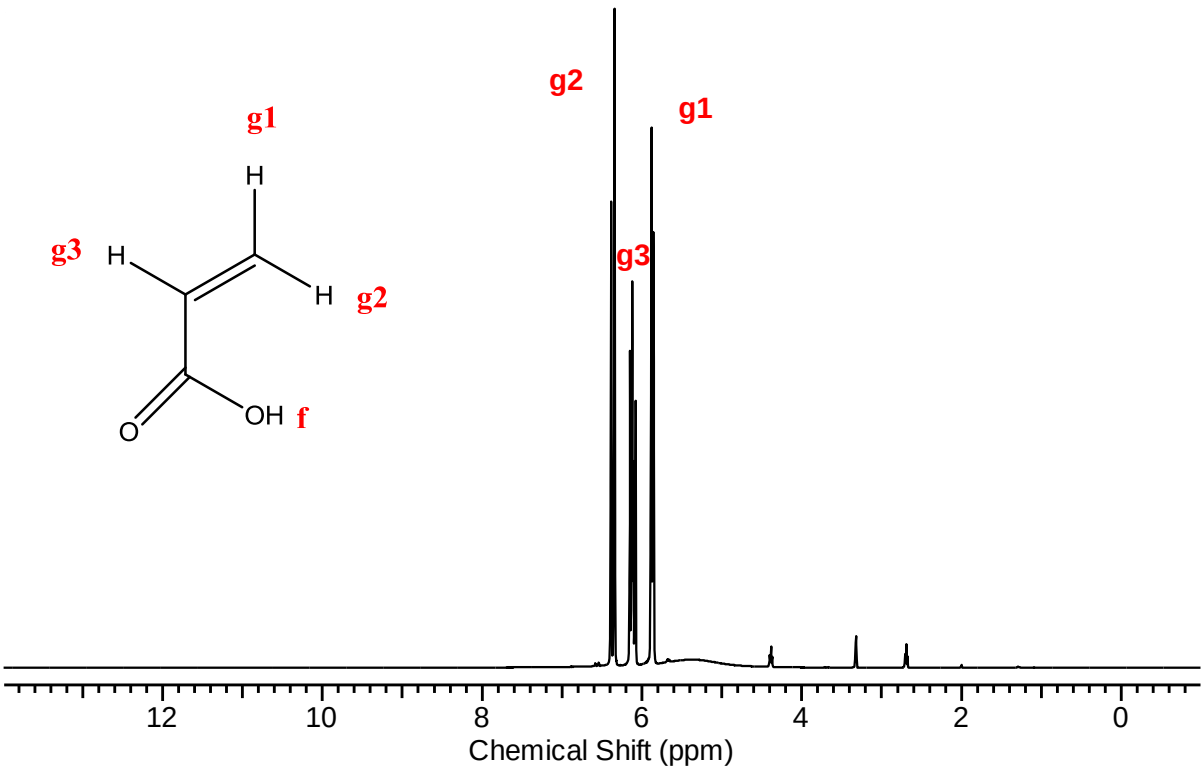


Figure 3.13 ^{1}H-NMR spectrum of AAc monomer

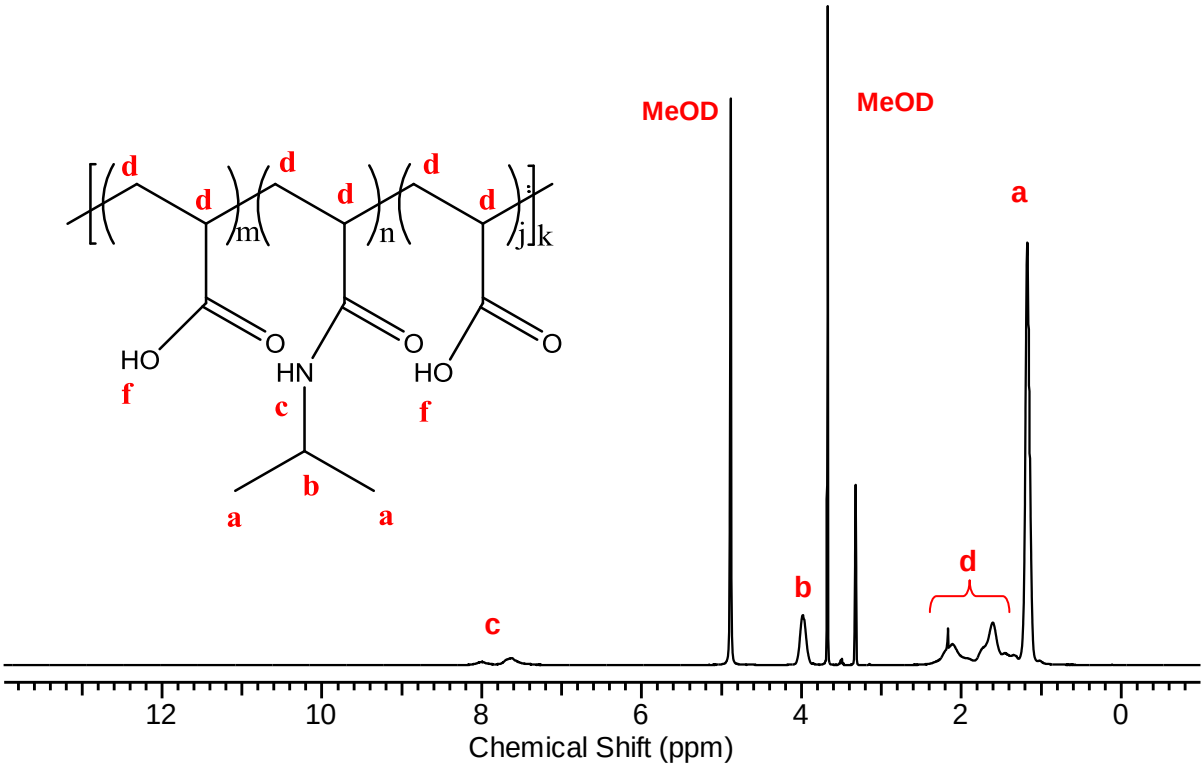


Figure 3.14 ^{1}H-NMR spectrum of P(NIPAAm-*co*-AAc-10%)

3.3.5 Phase transition of PNIPAAm copolymers

The series of poly(NIPAAm-*co*-AAc) and poly(NIPAAm-*co*-AAm) copolymer samples in aqueous solution (0.5 wt%, PH=7.4) was examined for optical absorbance change at various temperatures (Figure **3.15** and **3.16**). All copolymers demonstrated readily detectable phase transition behavior. PNIPAAm homopolymer demonstrated thermo-responsive properties and phase transition at 29 ℃. However, LCST of poly(NIPAAm-*co*-AAc) and poly(NIPAAm-*co*-AAm) copolymers considerably shifted to higher temperature and the temperature-sensitivity was decreased with increasing the AAc and AAm contents respectively. This is because the electrostatic repulsion or hydrophilicity of ionic or polar moieties prevents the intermolecular hydrophobic interaction and consequent aggregation of polymer chain (Aoyagi et al. 2000). The magnitude of this effect depends on the fraction of ionic or polar unit in the copolymer. Only the copolymers with LCST below 37 ℃ can be applied to the preparation of thermo-responsive microcarriers. Therefore, poly(NIPAAm-*co*-AAc-1%) (LCST = 32.5 ℃) and poly(NIPAAm-*co*-AAm-10%) (LCST = 34.5 ℃) were used for the preparation of looped PNIPAAm and double layer looped PNIPAAm grafted microsphere.

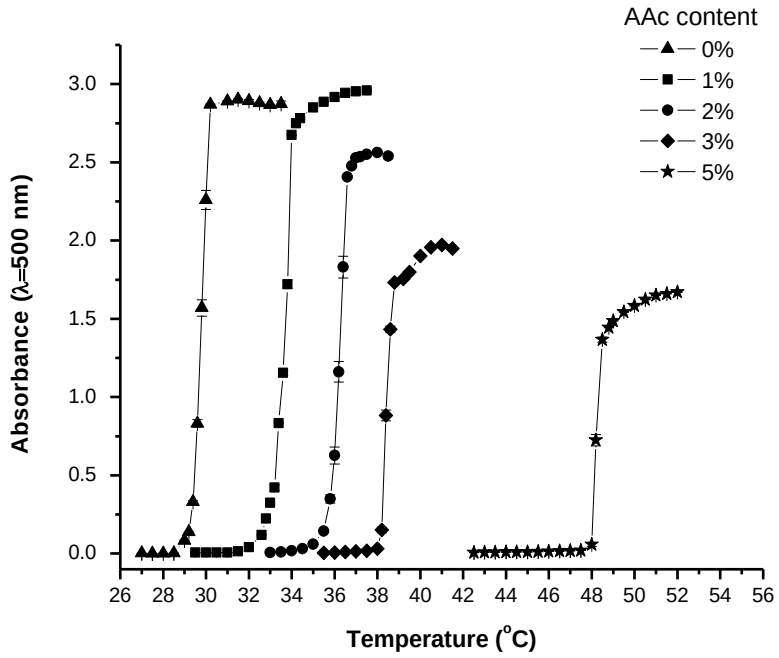


Figure 3.15 Phase transition profiles of poly(NIPAAm-*co*-AAc) with various AAc contents in pH 7.4 PBS at 500nm. Copolymer details refer to Table **3.6.**

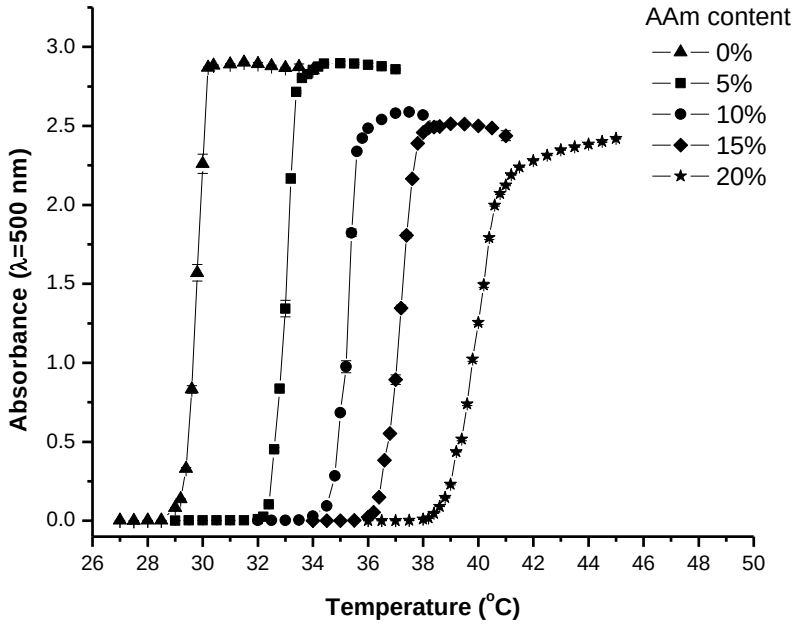


Figure 3.16 Phase transition profiles of poly(NIPAAm-*co*-AAm) with various AAm contents in pH 7.4 PBS at 500nm. Copolymer details refer to Table **3.7.**

3.3.6 Synthesis of looped PNIPAAm and double-layer looped PNIPAAm grafted microsphere

da Silva et al. (2007) proposed that, apart from molecular weight and grafting density, the molecular architecture of grafted PNIPAAm may also affect the adsorption of adhesive protein and subsequent cell attachment. Therefore, it is necessary to investigate the preparation of thermo-responsive microcarriers with various molecular architectures of grafted PNIPAAm. Takei (1994) prepared thermo-responsive surface with looped PNIPAAm molecular architecture by grafting poly(NIPAAm-*co*-AAc) copolymer to amino group modified surface. In this study, a similar strategy was used to graft poly(NIPAAm-*co*-AAc) copolymer to PS-OH microspheres through esterification mediated by DIC and DMAP (Figure **3.17**). Poly(NIPAAm-*co*-AAc-1%) copolymer was used for the modification, because copolymers with higher AAc content exhibited LSCT around or above 37 ℃, leading to the incompetence for the cell culture application of the resulting microcarrier. After conjugation, it is appropriate to consider the molecular architecture of the grafted polymer as "looped chain" due to the multi-point attachment between carboxyl groups on poly(NIPAAm-*co*-AAc) and hydroxyl groups on the PS-OH beads. FTIR spectroscopy was used to confirm the conjugation of poly(NIPAAm-*co*-AAc) to the surface of PS-OH microspheres (Figure **3.18**). The FTIR spectrum of the modified particles shows the peaks characteristic of PNIPAAm at 1640 cm^{-1} (amide I bond, arising from C=O stretching and little C-N stretching) and 1550 cm^{-1} (amide II bond, arising from N-H bending and C-N stretching), which were absent in the FTIR spectrum of unmodified PS-OH beads. Moreover, the covalent ester bond connecting poly(NIPAAm-*co*-AAc) and PS-OH bead was confirmed by the peak at 1735 cm^{-1} (ester C=O stretching). Also, the peak at 1705 cm^{-1} (carboxyl C=O stretching)

indicates the existence of residual –COOH groups on the grafted poly(NIPAAm-*co*-AAc).

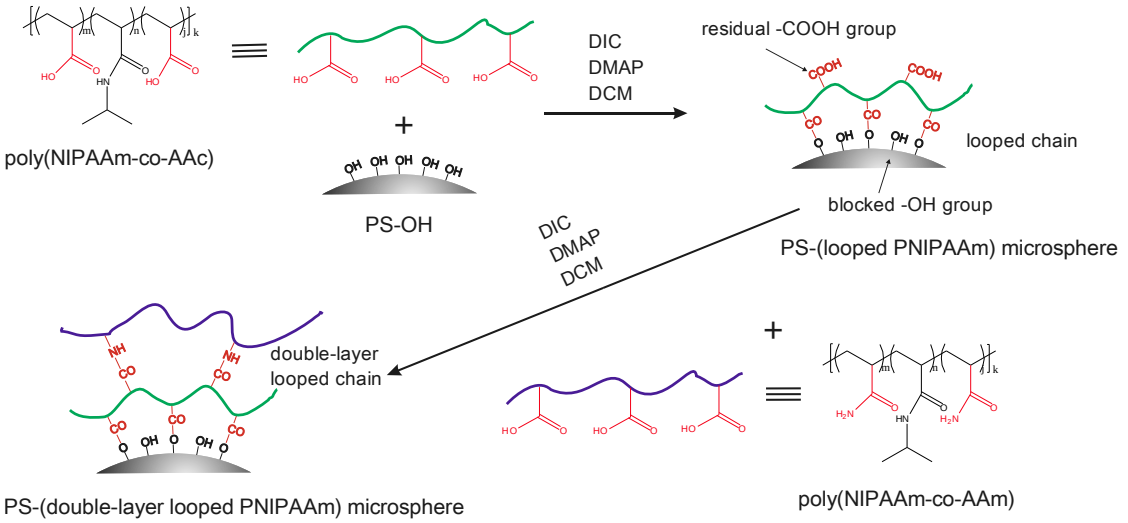


Figure 3.17 Synthesis of looped PNIPAAm and double-layer looped PNIPAAm grafted microsphere

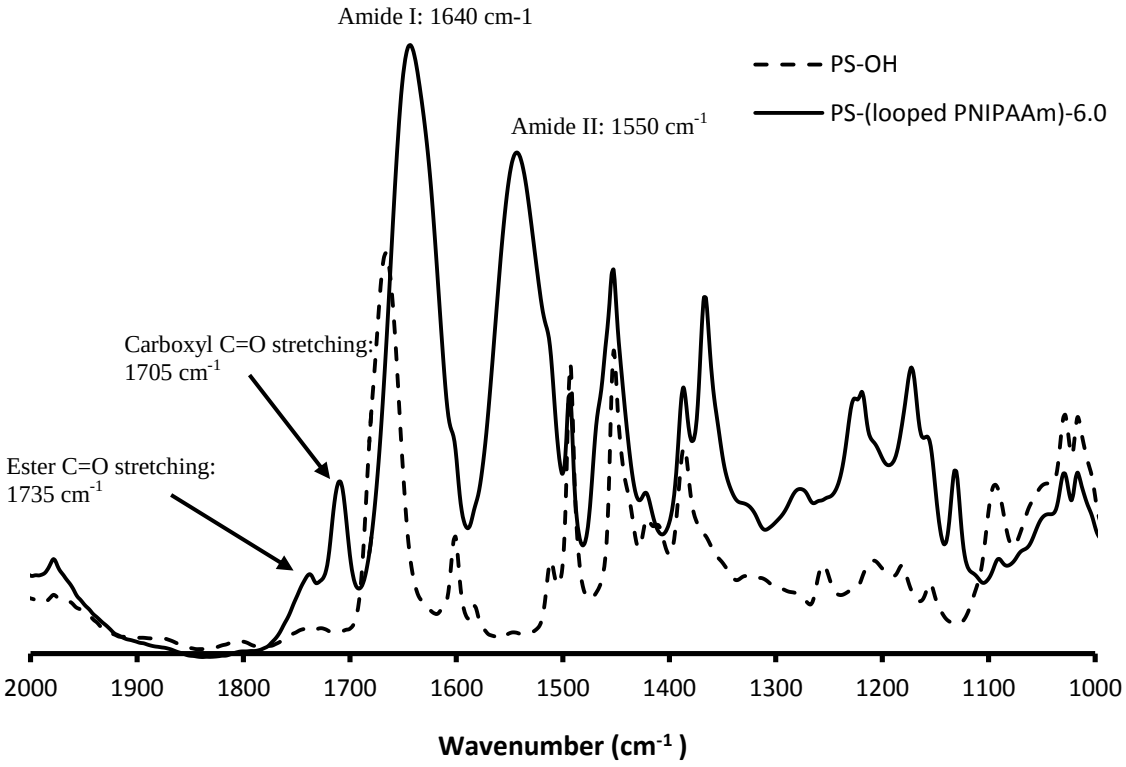


Figure 3.18 FTIR spectra of PS-OH and PS-(looped PNIPAAm)-6.0 microsphere

The grafted amount of poly(NIPAAm-*co*-AAc) on the PS-OH microsphere was regulated by varying the feed amount of poly(NIPAAm-*co*-AAc-1%) (M_n=61013, PD=3.51) (Table **3.8**). The maximum grafted amount of the copolymer on the PS-(looped PNIPAAm) particles was around 220 mg/g, which is less than that of PNIPAAm-COOH (300 mg/g) on the PS-O-OC-PNIPAAm particles. This is because the relatively larger molecular weight of poly(NIPAAm-*co*-AAc) copolymer and the looped chain molecular architecture lead to the increased effect of steric hindrance. The conjugation between the carboxyl groups in the copolymer mid-chain and the hydroxyl groups on the surface is a random process. The unreacted hydroxyl groups between the conjugating points might be blocked by the looped PNIPAAm chains and it is difficult for free copolymer chains to reach these blocked hydroxyl groups. Moreover, the residual negatively charged carboxyl groups in the copolymers might also cause Coulombic repulsion between the grafted copolymers and free copolymers in solvent. These issues increased the effect of steric hindrance caused by the existing polymer film.

Poly(NIPAAm-*co*-AAm) copolymer was introduced onto the poly(NIPAAm-*co*-AAc) grafted microspheres (PS-(looped PNIPAAm)-3.0) by utilizing residual carboxyl groups on the grafted poly(NIPAAm-*co*-AAc) copolymer. The introduction of poly(NIPAAm-*co*-AAm) (M_n=59502, PD=2.98) copolymer was confirmed by the increase of nitrogen content of the resulting microspheres. The molecular architecture of grafted PNIPAAm on the resulting microspheres was considered to be double layer looped chains (Figure **3.17**). In comparison with the single-layer structure, double-layer structure is considered to have more chain mobility and degree of freedom, because the second layer was grafted on the first layer of PNIPAAm copolymer rather than solid substrate. This might affect the magnitude and sensitivity of thermally induced collapse of the grafted PNIPAAm.

Bead code[a]	Feed amount of poly(NIPAAm-*co*-AAc) (g/50 mL)	Nitrogen content (wt%)[b]	Grafted amount of PNIPAAm (mg/g)
PS-OH	0	1.16 ±0.04	0
PS-(looped PNIPAAm)-0.1	0.1	1.42 ±0.06	22.9 ±1.4
PS-(looped PNIPAAm)-0.2	0.2	1.96 ±0.14	71.1 ±14.2
PS-(looped PNIPAAm)-0.5	0.5	2.21 ±0.04	93.7 ±3.1
PS-(looped PNIPAAm)-1.5	1.5	3.71 ±0.03	227.5 ±4.6
PS-(looped PNIPAAm)-3.0	3.0	3.61 ±0.09	218.9 ±7.7
PS-(looped PNIPAAm)-6.0	6.0	3.74 ±0.05	229.6 ±6.7
PS-(double-layer looped PNIPAAm)	3.0 g poly(NIPAAm-*co*-AAc-1%) 3.0 g poly(NIPAAm-*co*-AAm-10%)	4.06 ±0.06	258.5 ±8.1

a: Abbreviated as PS-(looped PNIPAAm)-X, where X represents the feed amount of poly(NIPAAm-*co*-AAc).

b: The data were expressed as the mean ± SD; n=3

Table 3.8 Characterization of PS-(looped PNIPAAm) or PS-(double-layer looped PNIPAAm) beads with various amounts of grafted PNIPAAm copolymer.

3.4 Summary

In this study, end-functionalized PNIPAAm polymers were synthesised via chain transfer polymerization. Carboxyl (-COOH), hydroxyl (-OH) and amino ($-NH_2$) end groups were incorporated to PNIPAAm polymer by using MPA, MetOH and MEA as chain transfer agents respectively. The molecular weight of the resulting end-functionalized PNIPAAm can be regulated by change the feed concentration of chain transfer agents. It was found that the phase transition behaviour of the resulting PNIPAAm-COOH was slightly affected by its molecular weight. PNIPAAm-COOH with smaller molecular weight demonstrated a higher phase transition temperature, decreased temperature-sensitivity and perhaps reduced magnitude of aggregation. Then, the end-functionalized PNIPAAm polymers were conjugated to various surface-functionalized particles via esterification or amidation. PNIPAAm-COOH was grafted

to hydroxyl groups on PS-OH microspheres and conversely, PNIPAAm-OH was grafted to carboxyl groups on PS-COOH microspheres via esterification. Similarly, PNIPAAm-COOH was grafted to the amino groups on PS-NH_2 microspheres, and conversely PNIPAAm-NH_2 was grafted to carboxyl groups on PS-COOH microspheres via amidation. The grafting density of PNIPAAm-COOH (M) on the PS-OH microsphere can be regulated by varying the feed amount of PNIPAAm-COOH (M) (M_n=10938, PD=1.78). The achievable grafting density of PNIPAAm was about 27 μmol/g.

The functional groups can also be introduced to PNIPAAm mid-chain by co-polymerization. In this case, carboxyl and amino groups were incorporated to PNIPAAm via radical copolymerization of NIPAAm with AAc and AAm respectively. Copolymers with various contents of carboxyl group or amino group were prepared by changing the feed mole ratio of AAc or AAm to NIPAAm. The phase transition temperatures of the copolymers were significantly increased with increasing the contents of the carboxyl group or amino group. The poly(NIPAAm-*co*-AAc) (M_n=61013, PD=3.51) copolymer was conjugated to the PS-OH microspheres forming a looped chain grafted surface. The grafted amount of poly(NIPAAm-*co*-AAc) on the PS-OH microsphere was regulated by varying the feed amount of poly(NIPAAm-*co*-AAc). However, the achievable grafted amount of the copolymer on the PS-(looped PNIPAAm) particles was less than that of PNIPAAm-COOH on the PS-O-OC-PNIPAAm particles, due to the increased effect of steric hindrance. Furthermore, the poly(NIPAAm-*co*-AAm-10%) (M_n=59502, PD=2.98) was conjugated to the looped chain grated microspheres forming a double-layer looped chain architecture.

The data presented in this chapter shows that PNIPAAm modification of the microspheres has been successful. The thermo-responsive character of such material

cannot, however, be easily measured by contact angle, and in any case, has normally been assessed in the literature by direct measurement of cell carrying capacity. The work undertaken to make this assessment on the modified microspheres is described in detail in Chapter 6.

4 ‘Grafting-from’ technique for microsphere modification

4.1 Introduction

As shown in Chapter 3, the ‘grafting-to’ technique was used to establish a chemical bond between the chain end of PNIPAAm molecules and the microsphere surfaces. Various end-functionalized PNIPAAm were synthesized and reacted with appropriate surface sites. However, it was reported that this method is intrinsically limited to low grafting densities due to a strong kinetic hindrance caused by the already deposited polymer chains (Prucker and Rühe 1998b). Once the surface becomes significantly covered, additional polymer chains have to diffuse through the existing polymer layer to reach the surface before they can be immobilised (Burtovyy et al. 2007).

A more promising approach for the preparation of covalently attached PNIPAAm monolayers is given by the “grafting-from” technique. It usually consists of two steps: immobilization of a polymerization initiator onto the surface of microspheres, and subsequent growth of PNIPAAm chains directly from the first immobilized initiators. As the growing chain only reacts with monomers or oligomers, the process is less affected by steric hindrance and leads to higher grafting density. Moreover, the grafting density of PNIPAAm chain can be regulated by changing the grafting density of immobilized initiator. In this study, two polymerization strategies were used, namely 1) conventional radical grafting polymerization and 2) atom transfer radical polymerization (ATRP). In the first strategy, an azo-initiator, ACVA, was first

immobilized onto polystyrene microspheres. The grafting density of ACVA can be regulated by changing the feed amount of ACVA. The subsequent polymerization of NIPAAm was initiated by thermal decomposition of ACVA, and the resulting chain molecular weight was found to be increased with increasing feed concentration of NIPAAm monomers. Using this strategy, three types of PNIPAAm molecular architecture were prepared, namely 1) linear PNIPAAm chain, 2) cross-linked PNIPAAm hydrogel and 3) branched PNIPAAm chain. In the second strategy, an ATRP initiator, 2-bromopropionyl bromide, was grafted onto cross-linked dextran microspheres. The grafting density of ATRP initiator can be also regulated by changing the feed amount of the ATRP initiator. PNIPAAm chains were then grown from the immobilized 2-bromopropionyl groups using aqueous ATRP. The effect of the grafting density on the molecular weight of the resulting PNIPAAm was also studied.

4.2 Materials and methods

4.2.1 Materials

1,4-Dioxane (99.8%), 4,4′-azobis(4-cyanovaleric acid) (ACVA, ≥98.0%), methanol (HPLC grade, ≥99.9%), (hydroxymethyl)polystyrene microspheres (PS-OH, 70-90 mesh, -OH group content: 2.0-3.0 mmol/g), *N*,*N*′-diisopropylcarbodiimide (DIC, 99%), 4-(dimethylamino)pyridine (DMAP, 99%) dichloromethane (DCM, ≥99.9%), 2-hydroxylethyl acrylate (HEA; 96%), styrene (≥99%), triethylamine (99%), 2-bromopropionyl bromide (97%), copper (I) bromide (CuBr, 99.999%), 2,2'-bipyridyl (≥99%), and dimethyl sulfoxide (DMSO; ≥99.9%) were purchased from Sigma-Aldrich (UK) and used as received. Sephadex® G-50 microspheres (coarse, wet particle size:

200 – 610 μm) and Cytodex®-1 microcarriers (wet particle size: 131 – 220 μm) were purchase from Amersham Bioscience (Sweden).

N-Isopropylacrylamide (NIPAAm, 97%, Sigma-Aldrich) was purified by recrystallisation from hexane/toluene followed by filtration and drying (see section **3.2.1**). Deionised water (DI water) used in this study was obtained from an ultrapure water purification system (Elix®, Millipore).

4.2.2 Conventional radical grafting polymerization

4.2.2.1 Azo-initiator immobilization

ACVA was immobilized onto PS-OH microspheres through esterification. A typical procedure (e.g. PS-ACVA-0.84 in Table **4.1**) was as follows: PS-OH microspheres (1 g), ACVA (0.84 g, 3 mmol) and DMAP (0.224 g, 1.8 mmol) were added to a round bottom flask containing 50 mL DCM. DIC (0.93 mL, 0.758g, 6 mmol) was then added to the mixture. The reaction was conducted at room temperature for 24 h. The resulting beads were washed with methanol thoroughly and dried by vacuum suction for 1 h. The dried microspheres were stored at 4 ℃ before use.

Bead code[a]	PS-OH bead (g)	ACVA (g/50 mL DCM)	DIC (mL)	DMAP (g)
PS-ACVA-0.05	1.0	0.05	0.06	0.015
PS-ACVA-0.10		0.10	0.12	0.030
PS-ACVA-0.21		0.21	0.23	0.060
PS-ACVA-0.42		0.42	0.46	0.112
PS-ACVA-0.84		0.84	0.93	0.224
PS-ACVA-1.68		1.68	1.86	0.448
PS-ACVA-3.36		3.36	3.92	0.900

a: Abbreviated as PS-ACVA-X, where X represents the feed amount of ACVA

Table 4.1 Immobilization of ACVA to PS-OH microspheres

4.2.2.2 Surfaced-initiated radical grafting polymerization

The free radical grafting polymerization was initiated from the azo-initiators immobilized on the PS-OH microsphere surface by thermo-decomposition. A typical procedure (e.g. PS-ACVA-1.68-PNIPAAm-9 in Table **4.2**) was as follows: NIPAAm (9 g, 0.08mol) and ACVA-immobilized microspheres (PS-ACVA-1.68, 0.5 g) were added in dioxane (50 mL), and the mixture was deoxygenated by nitrogen bubbling for 1 h at room temperature. The polymerization was then conducted at 70 ^{o}C for 24 h under nitrogen atmosphere. The resulting beads were washed with methanol thoroughly and dried by vacuum suction for 1 h. Similar experiments were performed by varying the feed amount of NIPAAm, while keeping all other quantities constant.

Bead code[a]	PS-ACVA-1.68 bead (g)	NIPAAm (g)	Dioxane (mL)
PS-ACVA-1.68-PNIPAAm-0.0	0.5	0.0	50
PS-ACVA-1.68-PNIPAAm-0.5		0.5	
PS-ACVA-1.68-PNIPAAm-1.5		1.5	
PS-ACVA-1.68-PNIPAAm-3.0		3.0	
PS-ACVA-1.68-PNIPAAm-6.0		6.0	
PS-ACVA-1.68-PNIPAAm-9.0		9.0	

a: Abbreviated as PS-ACVA-X-PNIPAAm-Y, where X represents the feed amount of ACVA in the initiator immobilization step, and Y represents the feed amount of NIPAAm in the polymerization step.

Table 4.2 Surfaced-initiated radical grafting polymerization

4.2.2.3 Preparation of microspheres grafted with PNIPAAm hydrogel

NIPAAm (2.0 g, 0.018 mol), MBAAm (0.1 g, 0.65 mmol) and ACVA-immobilized microspheres (PS-ACVA-1.68, 0.5 g) were added in dioxane (60 mL) and the mixture was deoxygenated by nitrogen bubbling for 1 h at room temperature. Then, the polymerization was conducted at 70 ^{o}C for 24 h under nitrogen atmosphere. The

resulting beads were washed with methanol thoroughly and dried by vacuum suction for 1 h.

4.2.2.4 Preparation of microspheres grafted with comb-type PNIPAAm hydrogel

4.2.2.4.1 Preparation of PNIPAAm macromonomer

PNIPAAm macromonomer (i.e., vinyl-terminated PNIPAAm) was synthesized by conjugating PNIPAAm-COOH with HEA through esterification. PNIPAAm-COOH (XS) (10.0 g), HEA (4.0 g) and DMAP (0.448 g, 3.6 mmol) were added to 50 mL DCM. DIC (1.96 mL, 12 mmol) was then added to the mixture. The reaction was kept under stirring at room temperature for 24 h. The solution was then concentrated *in vacuo* using a rotary evaporator (Büchi Rotavapor, FR-114) before 40 mL dioxane was added to the concentrated solution. The resulting PNIPAAm macromonomers were precipitated three times into an excess of diethyl ether from dioxane. Thereafter, the PNIPAAm macromonomers were dried by vacuum suction for 1 h at room temperature.

4.2.2.4.2 Preparation of comb-type hydrogel grafted microspheres

NIPAAm (3.0 g, 0.027 mol), MBAAm (0.3 g, 1.95 mmol), PNIPAAm macromonomer (0.5 g, about 0.2 mmol) and ACVA-immobilized microspheres (PS-ACVA-1.68, 0.5 g) were added in dioxane (60 mL) and the mixture was deoxygenated by nitrogen bubbling for 1 h at room temperature. The polymerization was then conducted at 70 ^{o}C for 24 h under nitrogen atmosphere. The resulting beads were washed with methanol thoroughly and dried by vacuum suction for 1 h.

4.2.2.5 Preparation of microspheres grafted with branched PNIPAAm

4.2.2.5.1 Synthesis of poly(2-hydroxylethyl acrylate) grafted polystyrene (PS-PHEA) microspheres

HEA (4 g, mol) and ACVA-immobilized microspheres (PS-ACVA-1.68, 0.5 g) were added in dioxane (50 mL), and the mixture was deoxygenated by nitrogen bubbling for 1 h at room temperature. The polymerization was then conducted at 70 ^{o}C for 24 h under nitrogen atmosphere. The resulting beads were washed with methanol thoroughly and dried by vacuum suction for 1 h.

4.2.2.5.2 Synthesis of poly(styrene-co-HEA) grafted polystyrene (PS-PSHEA) microspheres

HEA (4 g, mol), styrene (1 g, 0.08mol) and ACVA-immobilized microspheres (PS-ACVA-1.68, 0.5 g) were added in dioxane (50 mL), and the mixture was deoxygenated by nitrogen bubbling for 1 h at room temperature. The polymerization was then conducted at 70 ^{o}C for 24 h under nitrogen atmosphere. The resulting beads were washed with methanol thoroughly and dried by vacuum suction for 1 h.

4.2.2.5.3 Synthesis of PNIPAAm branches via 'grafting-to' technique

PS-PHEA or PS-PSHEA microspheres (0.5 g), PNIPAAm-COOH (XS) (M_n=1857, PD=2.26) (3.0 g) and DMAP (0.224 g, 1.8 mmol) were added to 50 mL DCM. DIC (0.93 mL, 0.758g, 6 mmol) was then added to the mixture. The reaction was kept under stirring at room temperature for 24 h. The resulting PS-PHEA-PNIPAAm or PS-PSHEA-PNIPAAm microspheres were washed thoroughly with methanol, and dried with vacuum suction for 1 h.

4.2.2.5.4 Immobilization of ACVA moieties to PS-PHEA or PS-PSHEA microspheres

ACVA molecules were immobilized to the PS-PHEA or PS-PSHEA microspheres by esterification. PS-PHEA or PS-PSHEA microspheres (1 g), ACVA (1.68 g, 6 mmol) and DMAP (0.448 g, 3.6 mmol) were added to a round bottom flask containing 50 mL DCM. DIC (1.86 mL, 1.516 g, 12 mmol) was then added to the mixture. The reaction was conducted at room temperature for 24 h. The resulting beads (PS-PHEA-ACVA or PS-PSHEA-ACVA) were washed with methanol thoroughly and dried by vacuum suction for 1 h.

4.2.2.5.5 Synthesis of PNIPAAm branches via 'grafting-from' technique

PNIPAAm branches were grafted from the PS-PHEA-ACVA or PS-PSHEA-ACVA microspheres by surfaced-initiated radical grafting polymerization. NIPAAm (6.0 g, 0.053 mol) and PS-PHEA-ACVA or PS-PSHEA-ACVA microspheres (0.5 g) were added in dioxane (50 mL), and the mixture was deoxygenated by nitrogen bubbling for 1 h at room temperature. The polymerization was then conducted at 70 ^{o}C for 24 h under nitrogen atmosphere. The resulting beads (PS-PHEA-ACVA-PNIPAAm) or PS-PSHEA-ACVA-PNIPAAm) were washed with methanol thoroughly and dried by vacuum suction for 1 h.

4.2.3 Atom transfer radical polymerization (ATRP)

The method of Kim et al. (2003) was used for the preparation of thermo-responsive microcarriers through ATRP.

4.2.3.1 ATRP initiator immobilization

The microspheres (Sephadex® G-50 or Cytodex®-1) (1 g) were dried at 85 ℃ for 1 h under vacuum to eliminate the trace water. The dried microspheres were then suspended in 10 mL of DMSO containing 0.7 mL of triethylamine for 1 h. Subsequently, 2-bromopropionyl bromide (0.2 mL) was added dropwise to the suspension. The reaction was kept under stirring at room temperature for 1 h. The resulting initiator-immobilized microspheres were thoroughly washed with DMSO and methanol and dried by vacuum suction at room temperature for 1 h. For Sephadex® G-50 microspheres, similar experiments were performed by varying the amount of 2-bromopropionyl bromide (0.2 mL, 0.5 mL and 1mL) added to the suspension, while keeping all other quantities constant.

4.2.3.2 ATRP of NIPAAm

The initiator-immobilized microspheres (0.2 g), NIPAAm (4.5 g, 0.04 mol), CuBr (0.114 g, 0.8 mmol), and 2,2'-bipyridyl (0.250 g, 1.6 mmol) were added to a 50 ml round bottom flask and the mixture was degassed under vacuum to remove oxygen. Degassed water (10 ml) was prepared by applying alternative vacuum/nitrogen cycles and subsequently added to the round bottom flask. The reaction was then kept under stirring for 24 h at room temperature. The resulting microspheres were washed thoroughly with DI water and methanol, and stored in methanol at room temperature.

4.2.4 Characterizations and measurements

4.2.4.1 FTIR spectroscopy measurements

Fourier transform infrared (FTIR) spectra were recorded using a FTIR spectrometer (FTS 6000, BIO-RAD) equipped with attenuated total reflectance (ATR) setup (DuraSampl*IR* II^{TM}, SensIR Technologies). 200 scans were averaged to yield the spectra at a resolution of 4.0 cm^{-1}. Before collecting sample spectra, the background spectrum was collected by measuring the response of the spectrometer without sample.

4.2.4.2 Combustion analysis

The mass percentages of C, H, N and Br of the unmodified and modified microspheres were tested by combustion analysis. The combustion analysis was conducted by MEDAC LTD (Surrey, UK).

4.2.4.2.1 Conventional radical grafting polymerization

The grafted amount (m_A) of ACVA on PS-OH bead surface was calculated from the increment in nitrogen content derived from the azo group and cyanide group of ACVA. It was calculated as follows:

$$m_A(\mathrm{mg/g}) = \frac{N_A\% - N_0\%}{N_{A,theory}\% - N_0\%} \times 10^3$$

where $N_A\%$ and $N_0\%$ represent the nitrogen contents in ACVA-modified and unmodified beads respectively, and $N_{A,theory}\%$ represents the theoretical nitrogen content of ACVA.

The grafting density (g_A) of ACVA on the PS-OH bead surface was calculated as follows:

$$g_A\ (\mu\text{mol/g}) = \frac{m_A}{M_{n,ACVA}} \times 10^3$$

where $M_{n,ACVA}$ represents the molecular weight of ACVA moiety.

The decomposition percentage (D%) of immobilized ACVA on PS-ACVA-1.68 beads was calculated as follows:

$$D\% = \frac{N_{A,1.68}\% - N_{d,1.68}\%}{g_{A,1.68}(3 \times N - 2 \times N \times N_{d,1.68}\% - N_{d,168}\% \times M_{n,CEA})} \times 100\%$$

where $g_{A,1.68}$ represents the grafting density of ACVA on the PS-ACVA-1.68 bead surface, $N_{A,1.68}$% represents the nitrogen content in PS-ACVA-1.68 beads, $N_{d,1.68}$% represents the nitrogen content in decomposed PS-ACVA-1.68 beads in the absence of NIPAAm monomer (i.e., PS-decomposed ACVA beads), N represents the atomic mass of nitrogen (=14), and $M_{n,CEA}$ represents the molecular weight of CEA (see Figure **4.4 (b)**).

The grafting density of PNIPAAm on the PS-OH bead surface was calculated as follows:

$$g_p\ (\mu\text{mol/g}) = g_{A,1.68} \times D\% \times R\%$$

where R% (=40%) represents the radical efficiency factor.

The grafted amount (m_p) of PNIPAAm on PS-ACVA bead surface was calculated as follows:

$$m_p(\text{mg/g}) = \frac{N_p\% - N_{d,1.68}\%}{N_{p,theory}\% - N_{d,1.68}\%} \times 10^3$$

where $N_p\%$ represents the nitrogen content in PNIPAAm grafted beads, and $N_{p,theory}\%$ represents the theoretical nitrogen content of PNIPAAm. The grafted amount of PNIPAAm on branched PNIPAAm grafted beads was calculated in a similar way.

The average molecular weight (M_n) of grafted PNIPAAm was calculated as follows:

$$M_n\ (\text{g/mol}) = \frac{m_p}{g_p \times 10^3}$$

4.2.4.2.2 ATRP

The grafting density (g_B) of 2-bromopropionyl bromide on Sephadex® G-50 bead surface was calculated as follows:

$$g_B(\text{mmol/g}) = \frac{Br\% - Br_0\%}{(Br_{theory}\% - Br_0\%) \times M_{n,initiator}} \times 10^3$$

where $Br\%$ and $Br_0\%$ represent the bromine contents in ATRP-initiator immobilized beads and unmodified beads respectively, $Br_{theory}\%$ represents the theoretical bromine content of 2-bromopropionyl moiety, and $M_{n,initiator}$ represents the molecular weight of 2-bromopropionyl moiety.

The grafted amount (m_p) of PNIPAAm on PNIPAAm-grafted Sephadex® G-50 bead surface was calculated as follows:

$$m_p(\text{mg/g}) = \frac{N_{p,ATRP}\% - N_{initiator}\%}{N_{p,theory}\% - N_{initiator}\%} \times 10^3$$

where $N_{p,ATRP}\%$ represents the nitrogen content in PNIPAAm grafted beads, $N_{initiator}\%$ represents the nitrogen content ATRP-initiator immobilized beads and $N_{p,theory}\%$ represents the theoretical nitrogen content of PNIPAAm

The average molecular weight (M_n) of grafted PNIPAAm was calculated as follows:

$$M_n \text{ (g/mol)} = \frac{m_p}{g_B}$$

4.2.4.3 SEM observations

The surface morphology of the unmodified and modified Sephadex® G-50 and Cytodex®-1 microspheres was observed by a SEM (Zeiss NVision 40) at an accelerating voltage of 5 kV. Before the SEM investigation, the samples were coated with platinum by sputtering. This investigation was kindly conducted by Dr. Fazlul Chowdhury (Nemaura Pharma Limited, Loughborough).

4.2.4.4 NMR measurements

^{1}H nuclear magnetic resonance (NMR) spectrum of PNIPAAm macromonomer was recorded on Bruker DQX400 (400 MHz) spectrometers at 27 ℃ using methanol-d_4 (Sigma-Aldrich) as a solvent. Chemical shifts (δH) were reported in parts per million (ppm) and were referenced to the residual protonated solvent peak.

4.3 Results and discussion

4.3.1 Conventional free radical grafting polymerization

4.3.1.1 Azo-initiator immobilization

ACVA is an azo compound containing carboxyl groups. It is a commonly used initiator for free radical polymerization. The immobilization of ACVA relies on a one-step esterification between the hydroxyl group on PS-OH microsphere surface and the carboxyl group of ACVA, using DIC as a coupling agent and DMAP as a catalyst (Figure **4.1**). In comparison with a stepwise generation of initiator monolayer, the one-step immobilization reaction leads to high grafting densities of the surface-immobilized initiator and consequently high grafting densities of the polymer (Prucker and Rühe 1998a). The immobilization was confirmed by FTIR spectroscopy. The FTIR spectrum (Figure **4.4 (b)**, Page **109**) of ACVA-modified beads (PS-ACVA) shows a signal for the ester groups (C=O stretching) at 1735 cm^{-1}, which was absent in the FTIR spectrum of unmodified beads (PS-OH). In order to regulate the grafting density of PNIPAAm chains growing from the immobilized ACVA moieties, it is necessary to control the grafting density of ACVA. Thus, several immobilization experiments were performed, in which the feed amount of ACVA (i.e., the starting ACVA/bead ratio) was

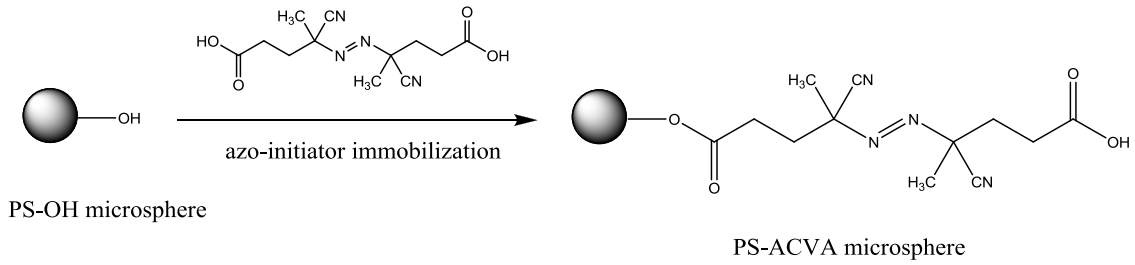


Figure 4.1 Immobilization of ACVA moieties to PS-OH microspheres

systematically varied. The grafting amounts and densities of the immobilized ACVA as determined by combustion analysis are summarized in Table **4.3**. The grafting density of ACVA on PS-OH microspheres was increased with increasing feed amount of ACVA in the immobilization reaction. Combustion analysis revealed that ACVA grafting onto the untreated bead surface occurred in a rapid linear fashion, with more than 650 μmol/g immobilized on the bead surface for the first 1500 μmol/g of feed concentration (Figure **4.2**). A saturation level was reached at 1500 μmol/g of ACVA feed concentration, and after this point, the density of ACVA increased at a much slower rate, with less than an extra 350 μmol/g immobilized onto the bead surface for next 10000 μmol/g of ACVA feed amount. The hydroxyl groups on PS-OH microspheres were consumed in the immobilization process. The content of hydroxyl group on PS-OH beads is about 2000-3000 μmol/g (manufacturer's data). However, in the case of PS-ACVA-0.42 (the saturation point), less than 35% of the hydroxyl groups were tethered with ACVA via esterification. The grafting density after this point was only slowly increased with ACVA feed amount. This indicates that the grafting density might be limited by the steric hindrance caused by the already immobilized ACVA moieties rather than the number of hydroxyl group on the PS-OH microspheres, as once the surface has become significantly covered, additional ACVA molecules, which were trying to reach the surface, have to diffuse through the existing layer of immobilized ACVA moieties. However, the grafting density of ACVA on PS-ACVA-0.42 microspheres already achieved around 682 μmol/g (180 mg/g). This number can be considered as a high grafting density in comparison with the numbers presented by relevant literature reports using similar methods (Prucker and Rühe 1998a; 1998b; Tang et al. 2012). Prucker and Rühe (1998a; 1998b) immobilized AIBN moieties to silica beads and achieved a grafting density of 550 μmol/g. Tang et al. (2012) immobilized

ACVA moieties to ZnO particles and achieved a grafted amount of 170 mg/g (647 μmol/g).

Bead code[a]	Feed amount of ACVA (g/50 mL)	Nitrogen content (wt%)[b]	Grafted amount of ACVA (mg/g)	Grafting density of ACVA (μmol/g)
PS-OH	0	1.16±0.04	0	0
PS-ACVA-0.05	0.05	1.22±0.06	2.6±2.8	9.8±10.6
PS-ACVA-0.10	0.10	2.11±0.09	41.1±3.9	156.3±15.1
PS-ACVA-0.21	0.21	3.62±0.14	106.1±6.2	402.8±23.4
PS-ACVA-0.42	0.42	5.32±0.17	179.5±7.2	681.7±27.3
PS-ACVA-0.84	0.84	5.65±0.13	194.0±5.7	736.7±21.5
PS-ACVA-1.68	1.68	6.18±0.10	216.7±4.4	823.2±16.8
PS-ACVA-3.36	3.36	6.72±0.29	240.3±12.5	912.6±47.3

a: Abbreviated as PS-ACVA-X, where X represents the feed amount of ACVA

b: The data were expressed as the mean ± SD; n=4

Table 4.3 Characterization of PS-ACVA microspheres

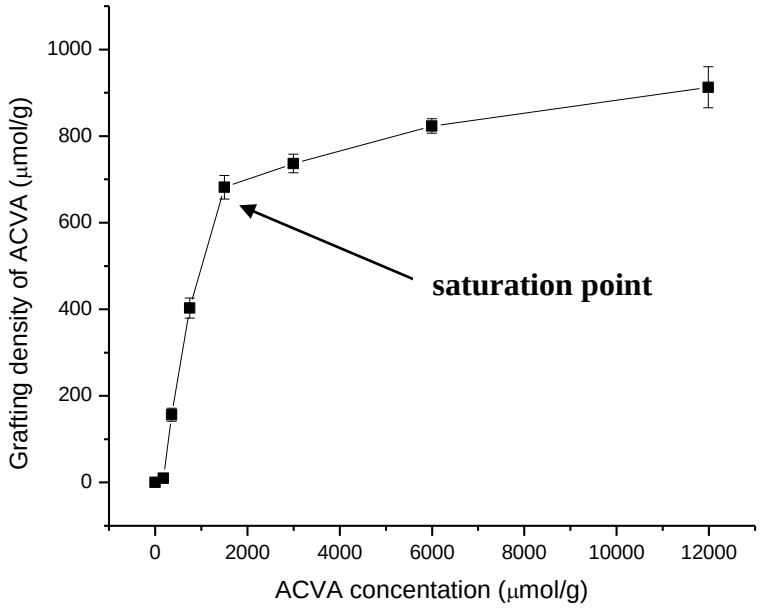


Figure 4.2 Grafting densities of ACVA moiety as a function of the feed amount of ACVA employed for immobilization. The ACVA concentration is given in the same unit as the grafting density to allow for comparison.

4.3.1.2 Surface-initiated radical polymerization

4.3.1.2.1 Thermal decomposition of grafted ACVA

Surface-immobilized azo-initiator undergoes thermal homolysis at 70 ℃ to yield a nitrogen molecule and a pair of initial radicals. The mechanism of the thermal decomposition of azo-initiator was shown in Figure **4.3** and Figure **4.4 (a)** (Engel 1980; Male et al. 1998). However, not all the immobilized azo molecules decompose immediately upon heating. Prucker and Rühe (1998a) grafted AIBN to silica particles and found that, up to 16 h polymerization at 60 ℃, only about 40% of the azo molecules had been thermally decomposed (step 1 in Figure **4.3**) and the other 70% were still intact. However, the decomposition percentage will increase with increasing reaction temperature and time. When this pair of initial radicals is generated by homolysis in solution, it is often considered to be a 'caged' radical pair. That is, the initially formed radicals are temporarily trapped by surrounding solvent molecules (i.e., solvent cage), causing them to remain as colliding neighbours for a short period of time before they either recombine or diffuse apart (Braden et al. 2001; Oelkers and Tyler 2008). This phenomenon is known as the 'cage effect' (Franck and Rabinowitsch 1934). In the case of surface immobilized initiator, upon decomposition, most of the generated radicals will be caught in the solvent cage and are therefore not able to start a polymerization reaction. It was reported that only about 30-40% of the initial radicals can leave the solvent cage (step 2 in Figure **4.3**) (Prucker and Rühe 1998a). This number is also referred as the radical efficiency factor. Once the newly formed pair radicals diffuse through the solvent cage, they start polymerization reactions and two macro-radicals grow to form the polymers, one tethered to the surface and the second in solution (step 3 in Figure **4.3**). In summary, following thermal decomposition and polymerization, the immobilized azo molecules will either remain intact or decompose

with or without initiating polymer chain formation. In order to calculate the grafting density of polymer chains tethered to the particle surfaces, it is necessary to investigate the percentage of decomposed azo-initiator and determine the radical efficiency factor.

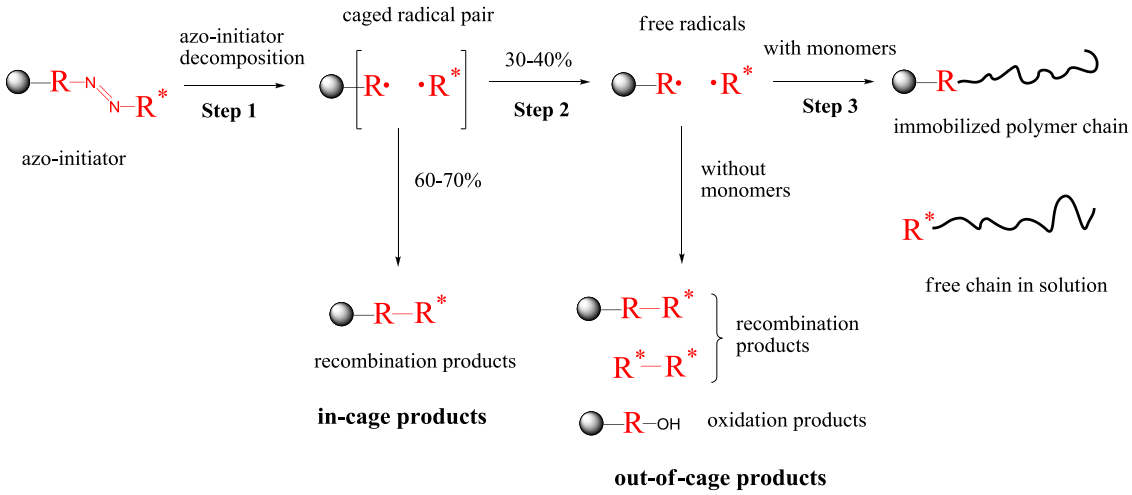


Figure 4.3 Thermal decomposition of grafted azo-initiator (note that in this drawing no distinction is made whether the termination occurs by recombination or disproportionation).

To investigate the percentage of thermally decomposed ACVA, the thermolysis reactions of surface-immobilized AVCA were performed in deoxygenated dioxane solutions under nitrogen atmosphere in the absence of vinyl monomers at 70 ℃. The initiator used in the experiments had a grafting density of about 823.22 μmol/g (PS-ACVA-1.68 microspheres). Upon decomposition, the initially generated radicals can react with each other inside the solvent cage to yield combination products, such as 4,5-dicyano-4,5-dimethyloctanedioic acid (DDOA) and 5-(4-carboxy-2-cyanobutan-2-ylimino)-4-methylpent-4-enoic acid (CCYMEA), and disproportionation products, 4-cyanopentanoic acid (COA) and 4-cyanopent-4-enoic acid (CEA) (Figure **4.4 (b)**). These products are referred as in-cage products (Abraham et al. 2012). CEA and CCYMEA are often not observed, because the former is susceptible to polymerization and the latter to thermal decomposition (Jaffe et al. 1972). As to the radicals which have diffused through the solvent cage, in the absence of NIPAAm monomers, they

eventually encounter each other (in solution or on surface) and undergo radical coupling to form the combination and disproportionation products similar with those in-cage products, except a minor proportion of the diffused radicals reacts with trace oxygen in solvent to form oxidation products, such as 4-cyano-4-hydroxypentanoic acid (CHA). These products are referred as out-of-cage products (Abraham et al. 2012). After both the in-cage and out-of-cage processes, the disproportionation products (i.e., COA moiety) were considered as the major products for the purpose of my calculation (Jaffe et al. 1972). Combustion analysis revealed a significant reduction in nitrogen content after thermal decomposition of the immobilized ACVA on PS-ACVA-1.68 microspheres. It is believed that the major products of the thermolysis resulted from disproportionation (i.e., COA moiety) (Jaffe et al. 1972). Therefore, the nitrogen content reduction was mainly attributed to the loss of the N_2 and CEA molecules. The percentage of decomposed ACVA on PS-ACVA microspheres after 24 h of homolysis was calculated from the decrement in nitrogen composition (see section **4.2.4.2.1**). It was found that about 100% of the immobilized ACVA was decomposed. From the literature (Prucker and Rühe 1998a; 1998b), a typical value of the radical efficiency factor of immobilized azo-initiator is 30-40%. This seems to be a reasonable value and will be assumed to also apply in the system discussed here (i.e., thermal decomposition of PS-ACVA microspheres).

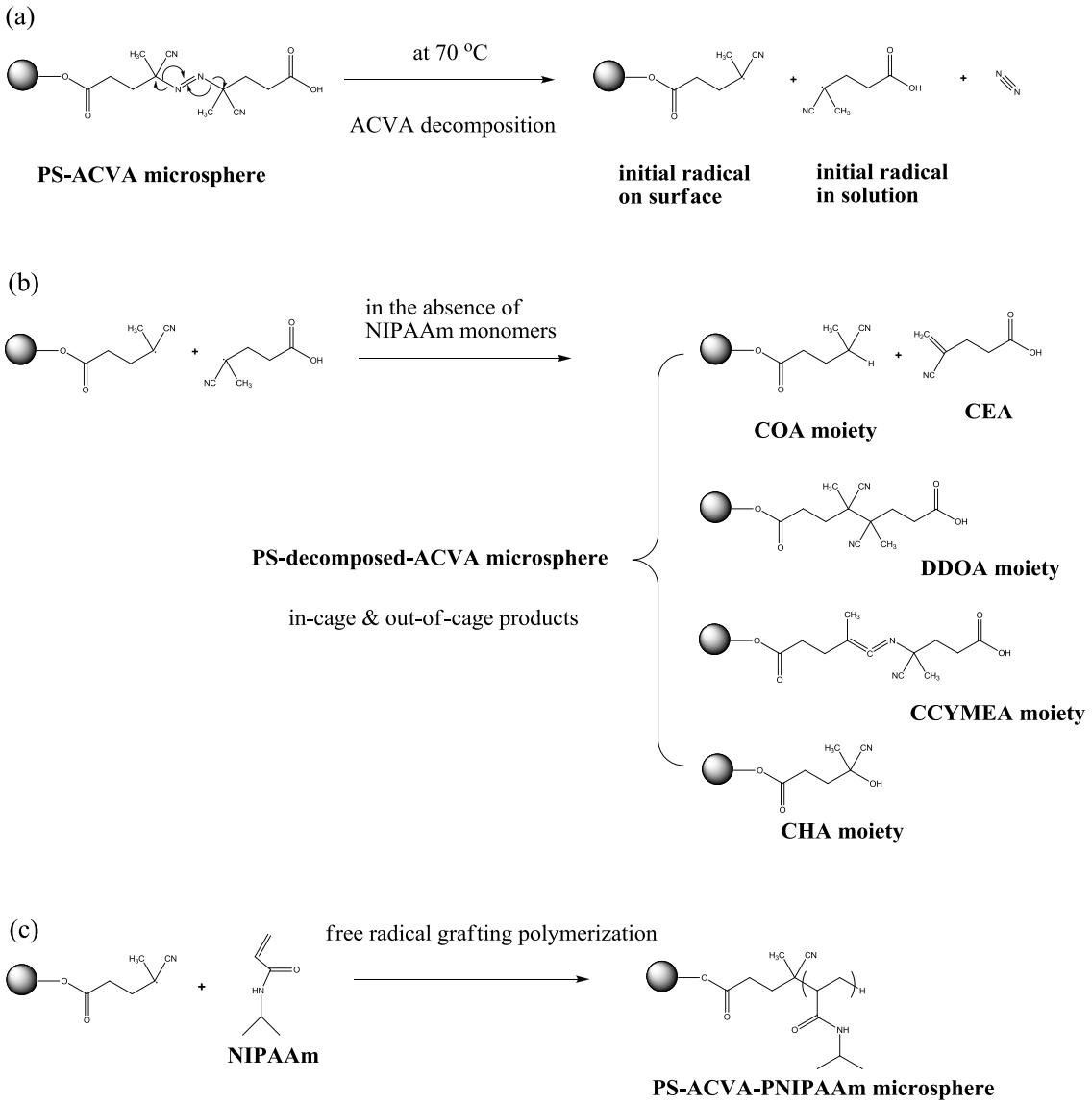


Figure 4.4 The decomposition of ACVA moiety and free radical grafting polymerization

4.3.1.2.2 Surface-initiated polymerization

The polymerization reactions of NIPAAm with surface-immobilized ACVA with grafting density of 823.22 μmol/g (PS-ACVA-1.68) were performed in dioxane solutions at 70 ℃ for 24 h. Each of reactions was identical in all parameters except for the initial concentration of NIPAAm monomer. In order to obtain quantitative information about the grafted amount of the covalently attached PNIPAAm layers, the resulting microspheres were studied by combustion analysis. The grafted amount of

PNIPAAm polymer on the modified microsphere surface was calculated from the increment in nitrogen composition in comparison with PS-decomposed-ACVA microspheres. This is because radical initiation may lead to products derived from disproportionation and recombination leading to the change in nitrogen content in the product, as well as the desired polymerisation process. It was therefore necessary to conduct a thermal decomposition of polymer modified with initiator, but in the absence of monomer, in order to obtain the level of change in nitrogen content for such a blank process. The nitrogen content of decomposed ACVA was then taken from each experimental run, less the value of this blank. It was found that the amount of grafted PNIPAAm was increased with increasing the initial concentration of NIPAAm monomer. It can be seen from Table **4.4** that the amount of immobilized PNIPAAm can achieve very high value using this 'grafting-from' method. For example, in the experiment employing 9 g NIPAAm monomers (PS-ACVA-1.68-PNIPAAm-9), a modified microsphere was obtained consisting of about 70 wt% PNIPAAm. This value corresponds to a grafted amount of about 2.3 g/g unmodified beads. It should be noted that this is not the maximum amount of PNIPAAm that can be covalently grafted onto ACVA-immobilized microspheres. If higher initial concentration of NIPAAm monomer is employed, even higher grafted amount can be obtained. By contrast, the microspheres prepared via 'grafting-to' method (see section **3.3.3**) only consist of maximum 30 wt% PNIPAAm. In 'grafting-to' method, once the surface has become significantly covered, additional polymer molecules, which are trying to reach the particle surface, have to diffuse against the concentration gradient caused by the already immobilized polymer chains (Prucker and Rühe 1998b). This leads to a strong kinetic hindrance and low grafted amount of PNIPAAm. However, in 'grafting-from' method, the growing chain

only reacts with small NIPAAm monomers or oligomers, therefore the process is less affected by steric hindrance and leads to higher grafted amount.

The study of thermal decomposition behaviour of grafted ACVA in the absence of NIPAAm monomers revealed that the percentage of decomposed ACVA on PS-ACVA-1.68 microspheres was 100% after 24 h at 70 °C. However, radical efficient factor was not able to be determined based on the combustion analysis results. For the purpose of calculation, it was assumed that 40% of the decomposed initiator molecules diffused through the solvent cage and successfully started polymerization reactions and form PNIPAAm chains, according to Prucker and Rühe (1998a). Therefore, it gave a potential convention of 40% overall. For all polymerizations, surface-immobilized ACVA with the same grafting density (823.22 μmol/g) was used. After polymerization 40% of them generated polymer chains, providing a PNIPAAm grafting density of about 329 μmol/g. The average molecular weight of the grafted PNIPAAm was calculated from the grafted amount and the grafting density as shown in Table **4.4**. The average molecular weight was also found to be increased with increasing the initial concentration of NIPAAm monomers.

Bead code[a]	Feed amount of NIPAAm (g/50 mL)	Nitrogen content (wt%)[b]	Grafted amount of PNIPAAm (mg/g)	Grafting density of PNIPAAm (μmol/g)	Average MW of PNIPAAm (g/mol)
PS-decomposed-ACVA	0	3.11 ±0.20	0	N/A	0
PS-ACVA-1.68-PNIPAAm-0.5	0.5	4.06 ±0.36	102.6 ±38.9	329	312 ±118
PS-ACVA-1.68-PNIPAAm-1.5	1.5	4.96 ±0.40	200.1 ±43.4		609 ±132
PS-ACVA-1.68-PNIPAAm-3.0	3.0	7.05 ±0.91	425.5 ±98.4		1294 ±299
PS-ACVA-1.68-PNIPAAm-6.0	6.0	9.12 ±0.67	649.4 ±71.9		1976 ±219
PS-ACVA-1.68-PNIPAAm-9.0	9.0	9.56 ±0.14	696.5 ±15.6		2119 ±47

a: Abbreviated as PS-ACVA-X-PNIPAAm-Y, where X represents the feed amount of ACVA in the initiator immobilization step, and Y represents the feed amount of NIPAAm in the polymerization step.

b: The data were expressed as the mean ± SD; n=4

MW: molecular weight

N/A: not applicable

Table 4.4 Characterization of PS-ACVA-1.68-PNIPAAm microspheres

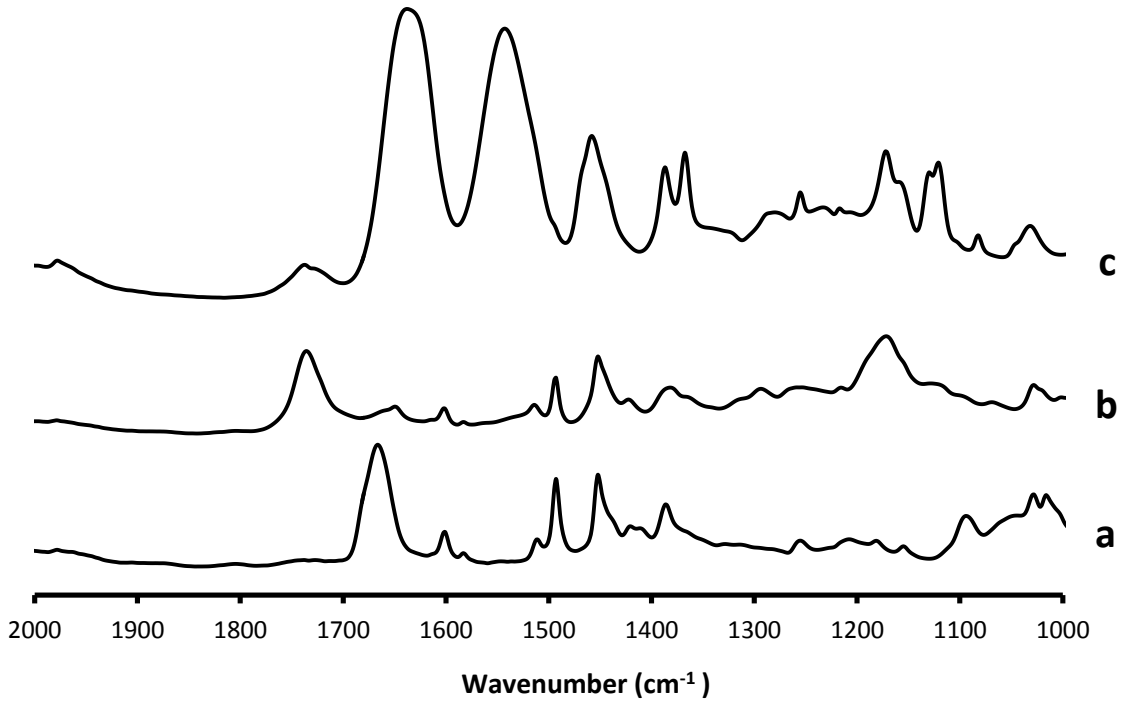


Figure 4.4 FTIR spectra of (a) unmodified PS-OH microspheres, (b) PS-ACVA-1.68 microspheres and (c) PS-ACVA-1.68-PNIPAAm-6 microspheres.

4.3.1.2.3 Reaction termination and molecular architecture of grafted PNIPAAm

Because the initiator is bound to the surface only by one end, the second part of decomposed ACVA can diffuse into solution and start a polymerization reaction there. Therefore, not all the growing chains which have formed are covalently attached to the microspheres. This results to different possibilities for bimolecular termination of the growing chains and they are schematically illustrated in Figure **4.5**. The molecular architecture is affected by the different termination pathways. One possibility is given by the termination reaction between a grafted and a freely growing chain (pathway A). The freely growing chains originate from the non-attached radical generated during thermal decomposition of the immobilized ACVA. This termination pathway is considered as predominant (Prucker and Rühe 1998a), and it finally generates linear polymer chains. The second possibility for termination reaction is the spontaneous deactivation of two simultaneously growing polymer radicals on particle surface (pathway B). This pathway forms a loop molecular architecture. However, it is considered as the minor product.

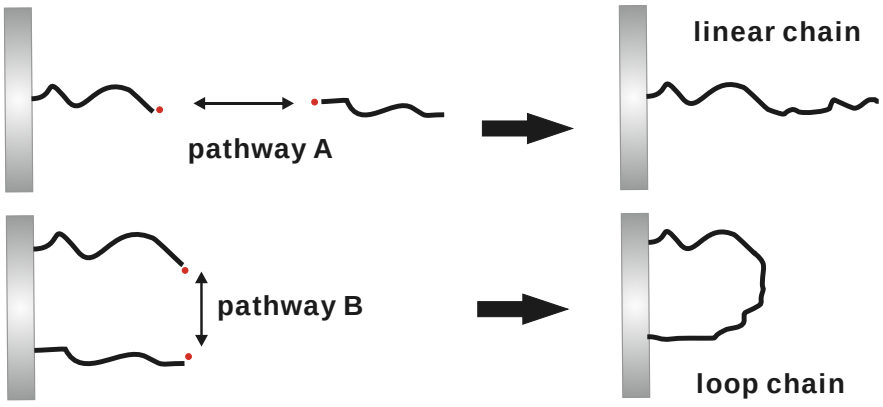


Figure 4.5 Reaction termination and molecular architecture of grafted PNIPAAm

4.3.1.3 Preparation of microspheres grafted with PNIPAAm hydrogel

This section describes the grafting of both a conventional PNIPAAm homopolymer hydrogel layer, and a comb-type PNIPAAm hydrogel layer onto the microsphere surface. The conventional PNIPAAm homopolymer hydrogel layer was prepared by copolymerizing NIPAAm with a cross-linker, MBAAm, on the surface of the ACVA-immobilized microspheres (PS-ACVA-1.68). The comb-type PNIPAAm hydrogel layer was prepared in a similar way in the presence of a PNIPAAm macromonomer (i.e., acrylate-terminated PNIPAAm), such that the free mobile PNIPAAm chains were grafted onto cross-linked networks. The PNIPAAm macromonomer was synthesised by conjugating HEA with PNIPAAm-COOH (XS) via esterification (Figure **4.6 (a)**). To confirm the successful conjugation, ^{1}H-NMR spectroscopy was carried out. Figure **4.7** shows the ^{1}H-NMR spectrum of PNIPAAm macromonomer. The signals around 5.9-6.5 ppm were assigned to CH_2=CH-, which are absent in the spectrum of PNIPAAm-COOH (Figure **3.6**). The microspheres modified with PNIPAAm hydrogel were characterized by means of FTIR spectroscopy. In both cases, FTIR spectra show the peaks characteristic of PNIPAAm at 1640 cm^{-1} (amide I bond, arising from C=O stretching and little C-N stretching) and 1550 cm^{-1} (amide II bond, arising from N-H bending and C-N stretching). However, both the cross-linked and comb-type architecture of the grafted hydrogel were not able to be confirmed via the FTIR spectra (Figure **4.8**).

Yoshida et al. (1995) found that the comb-type PNIPAAm hydrogel shrank much faster than the conventional homopolymer PNIPAAm hydrogel upon temperature change. The rapid deswelling of comb-type hydrogel was attributed to the immediate dehydration of these free mobile PNIPAAm chains grafted on the network. The dehydrated free chains

created hydrophobic regions, aiding the expulsion of water from the hydrogel network during collapse. By contrast, during de-swelling of the conventional PNIPAAm homopolymer hydrogel, a dense and dehydrated polymer skin impermeable to water was first formed near the hydrogel surface before the bulk gel collapse was initiated (Yoshida et al. 1992a; 1992b). This surface skin layer hindered the water permeation from the hydrogel interior outwards, leading to longer period of gel dehydration. However, it is worth mentioning that all the observations were based on bulk PNIPAAm hydrogel. In this study, PNIPAAm hydrogel was grafted onto microsphere surface, and the hydrogel layer is very thin in comparison with bulk gel particle. The difference in the de-swelling rate might not be significant between the two types of hydrogel layer on particle surface. However, the hydrogel architecture might have effects on cell attachment and detachment behaviour.

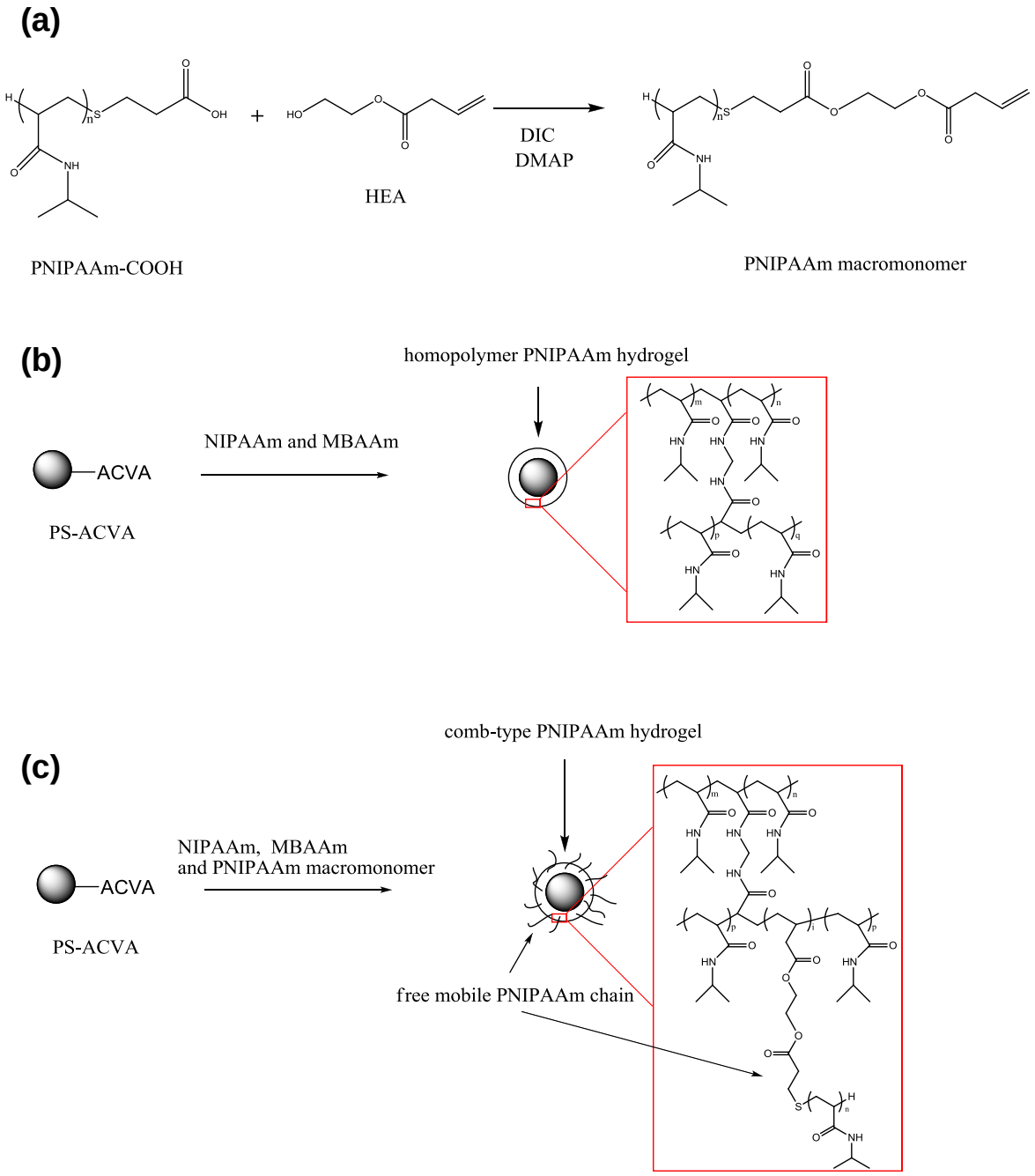


Figure 4.6 Synthesis of (a) PNIPAAm macromonomer, (b) PNIPAAm homopolymer hydrogel modified microsphere, and (c) comb-type PNIPAAm hydrogel modified microsphere.

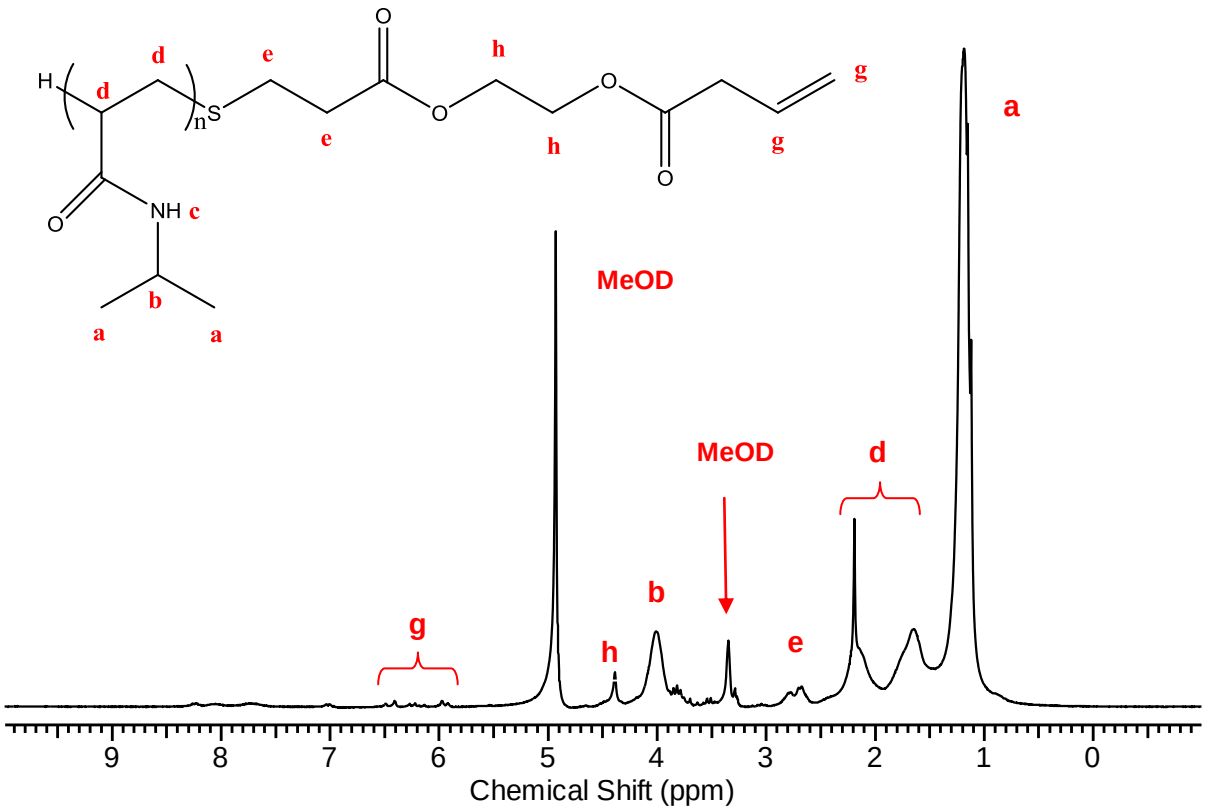


Figure 4.7 ^{1}H-NMR spectrum of PNIPAAm macromonomer

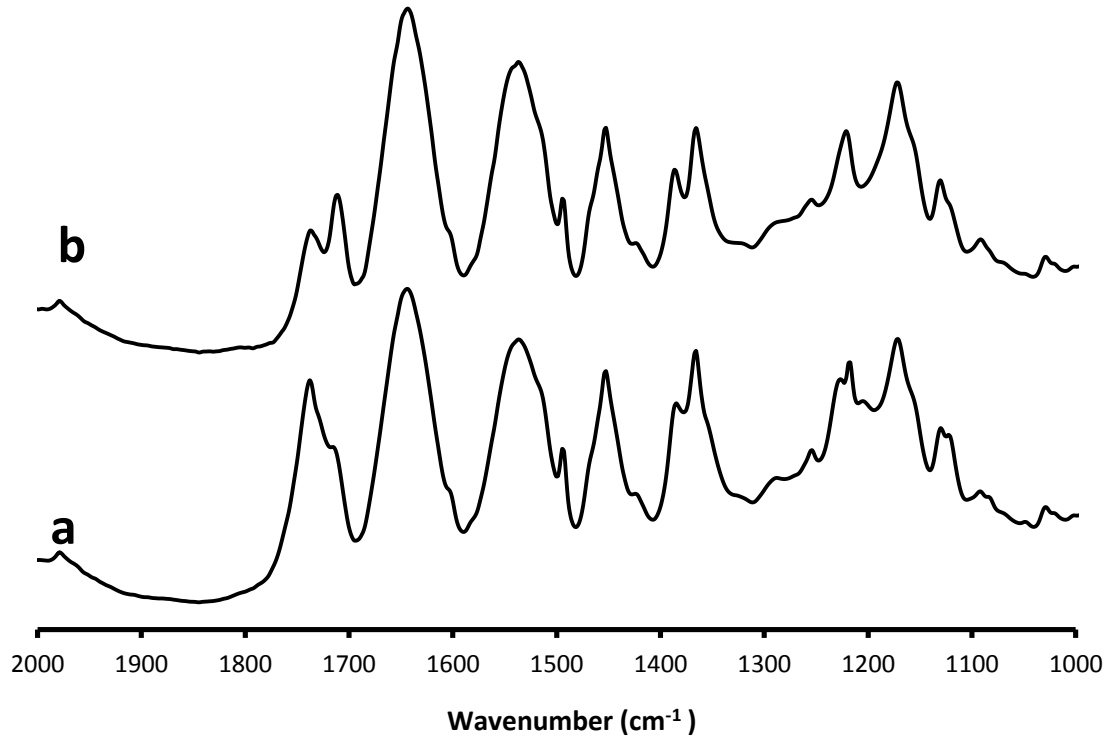


Figure 4.8 FTIR spectra of (a) microspheres grafted with PNIPAAm homopolymer hydrogel layer, and (b) microspheres grafted with comb-type hydrogel layer

4.3.1.4 Preparation of microspheres grafted with branched PNIPAAm

Branched polymer shows a 'multi-dimensional' architecture possessing a large number of chain ends per molecule. On one hand, the branched or hyperbranched polymers demonstrate different physical properties from their linear analogues, such as high solubility, globular or void-containing shapes, low melting point and solution viscosities (Hsieh et al. 2001; Magnusson et al. 2002; Carter et al. 2005; Tao and Yan 2010). In particular, it was found that the LCST values of branched PNIPAAm were significantly less than those of their linear counterparts and the LCST value was decreased with an increasing degree of branching (Carter et al. 2005; Vogt and Sumerlin 2008). The effect was primarily attributed to an increased contribution of hydrophobic end groups, the inclusion of which is associated with the increase of branching. However the reduction in LCST can also be partially attributed to the branching nature of the polymer, leading to increased molecular density (decreased free volume) (Vogt and Sumerlin 2008). On the other hand, the large number of chain ends can be used to add useful chemical functionality, which may differ from similar functionality added along the main chain (Carter et al. 2005). For example, Rimmer et al. (2007) prepared a highly branched PNIPAAm with a cell-adhesive peptide at the chain ends. This polymer can be used to gently detach and then transfer cultured cells to new substrates (Hopkins et al. 2007). According to these findings, it is reasonable to consider that thermo-responsive microcarriers grafted with branched PNIPAAm might show different cell attachment/detachment behaviour in comparison with those grafted with linear PNIPAAm.

In this study, branched PNIPAAm chains were incorporated to PS-ACVA microspheres through a two-step reaction (Figure **4.9** & **4.10**). The first step is to grow up a polymer

'backbone' from the PS-ACVA microsphere surface. In the second step, PNIPAAm branches were incorporated to the polymer backbone through 'grafting-to' or 'grafting-from' technique.

4.3.1.4.1 Synthesis of the backbone

Two types of polymer backbone were synthesized from the surface of PS-ACVA microspheres via surface-initiated radical polymerization (i.e., grafting-from technique). The polymer backbone is composed of poly(2-hydroxyethyl acrylate) (PHEA) homopolymer or poly(styrene-*co*-2-hydroxyethyl acrylate) (PSHEA) copolymer. Figure **4.11 (a)** and Figure **4.12 (a)** show the FTIR spectra of the PS-PHEA and PS-PSHEA microspheres. In both cases, the sharp peak at about 1735 cm^{-1} was attributed to the ester groups of HEA moieties. The polymer backbones consist of hydroxyl groups, which can be used for further modification.

4.3.1.4.2 Branch incorporation via 'grafting-to' technique

In this step, PNIPAAm branches were conjugated to the polymer backbones via esterification between the hydroxyl groups of the backbones and the carboxyl groups of PNIPAAm-COOH (XS) (M_n=1857, PD=2.26) using DIC as a coupling agent and DMAP as a catalyst. The incorporation of PNIPAAm branches was confirmed by FTIR spectroscopy. The FTIR spectra (Figure **4.11 (b)** & **4.12 (b)**) of PS-PHEA-PNIPAAm and PS-PSHEA-PNIPAAm beads show the peaks characteristic of PNIPAAm at 1640 cm^{-1} (amide I bond) and 1550 cm^{-1} (amide II bond), which were absent in the FTIR spectra of PS-PHEA and PS-PSHEA beads. This indicates that PNIPAAm branches were successfully grafted to the backbones. The amount of grafted PNIPAAm in both cases was calculated from an increment in nitrogen content, which was determined by combustion analysis (Table **4.5**). It was found that, with the same feed amount of

PNIPAAm-COOH polymer, the amount of PNIPAAm grafted on PS-PHEA microspheres was significantly higher that on PS-PSHEA microspheres. This was because the addition of styrene monomer decreased the concentration of HEA moieties (i.e., hydroxyl groups) in the PSHEA copolymer backbone. This indicates that the amount of grafted PNIPAAm might be regulated by changing the concentration of hydroxyl groups on the polymer backbones.

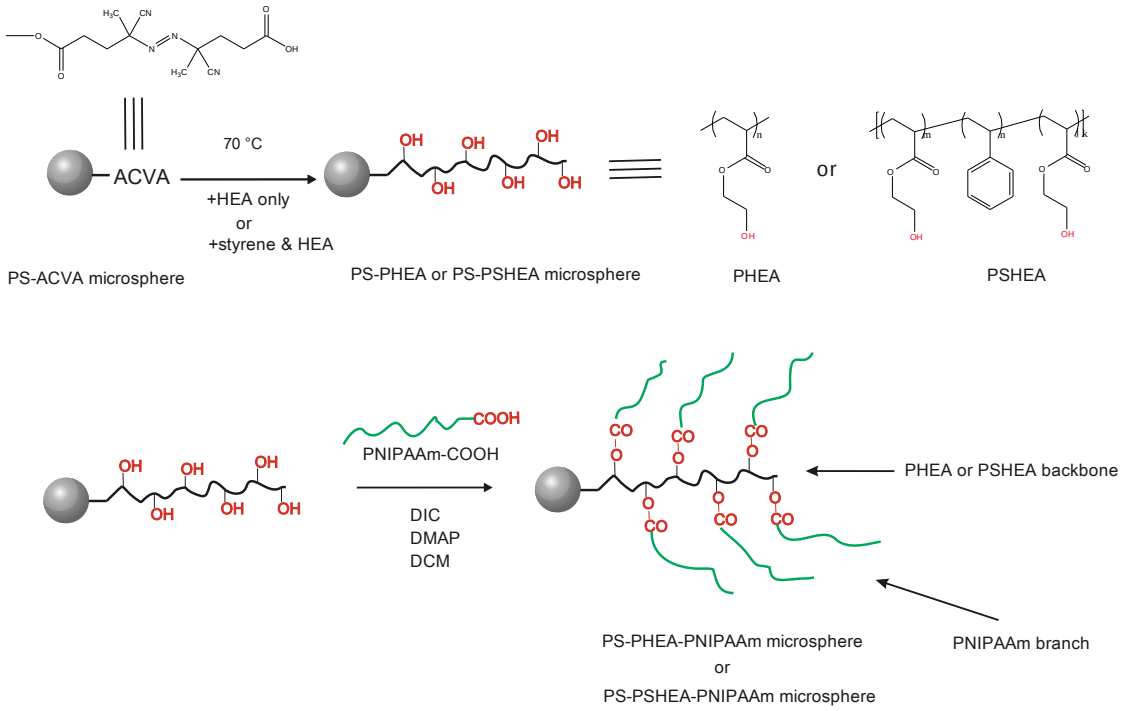


Figure 4.9 Synthesis of PHEA and PSHEA copolymer backbone and PNIPAAm branch incorporation via 'grafting-to' technique

Bead code	Feed amount of PNIPAAm-COOH (XS) (g/50 mL)	Nitrogen content (wt%)[a]	Grafted amount of PNIPAAm (mg/g)
PS-PHEA	N/A	1.48 ±0.06	0
PS-PSHEA	N/A	2.54 ±0.02	0
PS-PHEA-PNIPAAm	3	3.23 ±0.02	160.8 ±1.4
PS-PSHEA-PNIPAAm	3	3.31 ±0.04	78.6 ±3.7

a: The data were expressed as the mean ± SD; n=3

Table 4.5 Characterization of PHEA and PSHEA copolymer backbone and PNIPAAm branches

4.3.1.4.3 Branch incorporation via 'grafting-from' technique

PNIPAAm branches can also be grafted to the polymer backbones via grafting-from technique. First, the azo-initiator (ACVA) was immobilized to the hydroxyl groups on the PHEA or PSHEA backbones via esterification using DIC as a coupling agent and DMAP as a catalyst. The PNIPAAm branches were then synthesized from the ACVA-immobilized backbones by surface-initiated radical polymerization. The FTIR spectra (Figure **4.13 (b)** & **4.14 (b)**) of PS-PHEA-ACVA-PNIPAAm and PS-PSHEA-ACVA-PNIPAAm beads show the peaks characteristic of PNIPAAm at 1640 cm^{-1} (amide I bond) and 1550 cm^{-1} (amide II bond), which were absent in the FTIR spectra of the ACVA-immobilized backbones (i.e., PS- PS-PHEA-ACVA and PS-PSHEA-ACVA microspheres) (Figure **4.13 (a)** & **4.14 (a)**). This indicates that PNIPAAm branches were successfully grafted from the backbones in both cases.

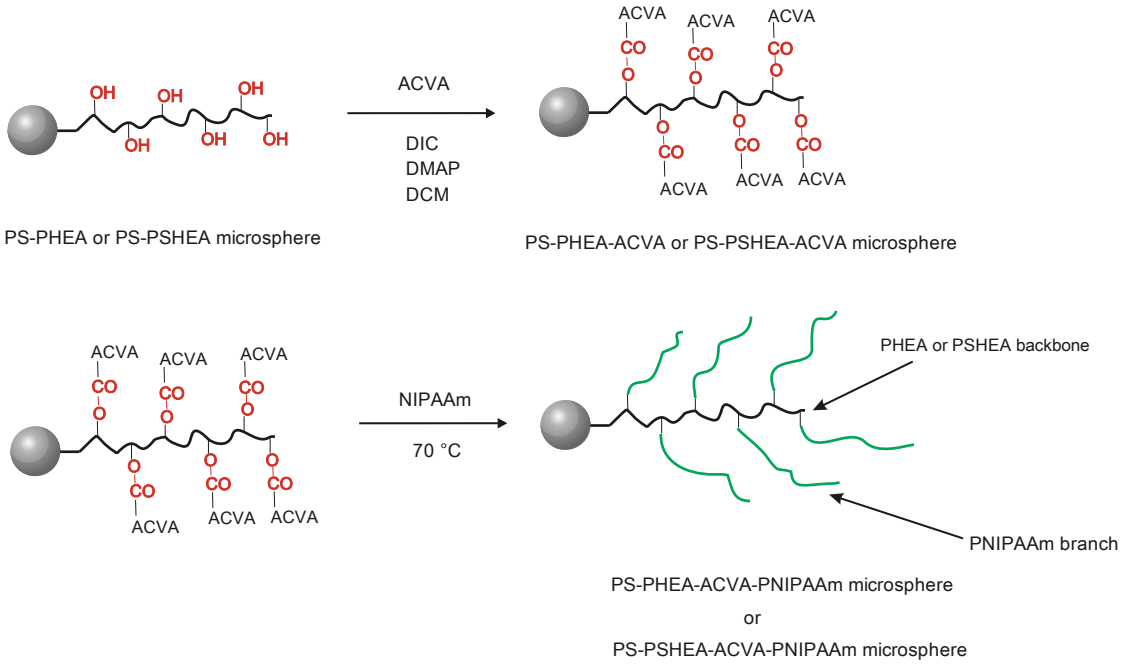


Figure 4.10 PNIPAAm branch incorporation via 'grafting-from' technique

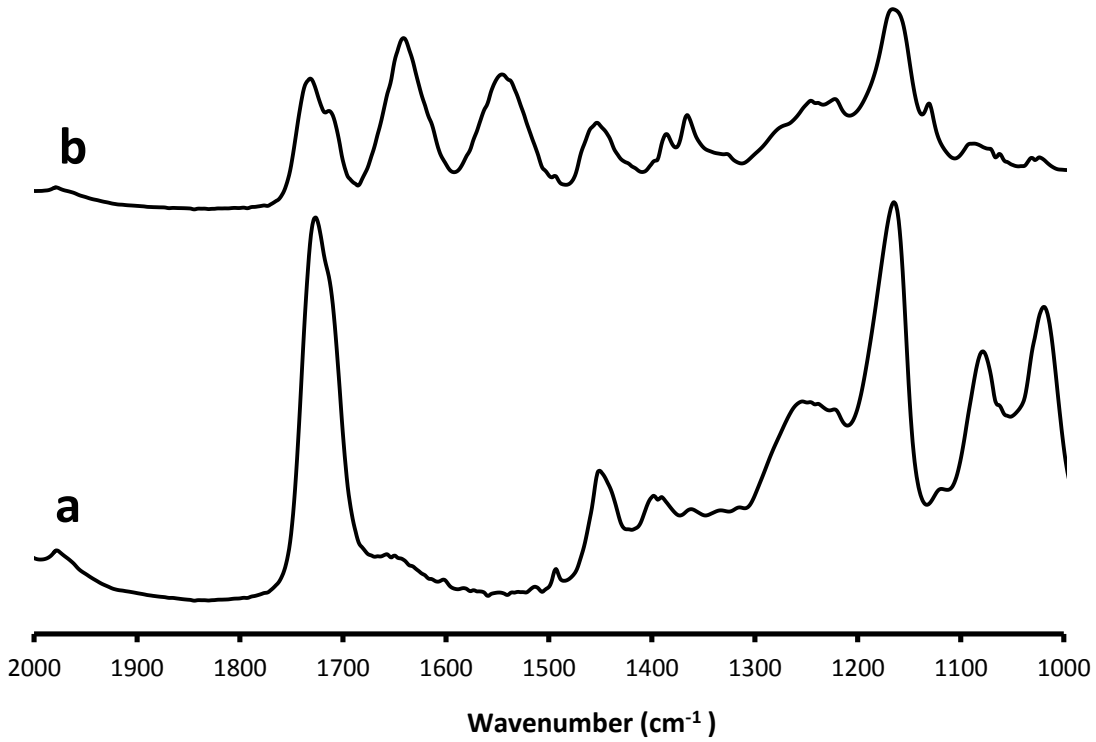


Figure 4.11 FTIR spectra of (a) PS-PHEA microsphere and (b) PS-PHEA-PNIPAAm microsphere

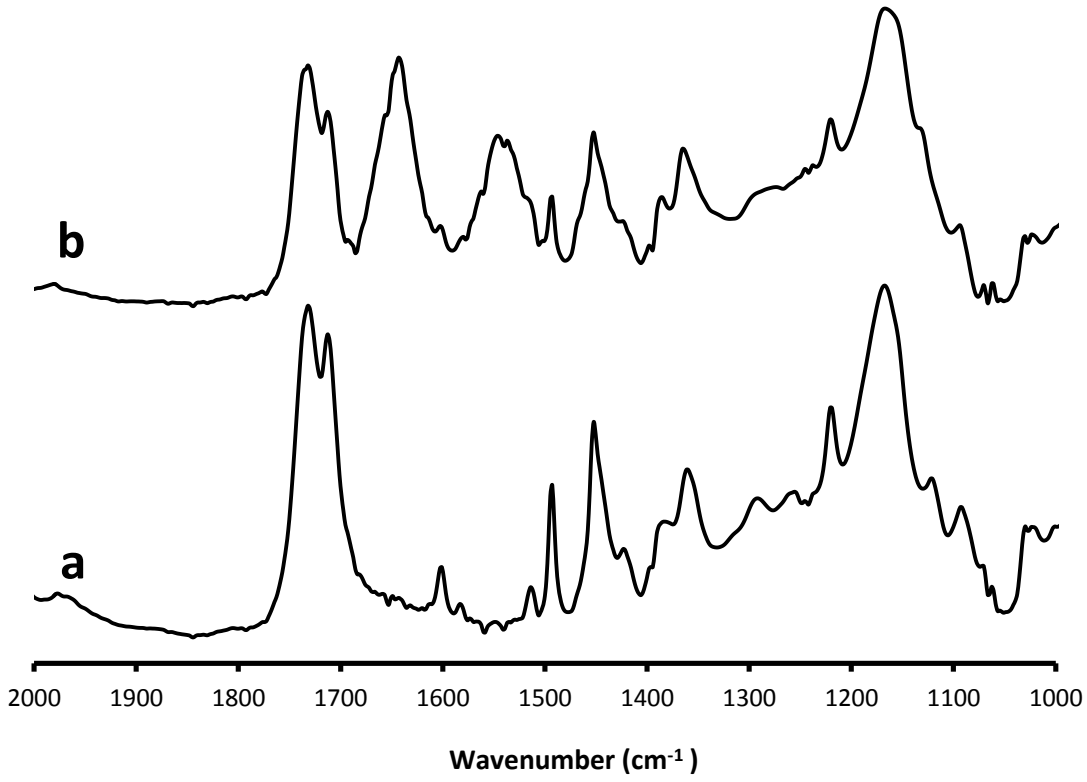


Figure 4.12 FTIR spectra of (a) PS-SHEA microsphere and (b) PS-PSHEA-PNIPAAm microsphere

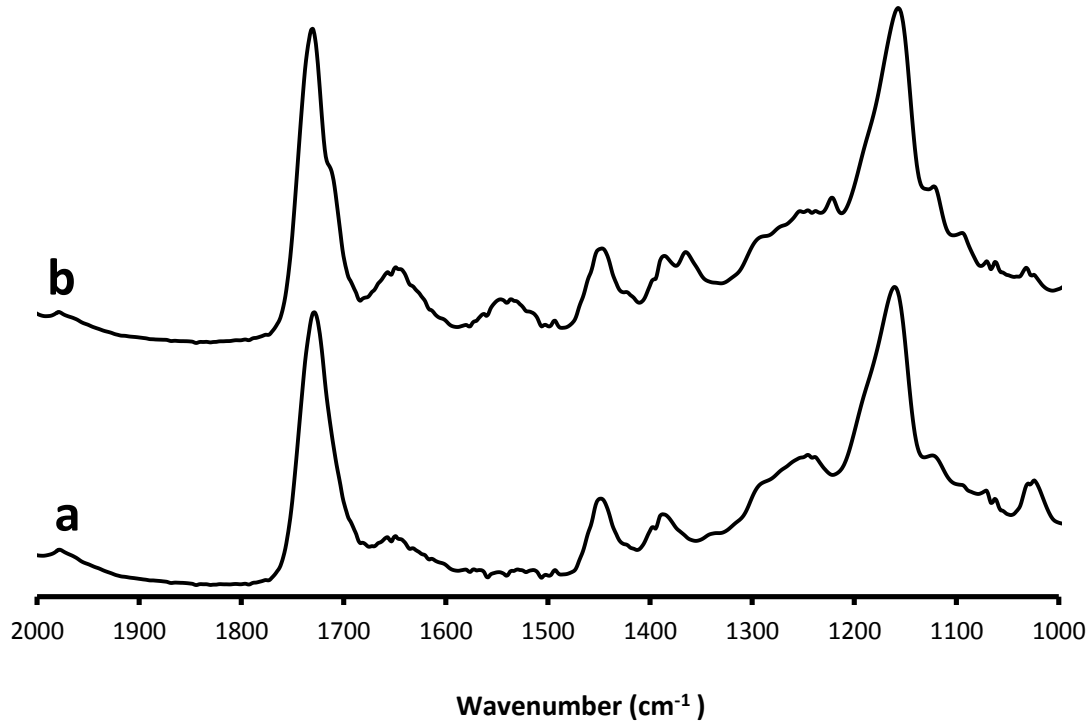


Figure 4.13 FTIR spectra of (a) PS-PHEA-ACVA microsphere and (b) PS-PHEA-ACVA-PNIPAAm microsphere

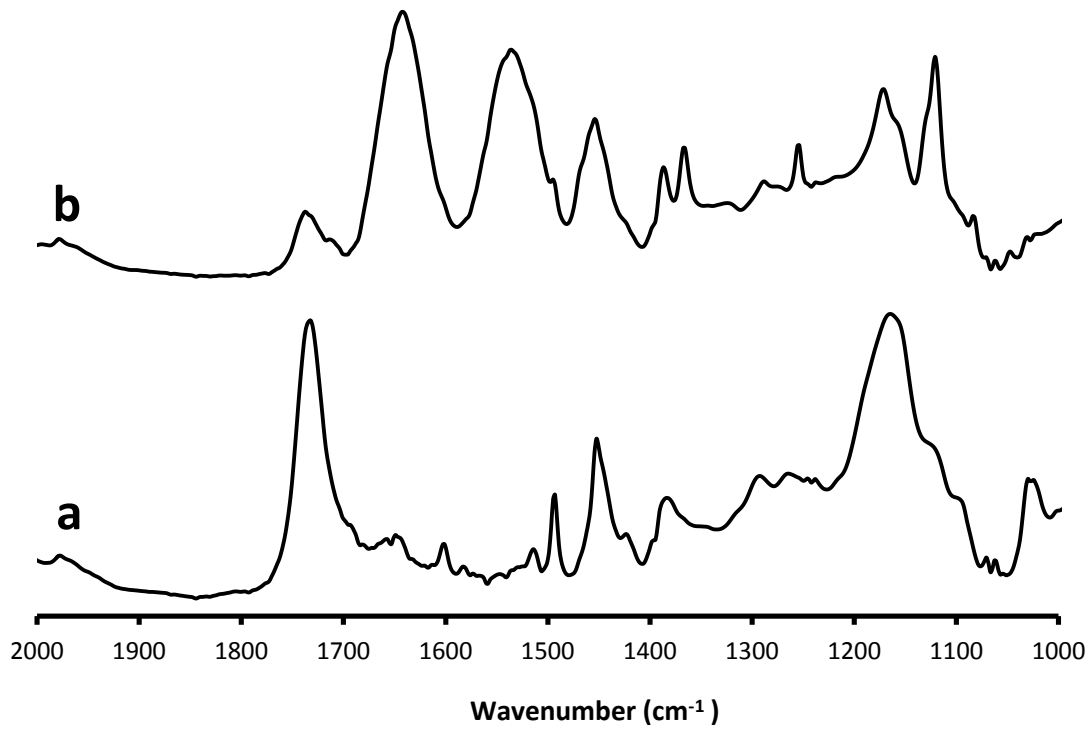


Figure 4.14 FTIR spectra of (a) PS-PSHEA-ACVA microsphere and (b) PS-PSHEA-ACVA-PNIPAAm microsphere

4.3.2 Surface-initiated ATRP

In this study, cross-linked dextran (CLD) based microspheres (Sephadex® G-50 and Cytodex®-1) were used as starting materials. Dextran is a D-glucose polymer composed of 95% 1,6'-linked glucose molecules with some single-unit glucose branches linked at 1,3' and 1,4' and, occasionally, 1,2' positions (Kim et al. 2003; Santos et al. 2005). Dextran has excellent biocompatibility so it has been widely used in the pharmaceutical industry and even food and textile industries (Santos et al. 2005). CLD microspheres, prepared by cross-linking dextran with epichlorohydrin, meet many requirements for the microcarriers. First, CLD microspheres with various sizes and cross-linking percentages are commercially available (Kim et al. 2003). Second, CLD microspheres are rigid enough to be used as cell attachment substrate under stirring condition. Third, most importantly, the density of CLD microsphere is slightly greater than that of the surrounding cell culture medium so that CLD microspheres can be easily suspended by gentle stirring when they are used as microcarriers. Sephadex® G-50 Coarse microspheres are CLD based gel filtration matrix without any surface modification. Cytodex®-1 microcarriers are based on a CLD matrix that is substituted with positively charged *N*,*N*-diethylaminoethyl (DEAE) groups. The charged groups are distributed throughout the entire matrix of the microcarrier. Cytodex®-1 microcarrier has been extensively used in large-scale culture of anchorage-dependant cells.

The modification method for both microspheres used in this study was adapted from Kim et al. (2003). It consists of two steps: 1) immobilization of an ATRP initiator, 2-bromopropionyl group, onto the surface of the microspheres (Figure **4.15**), and 2) subsequent PNIPAAm grafting through ATRP of NIPAAm from the initiator (Figure **4.16**).

4.3.2.1 Immobilization of ATRP initiator

The 2-bromopropionyl group was attached to Sephadex® G-50 microspheres through the ester bond formation between hydroxyl groups and 2-bromopropionyl bromide. Before this step, the microspheres were dried to eliminate the trace water trapped within them, which may terminate the reaction. After the attachment of the polymerization initiator, the presence of the ester groups (C=O stretching) was confirmed by a new peak in the FTIR spectrum at 1735 cm^{-1} (Figure **4.17 (b)**), which was absent in the FTIR spectrum of unmodified Sephadex® G-50 microspheres (Figure **4.17 (a)**). The same procedure was conducted for Cytodex®-1 microspheres and similar FTIR spectra (Figure **4.18 (a&b)**) were obtained. The combustion analysis revealed that the grafting density of 2-bromopropionyl group on Sephadex G50 microspheres was increased with increasing the feed amount of 2-bromopropionyl bromide in the immobilization reaction (Table **4.6**).

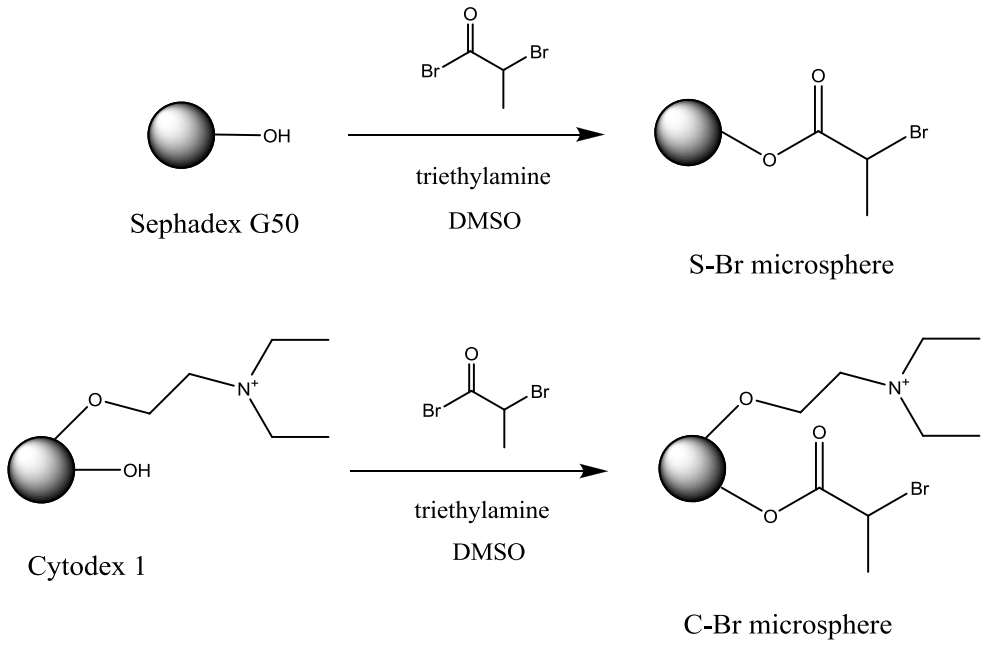


Figure 4.15 The attachment of 2-bromopropionyl polymerization initiator.

Bead code[a]	Feed amount of 2-bromopropionyl bromide (mL/10 mL)	Bromine content (wt%)[b]	Grafting density of ATRP initiator (mmol/g)
Sephadex G-50	0	0.06±0.11	0
S-Br-0.2	0.2	1.37±0.26	0.16±0.05
S-Br-0.5	0.5	2.42±0.52	0.29±0.06
S-Br-1.0	1.0	6.78±1.23	0.84±0.14

a: Abbreviated as S-Br-X, where X represents the feed amount of 2-bromopropionyl bromide in the initiator immobilization step

b: The data were expressed as the mean ± SD; n=3

Table 4.6 Characterization of Sephadex® G-50 microspheres after attachment of a polymerization initiator, 2-bromopropionyl bromide (S-Br microspheres).

4.3.2.2 Aqueous ATRP

Aqueous ATRP with a catalytic system of CuBr and 2,2'-dipyridyl was employed to synthesize PNIPAAm from the initiators coupled with Sephadex® G-50 and Cytodex®-1 microspheres. The mechanism of ATRP was illustrated in the section **2.5.2.2**. Degassed water was used as the solution due to the sensitivity of the CuBr to air. After ATRP, the resulting microspheres were washed with methanol thoroughly to remove unreacted monomers. The resulting PNIPAAm grafted Sephadex® G-50 microspheres and PNIPAAm grafted Cytodex®-1 microspheres were characterized by means of FTIR spectroscopy. The FTIR spectra (Figure **4.17 (c)** & **4.18 (c)**) show the peaks characteristic of PNIPAAm at 1640 cm^{-1} (C=O stretching) and 1550 cm^{-1} (N–H bending). Therefore, PNIPAAm was successfully grafted onto both microspheres. For the purpose of the calculation, it was assumed that all the initiators were activated to form PNIPAAm chains and the polymer chain length was uniform. However, it will not be true inside of the pores of the CLD microsphere, i.e., the external surface chain must be longer than the average number. PNIPAAm was grafted from the microspheres immobilized with different density of ATRP initiator. The achievable molecular weight

of grafted PNIPAAm polymer was found to be dependent on the density of the immobilized ATRP initiator (Table **4.7**). With increasing the density of immobilized ATRP initiator, both grafted amount and molecular weight of PNIPAAm were significantly decreased. This might be because higher density of ATRP initiator causes more polymer radicals grow simultaneously, leading to a higher concentration of growing radicals on the surface. This increases the possibility that two of them are generated and grow in such close vicinity that the active chains meet and terminate each other by recombination or disproportionation.

The surface morphology of the microspheres was characterized by means of SEM. Figure **4.19** presents SEM micrographs of unmodified Sephadex® G-50 microspheres and the microspheres after initiation and polymerization at two different magnifications. It can be noticed that the unmodified microspheres' surface is smooth and the particles are not uniform in size. After polymerization, the surface did not appear to be altered, although some degradation of the beads was observed in some cases. This could be consistant with the formation of thin PNIPAAm polymer shell over the surface of the Sephadex® G-50 microspheres. Figure **4.20** represents SEM micrographs of unmodified Cytodex®-1 microspheres and the microspheres after initiation and polymerization at two different magnifications. Similar with the previous case, there was no observable significant changes after polymerisation of NIPAAm on the surface of Cytodex®-1 microspheres, even though, after attachment of a polymerization initiator, the surface was observably rough.

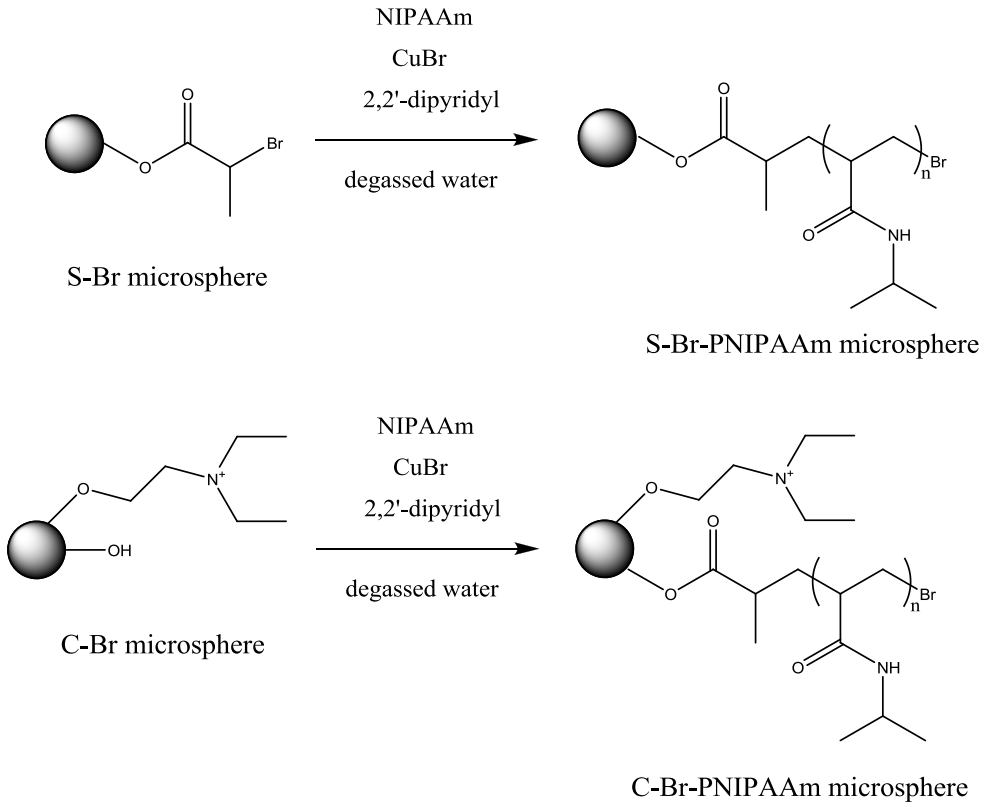


Figure 4.16 Schematic description of ATRP

Bead code[a]	Feed amount of NIPAAm (g/10 mL)	Nitrogen content (wt%)[b]	Grafting density of PNIPAAm chain (μmol/g)	Grafting amount of PNIPAAm (mg/g)	Average MW of PNIPAAm
Sephadex G-50	0	<0.1	0	0	0
S-Br-0.2-PNIPAAm-4.5	4.5	8.31 ±0.76	163.7 ±45.3	671.2 ±61.2	4281 ±987
S-Br-0.5-PNIPAAm-4.5	4.5	7.12 ±0.36	294.9 ±64.8	575.4 ±27.9	2024 ±518
S-Br-1.0-PNIPAAm-4.5	4.5	4.76 ±0.88	841.7 ±143.9	384.8 ±71.5	460 ±63

a: Abbreviated as S-Br-X-PNIPAAm-Y, where X represents the feed amount of 2-bromopropionyl bromide in the initiator immobilization step, and Y represents the feed amount of NIPAAm in the polymerization step.

b: The data were expressed as the mean ± SD; n=3

N/A: not applicable

Table 4.7 Characterization of PNIPAAm-grafted Sephadex® G-50 microspheres (S-Br-PNIPAAm microspheres).



Figure 4.17 FTIR spectra of (a) unmodified Sephadex® G-50 Coarse microspheres, (b) Sephadex® G-50 Coarse microspheres after attachment of a polymerization initiator, 2-bromopropionyl bromide, and (c) PNIPAAm grafted Sephadex® G-50 microspheres.



Figure 4.18 FTIR spectra of (a) unmodified Cytodex®-1 microspheres, (b) Cytodex®-1 microspheres after attachment of a polymerization initiator, 2-bromopropionyl bromide, and (c) PNIPAAm-grafted Cytodex®-1 microspheres

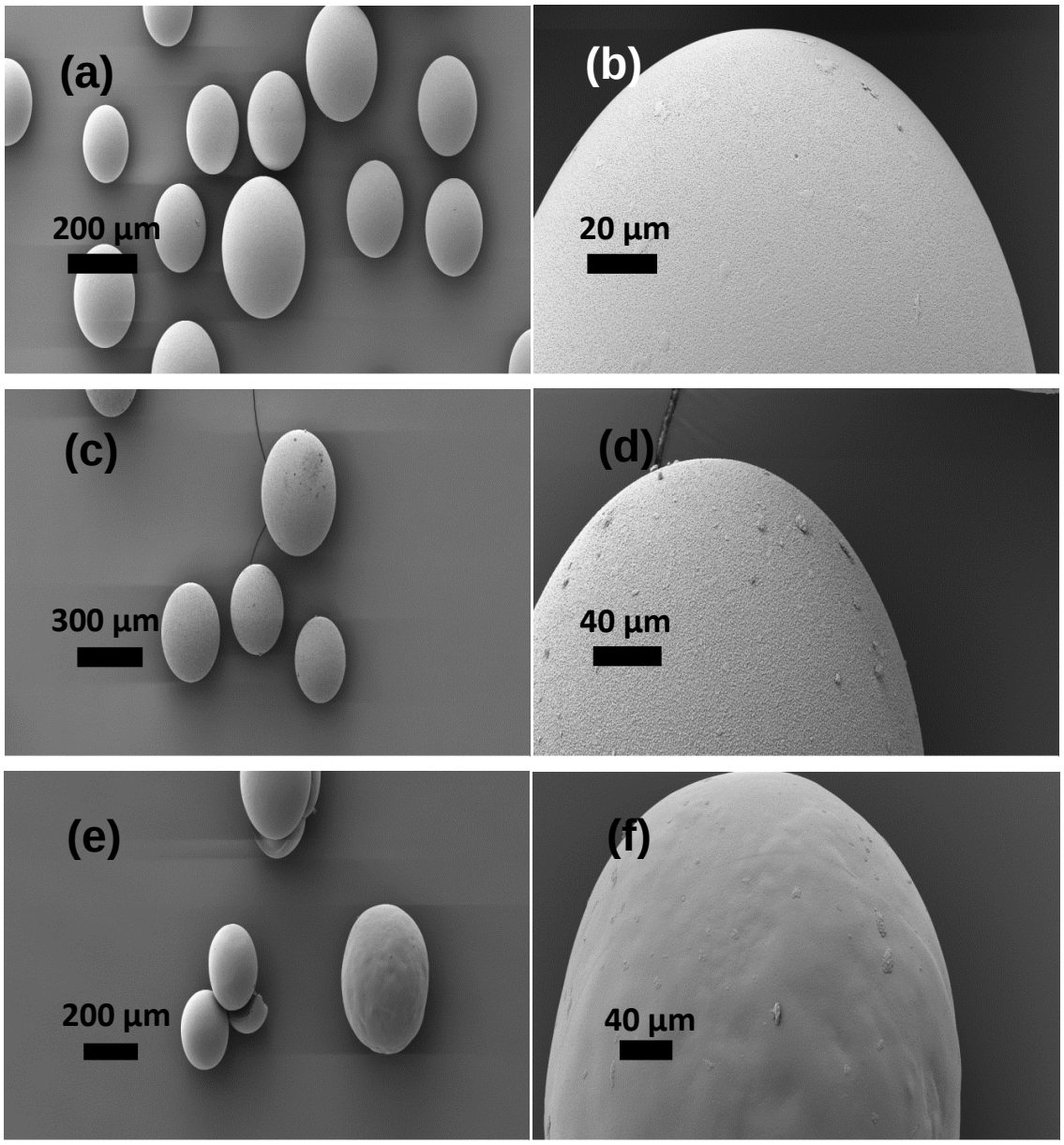


Figure 4.19 SEM characterization of (a) & (b) unmodified Sephadex® G-50 microspheres, (c) & (d) Sephadex® G-50 microspheres after attachment of a polymerization initiator, 2-bromopropionyl bromide (S-Br microspheres), and (e) & (f) PNIPAAm-grafted Sephadex® G-50 microspheres (S-Br-PNIPAAm microspheres). Courtesy of Dr. Fazlul Chowdhury.

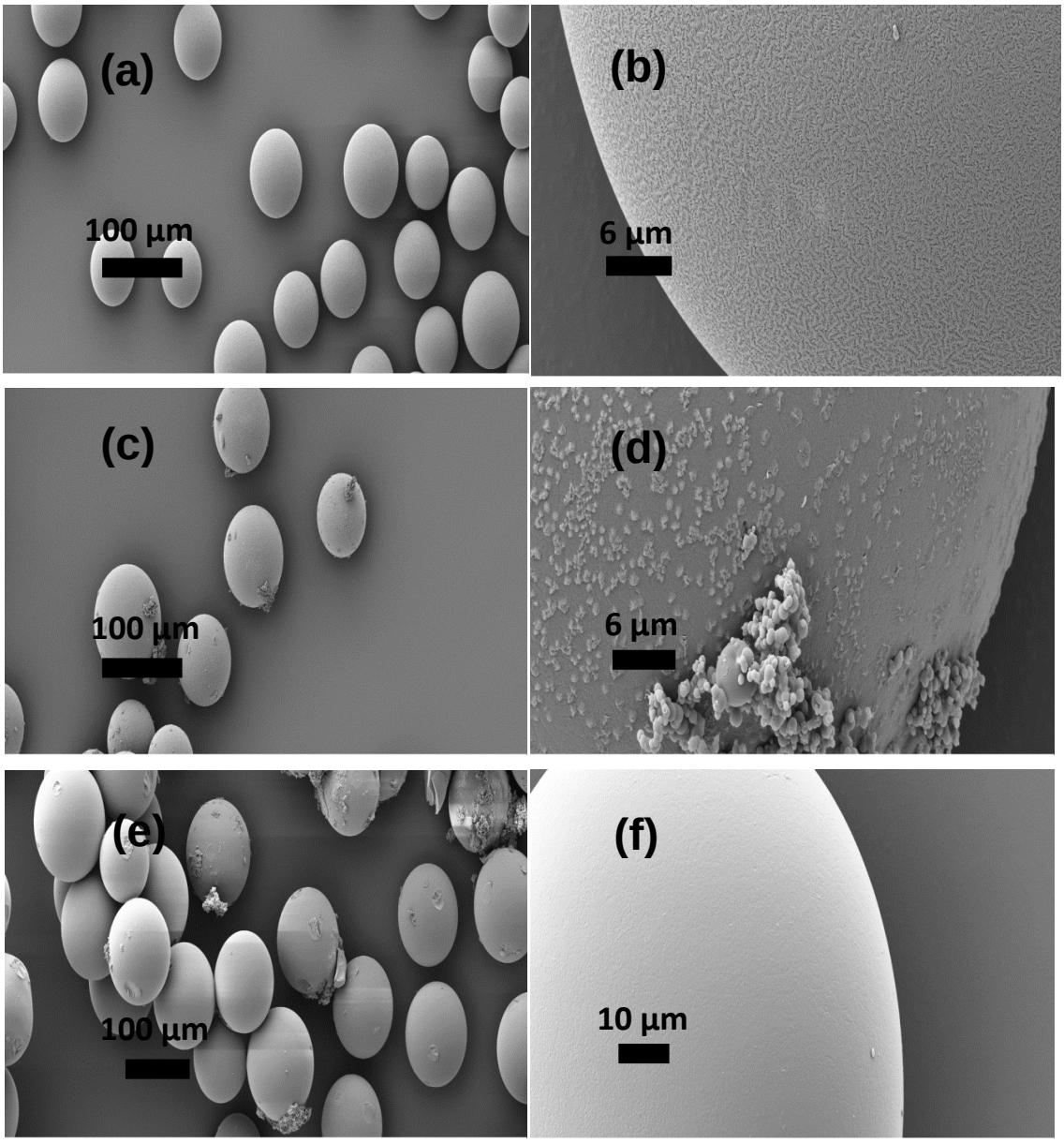


Figure 4.20 SEM characterization (a) & (b) unmodified Cytodex®-1 microspheres, (c) & (d) Cytodex®-1 microspheres after attachment of a polymerization initiator, 2-bromopropionyl bromide (i.e., C-Br microspheres), and (e) & (f) PNIPAAm-grafted Cytodex®-1 microspheres (i.e., C-Br-PNIPAAm microspheres). Courtesy of Dr. Fazlul Chowdhury.

4.4 Summary

The ‘grafting-from’ method consists of two steps: immobilization of a polymerization initiator onto the surface of microspheres, and subsequent growth of PNIPAAm chains directly from the first immobilized initiators. In this study, two ‘grafting-from’ strategies were employed, namely 1) conventional radical grafting polymerization and 2) atom transfer radical polymerization (ATRP).

In the strategy of conventional radical grafting polymerization, an azo-initiator, ACVA, was first immobilized onto polystyrene microspheres via esterification using DIC as a coupling agent and DMAP as a catalyst. The grafting density of ACVA can be regulated by changing the feed amount of ACVA. And the achievable grafting density (~913 μmol/g) is much higher than that proposed on literature (550 μmol/g). This simple way to control the grafting density of the azo-initiator clearly demonstrates the advantage of using this one-step esterification procedure. The subsequent polymerization reactions of NIPAAm with surface-immobilized ACVA with grafting density of 823.22 μmol/g (PS-ACVA-1.68) were performed in dioxane solutions at 70 ℃ for 24 h. It was found that 40% of the immobilized ACVA finally generates polymer chains, thus the PNIPAAm grafting density was ~329 μmol/g. This value is almost 12-fold higher than the maximum density of PS-O-OC-PNIPAAm beads (~27 μmol/g) prepared by ‘grafting-to’ method. The resulting PNIPAAm grafted amount was found to be increased with increasing the feed concentration of NIPAAm monomers. The achievable PNIPAAm grafted amount (~697 mg/g) is also much higher than that of PS-O-OC-PNIPAAm microspheres (~299 mg/g). Further, two types of PNIPAAm hydrogel were grafted to polystyrene microspheres via this strategy, namely PNIPAAm homopolymer hydrogel and comb-type hydrogel. The latter was prepared by copolymerizing NIPAAm with a

cross-linker, MBAAm, in the presence of a PNIPAAm macromonomer on the surface of the ACVA-immobilized microspheres, such that the free mobile PNIPAAm chains were grafted onto cross-linked networks. Finally, branched PNIPAAm architecture was prepared using PHEA or PSHEA as backbone. The PNIPAAm branches were immobilized to the backbones via either ‘grafting-to’ or ‘grafting-from’ technique.

In the ATRP strategy, an ATRP initiator, 2-bromopropionyl bromide, was grafted onto cross-linked dextran microspheres. The grafting density of ATRP initiator was increased with increasing the feed amount of 2-bromopropionyl bromide. PNIPAAm chains were then grafted from the immobilized 2-bromopropionyl groups using aqueous ATRP at room temperature. The PNIPAAm grafted amount and molecular weight were found to be dependent on the density of the immobilized ATRP initiator. With increasing the density of immobilized ATRP initiator, both grafted amount and molecular weight of PNIPAAm were significantly decreased. This might be because higher density of ATRP initiator causes more polymer radicals grow simultaneously, leading to a higher concentration of growing radicals on the surface. This increases the possibility that two of them are generated and grow in such close vicinity that the active chains meet and terminate each other by recombination or disproportionation.

5 Seeded precipitation polymerization for microsphere modification

5.1 Introduction

Seeded precipitation polymerization starts with a mixture containing NIPAAm monomers with a cross-linker, MBAAm, in the presence of seed particles. Upon polymerization, the formed cross-linked PNIPAAm hydrogel precipitates out and adsorbs on the surface of seed particles. There is likely to be no covalent bond between the adsorbed cross-linked PNIPAAm and the seed particles, unless reaction starts at a surface inhomogeneity. The stability of the modified PNIPAAm relies on the encapsulation of the cross-linked PNIPAAm on the seed particles. The particles encapsulated by PNIPAAm hydrogel suffer no problem from grafting density and PNIPAAm molecular weight, and this method is experimentally simple. However, the molecular architecture of grafted PNIPAAm is restricted because of the cross-linked form. Also, seeded polymerization is limited by side reactions. Upon initiation and propagation, a portion of the precipitated crosslinked PNIPAAm is unable to adsorb to the particles' surface. This causes a continuous nucleation and coagulation process which leads to the formation of bulk PNIPAAm hydrogel particles. Nevertheless, such hydrogel particles which are formed are usually much smaller than the seed particles and can be removed by filtration and decantation. In this study, cross-linked PNIPAAm hydrogel was grafted to carboxyl functionalized polystyrene particles via seeded precipitation polymerization. The amount of grafted PNIPAAm hydrogel was regulated

by changing the feed concentration of NIPAAm monomer with corresponding amount of MBAAm.

5.2 Materials and methods

5.2.1 Materials

4,4′-Azobis(4-cyanovaleric acid) (ACVA, ≥98.0%), methanol (HPLC grade, ≥99.9%), *N*,*N*′-methylenebis(acrylamide) (MBAAm) were purchased from Sigma-Aldrich (UK) and used as received. Polystyrene A COOH microspheres (PS-COOH, 160-200 μm, -COOH group content: 0.8-1.2 mmol/g) were obtained from RAPP POLYMERE (Germany) and used as received. Acetonitrile (HPLC grade) was purchased from Rathburn (UK).

N-Isopropylacrylamide (NIPAAm, 97%, Sigma-Aldrich) was purified by recrystallisation from hexane/toluene followed by filtration and drying (see Section #). Deionised water (DI water) used in this study was obtained from an ultrapure water purification system (Elix®, Millipore).

5.2.2 Preparation of PNIPAAm hydrogel-modified microsphere

NIPAAm (2.0 g, 0.018 mol), MBAAm (0.2 g, 1.3 mmol), ACVA (0.1 g, 0.36 mmol) and PS-COOH microspheres (0.5 g) were added in acetonitrile (50 mL) and the mixture was deoxygenated by nitrogen bubbling for 1 h at room temperature. Then, the polymerization was conducted at 70 ^{o}C for 24 h under nitrogen atmosphere. The

resulting beads were filtered and washed with methanol three times by decantation to remove any un-immobilized hydrogels. The particles were dried by vacuum suction for 1 h.

5.2.3 Characterizations and measurements

5.2.3.1 FTIR spectroscopy measurements

Fourier transform infrared (FTIR) spectra were recorded using an FTIR spectrometer (FTS 6000, BIO-RAD) equipped with attenuated total reflectance (ATR) setup (DuraSampl*IR* II^{TM}, SensIR Technologies). 200 scans were averaged to yield the spectra at a resolution of 4.0 cm^{-1}. Before collecting sample spectra, the background spectrum was collected by measuring the response of the spectrometer without sample.

5.2.3.2 Combustion analysis

The mass percentages of C, H and N of the unmodified and modified microspheres were tested by combustion analysis. The combustion analysis was conducted by MEDAC Ltd (Surrey, UK).

The grafted amount (m_p) of cross-linked PNIPAAm on PS-COOH bead surface was calculated from the increment in nitrogen content derived from the amide bond of cross-linked PNIPAAm. It was calculated as follows:

$$m_p(\mathrm{mg/g}) = \frac{N_p\% - N_0\%}{N_{p,theory}\% - N_0\%} \times 10^3$$

where $N_p\%$ and $N_0\%$ represent the nitrogen contents in modified and unmodified beads respectively, and $N_{p,theory}\%$ represents the theoretical nitrogen content of cross-linked PNIPAAm.

5.3 Results and discussion

The PNIPAAm hydrogel-modified microspheres were prepared by seeded precipitation polymerization of NIPAAm and a cross-linker, MBAAm, in acetonitrile using ACVA as an initiator. The mass ratio of NIPAAm to MBAAm was 10/1. Carboxyl functionalized polystyrene beads (PS-COOH) were used as the seeds for the growth of the PNIPAAm hydrogel layer. The mechanism of the seeded polymerization was illustrated in Figure **5.1**. The synergic hydrogen-bonding interaction between the carboxyl groups on the surface of PS-COOH seed particles and amide groups of NIPAAm and MBAAm was believed to play a key role as a driving force to promote the formation of the PNIPAAm hydrogel layer (Bai et al. 2004; Bai et al. 2007; Liu et al. 2007a; Li et al. 2008). Before polymerization, residual NIPAAm or MBAAm monomers can be adsorbed on the PS-COOH seed particles via the hydrogen-bonding interaction, providing the incorporated vinyl groups on the particle surface. Upon polymerization, these adsorbed vinyl groups captured the newly formed active oligomers, leading to the growth of the PNIPAAm hydrogel film on the surfaces of the seed particles. Any cross-linked PNIPAAm species formed in solution precipitated out of the homogeneous reaction system onto the newly formed PNIPAAm film on particle surface due to the strong hydrogen-bonding interaction between the amide groups, as the acetonitrile is a non-protonic polar solvent not interfering in the hydrogel-bonding

interaction (Liu et al. 2007b). However, the PNIPAAm hydrogel species or the oligomers formed in solution can also attract each other and aggregate together, resulting in small hydrogel particles during the polymerization, i.e., by nucleation and coagulation processes. However, these small hydrogel particles can be easily separated from the hydrogel grafted particles by repeat decantation.

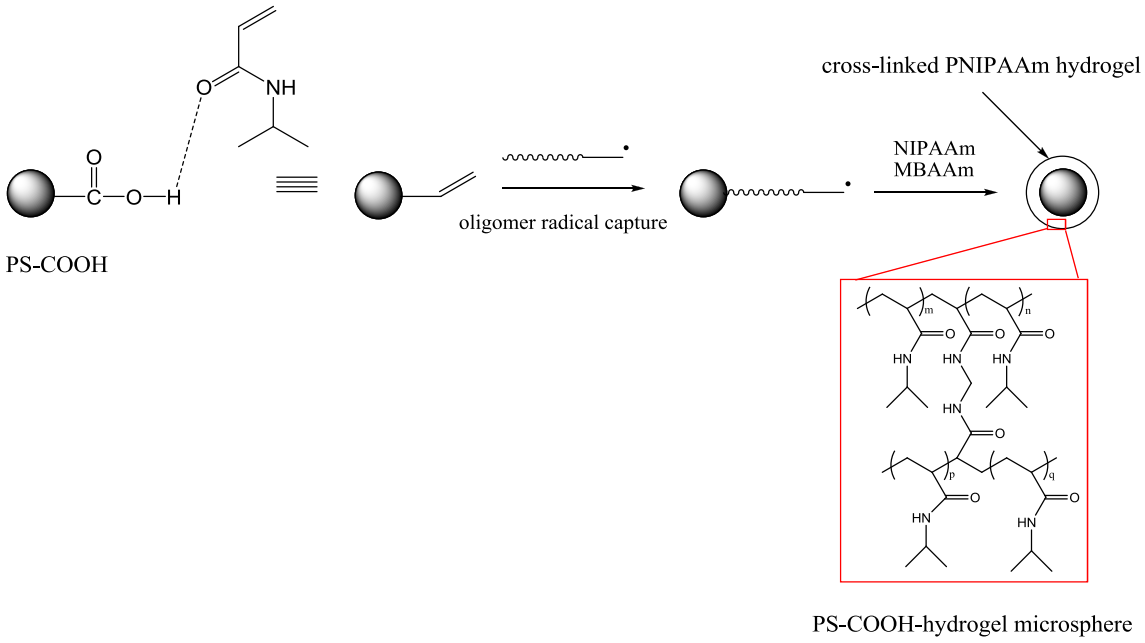


Figure 5.1 The mechanism of the seeded polymerization mediated by hydrogen-bonding

The encapsulation of PNIPAAm hydrogel onto the surface of PS-COOH microspheres was confirmed by FTIR spectroscopy. The FTIR spectrum (Figure **5.2**) of PNIPAAm hydrogel-modified beads (PS-COOH-hydrogel) shows the peaks characteristic of PNIPAAm at 1640 cm^{-1} (amide I bond, arising from C=O stretching and little C-N stretching) and 1550 cm^{-1} (amide II bond, arising from N-H bending and C-N stretching), which were absent in the FTIR spectrum of unmodified PS-COOH beads. The detailed chemical composition of the modified and unmodified particles was analyzed by combustion analysis (Table **5.1**). The nitrogen content of the PNIPAAm hydrogel-modified particles was much higher than that of the unmodified particles,

indicating successful introduction of the amide groups of PNIPAAm hydrogel. The grafted amount of PNIPAAm hydrogel on the modified particle surface was calculated from the increment in nitrogen composition in comparison with PS-COOH microspheres. It was also found that the grafted amount of hydrogel was increased with increasing the feed amount of NIPAAm monomer with corresponding amount of MBAAm.

Bead code[a]	Feed amount of NIPAAm (g/50 mL)	Feed amount of MBAAm (g/50 mL)	Nitrogen content (wt%)[b]	Grafted amount of PNIPAAm hydrogel (mg/g)
PS-COOH	N/A	N/A	1.06 ±0.02	0
PS-COOH-hydrogel-0.5/0.05	0.5	0.05	2.06 ±0.06	88.7 ±5.5
PS-COOH-hydrogel-1.0/0.1	1.0	0.1	2.27 ±0.02	107.0 ±2.0
PS-COOH-hydrogel-2.0/0.2	2.0	0.2	2.67 ±0.05	142.9 ±4.5

a: Abbreviated as PS-COOH-hydrogel-X/Y, where X and Y represent the feed amount of NIPAAm and MBAAm respectively

b: The data were expressed as the mean ± SD; n=3

Table 5.1 Characterization of PS-COOH-hydrogel microspheres

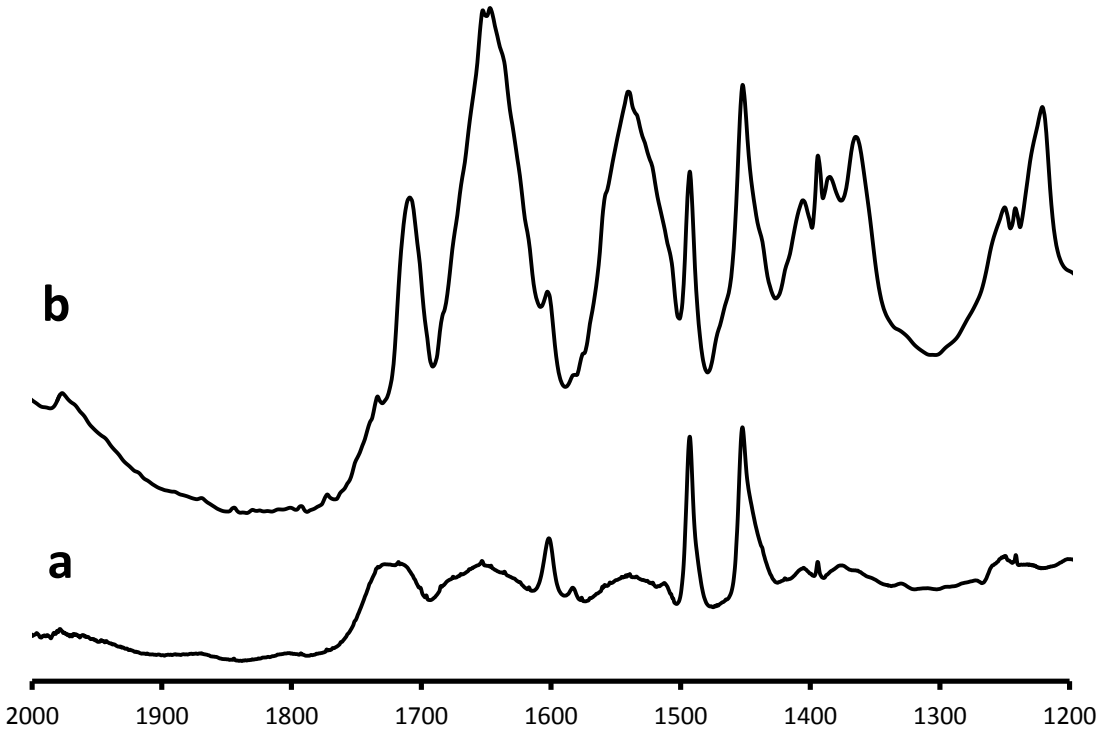


Figure 5.2 FTIR spectra of (a) PS-COOH microsphere and (b) PS-COOH-hydrogel microsphere.

5.4 Summary

In this study, cross-linked PNIPAAm hydrogel was grafted to carboxyl functionalized polystyrene (PS-COOH) particles via seeded precipitation polymerization in acetonitrile. The formation of PNIPAAm hydrogel layer was driven by the synergic hydrogen-bonding interaction between the carboxyl groups of PS-COOH seed particles and the amide groups of NIPAAm as well as MBAAm units. It was also found that the grafted amount of hydrogel was increased with increasing the feed amount of NIPAAm monomer with corresponding amount of MBAAm.

6 Characterisation of thermo-responsive properties of modified microspheres for cell culture

6.1 Introduction

The purpose of this study is to investigate the cytotoxicity of PNIPAAm-grafted microcarriers and the effects of physicochemical properties of PNIPAAm-grafted microcarriers on cell attachment and thermally-induced detachment behaviour. Such an investigation is necessary if these microspheres are to be used as microcarriers. In cytotoxicity assays, cells were co-cultured in normal 12-well plates for 7 days with representatives of each microcarrier grafting technique. The alamarBlue® reagent was employed to quantify the cell proliferation. In cell attachment experiments, cells were cultured for 24 h with the PNIPAAm-grafted beads of varied grafting parameters, such as PNIPAAm grafted amounts, grafting densities, molecular weights and molecular architectures. The experiments were conducted in a non-cell adhesive 12-well plate to prioritise the cell attachment to the microcarriers rather than the well plate. Finally, the microcarriers to which cells attached were incubated at 4 ℃ for 2 h to investigate thermally-induced cell detachment.

6.2 Materials and methods

6.2.1 Materials

Penicillin-streptomycin solution, puromycin dihydrochloride (10 mg/mL in H_2O), trypsin-EDTA solution, siliconizing reagent (Sigmacote®), ethylenediaminetetraacetic acid (EDTA; ≥99%) and ethanol were purchased from Sigma-Aldrich (UK). Dulbecco's modified Eagle's medium – high glucose (HG-DMEM) (without phenol red, Gibco®), RPMI-1640 medium (without phenol red, Gibco®) and fetal bovine serum (FBS) (Gibco®) and alamarBlue® (AB) reagent were obtained from Invitrogen (UK). Dulbecco's Phosphate-Buffered Saline (PBS, Ca^{2+} and Mg^{2+} free) was received from PAA Laboratories GmbH (Austria). Deionised water (DI water) used in this study was obtained from an ultrapure water purification system (Elix®, Millipore).

Non-cell adhesive 12-well plates (HydroCell) were from CellSeed (Japan) and all other tissue culture plastics used were from Corning (USA).

6.2.2 Methods

6.2.2.1 Isolation of rADSCs

Rat adipose-derived stem cells (rADSCs) were isolated using Zhu et al. (2009)'s method. The rat adipose tissue was kindly provided by the Department of Physiology, Anatomy and Genetics, Oxford University. Briefly, approximately 400–600 mg of rat adipose tissue was minced finely using surgical scissors and incubated in trypsin-EDTA solution at 37 ℃ with constant agitation for 25 min. The stromal–vascular fraction (SVF) was then collected by centrifugation at 1500 rpm for 10 min. The cell pellet was

resuspended in complete culture medium (HG-DMEM containing 10% (v/v) FBS, and 1% (v/v) penicillin-streptomycin solution). rADSC (Passage 0) suspension was cultured in a 25 cm^2 cell culture flask at 37 ℃ and 5.0% CO_2 in humidified incubators. Cells were fed every 3 to 4 days by replacing 100% of the medium.

6.2.2.2 Preparation of GFP cells

Breast cancer cells (NCI/ADR-RES) stably expressing enhanced green fluorescent protein (GFP) were engineered using self inactivating lenti virus (SIN) to deliver the enhanced GFP cassette under the control of human elongation factor promoter (EF1 alpha). The transfection experiments were kindly conducted by Dr. Yasser El-sherbini (Department of Engineering Science, Oxford). The cells expressing enhanced GFP are henceforth referred to as GFP cells. The GFP cells were cultured in RPMI-1640 medium containing 10% (v/v) FBS, 1% (v/v) penicillin-streptomycin and 10 μg/mL puromycin. Puromycin was used as a selection marker to ensure the maintenance of stably transfected cells and to prevent a dilution effect caused by non-transfected cells.

6.2.2.3 Monolayer cell cultivation

rADSCs and GFP cells were seeded in monolayers at a density of 1×10^4 cells per cm^2 in complete culture medium in 175 cm^2 cell culture flasks. Cells were fed every other day by replacing 100% of the medium. Having reached 80% confluence, cells were trypsinized and subcultured at the same seeding density. rADSCs of Passage 40 to 60 or GFP cells of Passage 30 to 40 were used in the experiments.

6.2.2.4 Preparation of microcarriers for culture

0.5 g dry unmodified Sephadex® G-50 and Cytodex®-1 microcarriers were added into a siliconized (i.e., Sigmacote® treated) glass bottle and swollen in 50 mL PBS overnight at room temperature with occasional gentle agitation. The supernatant was decanted and the microcarriers were washed twice and sedimented in 50 mL fresh PBS. The microcarriers were then sterilized by autoclaving (SES 2000, Eschmann, UK) with steam from purified water at 120 ℃ for 20 min. PS-OH, PS-COOH or PNIPAAm-grafted microcarriers (0.5 g) were washed thoroughly with deionized water and then sterilized by immersion in 70% (v/v) ethanol at room temperature overnight. The ethanol solution was decanted and the microcarriers were rinsed five times using 50 mL sterile PBS. All the sterile microcarriers were stored in PBS at 4 ℃.

Prior to use, the PBS solution was decanted and the microcarriers were rinsed 5 times using 50 mL warm culture medium to reduce dilution of the culture medium by PBS trapped between and within the microcarriers. The microcarriers were then allowed to settle again, the supernatant was removed and the microcarriers were resuspended in 50 mL fresh warm culture medium (final microcarrier concentration: 10 mg/mL).

6.2.2.5 Cytotoxicity assays

The cytotoxicity of the microcarriers was tested by co-culturing cells in normal 12-well plates for 7 days with the microcarriers prepared by various methods. The unmodified and modified Sephadex® G-50 microcarriers were co-cultured with rADSCs whilst the rest of the microcarriers were co-cultured with GFP cells. Cell viability was detected by alamarBlue® (AB) assay.

6.2.2.5.1 Standard curve

Cells were trypsinized from subconfluent cultures by adding 10 ml of trypsin solution to 175 cm^2 cell culture flasks followed by 5 min incubation at 37 ℃ with regular gentle shaking. The trypsin reaction was stopped by adding 20 ml of culture medium containing 10% (v/v) FBS. The cell suspension was then centrifuged at 1000 rpm for 5 min at 20 ℃. The cell pellet was resuspended in warm fresh medium and thoroughly mixed by repeated pipetting to generate single cell suspension. The cell number was counted using a Neubauer hemacytometer (Marienfeld, Germany) and then brought first to a concentration of 8×10^5 cells/ml and subsequently to serial dilutions, such as 6×10^5 cells/ml, 4×10^5 cells/ml, 2×10^5 cells/ml, 1×10^5 cells/ml, 0.5×10^5 cells/ml and 0.25×10^5 cells/ml. The resulting different cell suspensions were then seeded into duplicate wells of a 9-well plate (100 µL per well). 10 µl of AB solution was directly added to the medium resulting in a final concentration of 10%. As a negative control, 10 µl of AB was added to 100 µl of medium without cells. The plate was incubated for 2 h at 37 ℃. The fluorescent intensity of the solution in test and control wells was measured with an excitation wavelength at 485 nm and an emission wavelength at 590 nm using a microplate reader (Wallac Victor 1420 multilabel counter, PerkinElmer, USA). The number of viable cells correlates with the magnitude of dye reduction and is expressed as the percentage of AB reduction (Al-Nasiry et al. 2007). The calculation of the percentage of AB reduction (%AB reduction) is as follows according to the manufacturer's protocol:

$$\%AB\ reduction = \frac{\text{FI (sample)} - \text{FI (control)}}{\text{FI (100\%)} - \text{FI (control)}} \times 100$$

where :

FI (sample) = fluorescent intensity of test wells

FI (control) = fluorescent intensity of negative control wells (containing medium without cells)

FI (100%) = fluorescent intensity of 100% reduced alamar blue, which was produced by incubating cells (12×10^5 cells/mL) with AB for 24 h.

Finally, the percentage of AB reduction was plotted versus corresponding cell concentration giving a standard curve.

6.2.2.5.2 Cell inoculation with microcarriers

Prior to inoculation, the prepared microcarrier suspension (10 mg/mL) was homogenized by gentle agitation and 1 mL of microcarrier suspension was then transferred to each well of a normal 12-well plate. Cells were harvested from tissue culture flasks as described earlier. The cells were resuspended in warm fresh medium and the cell density was adjusted to 2×10^5 cells/mL. Then, 1 mL of cell suspension (2×10^5/mL) was transferred to the wells containing the microcarriers. The final cell density and microcarrier concentrations were 1×10^5 cells/mL and 5 mg/mL respectively in each well containing 2 mL of medium. The cultures were incubated in a 37℃ incubator with 5% CO_2 with a 20% media change every other day.

6.2.2.5.3 AB assay for cell proliferation

The AB assays were conducted at day 1, 3, 5 and 7. For each assay, 200 µL of AB was directly added to each culture and the plate was incubated for 2h. As a negative control, 200 µl AB was added to 2 mL of medium without cells. 110 µL of supernatant from each test and control well was then transferred into the wells of a 96-well plate. The fluorescence of each well in the 96-well plate was measured with an excitation

wavelength at 485 nm and an emission wavelength at 590 nm using a microplate reader (Wallac Victor 1420 multilabel counter, PerkinElmer, USA). The fluorescence number was converted to the percentage of AB reduction and the cell number was then calculated according to the standard curve.

6.2.2.5.4 Removal of copper ions

EDTA solution was used to remove Cu^{2+} trapped within the PNIPAAm-grafted Sephadex® G-50 and PNIPAAm-grafted Cytodex®-1 microspheres. The microspheres were washed thoroughly with DI water and resuspended in 20 mL of 0.1 M EDTA solution in a 50 mL centrifuge tube with agitation for 1 h. 1 mL of supernatant was then transferred into a rectangular UV-cuvette. The absorbance of the cuvette was then read at 326 nm with a spectrophotometer (HeλIOS, Thermo Spectronic, UK) and 1 mL EDTA solution was used as a negative control. The microspheres were separated from the used EDTA solution by filtration and the microspheres were resuspended and immersed in 10 mL of 0.1 M fresh EDTA solution for 1 h. The absorbance of the supernatant was measured again. The whole process was repeated 9 times.

6.2.2.6 Cell attachment experiments

GFP cells at Passage level 30 to 40 were seeded into a non-cell adhesive 12-well plate (HydroCell, CellSeed, Japan) at a density of 1×10^5 cells/mL. To each well, unmodified or PNIPAAm-grafted beads were added and the applied amount was adjusted to be 5 mg/mL. The final volume of the medium was adjusted to be 2 mL/well. After 24 h of incubation, 1 mL of medium was carefully changed to fresh warm medium (37 ℃). This procedure was repeated four times to remove single non-adhered cells. The attachment of GFP cells on the microcarriers was observed at 37 ℃ by an optical microscope (ECLIPSE 80i, Nikon, Japan).

6.2.2.7 Cell detachment experiments

After 24 hours of static cell culture, the temperature of the culture medium was reduced from 37 ℃ to 4 ℃. The attached GFP cells were then incubated at this lower temperature of 4 ℃ for 2 hours. The thermally-induced detachment of GFP cells was observed at room temperature by an optical microscope (ECLIPSE 80i, Nikon, Japan).

6.3 Results and discussion

In cytotoxicity assay, cell might die ether because the PNIPAAm-grafted microcarriers are toxic or because they are not able to attach anywhere. Therefore, normal 12-well plates were used for this assay to ensure that some cell attachment would be possible, and thus this avoids a false negative result from the assay. However, in cell attachment experiments, non-cell adhesive 12-well plates were used, because in this case it is necessary to force cell attachment to the beads and avoid preferential attachment to the plates.

6.3.1 Cytotoxicity assay of cross-linked dextran based microcarriers

Rat adipose-derived stem cells (rADSCs) were used preferentially in this experiment. The main benefit of rADSCs is that they can be easily harvested from adipose tissue by a simple, minimally invasive method and can also be easily cultured compared with other stem cells (Nakagami et al. 2006). The alamarBlue® (AB) assay was employed to analyze cell proliferation and cytotoxicity having co-cultured rADSCs with unmodified and modified Sephadex® G-50 microcarriers. Upon entering cells, the non-fluorescent

blue oxidized form of AB is converted to the fluorescent pink reduced form via mitochondrial enzyme activity in cytosol (Al-Nasiry et al. 2007). The shift in colour of the culture medium can be easily measured by colourimetric or fluorometric reading and converted to the magnitude of AB reduction. The AB standard curve (Figure **6.1**) shows the number of viable rADSCs correlated linearly (R^2=0.9474) with the percentage AB reduction after 2 hours of incubation.

The AB assays for microcarrier cell cultures were taken at days 1, 3, 5 and 7, and the cell densities were calculated according to the standard curve after measuring the percentage of dye reduction. For all experiments, rADSCs were inoculated at 1×10^5 cells/mL whilst the microcarrier concentration was 5 mg/mL. The numbers of rADSCs cultured with unmodified and modified Sephadex® G-50 microcarriers are shown in Figure **6.2**. It should be noted that the cells were cultured within a normal 12-well plate containing the beads. The data represented sums of both cells attached to the bead surfaces as well as the bottom of tissue culture wells. When cultured with unmodified Sephadex® G-50 microcarriers, rADSCs can proliferate over the 7-day period. There was a 13-fold increase in cell population by day 7. In contrast, when cells were cultured with modified microcarriers the growth of rADSCs was significantly inhibited and little change was seen in the cell density over a 7-day period. Cell proliferation inhibition correlates with cytotoxicity, so the modified microcarriers (without EDTA treatment) used in this study are toxic to cells. In the ATRP process, Cu^+ ions were used as catalysts and then oxidised to Cu^{2+} ions in the washing treatments. Cu^{2+} ions were not depleted from the PNIPAAm grafted microcarriers by the washing treatments at room temperature and might be released to the culture medium due to the increase of temperature required for cell culture. The propagation inhibition and death of rADSCs observed in modified microcarrier cell culture may result from the Cu^{2+} ions. Although

it could not be verified, it is possible that Cu^{2+} is present in the modified beads because the beads were green in colour. Therefore, 0.1 M EDTA solution was used to remove Cu^{2+} ions trapped in the modified microspheres, as EDTA can form strong complexes with Cu^{2+} and sequester them in aqueous solution. According to the absorbance of EDTA solution at 326 nm after each wash (Figure **6.3**), the green colour in EDTA solution was significantly decreased after washing 4 times with 0.1 M EDTA solution. This may suggest that the amount of Cu^{2+} ions trapped in the PNIPAAm-grafted beads was also significantly reduced. The cytotoxicity assay was conducted again using the modified beads following EDTA treatment (4 times). It was found that rADSCs can proliferate and cell number increased by 17-fold by over 3 days. The cell density then decreased as the cells reached confluence. This indicates that the EDTA treatment was able to remove the Cu^{2+} ions trapped in the PNIPAAm-grafted beads and the resulting beads were no longer toxic.

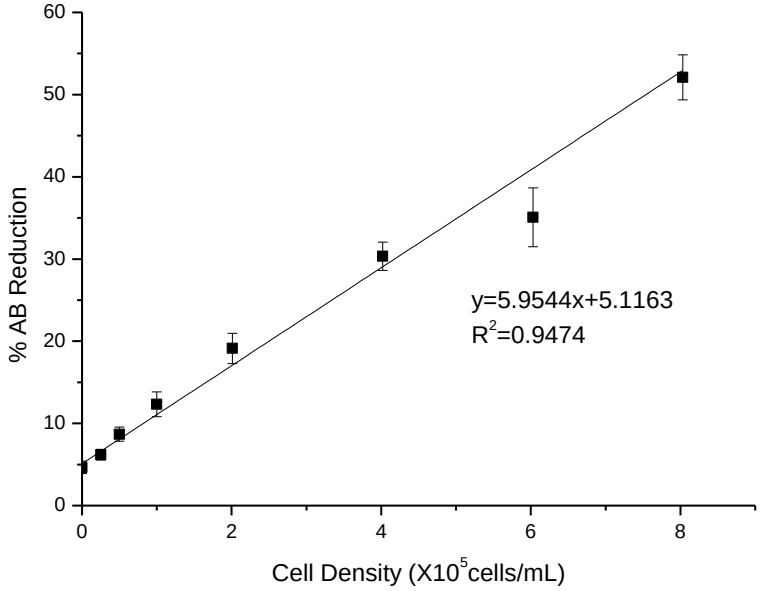


Figure 6.1 Standard curve of %AB reduction versus rADSC densities (n=8).

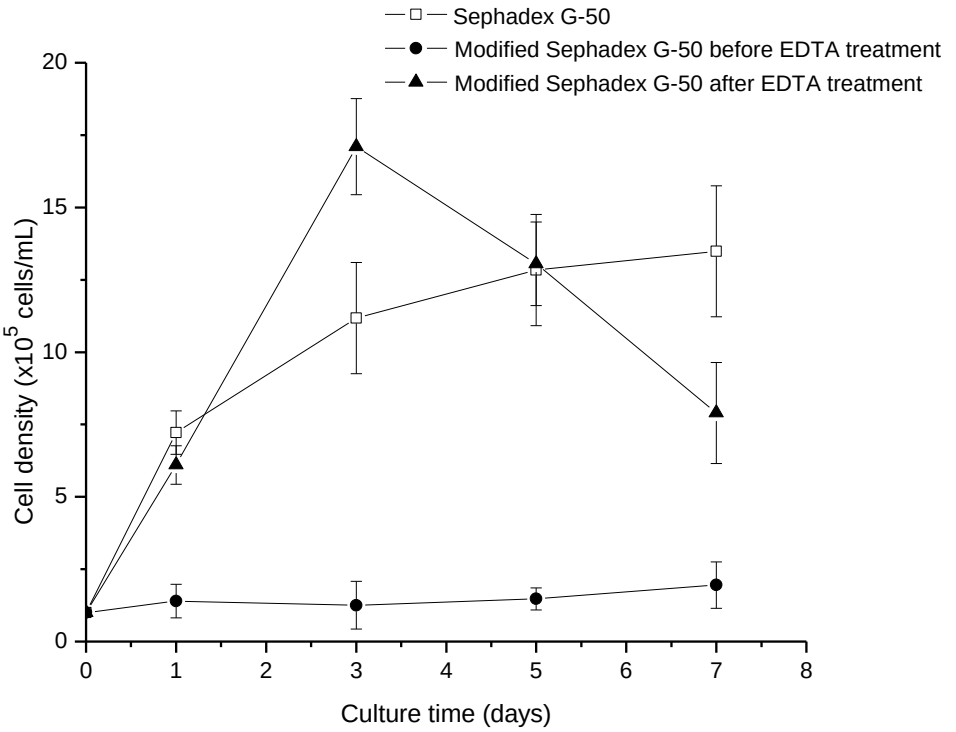


Figure 6.2 Growth of rADSCs in normal 12-well plates co-cultured with unmodified and modified Sephadex® G-50 microcarriers (n=4).

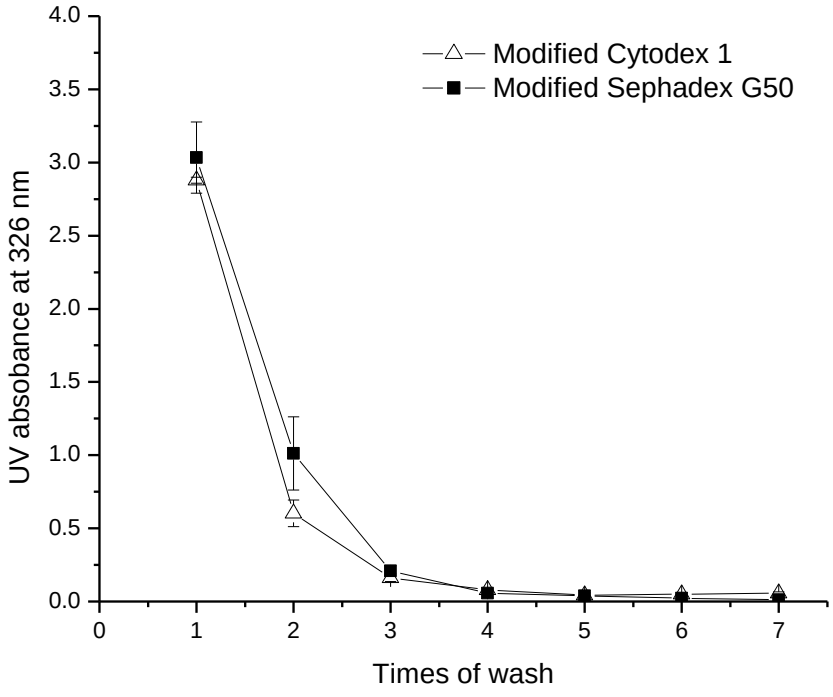


Figure 6.3 UV absorbance of EDTA solution at 326 nm (n=3).

6.3.2 Cytotoxicity assay of cross-linked polystyrene based microcarriers

The GFP cells were cultured with the modified and unmodified cross-linked polystyrene based microspheres to analyze the cytotoxicity of these beads, and the AB assay was used to quantify the cell number and viability. When the percentage of AB reduction was plotted against the cell concentrations, the standard curve was linear between 0 and 8×10^5 cells/mL (Figure **6.4**). Figure **6.5** demonstrates the growth profiles of GFP cells cultured with PNIPAAm-grafted microspheres prepared by the grafting-to technique. All groups showed an increase in cell number over the 7 day period, equivalent to the control group. It was found that the cells in PS-O-OC-PNIPAAm group proliferated more slowly, up to day 5, and then showed an increased proliferation rate. The reason for this observed difference is unknown and further investigations would be required. Figure **6.6** shows the growth profiles of GFP cells cultured with PNIPAAm-grafted microspheres prepared by the grafting-from technique. All groups were seen to survive and proliferate in culture. Although there are some differences between the profiles shown on the graph, these differences are likely to be due to unpredictable differences in initial cell proliferation rates and further investigations are required to determine if this effect is due to material characteristics or non-characterised experimental error. Figure **6.7** shows the growth profiles of GFP cells cultured with PNIPAAm-grafted microspheres prepared by seeded precipitation polymerization. Cells were seen to increase in number on both the control and modified beads. This shows that the cells were viable when cultured with the modified beads, and that the modification was not toxic to the cells.

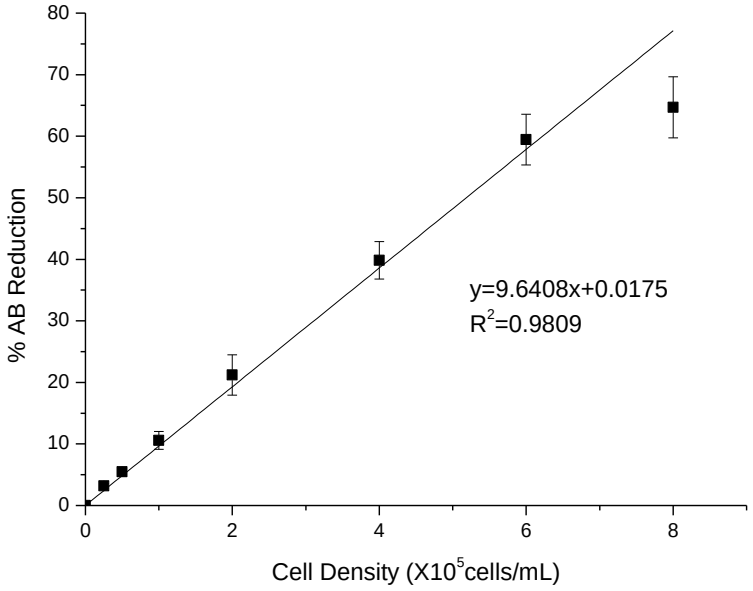


Figure 6.4 Standard curve of %AB reduction versus GFP cell densities (n=8).

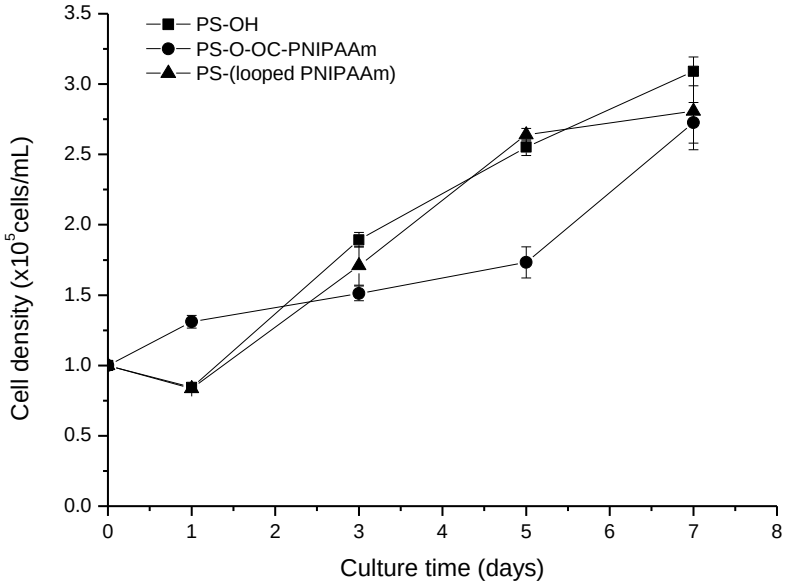


Figure 6.5 Growth of GFP cells in normal 12-well plates co-cultured with PNIPAAm-grafted microspheres prepared by grafting-to technique (n=4)

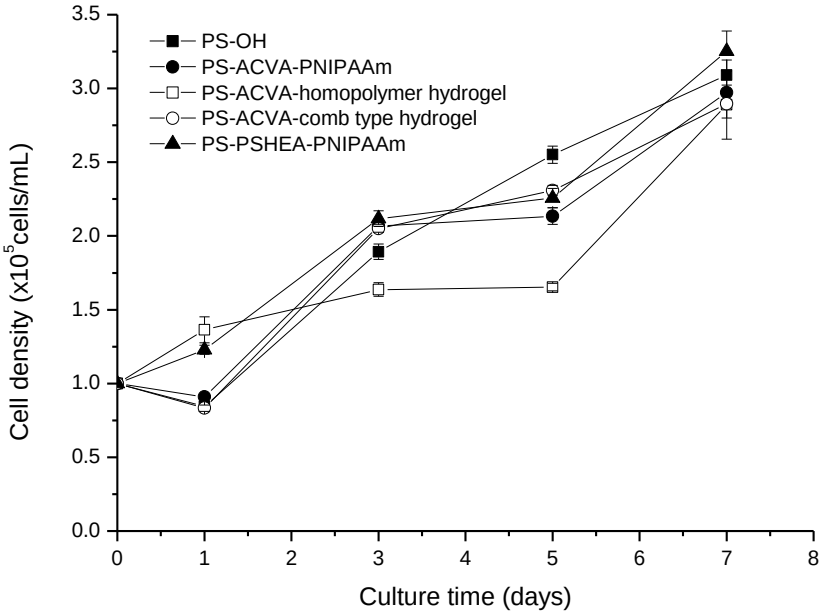


Figure 6.6 Growth of GFP cells in normal 12-well plates co-cultured with PNIPAAm-grafted microspheres prepared by grafting-from technique (n=4).

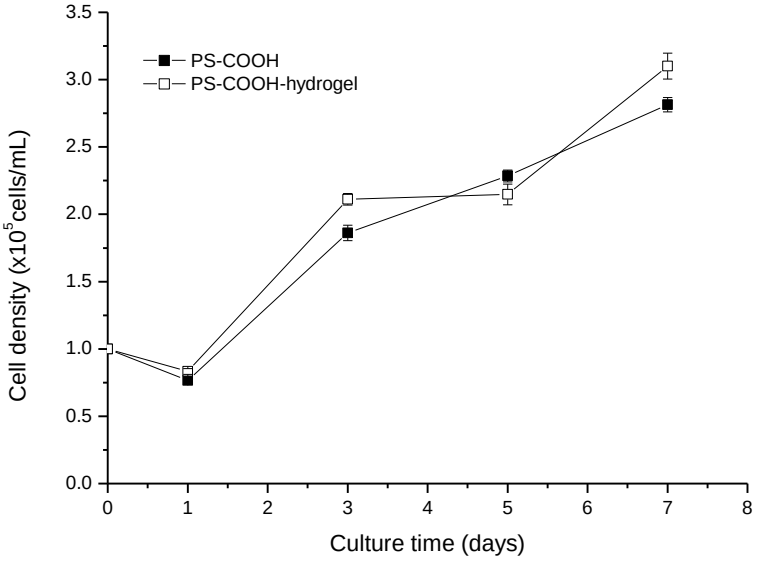


Figure 6.7 Growth of GFP cells in normal 12-well plates co-cultured with PNIPAAm-grafted microspheres prepared by seeded precipitation polymerization (n=4).

6.3.3 Cell attachment experiments

The cell attachment experiments were conducted in a non-cell adhesive 12-well plate in order to prioritise the cell attachment to the microcarriers rather than the well plate. After the incubation of the microcarriers with GFP cells for 24 h at 37 ℃, the single non-adherent cells in each well were removed by carefully exchanging the supernatant medium with fresh warm medium repeatedly without aspiration of the beads. Phase contrast and green fluorescent micrographs were then taken to investigate the attachment of GFP cells on the microcarriers.

6.3.3.1PS-O-OC-PNIPAAm microspheres

Figure **6.8** demonstrates GFP cells (green spots or aggregates) cultured with PS-O-OC-PNIPAAm microspheres with various PNIPAAm grafting densities. In the control group (Figure **6.8 (a)**), cells became attached to beads but were seen to remain rounded. This is thought to be because cell attachment was passive rather than active, i.e., cells were not able to form sufficiently large focal adhesion contacts, and for this reason, could not generate mature cytoskeleton morphology, remaining spherical. In the test groups (Figure **6.8 (b)-(h)**), cells aggregated but were not found to attach to the beads. This suggests that the beads did not attract cells or support attachment. This might be attributed to the low PNIPAAm grafting densities provided by the grating-to method, which would lead to insufficient contact points between the cell membrane and the PNIPAAm-grafted surface to support the binding of membrane bound receptors or the indirect cell attachment through interaction of cell membrane bound proteins.

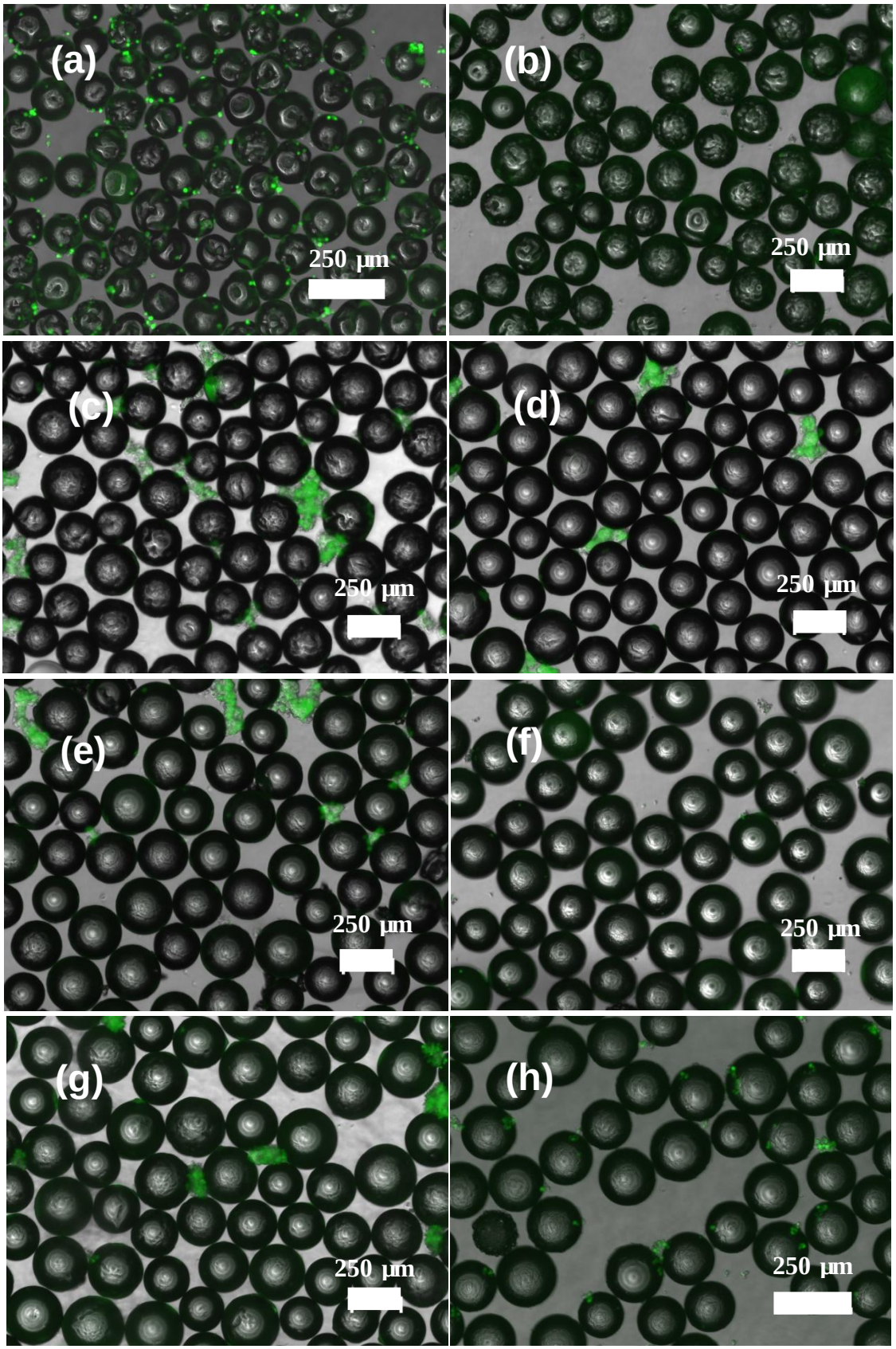


Figure 6.8 Phase contrast and green fluorescent micrographs of (a) PS-OH, (b) PS-O-OC-PNIPAAm-0.1, (c) PS-O-OC-PNIPAAm-0.3, (d) PS-O-OC-PNIPAAm-1.5, (e) PS-O-OC-PNIPAAm-3, (f) PS-O-OC-PNIPAAm-4.5, (g) PS-O-OC-PNIPAAm-6, and (h) PS-O-OC-PNIPAAm-9 microspheres in cell culture at 37 ℃ in non-cell adhesive 12-well plates. The phase contrast and the corresponding green fluorescent micrographs were combined into one image.

6.3.3.2 PS-(looped PNIPAAm) and PS-(double-layer looped PNIPAAm) microspheres

Figure **6.9** demonstrates the GFP cells cultured with the microspheres modified with looped or double-layer looped PNIPAAm with different grafted amounts. Cells were found to aggregated amongst the beads, forming discrete cell clusters, however, the cells from these clusters were not found to attach to beads, even when found in close proximity. This suggests that, as for the linear chain PNIPAAm grafted beads, the looped and double-layer looped PNIPAAM grafted beads did not support cell attachment. Again, it is thought that the PNIPAAm grafting densities was not sufficiently high to support cell attachment.

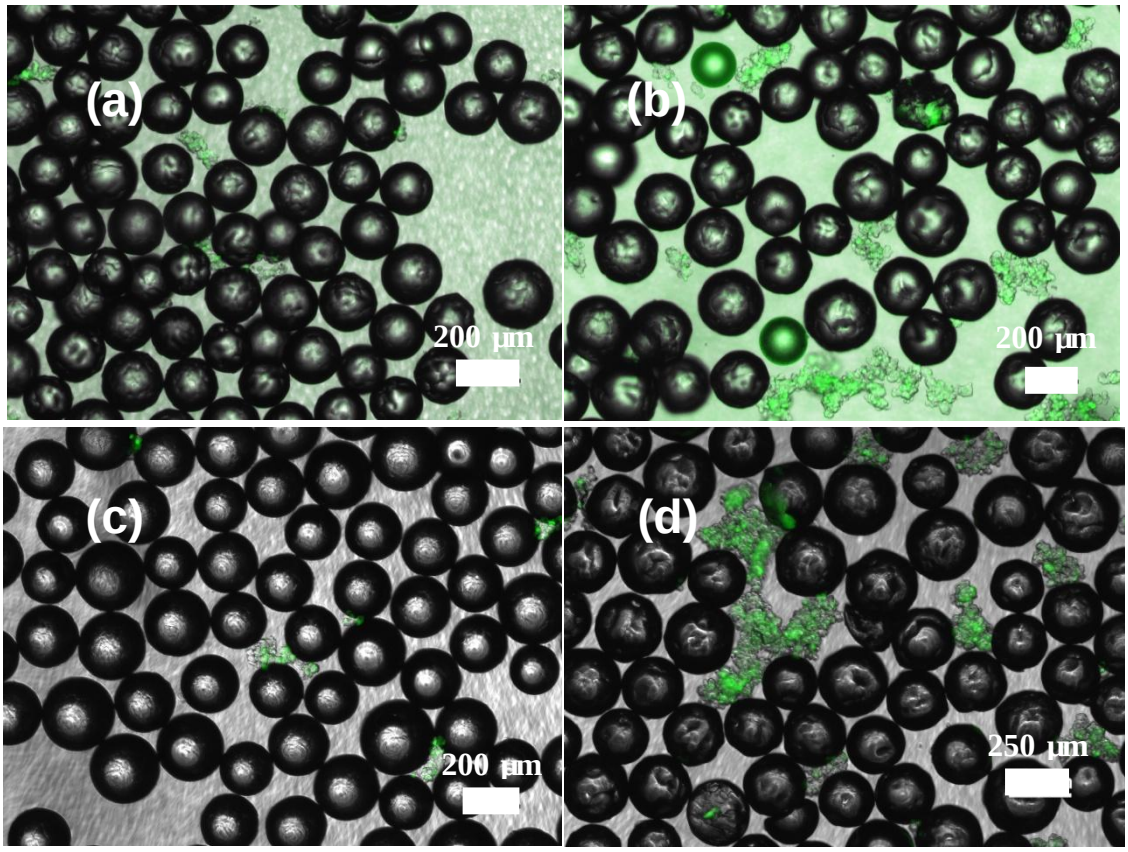


Figure 6.9 Phase contrast and green fluorescent micrographs of (a) PS-(looped PNIPAAm)-0.5, (b) PS-(looped PNIPAAm)-1.5, (c) PS-(looped PNIPAAm)-3, and (d) PS-(double-layer looped PNIPAAm) microspheres in cell culture at 37 ℃ in non-cell adhesive 12-well plates. The phase contrast and the corresponding green fluorescent micrographs were combined into one image.

6.3.3.3 PS-ACVA-PNIPAAm microspheres

Figure **6.10** demonstrates the GFP cells cultured within wells containing the PS-ACVA-PNIPAAm microspheres with PNIPAAm of different molecular weights (M_W=312 to 1976). Cells were not found to attach to the beads. This suggests that the beads did not attract cells or support attachment. This may be due to the low molecular weight of grafted PNIPAAm, leading to the absence of chain collapse above LCST. Both the PNIPAAm grafting density and the amount of polymer grafted onto the beads prepared using the grafting-from technique are much higher than those prepared by the grafting-to method. However, the molecular weights of the grafted PNIPAAm are relatively low. This is because the grafting-from method produces a higher grafting density, which increases the probability that two of the growing radicals will be generated and grow in such close vicinity that the active centres meet and terminate each other by recombination or disproportionation. It was reported that no thermally driven conformational change was detected for the end-grafted low-molecular weight PNIPAAm (M_W=2500 g/mol) (Zhu et al. 2006). Yim et al. (2003) also found that low-molecular weight end-grafted PNIPAAm-COOH (M_W=33000 g/mol) did not collapse with temperature change at the air-water interface. In this experiment, the highest molecular weight of grafted PNIPAAm is about 2000, and thus the microcarriers' surface might still remain swollen above LCST, leading to the repulsion to the cells.

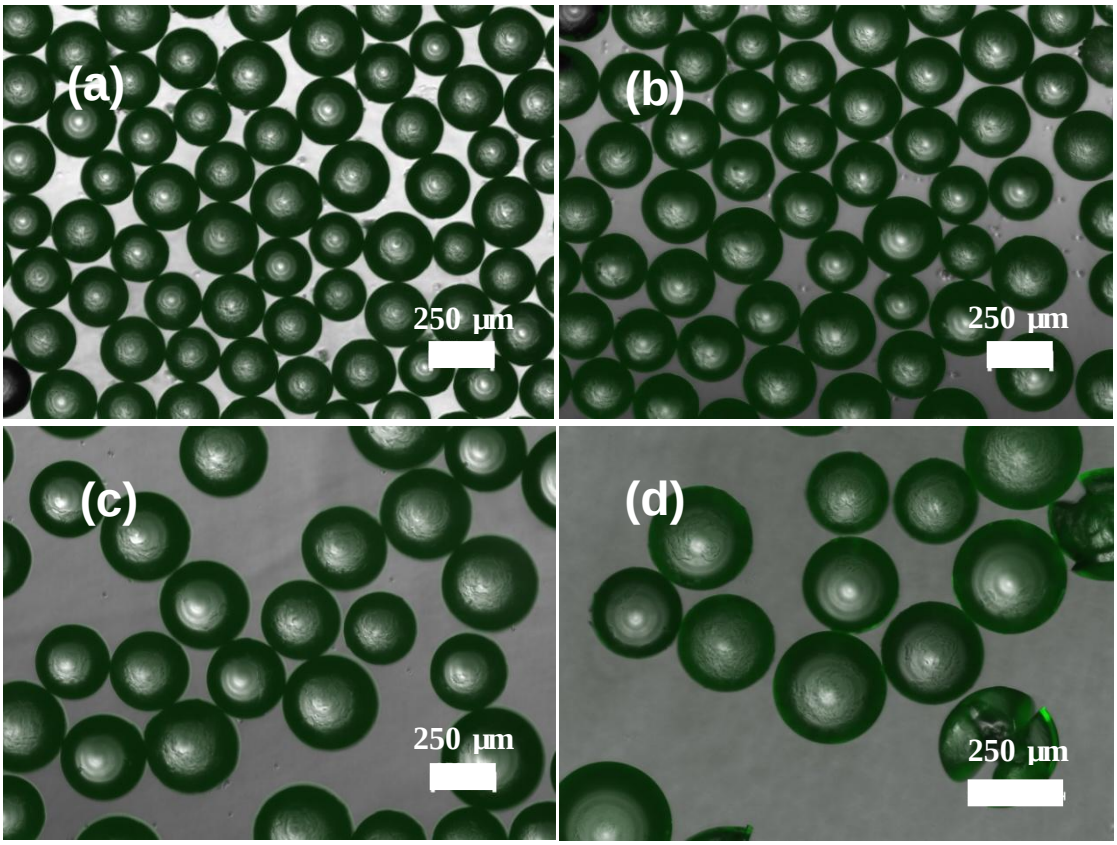


Figure 6.10 Phase contrast and green fluorescent micrographs of (a) PS-ACVA-1.68-PNIPAAm-0.5, (b) PS-ACVA-1.68-PNIPAAm-1.5, (c) PS-ACVA-1.68-PNIPAAm-3, and (d) PS-ACVA-1.68-PNIPAAm-6 microspheres in cell culture at 37 ℃ in non-cell adhesive 12-well plates. The phase contrast and the corresponding green fluorescent micrographs were combined into one image.

6.3.3.4 PS-ACVA-homopolymer hydrogel and PS-ACVA-comb type hydrogel microspheres

Figure **6.11** demonstrates the GFP cells cultured with those microcarriers coated with two different types of PNIPAAm hydrogel, namely PNIPAAm homopolymer hydrogel and comb-type hydrogel. The former was prepared by copolymerizing NIPAAm with a cross-linker, MBAAm, on the surface of the ACVA-immobilized microspheres. The latter was prepared by incorporating free mobile PNIPAAm chains onto cross-linked homopolymer hydrogel networks. Cells were not found to attach to either type of bead, although auto-fluorescence by the beads was noted. This suggests that neither type of bead attracted cells or supported attachment. As to the homopolymer hydrogel grafted

beads, this might be attributed to two reasons. Firstly, the grafted PNIPAAm hydrogel layer is too thin to show the conformational change above LCST. The thickness of the grafted hydrogel might be limited by the nature of the surface-initiated radical grafting polymerization as discussed in section **6.3.3.3**. The polymerization can be easily terminated by recombination or disproportionation due to a high density of the growing chains. Secondly, it was reported that the homopolymer hydrogel shrinks very slowly, requiring a very long period to squeeze the trapped water out from the gel interior. (Yoshida et al. 1995). Thus, the hydrogel-grafted surface may remain hydrophilic, and consequently resistant to cell attachment, for a long time after cell seeding. To increase the de-swelling rate, the free mobile PNIPAAm chains were incorporated into the hydrogel networks forming the comb-type hydrogel. However, the comb-type hydrogel grafted beads did not support cell adhesion either. This might be because the amount of incorporated PNIPAAm chains is not enough to aid the rapid expulsion of water from the gel network during collapse. Further investigations are required to determine if increasing the amount of the free PNIPAAm chains incorporated within gel network can accelerate the hydrogel dehydration so that the hydrogel grafted surface can quickly become hydrophobic and thus support cell adhesion.

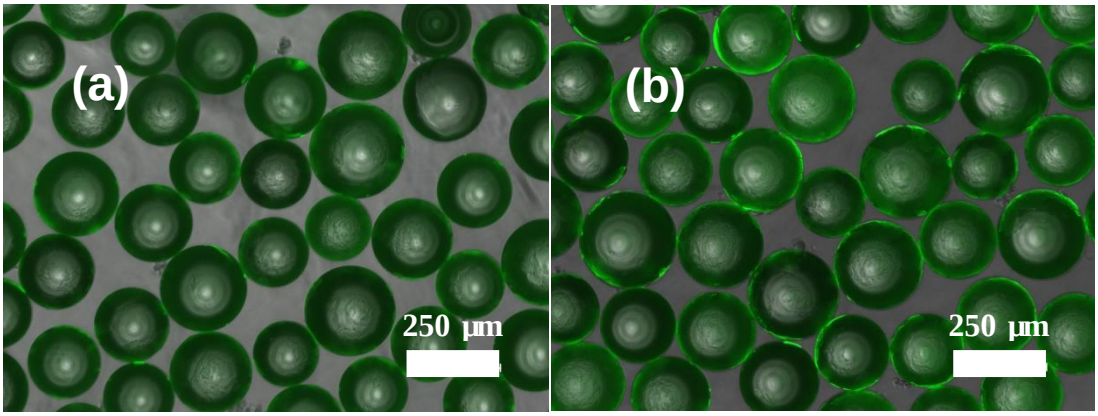


Figure 6.11 Phase contrast and green fluorescent micrographs of (a) PS-ACVA-homopolymer hydrogel, and (b) PS-ACVA-comb type hydrogel microspheres in cell culture at 37 ℃ in non-cell adhesive 12-well plates. The phase contrast and the corresponding green fluorescent micrographs were combined into one image.

6.3.3.5 PS-PSHEA-ACVA-PNIPAAm microspheres

Figure **6.12** demonstrates the GFP cells cultured alongside the microspheres grafted with branched PNIPAAm. Again, cells were not found to attach to the beads, suggesting that the bead in this case also did not attract cells or support attachment. Two potential reasons for this have been identified. Firstly, the PNIPAAm branches were prepared by radical polymerization on initiator-immobilized backbones. Due to a high grafting density, the molecular weight of resulting PNIPAAm branches was limited as two growing chains can easily meet and terminate each other by recombination or disproportionation. The low-molecular weight PNIPAAm branches may not show thermally driven conformational change at 37 ℃. Thus, the grafted surface might not be hydrophobic, and thus would be unable to support cell adhesion. Secondly, the PSHEA backbone may consist of unreacted hydrophilic HEA moieties, which are resistant to cell attachment.

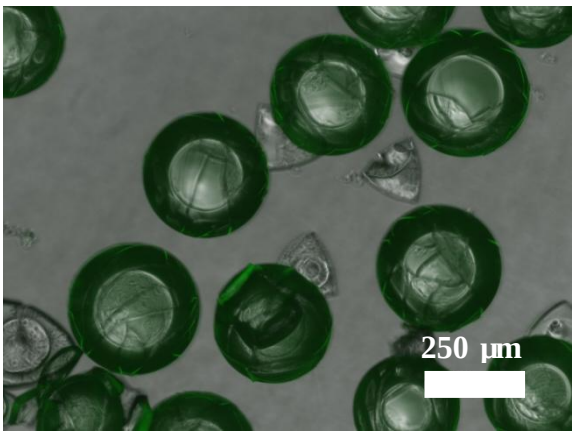


Figure 6.12 Phase contrast and green fluorescent micrographs of PS-PSHEA-ACVA-PNIPAAm microspheres in cell culture at 37 ℃ in non-cell adhesive 12-well plates. The phase contrast and the corresponding green fluorescent micrographs were combined into one image.

6.3.3.6 PS-COOH-hydrogel microspheres

Figure **6.13** demonstrates the GFP cells cultured with the microspheres modified with hydrogels of different grafted amounts prepared by seeded polymerization. In the

control group (Figure **6.13** (a)), cells did attach to the beads but were seen to remain rounded, i.e., passive attachment. It is believed that this cell-surface interaction occurs reversibly and that there is no metabolic signalling within the cell (Kikuchi and Okano 2005). In the test groups (Figure **6.13** (b)-(d)), cells aggregated but were not found to attach to the beads. These results suggest that the beads did not attract cells or support attachment, although strong auto-fluorescence by the beads was noted. This may be because of the low thickness or the slow shrinking of the grafted hydrogel, as noted for the PS-ACVA-homopolymer hydrogel and PS-ACVA-comb type hydrogel microspheres (section **6.3.3.4**). The low thickness of the grafted hydrogel may result from the side reactions in the seeded polymerization, where bulk PNIPAAm hydrogel particles formed in the reaction solution rather than precipitated on the beads' surfaces.

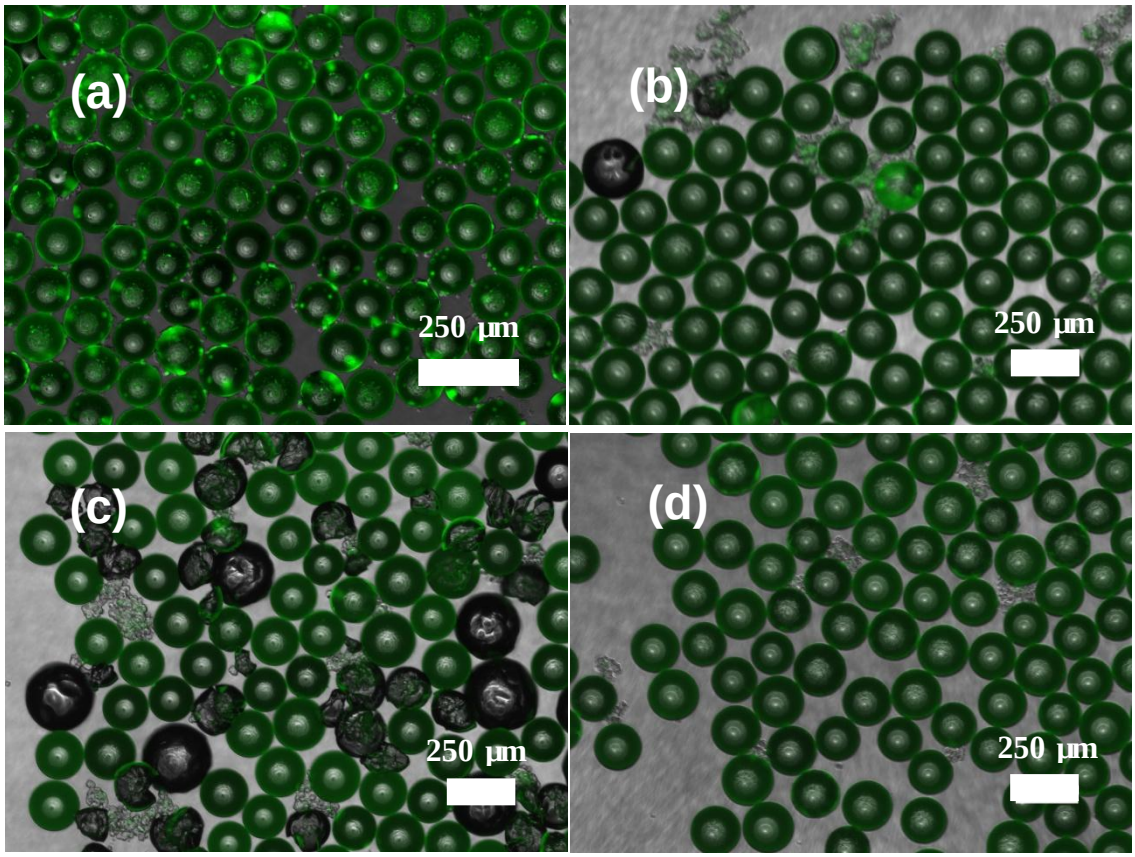


Figure 6.13 Phase contrast and green fluorescent micrographs of (a) PS-COOH, (b) PS-COOH-hydrogel-0.5/0.05, (c) PS-COOH-hydrogel-1.0/0.1, and (d) PS-COOH-hydrogel-2.0/0.2 microspheres in cell culture at 37 ℃ in non-cell adhesive 12-well plates. The phase contrast and the corresponding green fluorescent micrographs were combined into one image.

6.3.3.7 PNIPAAm-modified Sephadex® G-50 microcarriers

Figure **6.14** shows the GFP cells cultured with the PNIPAAm-modified Sephadex® G-50 microcarriers with different PNIPAAm grafting densities (from 385 to 671 mg/g) and molecular weights (from 460 to 4281). Discrete cell clusters of aggregated cells were found amongst the beads. However, no attachment was found between these cell clusters and the beads, despite close proximity in some cases. This finding suggests that PNIPAAm-modified Sephadex® G-50 microcarriers did not support cell attachment. This could be primarily due to low molecular weight of grafted PNIPAAm, leading to the absence of thermally driven conformational change above LCST.

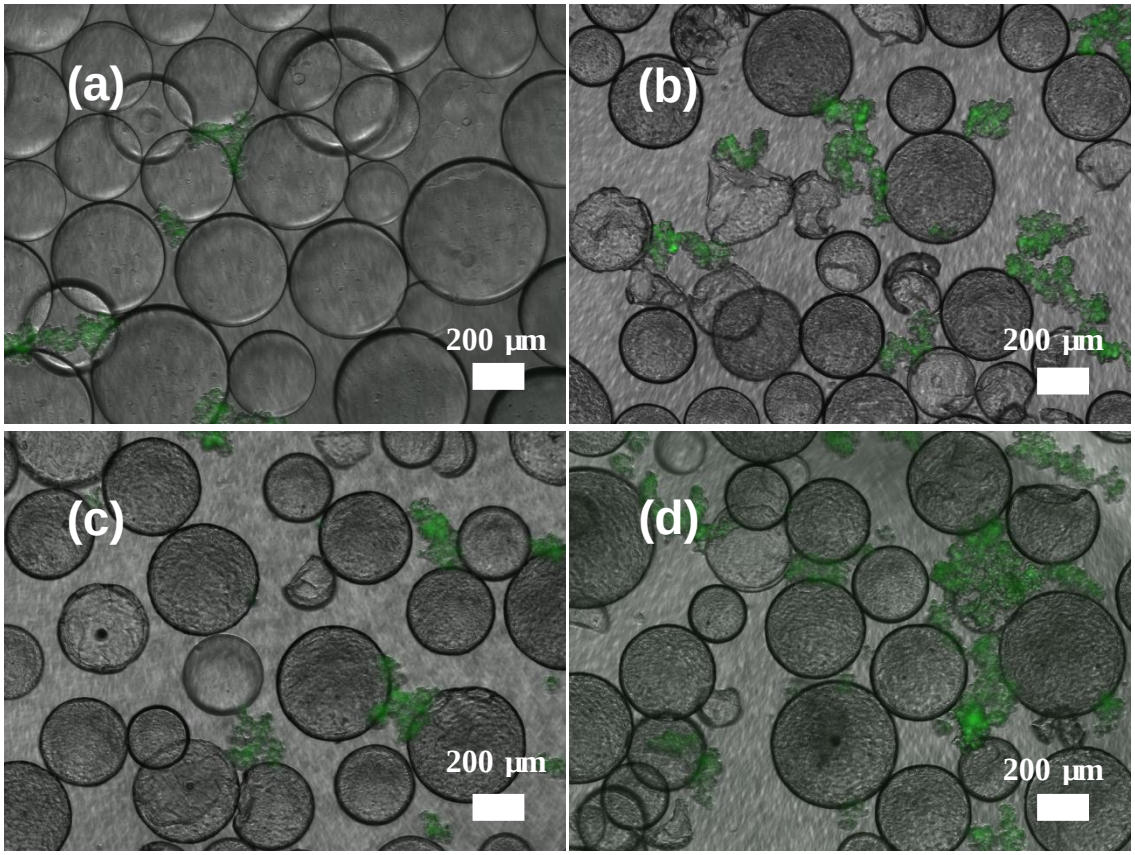


Figure 6.14 Phase contrast and green fluorescent micrographs of (a) unmodified Sephadex® G-50, (b) S-Br-0.2-PNIPAAm-4.5, (c) S-Br-0.5-PNIPAAm-4.5, and (d) S-Br-1.0-PNIPAAm-4.5 microspheres in cell culture at 37 ℃ in non-cell adhesive 12-well plates. The phase contrast and the corresponding green fluorescent micrographs were combined into one image.

6.3.3.8 PNIPAAm-modified Cytodex®-1 microcarriers

Commercial Cytodex®-1 microcarriers are based on a cross-linked dextran matrix that is substituted with positively charged *N,N*-diethylaminoethyl (DEAE) groups. The charged groups are distributed throughout the matrix of the microcarrier, and the total degree of DEAE substitution of the microcarriers has been optimized to give good growth and high yields for a wide variety of cells (GE-Healthcare 2005). GFP cells were found to successfully attach to the unmodified Cytodex®-1 microcarriers (Figure **6.15 (a)**, **(a')**). The morphology of the cells was also found to change from spherical to flat shapes (Figure **6.15 (b)**, **(b')**). This finding indicates that the attachment process can be considered to be 'active cell adhesion', whereby cells resident on the surfaces spontaneously activate receptor-mediated process, change their morphology to spread and commence signalling processes typical of attachment-dependent phenotypes (Kikuchi and Okano 2005).

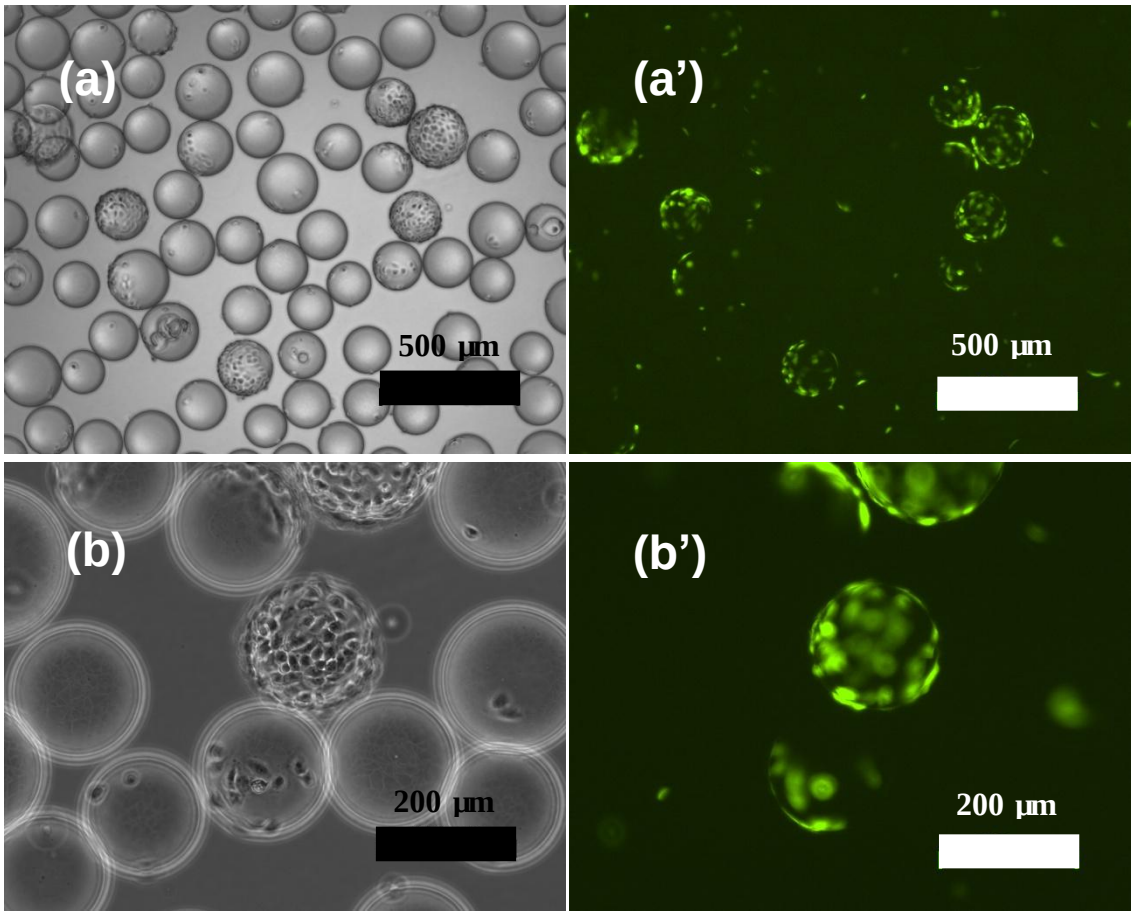


Figure 6.15 Phase contrast (a), (b) and corresponding green fluorescent (a'), (b') micrographs of unmodified Cytodex®-1 microcarriers in cell culture at 37 ℃ in non-cell adhesive 12-well plates at two different magnifications.

Figure **6.16** shows that GFP cells can also attach and spread onto PNIPAAm-grafted Cytodex®-1 microcarriers. After modification, the positively-charged DEAE groups remain present on the particle surfaces. The successful cell adhesion shown on the beads could be attributable to either or both of the effects mentioned, those being the presence of charged groups on the beads and the hydrophobicity of the grafted PNIPAAm above LCST. However, further investigations are required to determine the exact cause of the cell attachment in this case.

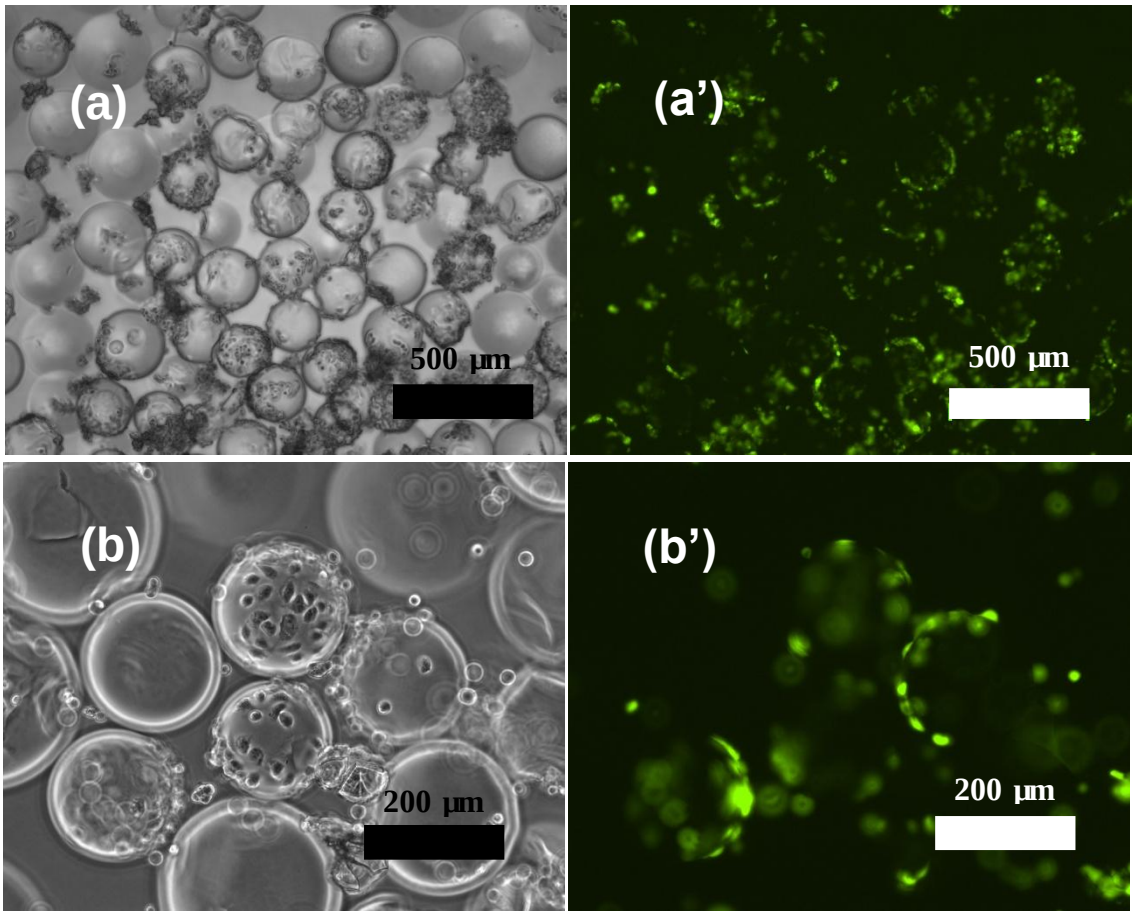


Figure 6.16 Phase contrast (a), (b) and corresponding green fluorescent (a'), (b') micrographs of PNIPAAm grafted Cytodex®-1 microcarriers in cell culture at 37 ℃ in non-cell adhesive 12-well plates at two different magnifications.

6.3.4 Cell detachment experiments

Cell detachment experiments were only conducted on PNIPAAm-grafted Cytodex®-1 microcarriers, since all other PNIPAAm-grafted microcarriers were not found to attract cells or support attachment. After 24 hours of static culture, the temperature of the culture medium was reduced from 37 ℃ to 4 ℃. The attached GFP cells were then incubated at this lower temperature of 4 ℃ for 2 hours. Phase contrast and green fluorescent micrographs were taken to investigate the thermally-induced detachment of GFP cells from the microcarriers. Results (Figure **6.17**) showed that there was no general cell detachment from the microcarriers, and that most remained of a flat

morphology. This suggests that the cell attachment on the PNIPAAm-grafted Cytodex®-1 microcarriers can be mainly attributed to the positively charged DEAE groups present on the particles surfaces rather than temperature-responsive conformational changes of the grafted PNIPAAm. The molecular weight of grafted-PNIPAAm might be too low to show the phase transition under temperature changes. Due to the negative charges distributed on the membrane surfaces of all vertebrate cells, the cells are able to remain attached to the PNIPAAm-grafted Cytodex®-1 microcarriers despite low temperatures due to the positively charged groups.

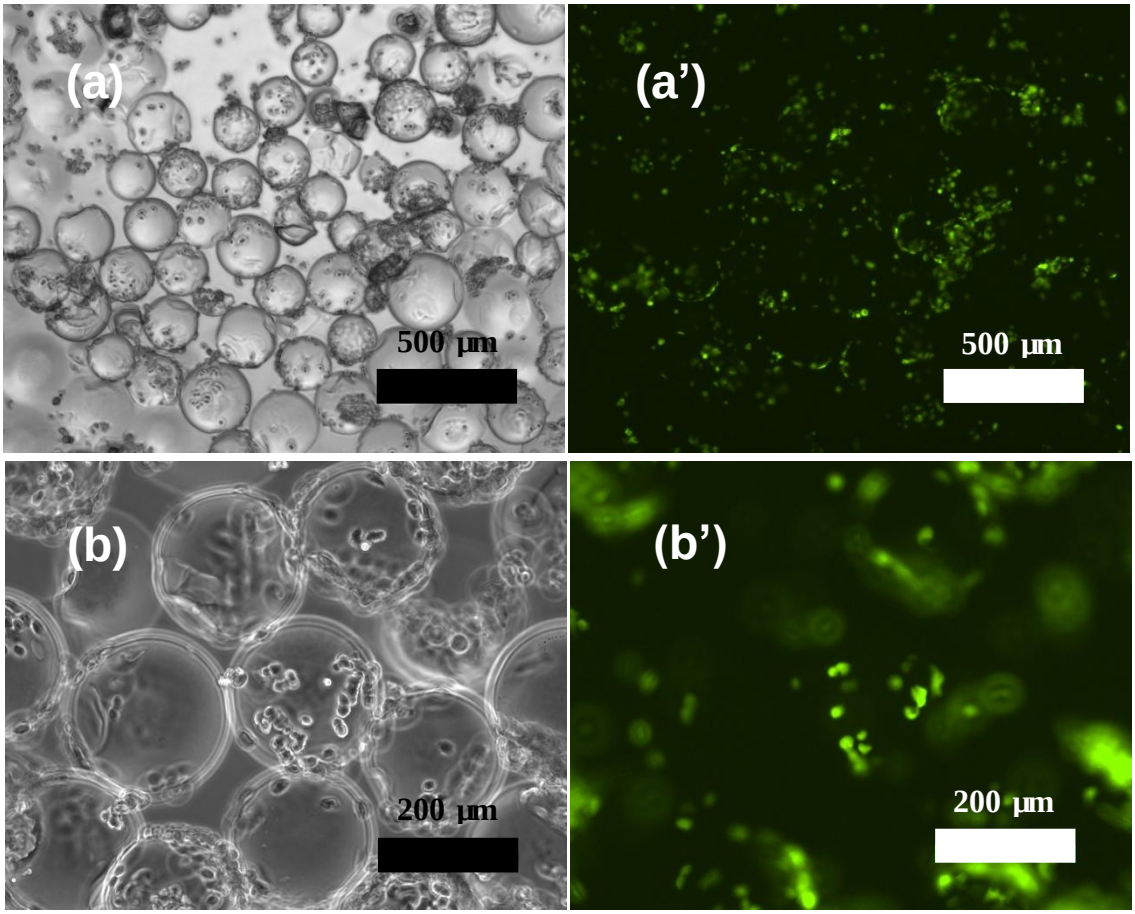


Figure 6.17 Phase contrast (a), (b) and corresponding green fluorescent (a'), (b') micrographs at two different magnifications of GFP cells cultured on PNIPAAm grafted Cytodex®-1 microcarriers after incubation for 2 h at 4 ℃.

6.4 Summary

In this study, AB assays were used to investigate the cytotoxicity of the PNIPAAm-grafted microcarriers prepared by various grafting techniques. PNIPAAm-grafted Sephadex® G-50 beads, prepared by ATRP might contain trapped Cu^{2+} ions, which inhibited the proliferation of the rADSCs over a 7 day culture period. However, it was found that the green colour of the modified beads can be significantly reduced by washing the beads 4 times with 1 M EDTA solution. This might indicate the loss of Cu^{2+} ions from the modified beads. rADSCs cultured with EDTA-treated beads can proliferate and increase in cell density 17-fold over a 3 day period. This indicates that the PNIPAAm-grafted microspheres after EDTA treatment were non-toxic to the rADSCs. GFP cells were used to test the cytotoxicity of all the polystyrene based microcarriers. All groups showed an increase in cell number over the 7 day period, equivalent to the corresponding control groups.

All cell attachment experiments were conducted using 12-well plates of non-cell adhesive material in order to manipulate cell attachment to only the microcarriers. Cells were found not to attach to the PNIPAAm-grafted beads prepared by the grafting-to technique, regardless of the grafting density and molecular morphology. This may be primarily because this method is intrinsically limited to low grafted amounts of polymer due to a strong kinetic hindrance caused by the already deposited polymer chains. Conventional radical grafting polymerization initiated from immobilized ACVA can be used to prepare 4 types of molecular architecture of grafted PNIPAAm, namely linear PNIPAAm, homopolymer hydrogel, comb-type hydrogel and branched PNIPAAm. However, none of them were found to support cell adhesion. It was thought this is primarily because high grafting density of immobilized initiator caused two major

effects, firstly to inhibit the molecular weight of the grafted PNIPAAm and secondly to limit the thickness of the grafted hydrogel in the polymerization process. This leads to the absence of conformational change of the resulting PNIPAAm chains or hydrogels when temperature increased. Thus, the grafted PNIPAAm chains or hydrogel may remain hydrophilic and cannot support cell adhesion. In addition, the low de-swelling rate of the homopolymer hydrogel, as well as the insufficient amount of free mobile chains incorporated in the comb-type hydrogel, and the hydrophilic HEA moieties in the backbone of branched PNIPAAm may be also attributed to the phenomenon. ATRP was used to graft PNIPAAm chains from the surfaces of two types of cross-linked dextran-based beads. Cells were not found to attach to the PNIPAAm-grafted Sephadex® G-50 beads. This could be primarily due to low molecular weight of grafted PNIPAAm, leading to the absence of thermally driven conformational change above LCST. In contrast, GFP cells were found to successfully attach to the PNIPAAm-grafted Cytodex®-1 microcarriers with a flat morphology, i.e., active attachment. As previously referred to, two reasons for this successful cell adhesion have been identified, those being the presence of charged groups on the beads and the hydrophobicity of the grafted PNIPAAm above LCST. Either or both of these effects may create the viability of cell adhesion. PS-COOH-hydrogel beads were prepared by the seeded polymerization. The resulting beads were not found to support cell adhesion. This may be attributed to the low thickness or the slow shrinking of the grafted hydrogel.

Cell detachment experiments were conducted on PNIPAAm-grafted Cytodex®-1 microcarriers at 4 ℃ for 2 hours. Following this treatment it was shown that the majority of cells remained attached to the microcarriers and maintained their flat morphologies. From this it can be inferred that cell attachment onto the PNIPAAm-grafted Cytodex®-1 microcarriers is due to the positively charged DEAE groups present

on the particles surfaces and not to temperature-responsive conformational changes of the grafted PNIPAAm. The low molecular weight of the grafted-PNIPAAm may cause the absence of phase transition under temperature changes. However, as the positively charged groups are unaffected by the reduced temperature the cells are able to remain attached to the microcarriers.

7 Conclusion and future work

This chapter provides a summary of the work presented in this thesis, before discussing the potential avenues for further work. In particular, two preliminary examples of bioreactor design are described in detail.

7.1 Preparation of PNIPAAm-grafted microspheres

In this study, thermo-responsive microcarriers were prepared by using three techniques, namely grafting-to, grafting-from and seeded polymerization. In each technique, the methods for controlling PNIPAAm grafting density, molecular weight, grafted amount and molecular architecture were also investigated.

In the grafting-to approach, various functional groups, such as carboxyl (-COOH), hydroxyl (-OH) and amino ($-NH_2$) groups, were introduced to the ends of PNIPAAm homopolymer chains by chain transfer polymerization. It was found that the molecular weight of resulting end-functionalized PNIPAAm can be controlled by regulating the feed concentration of chain transfer agent. However, the phase transition behaviour of the end-functionalized PNIPAAm was found to be slightly affected by its molecular weight. Generally, end-functionalized PNIPAAm (e.g., PNIPAAm-COOH) with smaller molecular weight demonstrated a higher phase transition temperature, decreased temperature-sensitivity, and reduced magnitude of aggregation. These end-functionalized PNIPAAm polymers were subsequently grafted to microspheres by the covalent tethering between the functional groups on PNIPAAm and complementary

reactive groups located on microsphere surfaces. It was found that the PNIPAAm grafting density (or amount) increased with increasing the feed amount of PNIPAAm. The grafting density (or amount) reached plateau at around 27 μmol/g (300 mg/g). The resulting grafted PNIPAAm demonstrated a linear molecular architecture. Carboxyl and amino functional groups were also introduced to the mid-chain of PNIPAAm copolymers by copolymerizing NIPAAm with AAc and AAm respectively. The content of carboxyl group or amino group was regulated by changing the feed mole ratio of AAc or AAm to NIPAAm. The LCST of the resulting copolymer was increased with increasing the content of the hydrophilic functional group. Using PNIPAAm copolymers, two types of molecular architecture were also prepared, namely looped PNIPAAm chain and double-layer looped PNIPAAm chain. The former was prepared by conjugating poly(NIPAAm-*co*-AAc) copolymer with PS-OH beads. The copolymer grafted amount was also increased with increasing the feed amount of the copolymer and reached plateau at around 220 mg/g. The latter was prepared by conjugating poly(NIPAAm-*co*-AAm) to the microsphere modified with looped PNIPAAm.

The grafting-to technique is experimentally simple and easy to control, but the grafting density obtained through this approach is limited because of steric hindrance. To achieve higher grafting densities (or grafted amounts), the grafting-from approach was also used in this study for the preparation of covalently attached PNIPAAm monolayers. The grafting-from approach consists of two steps: immobilization of a polymerization initiator onto the surface of microspheres, and subsequent growth of PNIPAAm chains directly from the first immobilized initiators. In this study, an azo-initiator, ACVA and an ATRP initiator, 2-bromopropionyl bromide, were grafted to the surfaces of cross-linked polystyrene and cross-linked dextran based microspheres respectively. In both cases, the initiator grafting density was increased with increasing the feed amount of the

initiator. The achievable grafting density of ACVA on PS-OH bead surface was around 913 μmol/g and the value of 2-bromopropionyl moieties on Sephadex® G-50 microsphere surface was around 840 μmol/g. The PNIPAAm was grafted from the surface-immobilized ACVA with grafting density of 823.22 μmol/g (PS-ACVA-1.68) by conventional radical grafting polymerization, which was initiated by ACVA decomposition. It was found that almost 100% immobilized ACVA decomposed and it was assumed 40% of the decomposed ACVA finally generates polymer chains, providing the final PNIPAAm grafting density was about 329 μmol/g. This value is almost 12-fold higher than the maximum density of PS-O-OC-PNIPAAm beads (~27 μmol/g) prepared by 'grafting-to' method. The resulting PNIPAAm grafted amount was found to be increased with increasing the feed concentration of NIPAAm monomers. The achievable PNIPAAm grafted amount (~697 mg/g) is also much higher than that of PS-O-OC-PNIPAAm microspheres (~299 mg/g). On the other hand, by using aqueous ATRP, the PNIPAAm chains were grafted from the ATRP initiators (i.e., 2-bromopropionyl moieties) on Sephadex® G-50 microsphere. However, the PNIPAAm grafted amount and molecular weight were found to be dependent on the density of the immobilized ATRP initiator. With increasing the density of immobilized ATRP initiator, both grafted amount and molecular weight of PNIPAAm were significantly decreased. The achievable grafted amount was about 670 mg/g at the density of 164 μmol/g, while this value was dropped to 385 mg/g when the density was increased to 841 μmol/g. However, these values are still much higher than those of the microspheres prepared by grafting from technique. The grafting-from technique not only can significantly increase the PNIPAAm grafting density, but also can be used to graft PNIPAAm with complicated molecular architectures. As well as the linear chains, cross-linked PNIPAAm hydrogel and branched PNIPAAm chains were also grafted to the ACVA-

immobilized surfaces. Two types of PNIPAAm hydrogel were synthesised, namely PNIPAAm homopolymer hydrogel and comb-type hydrogel. The former was prepared by copolymerizing NIPAAm with a cross-linker, MBAAm on the surface of the ACVA-immobilized microspheres. The latter was prepared in a similar way in the presence of a PNIPAAm macromonomer, thus the free mobile PNIPAAm chains were grafted onto cross-linked networks. Branched PNIPAAm architecture was prepared using PHEA or PSHEA as backbone. The PNIPAAm branches were then immobilized to the backbones via either ‘grafting-to’ or ‘grafting-from’ technique. `

The cross-linked PNIPAAm hydrogel was also grafted to the carboxyl functionalized polystyrene (PS-COOH) microspheres by seeded precipitation polymerization. There is likely to be no covalent bond between the adsorbed cross-linked PNIPAAm and the seed particles. The encapsulation of cross-linked PNIPAAm on the seed particles was driven by the hydrogen-bonding interaction between the carboxyl groups of PS-COOH seed particles and the amide groups of NIPAAm as well as MBAAm units. The grafted amount of hydrogel was increased with increasing the feed amount of NIPAAm monomer with corresponding amount of MBAAm. The resulting beads suffer no problem from grafting density and PNIPAAm molecular weight. However, the molecular architecture is restricted because of the cross-linked form, and the seeded polymerization is limited by side reactions.

7.2 PNIPAAm-grafted microspheres for cell culture

The aim of this study was to investigate the cytotoxicity of, cell attachment to and thermally-induced detachment from the PNIPAAm-grafted microspheres with different physiochemical property prepared by various grafting techniques. The results were summarized in Table **7.1**.

Alamar blue reagent was employed to quantify the cell proliferation over 7 days in the cytotoxicity assays. The cell proliferation profiles of modified beads were compared to ones of unmodified beads to determine if the toxic components were introduced by the PNIPAAm grafting procedures. All the modified beads are proven to be non-toxic to cell proliferation, excepting the PNIPAAm-grafted Sephadex® G-50 microspheres prepared by ATRP. The toxicity of the PNIPAAm-grafted Sephadex® G-50 microspheres was attributed to the trapped Cu^{2+} ions, which were used as the catalyst in the ATRP reaction. However, the trapped Cu^{2+} ions can be removed by washing the beads 4 times with 1 M EDTA solution. The beads after EDTA treatment showed no inhibition to cell proliferation.

Cell attachment experiments to the modified microspheres were conducted in non-cell adhesive 12-well plates at 37 ℃ for 24 h. The cell attachment behaviour is believed to be affected by the physicochemical properties of the PNIPAAm-grafted surfaces, which are primarily determined by the applied grafting techniques. The PNIPAAm-grafted microcarriers prepared by the grafting-to technique were found not to support cell adhesion. This is primarily because this method is intrinsically limited to low grafted amounts of polymer due to a strong kinetic hindrance caused by the already deposited polymer chains. The low grafting density would lead to insufficient contact points

between the cell membrane and the PNIPAAm-grafted surface to support the binding of membrane bound receptors or the indirect cell attachment through interaction of cell membrane bound proteins. To increase the grafting density, the grafting-from technique was employed to synthesize the PNIPAAm-grafted beads. In this technique, PNIPAAm chains were synthesised from previously-immobilized initiators. Because the growing chain only reacts with monomers or oligomers, the process is less affected by steric hindrance and leads to a higher grafting density. Two grafting-from strategies were used, namely 1) conventional radical grafting polymerization and 2) ATRP. However, PNIPAAm-grafted microcarriers prepared by the grafting-from technique (excepting PNIPAAm-grafted Cytodex®-1 beads) were found not to support cell adhesion. This is primarily because the high grafting density increases the probability that two of the growing radicals will be generated and grow in such close vicinity that the active centres meet and terminate each other by recombination or disproportionation. This may result in a low molecular weight for the resulting linear PNIPAAm chains or a limited thickness of the resulting PNIPAAm hydrogel, leading to the absence of chain collapse or hydrogel de-swelling above LCST. Thus the microcarriers' surfaces may still remain hydrophilic above LCST and do not support cell attachment. Conventional radical grafting polymerization was used to prepare four molecular architectures, namely linear PNIPAAm (PS-ACVA-PNIPAAm), homopolymer hydrogel (PS-ACVA-homopolymer hydrogel), comb-type hydrogel (PS-ACVA-comb type hydrogel) and branched PNIPAAm (PS-PSHEA-PNIPAAm). It should be noted that the low de-swelling rate of the homopolymer hydrogel, as well as the insufficient amount of free mobile chains incorporated in the comb-type hydrogel, and the hydrophilic HEA moieties in the backbone of branched PNIPAAm may be also attributed to the phenomenon. ATRP was only used to prepare linear grafted PNIPAAm. Cells were not found to attach to the

PNIPAAm-grafted Sephadex® G-50 beads. In contrast, cells can successfully attach to the PNIPAAm-grafted Cytodex®-1 microcarriers with a flat morphology, i.e., active attachment. This successful cell adhesion may be attributable to two points, firstly the presence of charged groups on the beads and secondly the hydrophobicity of the grafted PNIPAAm above LCST. Either or both of these effects may create the viability of cell adhesion. Seeded polymerization was used to coat PNIPAAm hydrogel on the PS-COOH microcarriers. The thickness of coated hydrogel was limited because of side reactions, i.e., the formation of bulk PNIPAAm hydrogel particles in the reaction solution. The limited thickness of the coated hydrogel leads to the absence of de-swelling above LCST. Thus, the resulting beads do not support the cell adhesion. In addition, the slow shrinking of the grafted hydrogel may be another explanation for the phenomenon, as noted for the PS-ACVA-homopolymer hydrogel and PS-ACVA-comb type hydrogel microspheres.

Cell detachment experiments were conducted on PNIPAAm-grafted Cytodex®-1 microcarriers at 4 ℃ for 2 hours. The outcome of this treatment confirmed that the majority of cells both remained attached to the microcarriers and maintained their flat morphologies. Thus it can be supposed that cell attachment onto the PNIPAAm-grafted Cytodex®-1 microcarriers is because of the positively charged DEAE groups distributed on the particles' surfaces and not due to thermo-responsive conformational changes within the grafted PNIPAAm. The absence of temperature-dependent phase transition may result from the low molecular weight of the grafted-PNIPAAm. Due to the positively charged groups remaining unaffected by the reduced temperature, however, the cells are able to maintain attachment to the microcarriers.

Bead code	Grafting technique	Grafting density (μmol/g)	MW	Grafted amount (g/mg)	Molecular architecture	Cytotoxicity	Cell attachment	Cell detachment
PS-O-OC-PNIPAAm	grafting-to	4-27	10938	40-299	linear chain	NO	NO	N/A
PS-(looped PNIPAAm)	grafting-to	N/A	61013	23-230	looped chain	NO	NO	N/A
PS-(double-layer looped PNIPAAm)	grafting-to	N/A	N/A	258	double layer looped chain	NO	NO	N/A
PS-ACVA-PNIPAAm	grafting-from	329	312-2119	103-697	linear chain	NO	NO	N/A
PS-ACVA-homopolymer hydrogel	grafting-from	N/A	N/D	N/D	cross-linked hydrogel	NO	NO	N/A
PS-ACVA-comb type hydrogel	grafting-from	N/A	N/D	N/D	cross-linked hydrogel incorporated with linear chains	NO	NO	N/A
PS-PSHEA-ACVA-PNIPAAm	grafting-from	N/A	N/A	N/D	branched PNIPAAm with PSHEA backbone	NO	NO	N/A
S-Br-PNIPAAm	grafting-from	164-842	460-4282	385-671	linear chain	YES before EDTA treatment; NO after EDTA treatment	NO	N/A
C-Br-PNIPAAm	grafting-from	N/D	N/D	N/D	linear chain	N/D, but treated with EDTA	YES	NO
PS-COOH-hydrogel	seeded polymerization	N/A	N/A	89-143	cross-linked hydrogel	NO	NO	N/A

N/D: not determined; **N/A**: not applicable; **MW**: molecular weight

Table 7.1 Cell culture experiments of thermo-responsive microcarriers with various PNIPAAm grafting parameters

7.3 Future work

7.3.1 Microsphere modification using RAFT polymerization

Surface-initiated free radical polymerization was used to grow PNIPAAm chains from the ACVA-immobilized microspheres (PS-ACVA). Although this technique can provide a high PNIPAAm grafting density, the molecular weight of the PNIPAAm chains was found to be limited. This is because the high grafting density increases the probability that two of the radicals will grow in close proximity, such that the active centres meet and terminate with each other by recombination or disproportionation. In order to overcome this difficulty, reversible addition-fragmentation chain transfer (RAFT) polymerization can be employed to increase the molecular weight of the resulting PNIPAAm chains grown from the ACVA-immobilized microspheres whilst maintaining a high grafting density. RAFT polymerization has proven to be a powerful controlled/living radical polymerization (CRP) technique, which relies on the use of a reversible chain transfer agent (normally a dithioester) and the resulting fast and dynamic equilibrium between active radical species and dormant species (thiocarbonylthio-terminated chains) (Moad et al. 2008; Pan et al. 2010). This equilibrium is thought to keep the concentration of propagating radicals on the microspheres' surface at a low level, leading to a suppression of bimolecular termination. Linear PNIPAAm with low polydispersity may be synthesised from the surface of the ACVA-immobilized microspheres by conducting the polymerization in the presence of NIPAAm monomers and a reversible chain transfer agent, benzyl-4(5)-imidazole dithioate (Figure **7.1 a**). In addition, highly branched PNIPAAm can be

grafted from the microspheres' surfaces by copolymerizing NIPAAm with a RAFT monomer, 3*H*-imidazole-4-carbodithioic acid 4-vinylbenzyl ester, which is a dithioate ester and also contains alkene functionality, and thus can act as both a monomer and a reversible chain transfer agent (Carter et al. 2005; Rimmer et al. 2007) (Figure **7.1 b**). Furthermore, the polymers generated via RAFT polymerization usually contain dithioate ester end groups, which are available for further modification. These dithioate ester end groups can be converted to carboxyl groups by reaction with ACVA. These carboxyl groups can be activated and then conjugated with RGD peptide via amidation (Rimmer et al. 2007). RGD-end groups allow accelerated cell adhesion and proliferation on PNIPAAm-grafted surfaces.

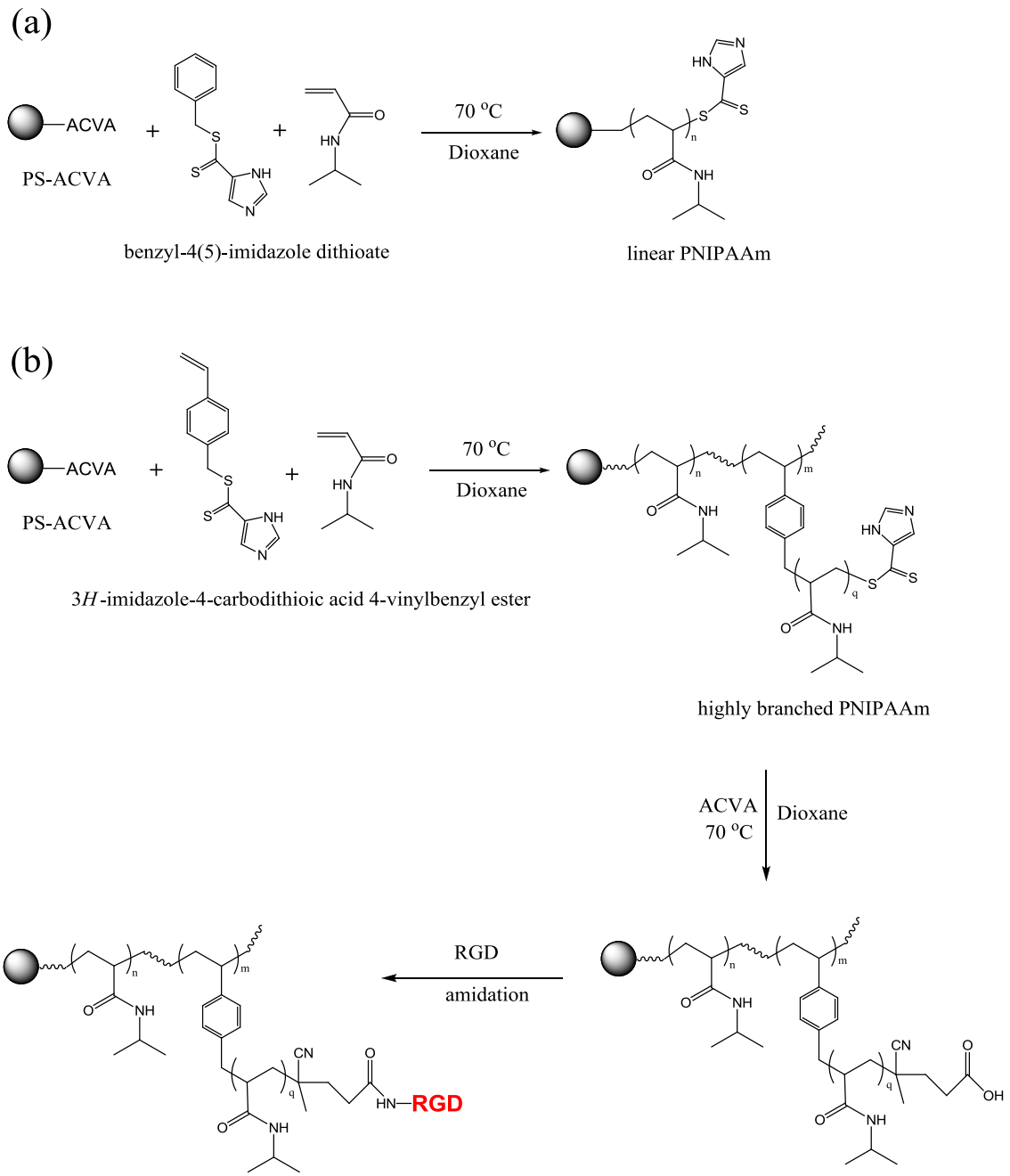


Figure 7.1 Synthesis of surface-grafted linear and highly branched PNIPAAm and end-group modification

7.3.2 Bioreactor design

Cell detachment from thermo-responsive microcarriers can be simply induced by a temperature reduction without the need for proteolytic enzyme treatment. Such thermally-induced cell harvesting enhances the viability and therapeutic efficiency of harvested cells. In addition, it simplifies the cell harvest procedure and most further operations. A cell culture system consists of microcarriers and a corresponding bioreactor. One future goal of research in this area should be the design of specific bioreactors for thermo-responsive microcarriers, which fully makes use of the advantages of thermally-induced cell detachment. Thermo-responsive microcarrier cell culture systems may provide the next generation of large scale cell culture methods in such clinical and industrial applications as tissue engineering, cell transplantation and biological production.

This section demonstrates two design examples for bioreactors containing thermo-responsive microcarriers. Both of these designs are based on the principles of a fluidized bed reactor, where thermo-responsive microcarriers act as the fluidizing particles and culture medium acts as the fluidizing medium. However, fluidization in both cases is not constant but occurs for a short time only, allowing for effective mixing. The first design, tapered fluidized bed bioreactor, requires the initial loading of all microcarriers. In contrast, the second design, columnar fluidized bed bioreactor, involves only the initial loading of a small proportion of the total microcarriers, with the remaining being held within the reservoir above. The preliminary conceptual designs, justifications and cell culture procedures are discussed as follows:

7.3.2.1 Design A: tapered fluidized-bed bioreactor

7.3.2.1.1 Conceptual design and justifications

Figure **7.2** shows a schematic diagram of the tapered fluidized-bed bioreactor. The bioreactor is mainly fabricated of poly(dimethylsiloxane) (PDMS). The reasons for the suitability of PDMS for the portable bioreactors can be summarized as: (1) the simplicity of fabrication, (2) its biocompatibility and non-toxic nature, (3) the high oxygen permeability, which can facilitate the microcarrier cell culture with a high cell concentration, (4) its optical transparency, which facilitates visual observation, and (5) its resistance to protein and cell attachment, which prioritises cell adhesion onto the microcarriers (Wu et al. 2006). The top and the bottom of the bioreactor are fabricated in Perspex® to provide sufficient mechanical stability. The bioreactor is designed for thermo-responsive microcarriers with a diameter of 100-200 μm. The total volume occupied by microcarriers is about 13 mL. All the microcarriers are loaded initially to form a tapered bed in chamber B on a plate with 80 μm holes. The plate and chamber A together act as a liquid distributor for the formation of plug flow allowing the incoming flow to pass through the microcarriers evenly. A cell seeding channel is placed at the top of the reactor for cell inoculation. Chamber B is separated from chamber C by a cell strainer (i.e., strong nylon mesh) with 70 μm pores (BD Falcon™, BD Biosciences) to restrain the microcarriers within chamber B when fluidized. After cell culture, cells are detached from the microcarriers by temperature reduction and the cells can then be separated from the microcarriers by the cell strainer using medium perfusion. The expected cell yield of the bioreactor is approximately 4×10^8 cells. This bioreactor can be considered as a packed-bed bioreactor or a fluidized-bed bioreactor, depending on the stage of the culture process.

This design relies on the hydrodynamic characteristics of fluidization in tapered fluidized beds. A fluidized bed is formed when the fluid flows through a packed bed at such a high superficial velocity that the packed bed is loosened and the particle-fluid mixture behaves as a fluid. The formed fluidized bed provides vigorous agitation of the particles and achieves an effective mixing. A dynamic equilibrium is formed as the fluid drag force acting upwards on the particles within the bed, combined with the buoyancy force, balance against the downwards-acting gravitational force. This fluid drag force, a function of superficial velocity, is constant within a columnar bed of uniform particles. In contrast, the increase of superficial velocity in the upward direction of a tapered bed causes an accompanying increase in fluid drag force (Peng and Fan 1995; 1997). This hydrodynamic characteristic in the tapered bed can lead to a phenomenon of partial fluidization, i.e., the particles in the upper part of the bed will first be fluidized upon an increase in the flow rate; in contrast, those in the lower part of the bed remain static. In other words, packed bed and fluidized bed can co-exist in the bioreactor. This peculiar characteristic is applied in this design to achieve stepwise mixing of the pecked microcarriers.

Another effect on which the design is based is the bead-to-bead cell transfer phenomenon. Using bead-to-bead cell transfer, a protease-free scale-up process can be completed simply by diluting the colonized microcarrier with fresh microcarriers and allowing the cells to migrate or crawl from the colonized beads via direct contact with the non-colonized beads (Kamiya et al. 1995; Wang and Ouyang 1999). In addition, using a fluidized-bed operation, the bead-to-bead cell transfer can be also achieved by physical detachment of cells from colonized beads and reattachment to non-colonized beads (Dürrschmid et al. 2003).

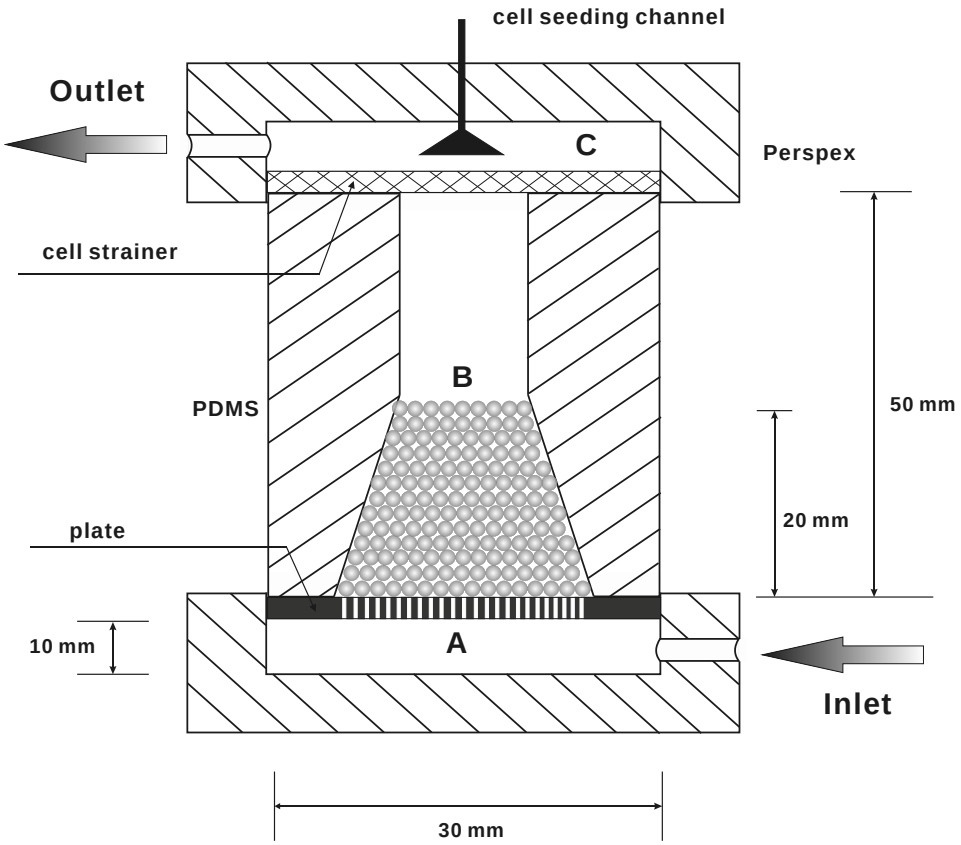


Figure 7.2 Schematic diagram of the tapered fluidized-bed bioreactor

7.3.2.1.2 Cell culture procedure

The intended cell culture procedure is as follows (Figure **7.3**):

1) The microcarriers are settled into a tapered bed and submerged in warm culture medium.

2) Cells are seeded from the top of the bioreactor through the seeding channel onto the first layer(s) of the microcarrier bed. After cells attach and spread on the microcarriers, an upward continuous perfusion of warm medium is applied to the bed with a flow rate which is lower than the minimum velocity of partial fluidization, i.e., the fluid simply passes upward through the bed without disturbing the microcarriers. The flow rate of continuous perfusion for cell culture can be increased proportional to the total cell

number as long as it is lower than the minimum velocity of partial fluidization. The bioreactor is kept in an incubator.

3) Once cells achieve confluence on the first layer(s) of the microcarriers, the flow rate is increased until the particles on the top layers are fluidized whilst the middle layers and bottom layers remain static. The partial fluidization is kept for a certain period until colonized microcarriers are mixed with fresh ones at the top layers. The flow rate is then reduced below the minimum velocity of partial fluidization to allow the particles to settle. The upward continuous perfusion is kept for cell proliferation.

4) Cells can migrate from the confluent beads to the non-colonized ones within the top layers through bead-to-bead transfer. Once cells achieve confluence on the top layers of microcarriers, the flow rate is increased until the particles of top and middle layers are fluidized whilst the bottom layers remain static. The flow rate is then reduced to allow for bead settlement. The upward continuous perfusion is kept for cell proliferation.

5) Similarly, once cells achieve confluence on both the top and middle layers of microcarriers, the flow rate is increased to allow all microcarriers to reach the full fluidization stage. All the beads are mixed in the turbulence. The beads are then allowed to settle. The upward continuous perfusion is kept for cell proliferation.

7) Once cells achieve confluence on all the microcarriers, cold medium (4℃) is perfused into the bed until all the microcarriers are submerged. Then the perfusion is stopped for a period to allow the cells to detach from the thermo-responsive microcarriers.

8) Finally, a rapid upward flow of cold medium is applied to the bed, allowing full fluidization of the bed in order to wash out the cells through the top of the bioreactor. The cells can be separated from the beads by the cell strainer.

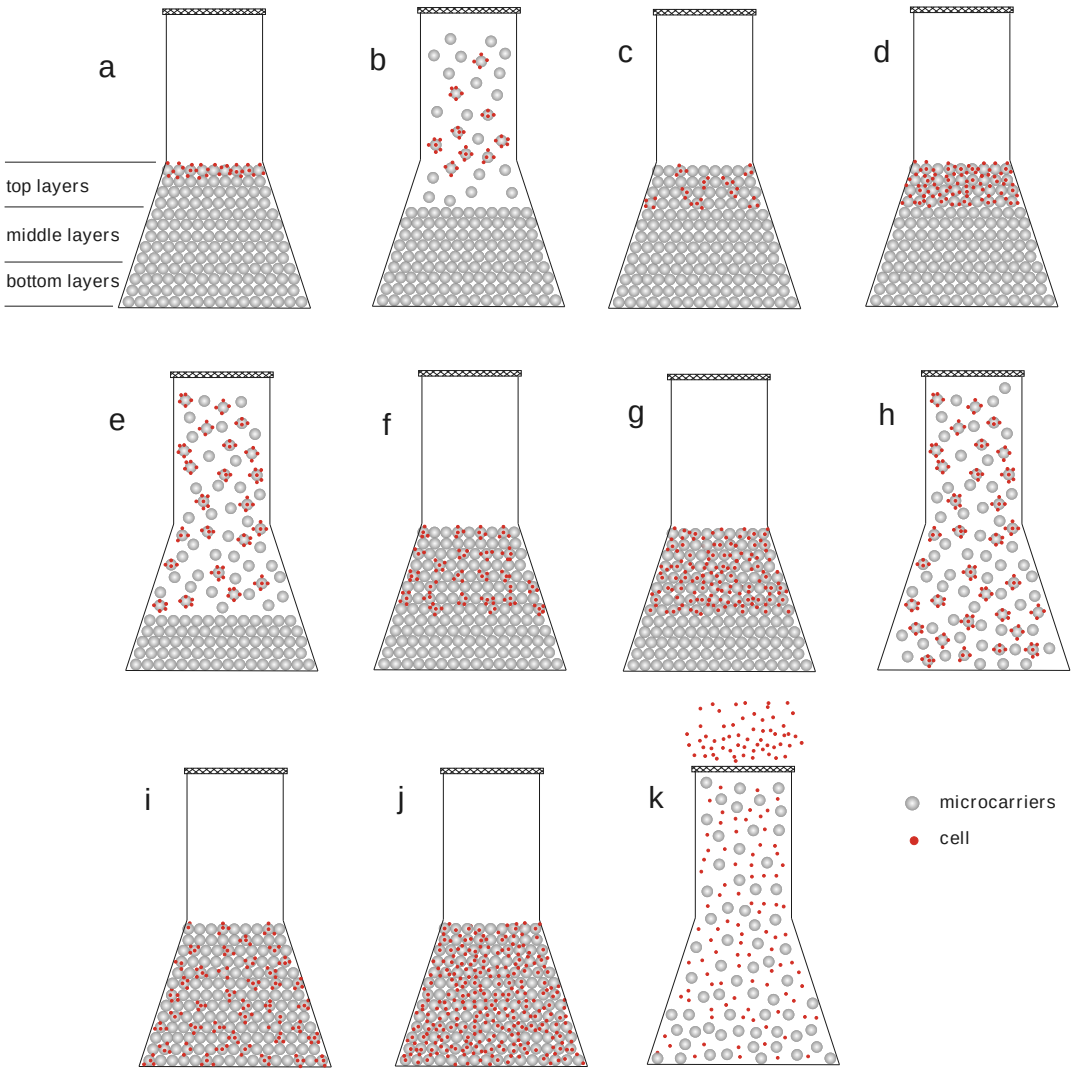


Figure 7.3 Schematic diagram of the cell culture procedure using the tapered fluidized-bed bioreactor: (a) cell are seeded and achieve confluence on the first layer, (b) colonized microcarriers are mixed with fresh ones within the top layers by partial fluidization, (c) microcarriers are allowed to settle and cells immigrate to fresh microcarriers via bead-to-bead transfer, (d) cells achieve confluence on the top layer, (e) colonized microcarriers are mixed with fresh ones within the top and middle layers by partial fluidization, (f) the microcarriers are allowed to settle and bead-to-bead transfer occurs, (g) cells achieve confluence on the top and middle layers, (h) colonized microcarriers are mixed with all remaining fresh ones by full fluidization, (i) the microcarriers are allowed to settle and bead-to-bead transfer occurs, (j) cells achieve confluence on all the microcarriers and cold medium is applied to allow thermally-induced cell detachment, (k) cells are washed out from the bioreactor by full fluidization and separated from the microcarriers by the cell strainer.

7.3.2.2 Design B: columnar fluidized-bed bioreactor

7.3.2.2.1 Conceptual design and justifications

Figure **7.4** shows a schematic diagram of the columnar fluidized-bed bioreactor. The bioreactor is fabricated using Perspex®. Perspex® is transparent and visual observations can be easily made when analysing the fluidization of the microcarriers. The bioreactor is designed for thermo-responsive microcarriers with a diameter of about 590 μm. The microcarriers are rested on a plate with 500 μm holes. The target number of cells for the whole culture process is decided to be 1×10^8 cells. In contrast with the previous design, this bioreactor involves only the initial loading of a small proportion of the microcarriers, with the remaining being held within the reservoir above (chamber C). In addition, the cell culture is conducted a static condition rather than a perfusion manner. Once cells achieve confluency on the microcarriers existing in the chamber B, a controlled amount of fresh microcarriers from chamber C is added to the colonized microcarrier. The extensive mixing is then achieved by full fluidization through applying a rapid upward flow from inlet B. A tap is placed at the bottom of the bioreactor for medium drainage. Chambers B and C are connected by a tapered section with an angle of 45 °, thus guiding cells to the exit point when an upward flow is applied during the cell harvesting stage. This is due to the increased superficial velocity of the applied medium in the tapered section in comparison with that in the columnar section of chamber B, leading to an accelerated washing-out of the cells. An air filter is placed as shown and can be removed easily when required, which is necessary when adding the initially colonized microcarriers or harvesting detached cells through the same inlet A. The air filter allows oxygen into the bioreactor while filtering out microbes.

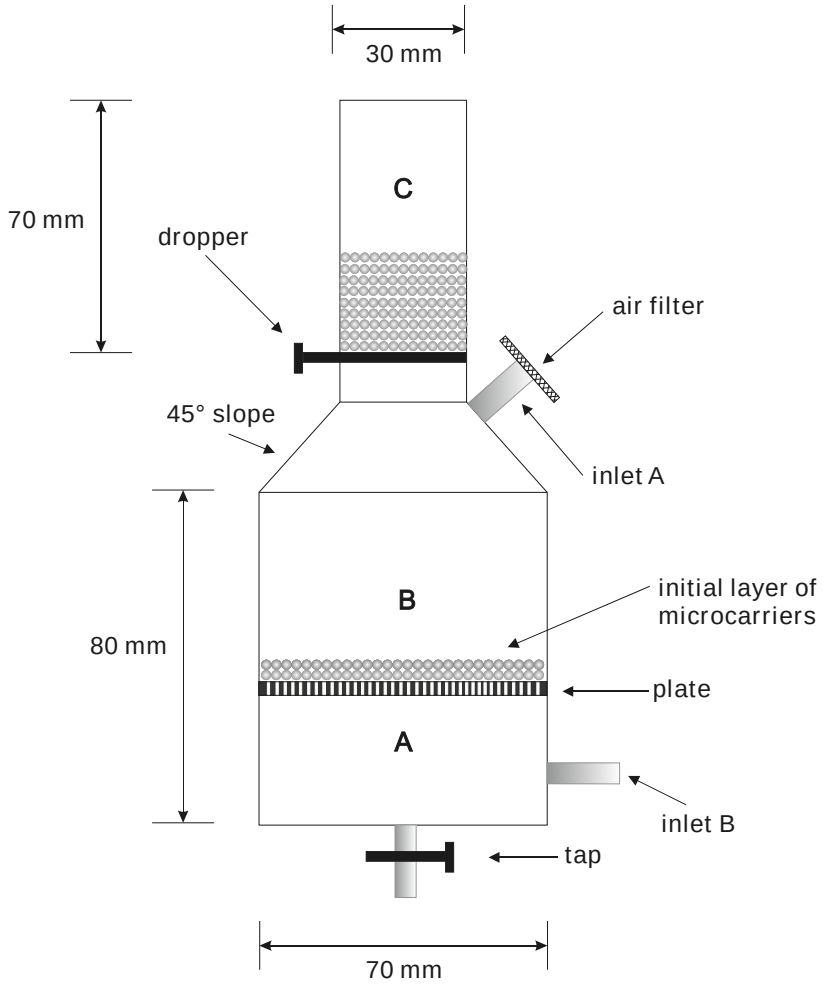


Figure 7.4 Schematic diagram of the columnar fluidized-bed bioreactor.

7.3.2.2.2 Cell culture procedure

The intended cell culture procedure is as follows (Figure **7.5**):

1) Cells are inoculated onto a small number of microcarriers and the colonized microcarriers are added to the bioreactor through inlet A by removing the air filter temporarily. Warm medium is pumped into the reactor until all the microcarriers are immersed in the medium. The cells will then proliferate on the small number of microcarriers. Cells require fresh medium on a regular basis and therefore the design allows old medium to be drained from the tap at the bottom and replaced with fresh medium when necessary.

2) Once cells achieve confluence, more fresh microcarriers are added to chamber B from chamber C by turning the handle of the dropper. A rapid upward flow of warm medium is applied to the bed for a short period allowing full fluidization of all the microcarriers without filling fully chamber B. The critical flow rate required to fluidize the microcarriers will depend on the amount of microcarriers to be fluidized. After the sedimentation of the microcarriers, the medium is then drained out through the tap placed at the bottom until the medium reaches a proper level. The cells will migrate or crawl from the confluent beads to the non-colonized ones through bead-to-bead transfer, leading to a higher cell density. This whole step is repeated until the target number of cells is achieved.

3) The last stage is cell harvesting. The used medium in the bioreactor is drained before cold medium is pumped into the bioreactor. All the microcarriers are submerged in the cold medium for the required time to allow for thermally-induced cell detachment from the microcarriers. By applying a continuous upward flow with a certain flow rate, the microcarriers can be suspended in equilibrium (i.e., stable expanded bed) due to the balance between particle sedimentation velocity and upward liquid flow velocity. The height of the expanded bed can be controlled by regulating the flow rate to allow the detached cells to pass through the bed unhindered without having the particles carried out with the fluid at the exit. Thus, the detached cells can be washed out through inlet A at the top after removing the air filter.

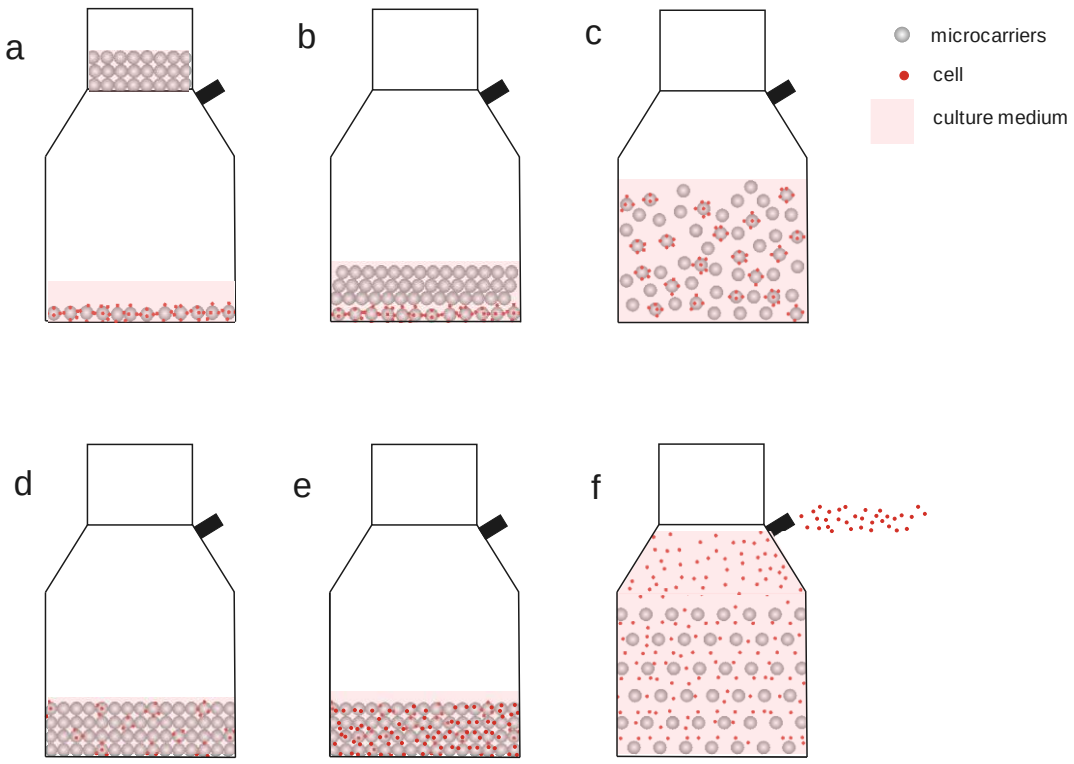


Figure 7.5 Schematic diagram of the cell culture procedure using the columnar fluidized-bed bioreactor: (a) initially colonized microcarriers are added to the bioreactor and cells achieve confluence, (b) fresh microcarriers are added to the colonized ones, (c) colonized microcarriers are mixed with fresh ones by full fluidization, (d) the microcarriers are allowed to settle and cells immigrate to fresh microcarriers via bead-to-bead transfer, (e) cells achieve confluence and cold medium is applied to allow thermally-induced cell detachment, (f) cells are washed out from the stable expanded bed of the microcarriers.

Appendix A: Combustion analysis characterization

Bead code[a]	Element Mass Percentage (%)		
	C	H	N
PS-OH	83.56	7.47	1.13
	83.66	7.49	1.21
	83.90	7.48	1.15
PS-O-OC-PNIPAAm-0.1	79.81	7.72	1.63
	79.72	7.83	1.61
	79.74	7.70	1.60
PS-O-OC-PNIPAAm-0.3	76.06	7.96	2.99
	76.63	8.04	2.94
	76.28	7.97	2.96
PS-O-OC-PNIPAAm-0.5	75.48	8.19	3.11
	75.76	8.02	3.39
	76.25	8.03	3.29
PS-O-OC-PNIPAAm-1.5	73.50	8.09	3.69
	74.55	7.90	3.96
	75.19	8.31	4.04
PS-O-OC-PNIPAAm-3.0	72.39	8.39	4.50
	70.16	7.86	4.47
	73.87	8.23	3.94
PS-O-OC-PNIPAAm-4.5	70.86	8.12	4.33
	70.03	7.98	4.81
	72.05	8.10	4.46
PS-O-OC-PNIPAAm-6.0	70.87	8.10	4.42
	73.40	8.60	4.45
	69.71	7.85	4.57
PS-O-OC-PNIPAAm-9.0	71.05	8.19	4.73
	75.07	8.58	4.27
	69.94	7.96	4.54

a: Abbreviated as PS-O-OC-PNIPAAm-X, where X represents the feed concentration of PNIPAAm-COOH (M)

Table A.1 Characterization of PS-O-OC-PNIPAAm beads prepared with various feed amount of PNIPAAm-COOH (M)

Bead code[a]	Element Mass Percentage (%)		
	C	H	N
PS-(looped PNIPAAm)-0.1	80.45	7.53	1.41
	80.20	7.52	1.37
	80.12	7.50	1.48
PS-(looped PNIPAAm)-0.2	77.93	7.66	1.90
	77.15	7.60	1.86
	77.06	7.75	2.12
PS-(looped PNIPAAm)-0.5	78.35	7.74	2.17
	77.49	7.92	2.23
	77.69	7.92	2.24
PS-(looped PNIPAAm)-1.5	76.06	8.37	3.71
	74.04	7.82	3.69
	73.13	8.43	3.74
PS-(looped PNIPAAm)-3.0	76.30	8.20	3.66
	75.56	7.93	3.68
	75.88	8.23	3.51
PS-(looped PNIPAAm)-6.0	75.52	8.19	3.73
	72.50	7.75	3.69
	75.50	8.54	3.79
PS-(double layer looped PNIPAAm)	74.57	8.32	4.08
	74.52	8.34	3.99
	74.08	8.10	4.11

a: Abbreviated as PS-(looped PNIPAAm)-X, where X represents the feed amount of poly(NIPAAm-*co*-AAc).

Table A.2 Characterization of PS-(looped PNIPAAm) or PS-(double-layer looped PNIPAAm) beads with various amounts of grafted PNIPAAm copolymer.

Bead code[a]	Element Mass Percentage (%)		
	C	H	N
PS-ACVA-0.05	82.90	7.20	1.26
	83.22	7.24	1.17
	83.51	7.36	1.29
	80.20	7.17	1.16
PS-ACVA-0.10	80.59	7.07	2.19
	81.23	7.09	2.15
	80.58	7.14	1.98
	80.59	7.26	2.13
PS-ACVA-0.21	77.97	6.81	3.53
	77.96	6.97	3.65
	79.80	7.06	3.48
	75.92	6.83	3.80
PS-ACVA-0.42	77.53	6.74	5.25
	77.61	6.82	5.46
	77.50	7.22	5.44
	73.62	6.59	5.11
PS-ACVA-0.84	76.15	6.68	5.52
	75.90	7.10	5.81
	74.44	6.60	5.70
	74.37	6.89	5.57
PS-ACVA-1.68	74.46	6.57	6.03
	74.46	6.59	6.26
	72.87	6.64	6.19
	75.26	7.09	6.23
PS-ACVA-3.36	74.34	6.85	6.76
	73.52	6.67	6.97
	68.71	6.40	6.31
	74.20	7.02	6.85

a: Abbreviated as PS-ACVA-X, where X represents the feed amount of ACVA

Table A.3 Characterization of PS-ACVA microspheres

Bead code[a]	Element Mass Percentage (%)		
	C	H	N
PS-ACVA-1.68-PNIPAAm-0.0	79.81	7.31	3.06
	73.96	6.97	2.94
	78.65	7.18	3.33
PS-ACVA-1.68-PNIPAAm-0.5	75.97	7.13	3.74
	75.44	7.33	4.45
	76.04	7.37	3.99
PS-ACVA-1.68-PNIPAAm-1.5	71.02	7.63	5.17
	71.23	7.73	5.22
	75.96	7.66	4.50
PS-ACVA-1.68-PNIPAAm-3.0	60.13	7.97	7.71
	67.55	8.07	6.01
	64.68	8.40	7.43
PS-ACVA-1.68-PNIPAAm-6.0	56.59	8.80	9.81
	58.32	8.61	8.48
	57.60	8.85	9.08
PS-ACVA-1.68-PNIPAAm-9.0	55.80	8.82	9.52
	57.67	9.25	9.72
	56.86	9.36	9.44

a: Abbreviated as PS-ACVA-X-PNIPAAm-Y, where X represents the feed amount of ACVA in the initiator immobilization step, and Y represents the feed amount of NIPAAm in the polymerization step.

Table A.4 Characterization of PS-ACVA-1.68-PNIPAAm microspheres

Bead code	Element Mass Percentage (%)		
	C	H	N
PS-PHEA	60.88	6.90	1.42
	62.01	6.82	1.53
	61.71	6.91	1.50
PS-PSHEA	77.33	7.21	2.52
	77.40	7.27	2.54
	77.42	7.37	2.55
PS-PHEA-PNIPAAm	63.01	7.55	3.25
	63.50	7.66	3.22
	63.22	7.64	3.23
PS-PSHEA-PNIPAAm	73.32	7.66	3.30
	73.30	7.59	3.28
	73.60	7.40	3.35

Table A.5 Characterization PS-PHEA and PS-PSHEA beads and subsequent PNIPAAm branch incorporation via 'grafting-to' technique.

Bead code	Element Mass Percentage (%)			
	C	H	N	Br
Unmodified Sephadex G50	42.76	6.81	<0.10	0.19
	42.82	6.76	<0.10	<0.10
	42.54	6.69	<0.10	<0.10
S-Br-0.2[a]	40.88	6.54	<0.10	1.08
	39.75	6.41	0.36	1.47
	39.59	6.66	<0.10	1.56
S-Br-0.5[a]	38.64	6.34	0.41	2.48
	39.93	6.47	0.48	1.87
	39.05	6.27	0.17	2.90
S-Br-1.0[a]	35.77	5.91	<0.10	7.93
	37.35	6.24	<0.10	5.49
	36.27	6.02	<0.10	6.92
S-Br-0.2-PNIPAAm-4.5[b]	49.88	8.53	7.50	0.28
	51.12	8.79	8.43	<0.10
	54.35	9.77	9.00	<0.10
S-Br-0.5-PNIPAAm-4.5[b]	48.60	8.00	6.82	0.14
	49.77	8.19	7.50	0.22
	50.14	8.44	7.05	<0.10
S-Br-1.0-PNIPAAm-4.5[b]	47.82	8.04	5.78	0.23
	45.33	7.64	4.34	0.12
	45.51	8.51	4.17	<0.10

a: Abbreviated as S-Br-X, where X represents the feed amount of 2-bromopropionyl bromide in the initiator immobilization step

b: Abbreviated as S-Br-X-PNIPAAm-Y, where X represents the feed amount of 2-bromopropionyl bromide in the initiator immobilization step, and Y represents the feed amount of NIPAAm in the polymerization step.

Table 4.6 Characterization of Sephadex® G-50 microspheres after attachment of a polymerization initiator, 2-bromopropionyl bromide (S-Br microspheres) and PNIPAAm-grafted Sephadex® G-50 microspheres (S-Br-PNIPAAm microspheres).

Bead code[a]	Element Mass Percentage (%)		
	C	H	N
PS-COOH	84.88	7.86	1.06
	84.88	7.96	1.04
	84.93	8.01	1.07
PS-COOH-hydrogel-0.5/0.05	79.39	7.37	2.01
	80.62	7.58	2.13
	80.84	7.54	2.04
PS-COOH-hydrogel-1.0/0.1	79.68	7.42	2.28
	80.25	7.60	2.28
	80.40	7.66	2.24
PS-COOH-hydrogel-2.0/0.2	79.69	7.61	2.72
	78.86	7.73	2.62
	79.40	7.70	2.68

a: Abbreviated as PS-COOH-hydrogel-X/Y, where X and Y represent the feed amount of NIPAAm and MBAAm respectively

Table A.7 Characterization of PS-COOH-hydrogel microspheres

Appendix B: FTIR characterization

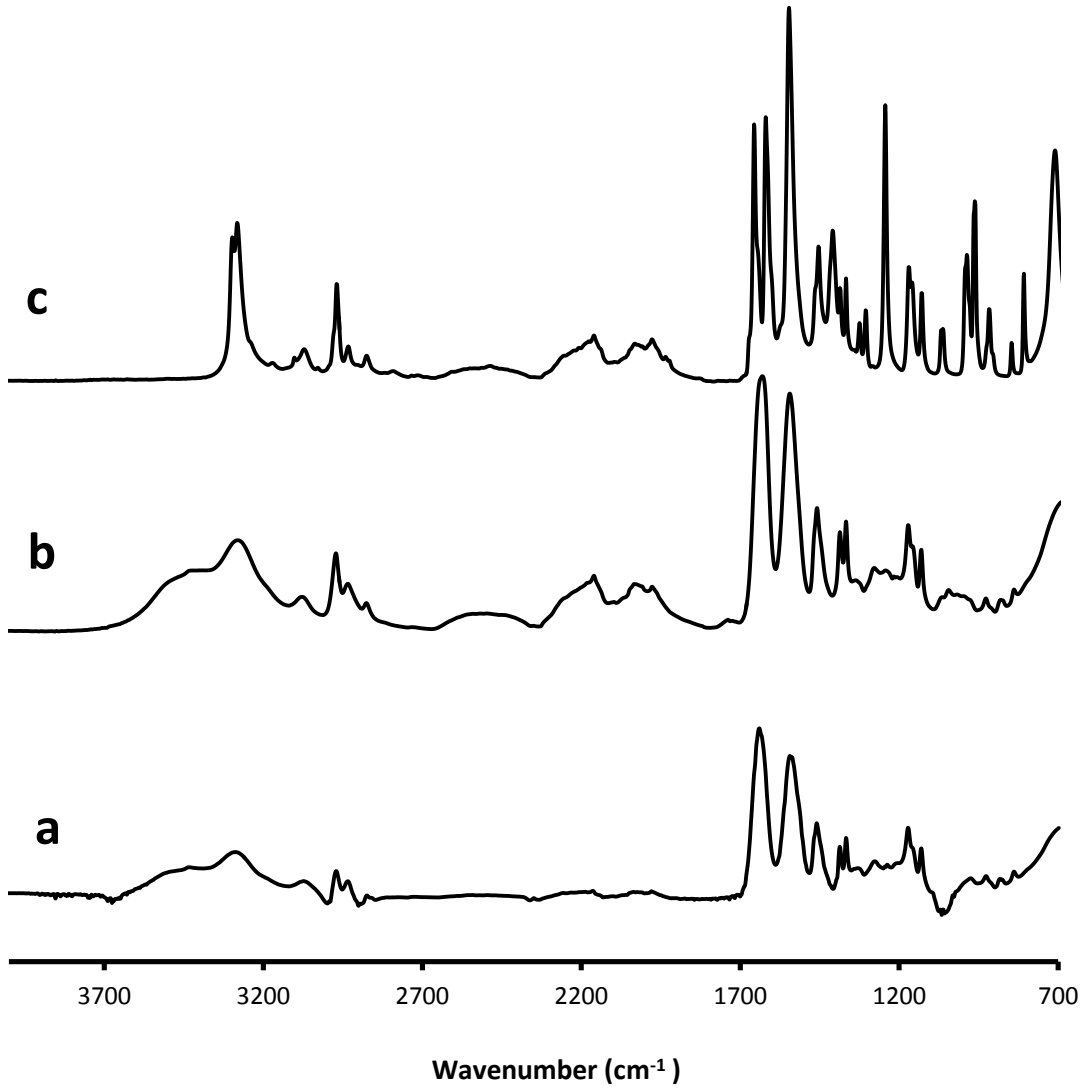


Figure B.1 FTIR spectra of (a) PNIPAAm-NH_2 , (b) PNIPAAm-OH and (c) NIPAAm monomer

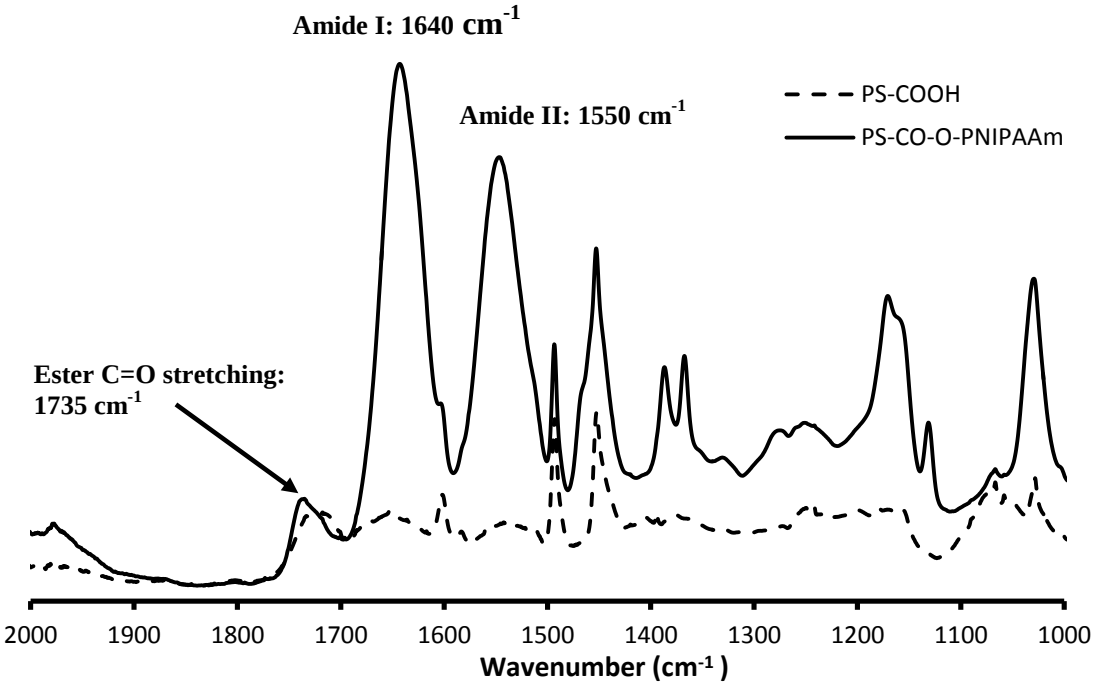


Figure B.2 FTIR spectra of PS-COOH and PS-CO-O-PNIPAAm microspheres

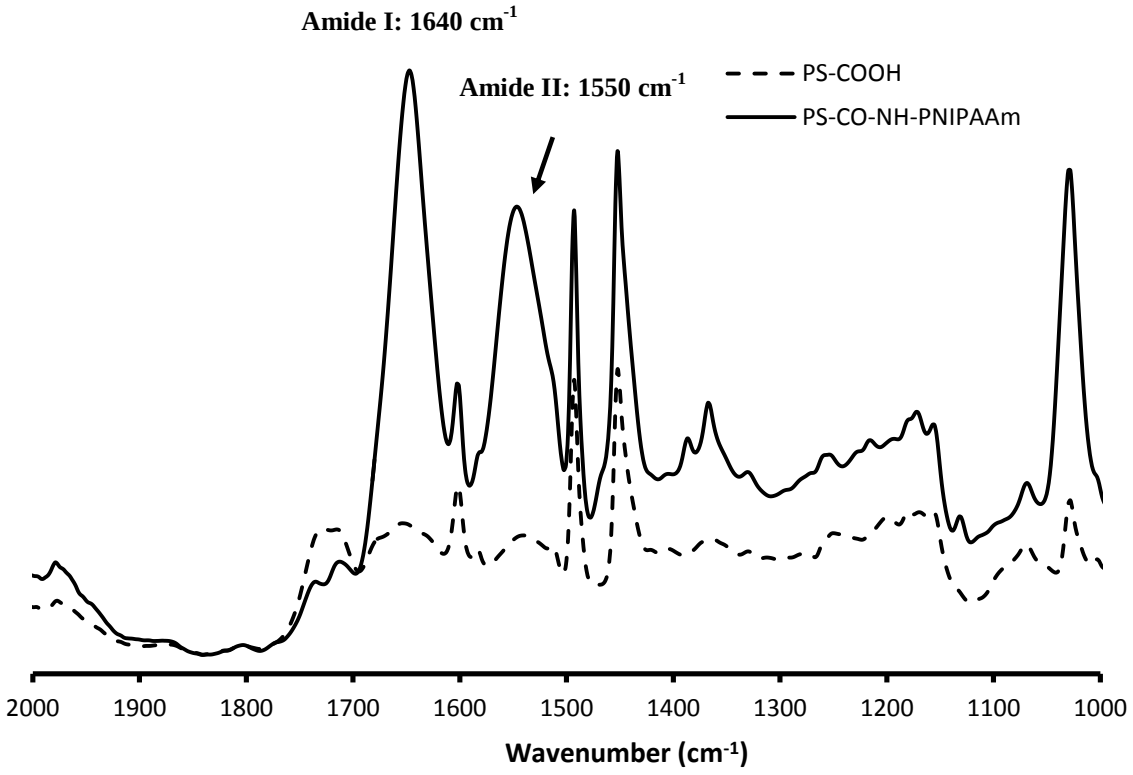


Figure B.3 FTIR spectra of PS-COOH and PS-CO-NH-PNIPAAm microspheres

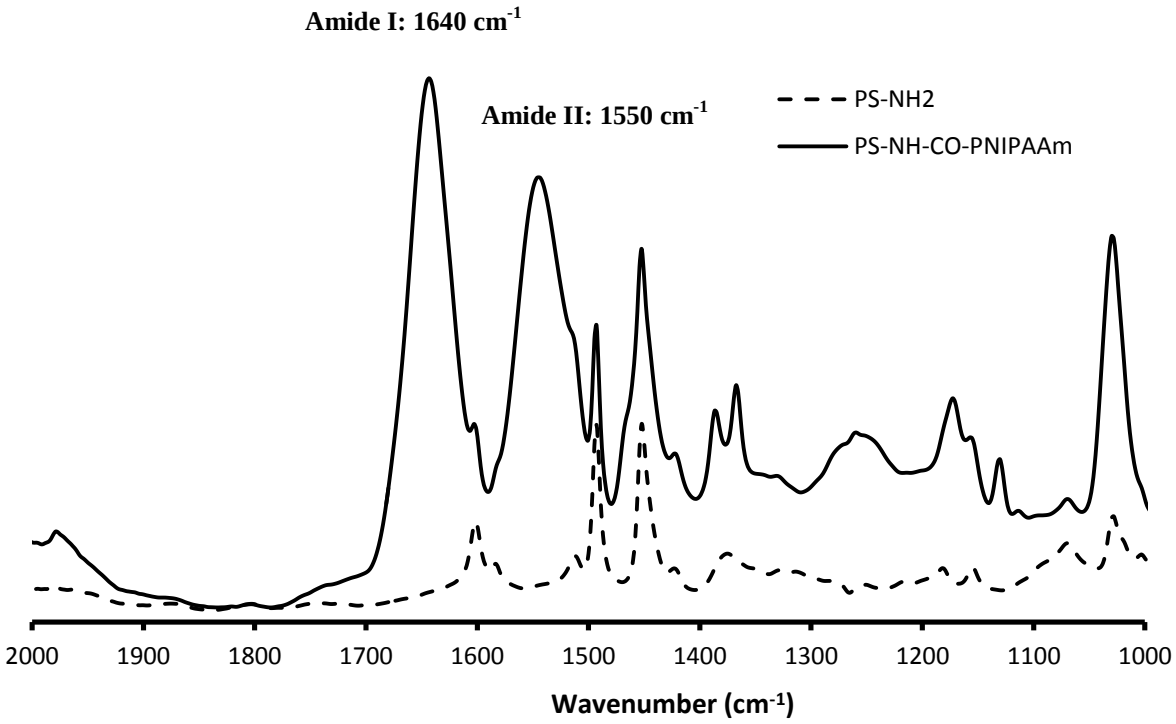


Figure B.4 FTIR spectra of PS-NH_2 and PS-NH-CO-PNIPAAm microspheres

Appendix C: ^{1}H-NMR characterization

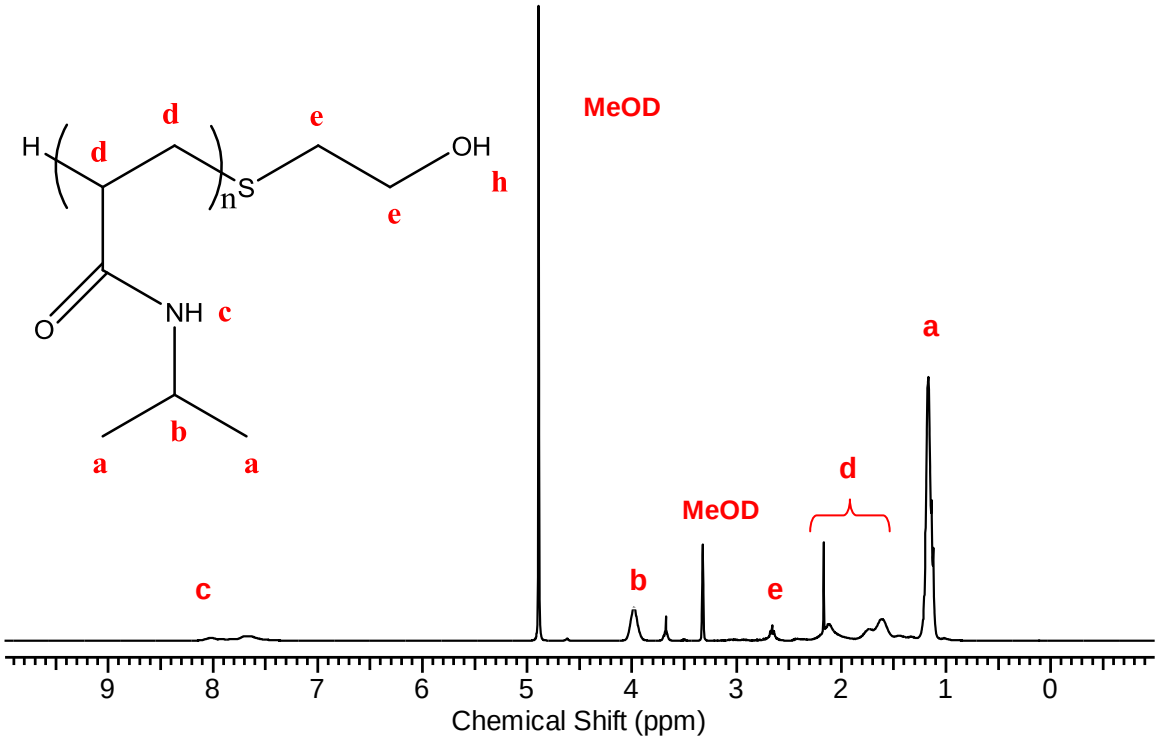


Figure C.1 ^{1}H-NMR spectrum of PNIPAAm-OH

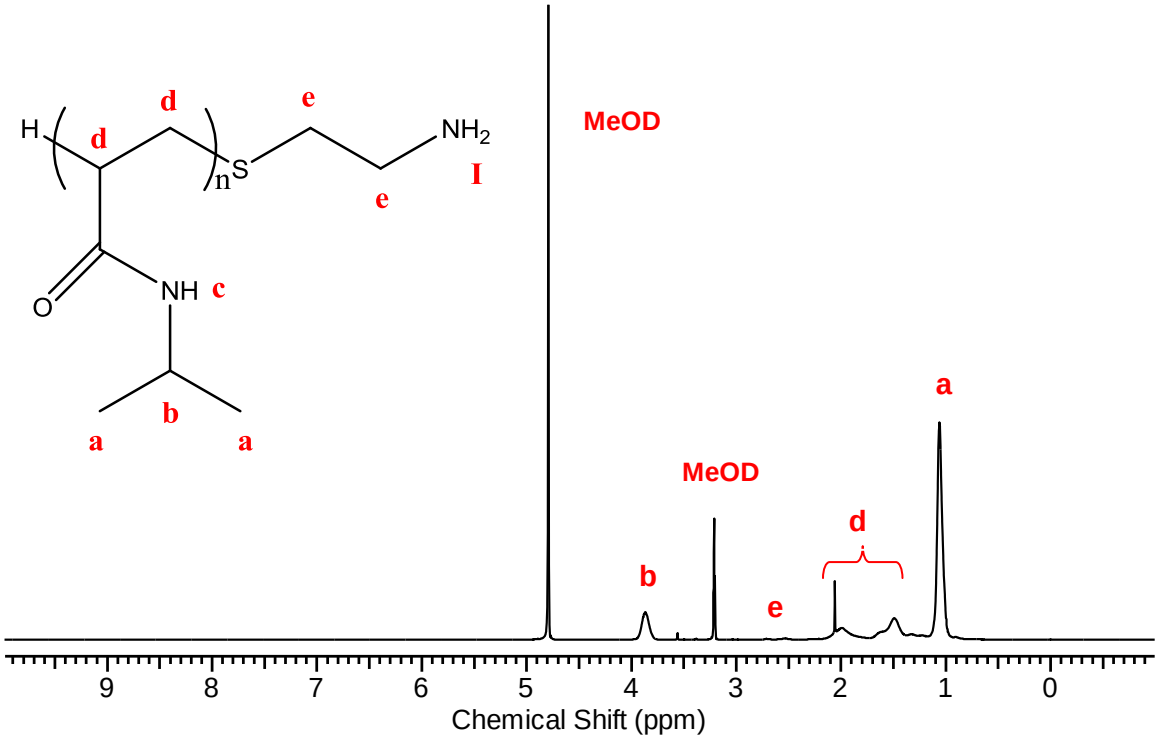


Figure C.2 ^{1}H-NMR spectrum of PNIPAAm-NH_2

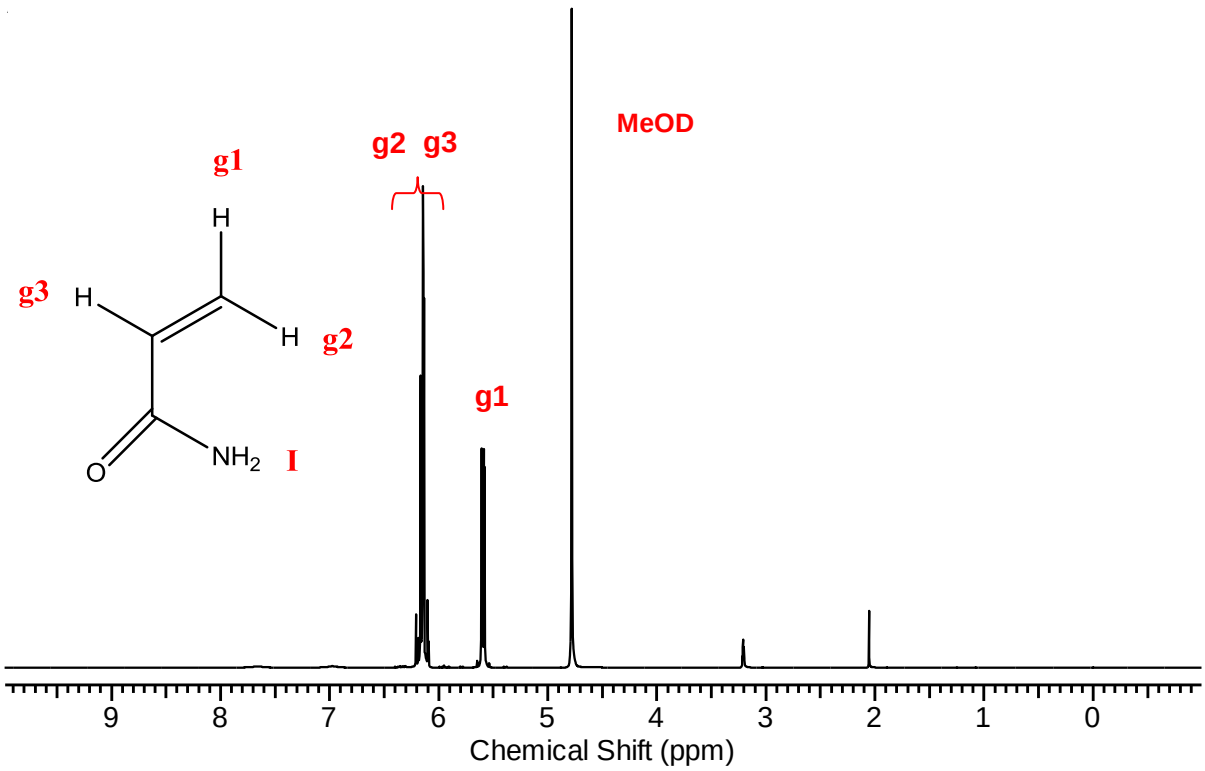


Figure C.3 ^{1}H-NMR spectrum of AAm

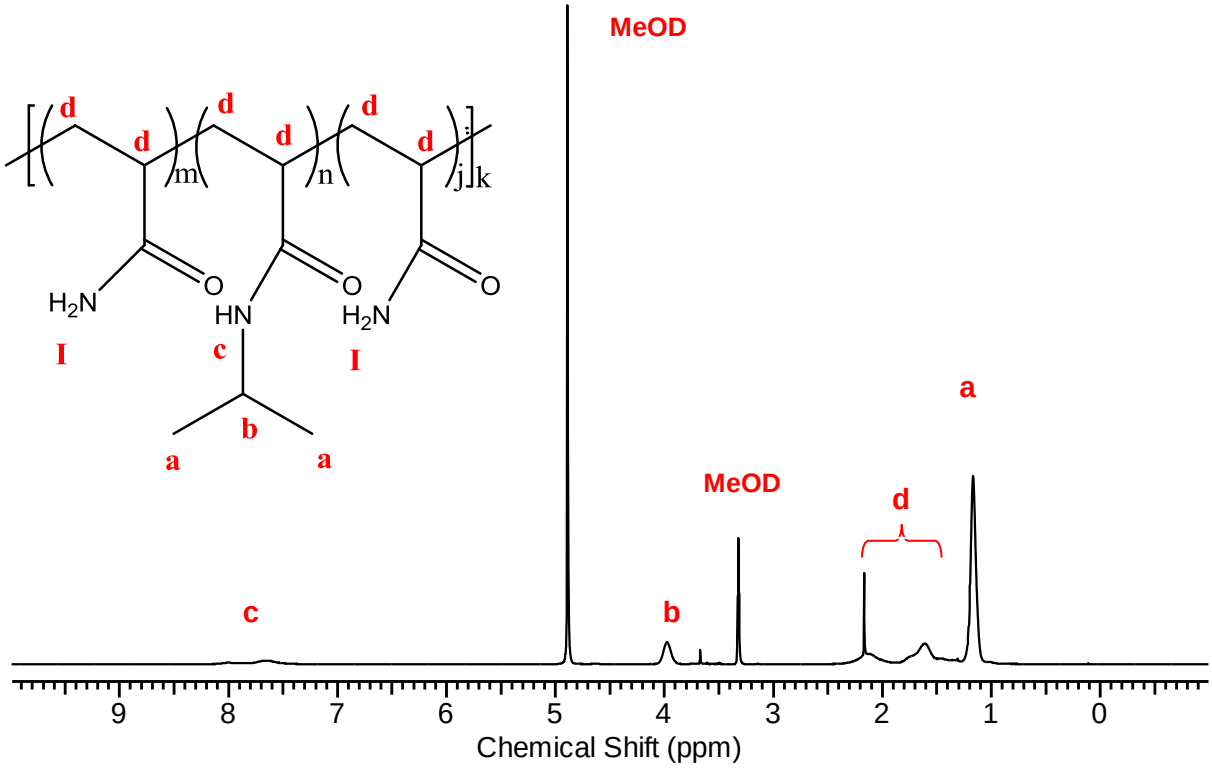


Figure C.4 ^{1}H-NMR spectrum of P(NIPAAm-*co*-AAm-20%)

Appendix D: SEM characterization

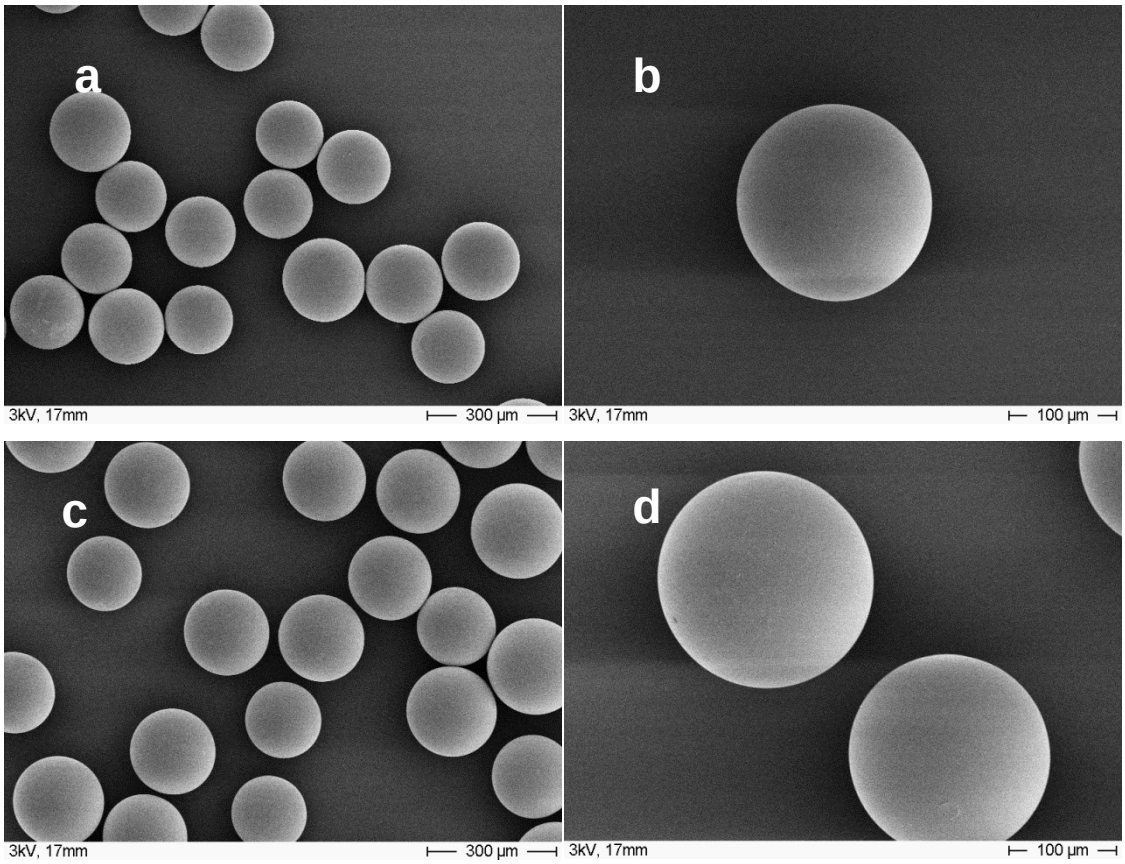


Figure D.1 SEM characterization of (a) & (b) unmodified PS-NH_2 microspheres, (c) & (d) PS-NH-OC-PNIPAAm.

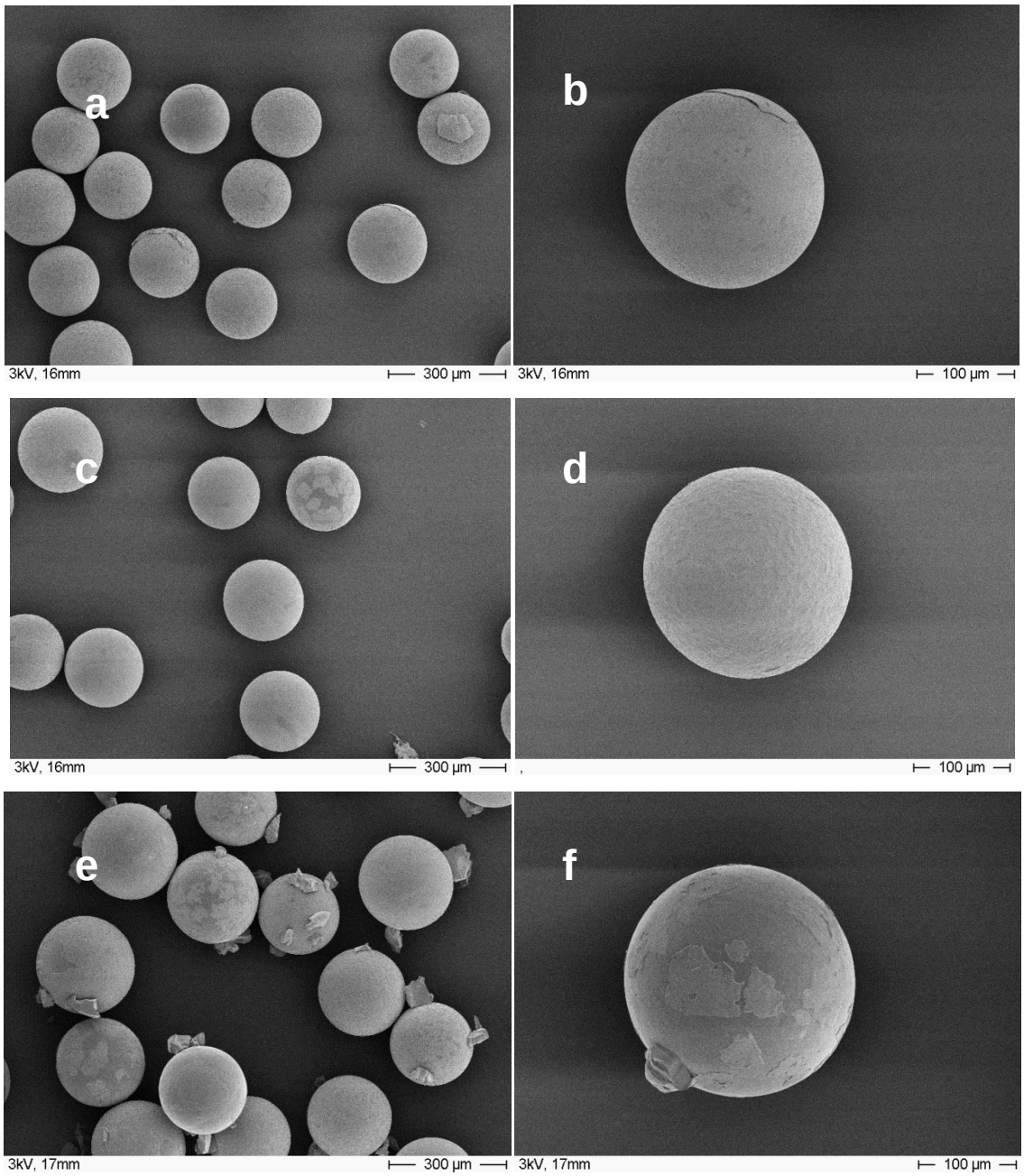


Figure D.2 SEM characterization of (a) & (b) unmodified PS-COOH microspheres, (c) & (d) PS-CO-NH-PNIPAAm microspheres, (e) & (f) PS-CO-O-PNIPAAm.

References

Abraham, S., Ghosh, I., Nau, W. M., Chesta, C., Pas, S. J., Hill, A. J. and Weiss, R. G. (2012). "In-cage and out-of-cage combinations of benzylic radical pairs in the glassy and melted states of poly(alkyl methacrylate)s." *Photochemical & Photobiological Sciences* **11**(6): 914-924.

Akiyama, Y., Kikuchi, A., Yamato, M. and Okano, T. (2004). "Ultrathin Poly(N-isopropylacrylamide) Grafted Layer on Polystyrene Surfaces for Cell Adhesion/Detachment Control." *Langmuir* **20**(13): 5506-5511.

Al-Nasiry, S., Geusens, N., Hanssens, M., Luyten, C. and Pijnenborg, R. (2007). "The use of Alamar Blue assay for quantitative analysis of viability, migration and invasion of choriocarcinoma cells." *Hum Reprod* **22**(5): 1304-1309.

Andersson, M., Hietala, S., Tenhu, H. and Maunu, S. (2006). "Polystyrene latex particles coated with crosslinked poly(N-isopropylacrylamide)." *Colloid & Polymer Science* **284**(11): 1255-1263.

Aoki, T., Kawashima, M., Katono, H., Sanui, K., Ogata, N., Okano, T. and Sakurai, Y. (1994). "Temperature-Responsive Interpenetrating Polymer Networks Constructed with Poly(acrylic acid) and Poly(N,N-dimethylacrylamide)." *Macromolecules* **27**(4): 947-952.

Aoyagi, T., Ebara, M., Sakai, K., Sakurai, Y. and Okano, T. (2000). "Novel bifunctional polymer with reactivity and temperature sensitivity." *Journal of Biomaterials Science, Polymer Edition* **11**(1): 101-110.

Bachmann, S., Wang, H., Albert, K. and Partch, R. (2007). "Graft polymerization of styrene initiated by covalently bonded peroxide groups on silica." *J Colloid Interface Sci* **309**(1): 169-175.

Bai, F., Huang, B., Yang, X. and Huang, W. (2007). "Synthesis of monodisperse poly(methacrylic acid) microspheres by distillation–precipitation polymerization." *European Polymer Journal* **43**(9): 3923-3932.

Bai, F., Yang, X. and Huang, W. (2004). "Synthesis of narrow or monodisperse poly(divinylbenzene) microspheres by distillation-precipitation polymerization." *Macromolecules* **37**(26): 9746-9752.

Balamurugan, S., Mendez, S., Balamurugan, S. S., O'Brien Ii, M. J. and López, G. P. (2003). "Thermal response of poly(N-isopropylacrylamide) brushes probed by surface plasmon resonance." *Langmuir* **19**(7): 2545-2549.

Bamford, C. H. and Al-Lamee, K. G. (1994). "Polymer surface functionalisation and grafting by a simple and inexpensive method." *Macromolecular Rapid Communications* **15**(4): 379-384.

Binder, K., Baschnagel, J., Müller, M., Paul, W. and Rampf, F. (2006). "Simulation of phase transitions of single polymer chains: Recent advances." *Macromolecular Symposia* **237**: 128-138.

Braden, D. A., Parrack, E. E. and Tyler, D. R. (2001). "Solvent cage effects. I. Effect of radical mass and size on radical cage pair recombination efficiency. II. Is geminate recombination of polar radicals sensitive to solvent polarity?" *Coordination Chemistry Reviews* **211**(1): 279-294.

Brun-Graeppi, A. K. A. S., Richard, C., Bessodes, M., Scherman, D. and Merten, O.-W. (2010). "Thermoresponsive surfaces for cell culture and enzyme-free cell detachment." *Progress in Polymer Science* **35**(11): 1311-1324.

Burtovyy, O., Klep, V., Chen, H.-C., Hu, R.-K., Lin, C.-C. and Luzinov, I. (2007). "Hydrophobic Modification of Polymer Surfaces via "Grafting to" Approach." *Journal of Macromolecular Science, Part B* **46**(1): 137-154.

Canavan, H. E., Cheng, X., Graham, D. J., Ratner, B. D. and Castner, D. G. (2005). "Cell sheet detachment affects the extracellular matrix: A surface science study comparing thermal liftoff, enzymatic, and mechanical methods." *Journal of Biomedical Materials Research Part A* **75A**(1): 1-13.

Carter, S., Hunt, B. and Rimmer, S. (2005). "Highly Branched Poly(N-isopropylacrylamide)s with Imidazole End Groups Prepared by Radical Polymerization in the Presence of a Styryl Monomer Containing a Dithioester Group." *Macromolecules* **38**(11): 4595-4603.

Cetinkaya, G., Kahraman, A. S., Gumusderelioglu, M., Arat, S. and Onur, M. A. (2011). "Derivation, characterization and expansion of fetal chondrocytes on different microcarriers." *Cytotechnology* **63**(6): 633-643.

Cheng, X., Canavan, H. E., Stein, M. J., Hull, J. R., Kweskin, S. J., Wagner, M. S., Somorjai, G. A., Castner, D. G. and Ratner, B. D. (2005). "Surface chemical and mechanical properties of plasma-polymerized N-isopropylacrylamide." *Langmuir* **21**(17): 7833-7841.

Chern, C. S. (2006). "Emulsion polymerization mechanisms and kinetics." *Progress in Polymer Science* **31**(5): 443-486.

Cole, M. A., Voelcker, N. H., Thissen, H. and Griesser, H. J. (2009). "Stimuli-responsive interfaces and systems for the control of protein-surface and cell-surface interactions." *Biomaterials* **30**(9): 1827-1850.

Collett, J., Crawford, A., Hatton, P. V., Geoghegan, M. and Rimmer, S. (2007). "Thermally responsive polymeric hydrogel brushes: synthesis, physical properties and use for the culture of chondrocytes." *Journal of The Royal Society Interface* **4**(12): 117-126.

da Silva, R. M. P., Mano, J. F. and Reis, R. L. (2007). "Smart thermoresponsive coatings and surfaces for tissue engineering: switching cell-material boundaries." *Trends in Biotechnology* **25**(12): 577-583.

Demetriou, A. A., Reisner, A., Sanchez, J., Levenson, S. M., Moscioni, A. D. and Chowdhury, J. R. (1988). "Transplantation of microcarrier-attached hepatocytes into 90% partially hepatectomized rats." *Hepatology* **8**(5): 1006-1009.

Dürrschmid, M., Landauer, K., Simic, G., Blüml, G. and Doblhoff-Dier, O. (2003). "Scalable inoculation strategies for microcarrier-based animal cell bioprocesses." *Biotechnology and Bioengineering* **83**(6): 681-686.

Ebara, M., Yamato, M., Aoyagi, T., Kikuchi, A., Sakai, K. and Okano, T. (2008). "A Novel Approach to Observing Synergy Effects of PHSRN on Integrin–RGD Binding Using Intelligent Surfaces." *Advanced Materials* **20**(16): 3034-3038.

Eibes, G., dos Santos, F., Andrade, P. Z., Boura, J. S., Abecasis, M. M. A., da Silva, C. L. and Cabral, J. M. S. (2010). "Maximizing the ex vivo expansion of human mesenchymal stem cells using a microcarrier-based stirred culture system." *Journal of Biotechnology* **146**(4): 194-197.

Engel, P. S. (1980). "Mechanism of the thermal and photochemical decomposition of azoalkanes." *Chemical Reviews* **80**(2): 99-150.

Franck, J. and Rabinowitsch, E. (1934). "Some remarks about free radicals and the photochemistry of solutions." *Transactions of the Faraday Society* **30**(0): 120-130.

Fujishige, S., Kubota, K. and Ando, I. (1989). "Phase transition of aqueous solutions of poly(N-isopropylacrylamide) and poly(N-isopropylmethacrylamide)." *The Journal of Physical Chemistry* **93**(8): 3311-3313.

GE-Healthcare (2005). "Microcarrier Cell Culture Principles and Methods."

Gewehr, M., Nakamura, K., Ise, N. and Kitano, H. (1992). "Gel permeation chromatography using porous glass beads modified with temperature-responsive polymers." *Die Makromolekulare Chemie* **193**(1): 249-256.

Gil, E. S. and Hudson, S. M. (2004). "Stimuli-reponsive polymers and their bioconjugates." *Progress in Polymer Science* **29**(12): 1173-1222.

Go, H., Sudo, Y., Hosoya, K., Ikegami, T. and Tanaka, N. (1998). "Effects of Mobile-Phase Composition and Temperature on the Selectivity of Poly(N-isopropylacrylamide)-Bonded Silica Gel in Reversed-Phase Liquid Chromatography." *Analytical Chemistry* **70**(19): 4086-4093.

Gokmen, M. T. and Du Prez, F. E. (2012). "Porous polymer particles—A comprehensive guide to synthesis, characterization, functionalization and applications." *Progress in Polymer Science* **37**(3): 365-405.

Griesbaum, K. (1970). "Problems and Possibilities of the Free-Radical Addition of Thiols to Unsaturated Compounds." *Angewandte Chemie International Edition in English* **9**(4): 273-287.

Griesser, H. J., Chatelier, R. C., Gengenbach, T. R., Johnson, G. and Steele, J. G. (1994). "Growth of human cells on plasma polymers: Putative role of amine and amide groups." *Journal of Biomaterials Science, Polymer Edition* **5**(6): 531-554.

Grinnell, F. (1978). Cellular Adhesiveness and Extracellular Substrata. International Review of Cytology. G. H. Bourne and J. F. Danielli, Academic Press. **Volume 53:** 65-144.

Grinnell, F. and Feld, M. K. (1979). "Initial adhesion of human fibroblasts in serum-free medium: Possible role of secreted fibronectin." *Cell* **17**(1): 117-129.

Grinnell, F., Hays, D. G. and Minter, D. (1977). "Cell adhesion and spreading factor: Partial purification and properties." *Experimental Cell Research* **110**(1): 175-190.

Hatakeyama, H., Kikuchi, A., Yamato, M. and Okano, T. (2006). "Bio-functionalized thermoresponsive interfaces facilitating cell adhesion and proliferation." *Biomaterials* **27**(29): 5069-5078.

Hendrick, V., Muniz, E., Geuskens, G. and Wérenne, J. (2001). "Adhesion, growth and detachment of cells on modified polystyrene surface." *Cytotechnology* **36**(1-3): 49-53.

Henríquez, C., Bueno, C., Lissi, E. A. and Encinas, M. V. (2003). "Thiols as chain transfer agents in free radical polymerization in aqueous solution." *Polymer* **44**(19): 5559-5561.

Hoffman, A. S., Stayton, P. S., Bulmus, V., Chen, G., Chen, J., Cheung, C., Chilkoti, A., Ding, Z., Dong, L., Fong, R., Lackey, C. A., Long, C. J., Miura, M., Morris, J. E., Murthy, N., Nabeshima, Y., Park, T. G., Press, O. W., Shimoboji, T., Shoemaker, S., Yang, H. J., Monji, N., Nowinski, R. C., Cole, C. A., Priest, J. H., Harris, J. M., Nakamae, K., Nishino, T. and Miyata, T. (2000). "Really smart bioconjugates of smart polymers and receptor proteins." *Journal of Biomedical Materials Research* **52**(4): 577-586.

Hopkins, S., Carter, S., Swanson, L., MacNeil, S. and Rimmer, S. (2007). "Temperature-dependent phagocytosis of highly branched poly(N-isopropyl acrylamide-co-1,2 propandiol-3-methacrylate)s prepared by RAFT polymerization." *Journal of Materials Chemistry* **17**(38): 4022-4027.

Hsieh, T. T., Tiu, C. and Simon, G. P. (2001). "Melt rheology of aliphatic hyperbranched polyesters with various molecular weights." *Polymer* **42**(5): 1931-1939.

Ista, L. K., Mendez, S., Pérez-Luna, V. H. and López, G. P. (2001). "Synthesis of poly(N-isopropylacrylamide) on initiator-modified self-assembled monolayers." *Langmuir* **17**(9): 2552-2555.

Jaffe, A. B., Skinner, K. J. and McBride, J. M. (1972). "Solvent steric effects. II. Free-radical chemistry of azobisisobutyronitrile and azobis-3-cyano-3-pentane in viscous and crystalline media." *Journal of the American Chemical Society* **94**(24): 8510-8515.

Jeong, B. and Gutowska, A. (2002). "Lessons from nature: stimuli-responsive polymers and their biomedical applications." *Trends in Biotechnology* **20**(7): 305-311.

Ju, H. K., Kim, S. Y. and Lee, Y. M. (2001). "pH/temperature-responsive behaviors of semi-IPN and comb-type graft hydrogels composed of alginate and poly(N-isopropylacrylamide)." *Polymer* **42**(16): 6851-6857.

Kamiya, K., Yanagida, K. and Shirokaze, J. (1995). Subculture Method for Large Scale Cell Culture Using Macroporous MicroCarrier. Animal Cell Technology: Developments Towards the 21st Century. E. C. Beuvery, J. B. Griffiths and W. P. Zeijlemaker, Springer Netherlands**:** 759-763.

Kikuchi, A. and Okano, T. (2002). "Intelligent thermoresponsive polymeric stationary phases for aqueous chromatography of biological compounds." *Progress in Polymer Science* **27**(6): 1165-1193.

Kikuchi, A. and Okano, T. (2005). "Nanostructured designs of biomedical materials: applications of cell sheet engineering to functional regenerative tissues and organs." *Journal of Controlled Release* **101**(1-3): 69-84.

Kim, D. J., Heo, J.-y., Kim, K. S. and Choi, I. S. (2003). "Formation of Thermoresponsive Poly(N-isopropylacrylamide)/Dextran Particles by Atom Transfer Radical Polymerization." *Macromolecular Rapid Communications* **24**(8): 517-521.

Kim, M. H., Kim, J.-C., Lee, H. Y., Kim, J. D. and Yang, J. H. (2005a). "Release property of temperature-sensitive alginate beads containing poly(N-isopropylacrylamide)." *Colloids and Surfaces B: Biointerfaces* **46**(1): 57-61.

Kim, M. R., Jeong, J. H. and Park, T. G. (2002). "Swelling Induced Detachment of Chondrocytes Using RGD-Modified Poly(N-isopropylacrylamide) Hydrogel Beads." *Biotechnology Progress* **18**(3): 495-500.

Kim, S.-S., Gwak, S.-J., Choi, C. Y. and Kim, B.-S. (2005b). "Skin regeneration using keratinocytes and dermal fibroblasts cultured on biodegradable microspherical polymer scaffolds." *Journal of Biomedical Materials Research Part B: Applied Biomaterials* **75B**(2): 369-377.

Kumar, A., Srivastava, A., Galaev, I. Y. and Mattiasson, B. (2007). "Smart polymers: Physical forms and bioengineering applications." *Progress in Polymer Science* **32**(10): 1205-1237.

Kwon, O. H., Kikuchi, A., Yamato, M., Sakurai, Y. and Okano, T. (2000). "Rapid cell sheet detachment from Poly(N-isopropylacrylamide)-grafted porous cell culture membranes." *Journal of Biomedical Materials Research* **50**(1): 82-89.

LaFlamme, S. E., Akiyama, S. K. and Yamada, K. M. (1992). "Regulation of fibronectin receptor distribution." *J Cell Biol* **117**(2): 437-447.

Lee, Y.-G., Park, C.-Y., Song, K.-H., Kim, S.-S. and Oh, S.-G. (2012). "Preparation of monodispersed PNIPAm/silica composites and characterization of their thermal behaviors." *Journal of Industrial and Engineering Chemistry* **18**(2): 744-751.

Li, G., Yang, X., Wang, B., Wang, J. and Yang, X. (2008). "Monodisperse temperature-responsive hollow polymer microspheres: Synthesis, characterization and biological application." *Polymer* **49**(16): 3436-3443.

Lin, S.-Y., Chen, K.-S. and Liang, R.-C. (1999). "Thermal micro ATR/FT-IR spectroscopic system for quantitative study of the molecular structure of poly(N-isopropylacrylamide) in water." *Polymer* **40**(10): 2619-2624.

Liu, G., Yang, X. and Wang, Y. (2007a). "Preparation of monodisperse hydrophilic polymer microspheres with N,N′-methylenediacrylamide as crosslinker by distillation precipitation polymerization." *Polymer International* **56**(7): 905-913.

Liu, G., Yang, X. and Wang, Y. (2007b). "Silica/poly(N,N′-methylenebisacrylamide) composite materials by encapsulation based on a hydrogen-bonding interaction." *Polymer* **48**(15): 4385-4392.

Luo, Y.-L., Yu, W., Xu, F. and Zhang, L.-L. (2012). "Novel thermo-responsive self-assembly micelles from a double brush-shaped PNIPAM-g-(PA-b-PEG-b-PA)-g-PNIPAM block copolymer with PNIPAM polymers as side chains." *Journal of Polymer Science Part A: Polymer Chemistry* **50**(10): 2053-2067.

Magnusson, H., Malmström, E., Hult, A. and Johansson, M. (2002). "The effect of degree of branching on the rheological and thermal properties of hyperbranched aliphatic polyethers." *Polymer* **43**(2): 301-306.

Maharjan, P., Woonton, B. W., Bennett, L. E., Smithers, G. W., DeSilva, K. and Hearn, M. T. W. (2008). "Novel chromatographic separation — The potential of smart polymers." *Innovative Food Science & Emerging Technologies* **9**(2): 232-242.

Makino, K., Yamamoto, S., Fujimoto, K., Kawaguchi, H. and Ohshima, H. (1994). "Surface Structure of Latex Particles Covered with Temperature-Sensitive Hydrogel Layers." *Journal of Colloid and Interface Science* **166**(1): 251-258.

Malda, J. and Frondoza, C. G. (2006). "Microcarriers in the engineering of cartilage and bone." *Trends in Biotechnology* **24**(7): 299-304.

Male, J. L., Lindfors, B. E., Covert, K. J. and Tyler, D. R. (1998). "The Effect of Radical Size and Mass on the Cage Recombination Efficiency of Photochemically Generated Radical Cage Pairs." *Journal of the American Chemical Society* **120**(50): 13176-13186.

Malham, I. B. and Bureau, L. (2009). "Density Effects on Collapse, Compression, and Adhesion of Thermoresponsive Polymer Brushes." *Langmuir* **26**(7): 4762-4768.

Mano, J. F. (2008). "Stimuli-Responsive Polymeric Systems for Biomedical Applications." *Advanced Engineering Materials* **10**(6): 515-527.

Martin, Y., Eldardiri, M., Lawrence-Watt, D. J. and Sharpe, J. R. (2011). "Microcarriers and their potential in tissue regeneration." *Tissue Eng Part B Rev* **17**(1): 71-80.

Matsuda, N., Shimizu, T., Yamato, M. and Okano, T. (2007). "Tissue Engineering Based on Cell Sheet Technology." *Advanced Materials* **19**(20): 3089-3099.

Matyjaszewski, K. (2001). Atom Transfer Free Radical Polymerization. Encyclopedia of Materials: Science and Technology (Second Edition). K. H. J. B. Editors-in-Chief: , W. C. Robert, C. F. Mertonet al. Oxford, Elsevier**:** 356-365.

Matyjaszewski, K. and Tsarevsky, N. V. (2009). "Nanostructured functional materials prepared by atom transfer radical polymerization." *Nat Chem* **1**(4): 276-288.

Mendez, S., Curro, J. G., McCoy, J. D. and Lopez, G. P. (2004). "Computational Modeling of the Temperature-Induced Structural Changes of Tethered Poly(N-isopropylacrylamide) with Self-Consistent Field Theory." *Macromolecules* **38**(1): 174-181.

Mino, G. and Kaizerman, S. (1958). "A new method for the preparation of graft copolymers. Polymerization initiated by ceric ion redox systems." *Journal of Polymer Science* **31**(122): 242-243.

Mittal, V., Matsko, N. B., Butté, A. and Morbidelli, M. (2007a). "Functionalized polystyrene latex particles as substrates for ATRP: Surface and colloidal characterization." *Polymer* **48**(10): 2806-2817.

Mittal, V., Matsko, N. B., Butté, A. and Morbidelli, M. (2007b). "Synthesis of temperature responsive polymer brushes from polystyrene latex particles functionalized with ATRP initiator." *European Polymer Journal* **43**(12): 4868-4881.

Mizutani, A., Nagase, K., Kikuchi, A., Kanazawa, H., Akiyama, Y., Kobayashi, J., Annaka, M. and Okano, T. (2010). "Thermo-responsive polymer brush-grafted porous polystyrene beads for all-aqueous chromatography." *Journal of Chromatography A* **1217**(4): 522-529.

Moad, G., Rizzardo, E. and Thang, S. H. (2008). "Radical addition–fragmentation chemistry in polymer synthesis." *Polymer* **49**(5): 1079-1131.

Nagase, K., Kobayashi, J., Kikuchi, A., Akiyama, Y., Kanazawa, H. and Okano, T. (2007). "Effects of Graft Densities and Chain Lengths on Separation of Bioactive Compounds by Nanolayered Thermoresponsive Polymer Brush Surfaces." *Langmuir* **24**(2): 511-517.

Nakagami, H., Morishita, R., Maeda, K., Kikuchi, Y., Ogihara, T. and Kaneda, Y. (2006). "Adipose tissue-derived stromal cells as a novel option for regenerative cell therapy." *J Atheroscler Thromb* **13**(2): 77-81.

Oddo, L., Masci, G., Di Meo, C., Capitani, D., Mannina, L., Lamanna, R., De Santis, S., Alhaique, F., Coviello, T. and Matricardi, P. (2010). "Novel thermosensitive calcium alginate microspheres: Physico-chemical characterization and delivery properties." *Acta Biomaterialia* **6**(9): 3657-3664.

Oelkers, A. B. and Tyler, D. R. (2008). "Radical cage effects: A method for measuring recombination efficiencies of secondary geminate radical cage pairs using pump-probe transient absorption methods." *Photochemical & Photobiological Sciences* **7**(11): 1386-1390.

Oh, S. K. W., Chen, A. K., Mok, Y., Chen, X., Lim, U. M., Chin, A., Choo, A. B. H. and Reuveny, S. (2009). "Long-term microcarrier suspension cultures of human embryonic stem cells." *Stem Cell Research* **2**(3): 219-230.

Okano, T., Yamada, N., Okuhara, M., Sakai, H. and Sakurai, Y. (1995). "Mechanism of cell detachment from temperature-modulated, hydrophilic-hydrophobic polymer surfaces." *Biomaterials* **16**(4): 297-303.

Pan, G., Zhang, Y., Guo, X., Li, C. and Zhang, H. (2010). "An efficient approach to obtaining water-compatible and stimuli-responsive molecularly imprinted polymers by the facile surface-grafting of functional polymer brushes via RAFT polymerization." *Biosensors and Bioelectronics* **26**(3): 976-982.

Park, T. G. and Hoffman, A. S. (1990a). "Immobilization and characterization of β-galactosidase in thermally reversible hydrogel beads." *Journal of Biomedical Materials Research* **24**(1): 21-38.

Park, T. G. and Hoffman, A. S. (1990b). "Immobilization of Arthrobacter simplex in a thermally reversible hydrogel: Effect of temperature cycling on steroid conversion." *Biotechnology and Bioengineering* **35**(2): 152-159.

Park, T. G. and Hoffman, A. S. (1992). "Preparation of large, uniform size temperature-sensitive hydrogel beads." *Journal of Polymer Science Part A: Polymer Chemistry* **30**(3): 505-507.

Park, Y., Subramanian, K., Verfaillie, C. M. and Hu, W. S. (2010). "Expansion and hepatic differentiation of rat multipotent adult progenitor cells in microcarrier suspension culture." *Journal of Biotechnology* **150**(1): 131-139.

Patrizi, M. L., Diociaiuti, M., Capitani, D. and Masci, G. (2009). "Synthesis and association properties of thermoresponsive and permanently cationic charged block copolymers." *Polymer* **50**(2): 467-474.

Peleshanko, S. and Tsukruk, V. V. (2008). "The architectures and surface behavior of highly branched molecules." *Progress in Polymer Science* **33**(5): 523-580.

Pelton, R. H. and Chibante, P. (1986). "Preparation of aqueous latices with N-isopropylacrylamide." *Colloids and Surfaces* **20**(3): 247-256.

Peng, Y. and Fan, L. T. (1995). "Hysteresis in liquid-solid tapered fluidized beds." *Chemical Engineering Science* **50**(16): 2669-2671.

Peng, Y. and Fan, L. T. (1997). "Hydrodynamic characteristics of fluidization in liquid-solid tapered beds." *Chemical Engineering Science* **52**(14): 2277-2290.

Phillips, B. W., Horne, R., Lay, T. S., Rust, W. L., Teck, T. T. and Crook, J. M. (2008). "Attachment and growth of human embryonic stem cells on microcarriers." *Journal of Biotechnology* **138**(1–2): 24-32.

Plunkett, K. N., Zhu, X., Moore, J. S. and Leckband, D. E. (2006). "PNIPAM Chain Collapse Depends on the Molecular Weight and Grafting Density." *Langmuir* **22**(9): 4259-4266.

Prucker, O. and Rühe, J. (1998a). "Mechanism of Radical Chain Polymerizations Initiated by Azo Compounds Covalently Bound to the Surface of Spherical Particles." *Macromolecules* **31**(3): 602-613.

Prucker, O. and Rühe, J. (1998b). "Synthesis of Poly(styrene) Monolayers Attached to High Surface Area Silica Gels through Self-Assembled Monolayers of Azo Initiators." *Macromolecules* **31**(3): 592-601.

Qiu, J., Charleux, B. and Matyjaszewski, K. (2001). "Controlled/living radical polymerization in aqueous media: homogeneous and heterogeneous systems." *Progress in Polymer Science* **26**(10): 2083-2134.

Ranby, B. and Zuchowska, D. (1987). "Graft Copolymerization of Vinyl Monomers onto Pure Cotton Cellulose Using Mn^{3+} Ions as Initiator." *Polymer Journal* **19**(5): 623-630.

Rimmer, S., Carter, S., Rutkaite, R., Haycock, J. W. and Swanson, L. (2007). "Highly branched poly-(N-isopropylacrylamide)s with arginine-glycine-aspartic acid (RGD)- or COOH-chain ends that form sub-micron stimulus-responsive particles above the critical solution temperature." *Soft Matter* **3**(8): 971-973.

Rimmer, S., Mohd. Ramli, A. N. and Lefèvre, S. (1996). "Preparation of polystyrene-poly (styrene-g-N-isopropylacrylamide) core-shell particles: copolymerization of oligo (N-isopropylacrylamide) macromonomers and styrene onto polystyrene seed particles and stability of the resultant particles." *Polymer* **37**(18): 4135-4139.

Sakamoto, C., Okada, Y., Kanazawa, H., Ayano, E., Nishimura, T., Ando, M., Kikuchi, A. and Okano, T. (2004). "Temperature- and pH-responsive aminopropyl-silica ion-exchange columns grafted with copolymers of N-isopropylacrylamide." *Journal of Chromatography A* **1030**(1–2): 247-253.

Santos, M., Rodrigues, A. and Teixeira, J. A. (2005). "Production of dextran and fructose from carob pod extract and cheese whey by Leuconostoc mesenteroides NRRL B512(f)." *Biochemical Engineering Journal* **25**(1): 1-6.

Schild, H. G. (1992). "Poly(N-isopropylacrylamide): experiment, theory and application." *Progress in Polymer Science* **17**(2): 163-249.

Schmaljohann, D. (2006). "Thermo- and pH-responsive polymers in drug delivery." *Advanced Drug Delivery Reviews* **58**(15): 1655-1670.

Seino, M., Yokomachi, K., Hayakawa, T., Kikuchi, R., Kakimoto, M.-a. and Horiuchi, S. (2006). "Preparation of poly(N-isopropylacrylamide) grafted silica bead using hyperbranched polysiloxysilane as polymer brush and application to temperature-responsive HPLC." *Polymer* **47**(6): 1946-1952.

Shamim, N., Hong, L., Hidajat, K. and Uddin, M. S. (2006). "Thermosensitive-polymer-coated magnetic nanoparticles: Adsorption and desorption of Bovine Serum Albumin." *Journal of Colloid and Interface Science* **304**(1): 1-8.

Shefer, A., Grodzinsky, A. J., Prime, K. L. and Busnel, J. P. (1993). "Free-radical telomerization of tert-butyl acrylate in the presence of bis(4-aminophenyl) disulfide as a useful route to amino-terminated telomers of poly(acrylic acid)." *Macromolecules* **26**(9): 2240-2245.

Shi, J., Alves, N. M. and Mano, J. F. (2006). "Drug Release of pH/Temperature-Responsive Calcium Alginate/Poly(N-isopropylacrylamide) Semi-IPN Beads." *Macromolecular Bioscience* **6**(5): 358-363.

Shimizu, H., Wada, R. and Okabe, M. (2009). "Preparation and Characterization of Micrometer-Sized Poly(N-isopropylacrylamide) Hydrogel Particles." *Polym. J* **41**(9): 771-777.

Siegwart, D. J., Oh, J. K. and Matyjaszewski, K. (2012). "ATRP in the design of functional materials for biomedical applications." *Progress in Polymer Science* **37**(1): 18-37.

Takei, Y. G., Aoki, T., Sanui, K., Ogata, N., Okano, T. and Sakurai, Y. (1993). "Temperature-responsive bioconjugates. 1. Synthesis of temperature-responsive oligomers with reactive end groups and their coupling to biomolecules." *Bioconjugate Chemistry* **4**(1): 42-46.

Takei, Y. G., Aoki, T., Sanui, K., Ogata, N., Sakurai, Y. and Okano, T. (1994). "Dynamic Contact Angle Measurement of Temperature-Responsive Surface Properties for Poly(N-isopropylacrylamide) Grafted Surfaces." *Macromolecules* **27**(21): 6163-6166.

Takeuchi, S., Oike, M., Kowitz, C., Shimasaki, C., Hasegawa, K. and Kitano, H. (1993). "Microspheres prepared with a temperature-responsive macromonomer." *Die Makromolekulare Chemie* **194**(2): 551-558.

Tamura, A., Kobayashi, J., Yamato, M. and Okano, T. (2012a). "Temperature-responsive poly(N-isopropylacrylamide)-grafted microcarriers for large-scale non-invasive harvest of anchorage-dependent cells." *Biomaterials* **33**(15): 3803-3812.

Tamura, A., Kobayashi, J., Yamato, M. and Okano, T. (2012b). "Thermally responsive microcarriers with optimal poly(N-isopropylacrylamide) grafted density for facilitating cell adhesion/detachment in suspension culture." *Acta Biomaterialia* **8**(11): 3904-3913.

Tamura, A., Nishi, M., Kobayashi, J., Nagase, K., Yajima, H., Yamato, M. and Okano, T. (2012c). "Simultaneous Enhancement of Cell Proliferation and Thermally

Induced Harvest Efficiency Based on Temperature-Responsive Cationic Copolymer-Grafted Microcarriers." *Biomacromolecules* **13**(6): 1765-1773.

Tang, E., Fu, C., Wang, S., Dong, S., Zhao, F. and Zhao, D. (2012). "Graft polymerization of styrene monomer initiated by azobis(4-cyanovaleric acid) anchored on the surface of ZnO nanoparticles and its PVC composite film." *Powder Technology* **218**(0): 5-10.

Tao, W. and Yan, L. (2010). "Thermogelling of highly branched poly(N-isopropylacrylamide)." *Journal of Applied Polymer Science* **118**(6): 3391-3399.

Teal, H. E., Hu, Z. and Root, D. D. (2000). "Native Purification of Biomolecules with Temperature-Mediated Hydrophobic Modulation Liquid Chromatography." *Analytical Biochemistry* **283**(2): 159-165.

Tsuda, Y., Kikuchi, A., Yamato, M., Nakao, A., Sakurai, Y., Umezu, M. and Okano, T. (2005). "The use of patterned dual thermoresponsive surfaces for the collective recovery as co-cultured cell sheets." *Biomaterials* **26**(14): 1885-1893.

Tsuda, Y., Kikuchi, A., Yamato, M., Sakurai, Y., Umezu, M. and Okano, T. (2004). "Control of cell adhesion and detachment using temperature and thermoresponsive copolymer grafted culture surfaces." *Journal of Biomedical Materials Research Part A* **69A**(1): 70-78.

Van Wezel, A. L. (1967). "Growth of cell-strains and primary cells on micro-carriers in homogeneous culture [17]." *Nature* **216**(5110): 64-65.

Vogt, A. P. and Sumerlin, B. S. (2008). "Tuning the Temperature Response of Branched Poly(N-isopropylacrylamide) Prepared by RAFT Polymerization." *Macromolecules* **41**(20): 7368-7373.

Von Recum, H. A., Okano, T., Kim, S. W. and Bernstein, P. S. (1999). "Maintenance of Retinoid Metabolism in Human Retinal Pigment Epithelium Cell Culture." *Experimental Eye Research* **69**(1): 97-107.

Wang, H., Peng, M., Zheng, J. and Li, P. (2008). "Encapsulation of silica nanoparticles by redox-initiated graft polymerization from the surface of silica nanoparticles." *Journal of Colloid and Interface Science* **326**(1): 151-157.

Wang, Y. and Ouyang, F. (1999). "Bead-to-bead transfer of Vero cells in microcarrier culture." *Bioprocess Engineering* **21**(3): 211-213.

Wardman, P. and von Sonntag, C. (1995). [3] Kinetic factors that control the fate of thiyl radicals in cells. Methods in Enzymology. P. Lester, Academic Press. **Volume 251:** 31-45.

Weisz, O. A. and Schnaar, R. L. (1991). "Hepatocyte adhesion to carbohydrate-derivatized surfaces. I. Surface topography of the rat hepatic lectin." *J Cell Biol* **115**(2): 485-493.

Wu, M. H., Urban, J. P., Cui, Z. and Cui, Z. F. (2006). "Development of PDMS microbioreactor with well-defined and homogenous culture environment for chondrocyte 3-D culture." *Biomed Microdevices* **8**(4): 331-340.

Xu, F. J., Neoh, K. G. and Kang, E. T. (2009). "Bioactive surfaces and biomaterials via atom transfer radical polymerization." *Progress in Polymer Science* **34**(8): 719-761.

Yakushiji, T., Sakai, K., Kikuchi, A., Aoyagi, T., Sakurai, Y. and Okano, T. (1998). "Graft Architectural Effects on Thermoresponsive Wettability Changes of Poly(N-isopropylacrylamide)-Modified Surfaces." *Langmuir* **14**(16): 4657-4662.

Yakushiji, T., Sakai, K., Kikuchi, A., Aoyagi, T., Sakurai, Y. and Okano, T. (1999). "Effects of Cross-Linked Structure on Temperature-Responsive Hydrophobic Interaction of Poly(N-isopropylacrylamide) Hydrogel-Modified Surfaces with Steroids." *Analytical Chemistry* **71**(6): 1125-1130.

Yamada, N., Okano, T., Sakai, H., Karikusa, F., Sawasaki, Y. and Sakurai, Y. (1990). "Thermo-responsive polymeric surfaces; control of attachment and detachment of cultured cells." *Die Makromolekulare Chemie, Rapid Communications* **11**(11): 571-576.

Yamato, M., Akiyama, Y., Kobayashi, J., Yang, J., Kikuchi, A. and Okano, T. (2007). "Temperature-responsive cell culture surfaces for regenerative medicine with cell sheet engineering." *Progress in Polymer Science* **32**(8–9): 1123-1133.

Yamato, M., Okuhara, M., Karikusa, F., Kikuchi, A., Sakurai, Y. and Okano, T. (1999). "Signal transduction and cytoskeletal reorganization are required for cell detachment from cell culture surfaces grafted with a temperature-responsive polymer." *Journal of Biomedical Materials Research* **44**(1): 44-52.

Yang, H. S., Jeon, O., Bhang, S. H., Lee, S.-H. and Kim, B.-S. (2010). "Suspension Culture of Mammalian Cells Using Thermosensitive Microcarrier That Allows Cell Detachment Without Proteolytic Enzyme Treatment." *Cell Transplantation* **19**(9): 1123-1132.

Yang, J., Yamato, M., Kohno, C., Nishimoto, A., Sekine, H., Fukai, F. and Okano, T. (2005). "Cell sheet engineering: Recreating tissues without biodegradable scaffolds." *Biomaterials* **26**(33): 6415-6422.

Yim, H., Kent, M. S., Huber, D. L., Satija, S., Majewski, J. and Smith, G. S. (2003). "Conformation of End-Tethered PNIPAM Chains in Water and in Acetone by Neutron Reflectivity." *Macromolecules* **36**(14): 5244-5251.

Yim, H., Kent, M. S., Mendez, S., Balamurugan, S. S., Balamurugan, S., Lopez, G. P. and Satija, S. (2004). "Temperature-Dependent Conformational Change of PNIPAM Grafted Chains at High Surface Density in Water." *Macromolecules* **37**(5): 1994-1997.

Yim, H., Kent, M. S., Mendez, S., Lopez, G. P., Satija, S. and Seo, Y. (2006). "Effects of Grafting Density and Molecular Weight on the Temperature-Dependent Conformational Change of Poly(N-isopropylacrylamide) Grafted Chains in Water." *Macromolecules* **39**(9): 3420-3426.

Yoshida, R., Sakai, K., Okano, T. and Sakurai, Y. (1992a). "Surface-modulated skin layers of thermal responsive hydrogels as on-off switches: II. Drug permeation." *Journal of Biomaterials Science, Polymer Edition* **3**(3): 243-252.

Yoshida, R., Sakai, K., Okano, T., Sakurai, Y., You Han, B. and Sung Wan, K. (1992b). "Surface-modulated skin layers of thermal responsive hydrogels as on-off switches: I. Drug release." *Journal of Biomaterials Science, Polymer Edition* **3**(2): 155-162.

Yoshida, R., Uchida, K., Kaneko, Y., Sakai, K., Kikuchi, A., Sakurai, Y. and Okano, T. (1995). "Comb-type grafted hydrogels with rapid deswelling response to temperature changes." *Nature* **374**(6519): 240-242.

Zhang, F. and Wang, C.-C. (2008). "Preparation of thermoresponsive core–shell polymeric microspheres and hollow PNIPAM microgels." *Colloid & Polymer Science* **286**(8): 889-895.

Zhu, X., Yan, C., Winnik, F. M. and Leckband, D. (2006). "End-Grafted Low-Molecular-Weight PNIPAM Does Not Collapse above the LCST†." *Langmuir* **23**(1): 162-169.

Zhu, Y., Liu, T., Song, K., Ning, R., Ma, X. and Cui, Z. (2009). "ADSCs differentiated into cardiomyocytes in cardiac microenvironment." *Mol Cell Biochem* **324**(1-2): 117-129.